JOURNAL OF THE AERONAUTICAL SCIENCES

VOLUME 23 APRIL, 1956 NUMBER 4

ST. LOUIS PUBLIC LIBRARY APR 17 1956

CONTENTS

Some Structural and Aeroelastic Considerations of High-Speed Flight (Nineteenth Wright Brothers Lecture) ..... R. L. BISPLINGHOFF 289

A Method for Predicting Lift Effectiveness of Spoilers at Subsonic Speeds ..... ARTHUR L. JONES, OWEN P. LAMB, AND ALFRED E. CRONK 330

An Investigation of the Flutter Characteristics of Compressor and Turbine Blade Systems ..... CHI-TEH WANG, FRANK LANE, AND ROBERT J. VACCARO 335

An Investigation of Helicopter Descent and Landing Characteristics Following Power Failure ..... E. F. KATZENBERGER AND M. J. RICH 345

Dynamic Derivatives in Yaw and Sideslip of Thin Wings at Supersonic Speeds ..... THEODORE R. GOODMAN 357

The Flow over a Body in a Choked Wind Tunnel and in a Sonic Free Jet ..... BERNARD W. MARSCHNER 368

Readers' Forum 377–400

Published by
INSTITUTE OF THE AERONAUTICAL SCIENCES, INC.

JOURNAL OF THE AERONAUTICAL SCIENCES

Editor: W. R. SEARS

Director, Graduate School of Aeronautical Engineering, Cornell University

Associate Editor: ROBERT R. DEXTER *Managing Editor:* RITA J. TURINO

Editorial Assistant: CAROLINE TAYLOR

Editorial Committee

Aerodynamics and Fluid Mechanics

Holt Ashley
H. Julian Allen
Dean R. Chapman
Francis H. Clauser
Hugh L. Dryden
John C. Evvard
Antonio Ferri
Alexander Flax
Wallace D. Hayes
R. T. Jones
Carl Kaplan
H. W. Liepmann
C. C. Lin
H. F. Ludloff
Harold Luskin
Clark B. Millikan
C. D. Perkins
H. J. E. Reid
George S. Schairer
G. B. Schubauer
John Stack
Theodore Theodorsen
Arthur N. Tifford
Th. von Karman

Flight Testing

R. R. Gilruth
Melvin N. Gough
W. L. Howland
W. F. Milliken, Jr.

Rotating Wing Aircraft

F. B. Gustafson
K. H. Hohenemser
Bartram Kelley
R. B. Maloy
Ralph McClarren
R. H. Miller
R. H. Prewitt
Igor I. Sikorsky

Structures

John E. Duberg
N. J. Hoff
Samuel Levy
J. F. McBrearty
W. Ramberg
E. E. Sechler
F. R. Shanley
C. R. Strang
S. Timoshenko

Meteorology

C. F. Brooks
D. M. Little
F. W. Reichelderfer
K. C. Spengler

Vibration and Flutter

Lee Arnold
M. A. Biot
R. L. Bisplinghoff
Harold A. Cheilek
I. E. Garrick
Martin Goland

Aircraft Design

W. E. Beall
E. H. Heinemann
Hall L. Hibbard
Richard Hutton
C. L. Johnson
A. A. Kartveli
E. G. Stout
F. K. Teichmann
Robert J. Woods

Electronics

Welcome W. Bender
K. C. Black
M. V. Kiebert, Jr.
David S. Little
S. B. Rogers
Paul Rosenberg
L. M. Sherer

Physiologic Problems

H. G. Armstrong
Louis H. Bauer
Robert J. Benford
W. Randolph Lovelace, II
Ross A. MacFarland

Flight Propulsion

William Bollay
George W. Brady
R. P. Kroon
Frank E. Marble
Abe Silverstein
Martin Summerfield
E. S. Taylor

Instruments

Alan G. Binnie
Charles H. Colvin
Frank R. Cook
C. S. Draper
S. G. Eskin
C. F. Savage
R. C. Sylvander

SUBSCRIPTION RATES

JOURNAL OF THE AERONAUTICAL SCIENCES, Published Monthly.—United States and Possessions: 1 Year, $15.00; Single Copies, $1.50. Foreign Countries Including Canada (American Currency Rates): 1 Year, $16.00; Single Copies, $1.50.

AERONAUTICAL ENGINEERING REVIEW, Published Monthly.—United States and Possessions: 1 Year, $3.00; Single Copies, $0.50. Foreign Countries Including Canada (American Currency Rates): 1 Year, $3.50; Single Copies, $0.50.

Notices of change of address should be sent to the Institute at least 30 days prior to actual change of address.

Manuscripts for publication, proofs, and all correspondence should be addressed to the Editorial Office of the JOURNAL.

Correspondence regarding subscriptions may be addressed to the Editorial Office of the JOURNAL OF THE AERONAUTICAL SCIENCES, 2 East 64th Street, New York 21, N.Y., or to the Publication Office, 20th and Northampton Sts., Easton, Pa.

© *Copyright, 1956, by the Institute of the Aeronautical Sciences, Inc.*

Entered as Second Class Matter at the Post Office, Easton, Pa., May 1, 1937. Acceptance for mailing at a special rate of Postage provided for in the Act of August 24, 1912. Authorized April 29, 1937.

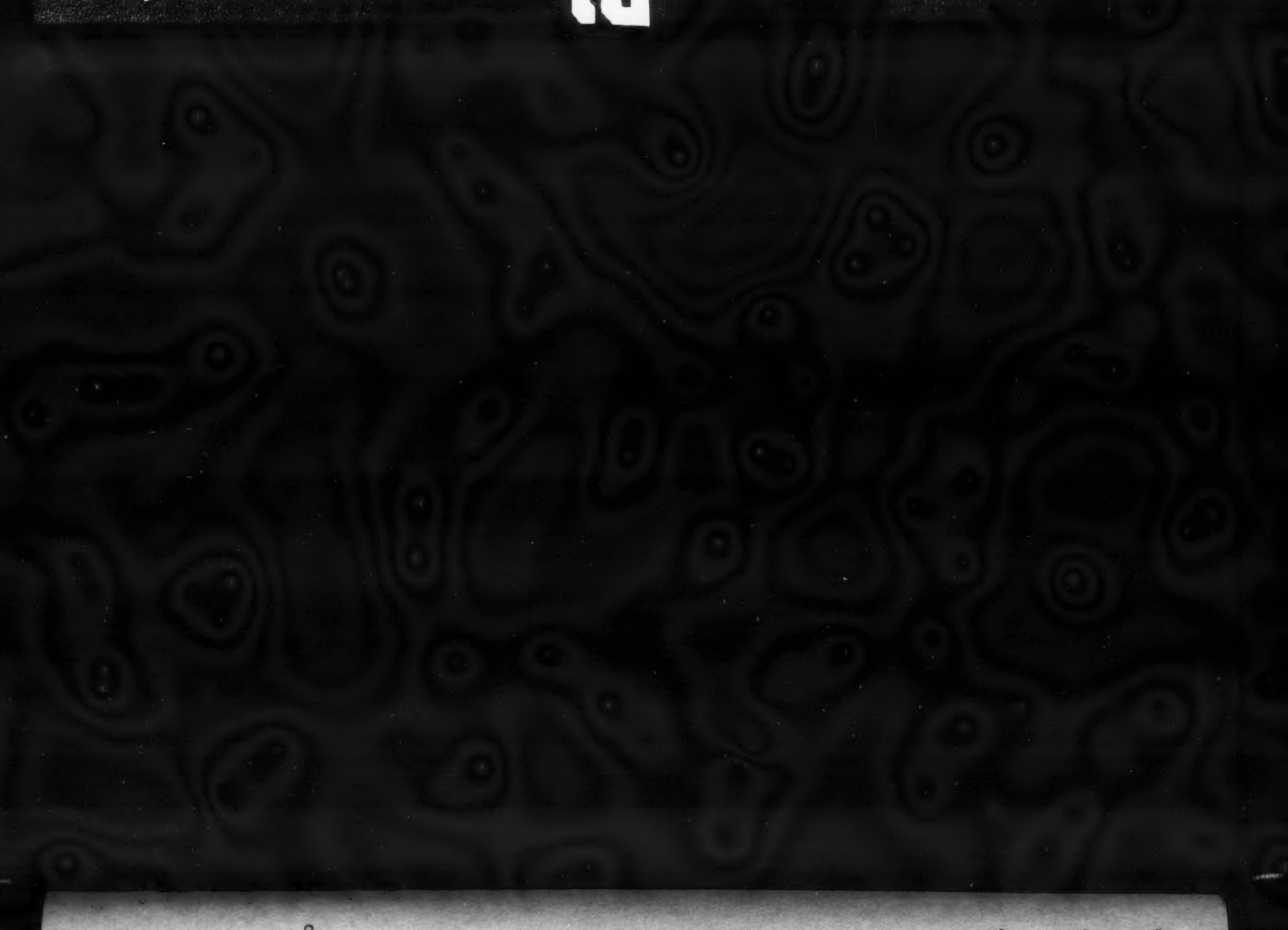

JOURNAL OF THE AERONAUTICAL SCIENCES

VOLUME 23 APRIL, 1956 NUMBER 4

Some Structural and Aeroelastic Considerations of High-Speed Flight

The Nineteenth Wright Brothers Lecture

R. L. BISPLINGHOFF*

Massachusetts Institute of Technology

SUMMARY

The dominating factors in structural design of high-speed aircraft are thermal and aeroelastic in origin. The subject matter is concerned largely with a discussion of these factors and their interrelation with one another. A summary is presented of some of the analytical and experimental tools available to aeronautical engineers to meet the demands of high-speed flight upon aircraft structures. The state of the art with respect to heat transfer from the boundary layer into the structure, modes of failure under combined load as well as thermal inputs and aerothermoelasticity is discussed. Methods of attacking and alleviating structural and aeroelastic problems of high-speed flight are summarized. Finally, some avenues of fundamental research are suggested.

(1) INTRODUCTION

MAY I FIRST express my sincere appreciation of the invitation of the Council to present this lecture. It is an honor of which I am deeply appreciative. As a teacher and research worker, I am especially conscious of the privilege and opportunity which has been presented me.

Now that we have achieved supersonic flight, aircraft structures are of greater concern than ever before. It has been customary to think of advances in airplane performance as a direct result of technical advances in propulsion and aerodynamics. Consequently, research and development in these areas has been greatly emphasized. Improvements in structures contribute less directly and have generally come as a result of pressures to create air frames which can exploit the new power-plant and aerodynamic innovations. Since the close of World War II, advances in propulsion and aerodynamics have been phenomenal. The resulting demands for a safe and adequate structure are approaching the limit of what the structural engineer can do with the materials at hand or even in sight.

This paper has three aims; to review some of the structural demands of supersonic flight, to discuss possible ways of meeting these demands, and to assess, at least qualitatively, their influence on design. I limit myself to the forseeable problems of manned aircraft and avoid consideration of the extreme speeds and altitudes of ballistic missiles.

I am aware of the classified nature of much material pertinent to the subject. However, some of the classified matter relates to characteristics and details of military air weapons and not necessarily to the more fundamental considerations which are emphasized here. Thus there appears to be a great deal that can and should be said about the unclassified portion of our subject. The paper cannot be a complete survey of all structural problems of high-speed flight for space will not permit comprehensive discussion of more than a small portion of the major factors involved.

(2) SYMBOLS

AF	=	alleviation factor
b	=	half chord
BM	=	bending moment
c	=	specific heat
e	=	nondimensional location of elastic axis behind the mid-chord
EI	=	flexural rigidity
E_{sec}	=	secant modulus
GJ	=	torsional rigidity
h	=	heat-transfer coefficient
J	=	Joule's constant; torsion constant
k	=	thermal conductivity; reduced frequency
l	=	wing structural semispan
M	=	Mach Number

Presented before the Institute of the Aeronautical Sciences in the U.S. Chamber of Commerce Auditorium, Washington, D.C., December 17, 1955.

* Professor of Aeronautical Engineering.

p = pressure; rolling moment
Pr = Prandtl Number
q = heat flux; dynamic pressure
Q = total heat
r = recovery factor
RN = Reynolds Number
s = nondimensional distance in half chords
S = entropy; wing area
t = time; thickness
T = temperature
u,v,w = displacements in x,y,z directions
U = airplane speed; energy
V = volume
w = displacement; gust intensity
W = airplane weight; virtual work
x,y,z / x_1,x_2,x_3 = rectangular coordinates
α = coefficient of thermal expansion; absorptivity coefficient; angle of attack
γ = ratio of specific heats
δ = thickness; thickness ratio of airfoil
δ_{ij} = Kronecker delta
ϵ = emissivity; strain
ζ = reduced frequency based on turbulence scale
θ = nondimensional joint thermal conductance; radiation incidence angle
μ = nondimensional mass parameter
ν = kinematic viscosity; Poisson's ratio
ρ = density
σ = stress; Stefan-Boltzman constant
ϕ = heat flux of radiation; Airy's stress function
ω = frequency

Subscripts

a = air; ambient
aw = adiabatic wall
e = equilibrium
F = flexible
h = bending
H = maximum level flight speed
0 = room temperature
R = rigid
s = stagnation
α = torsion

(3) Trends in the Form of the Vehicle and Its Environment

The evolution of the structural form of the airplane since the Wright biplane of 1903 is a familiar story. The Wrights' success inspired designers to adopt the trussed biplane and retain it, largely for structural reasons, for over 30 years. The biplane lift truss and Bleriot's tractor configuration merged to form the familiar airplane of World War I and the 1920's. The semimonocoque aluminum-alloy structure made its appearance in the early 1930's, and the past 25 years have been a period of refinement.

An airplane structure, like most engineering structures, sustains its loads by means of beams. There have been remarkable changes in the proportions of fuselage and wing beams during the period of refinement of the semimonocoque structure. It is worth taking notice of some of these changes.

Fig. 3-1 illustrates the average upward trend of fuselage slenderness of fighter and transport airplanes. Fuselage slenderness is defined as the ratio of fuselage length to maximum depth. We observe that the average fuselage beam is nearly twice as slender now as it was in 1920 and that, if these trends should continue, slenderness values of 10 to 15 will be common by 1965. It is interesting to notice that the current proportions of airplane fuselages and seagoing ship hulls are nearly the same.

Fig. 3-2 illustrates the average upward trend in wing slenderness—that is, the ratio of wing structural semispan to maximum thickness at the wing root. The term structural semispan denotes a distance measured along the beam axis of the wing. Wing beams in the principal bending direction have become very slender by structural engineering standards; a trend which has been responsible for the growing importance of aeroelasticity. We might infer from these trends that the wing slenderness of transports and fighters will approach values of 20 and 30, respectively, by 1965. It can be mentioned in contrast that civil engineering structures rarely exceed slenderness values of about 15.

Fig. 3-3 illustrates the trend of wing structural aspect ratio. Wing structural aspect ratio is defined as the ratio of the square of the structural span to the wing area. Here we observe that wing beams tended to higher aspect ratios—that is, to higher degrees of slenderness in the chordwise bending direction—until the advent of supersonic fighters, at which time a reversal in the trend appears. This reversal was evidently brought about largely for structural reasons, although the lessened importance of induced drag must certainly be a factor.

In addition to changes in outward appearance, it is interesting to take notice of corresponding trends in strength and stiffness. For example, although there has been a phenomenal increase in maximum speed, there have been no significant changes in design load factors. Fig. 3-4 portrays the average trend of fighter and transport ultimate positive load factors. High values were set for fighters in about 1930 based on human capabilities of withstanding accelerations, and there appears to be little change since that time. Transport ultimate load factors seem to be drifting slowly downward from a peak value of about 6 in 1925.

An exacting lesson learned by structural designers as speeds have increased is that structural stiffness and vibration frequencies must be considered as well as strength. Fig. 3-5 illustrates an interesting upward trend of the reduced velocity parameter, $U_H / b_{3/4}\omega_\alpha$ for fighter aircraft. Here we have plotted maximum level flight speed at sea level divided by the wing semichord at the three-quarter semispan and the frequency of the first torsion wing mode. Such a parameter has special significance to the flutter engineer. The trend also has a rather simple interpretation. It can be said that for aircraft of the same size, the maximum level flight speed has increased at a greater rate than the wing torsional frequency. Such a trend could mean one or both of the following: either flutter margins are being reduced in modern fighter aircraft or flutter design con-

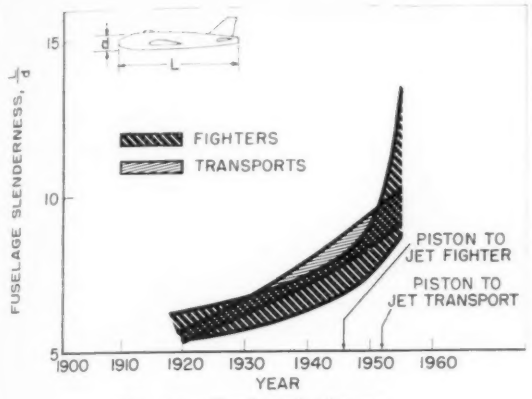

FIG. 3-1. Fuselage slenderness.

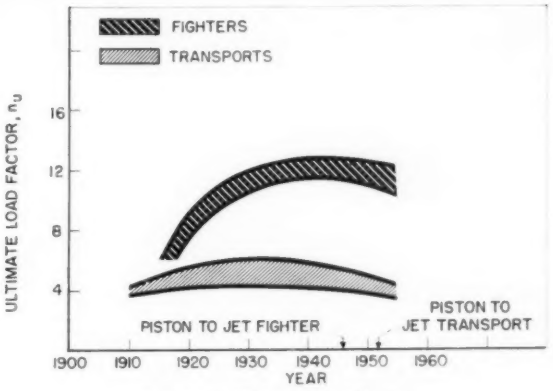

FIG. 3-4. Ultimate load factor.

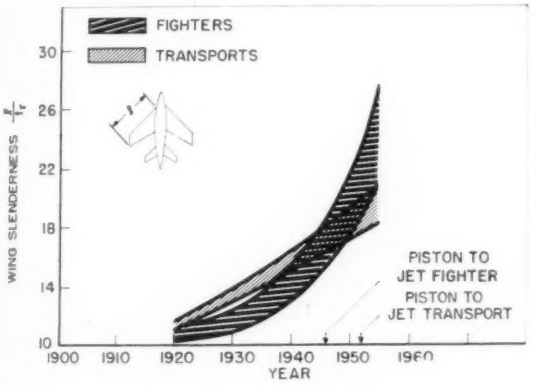

FIG. 3-2. Wing slenderness.

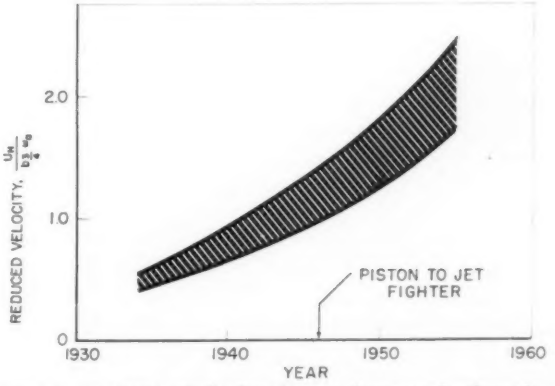

FIG. 3-5. Reduced velocity based on maximum sea-level speed—fighters.

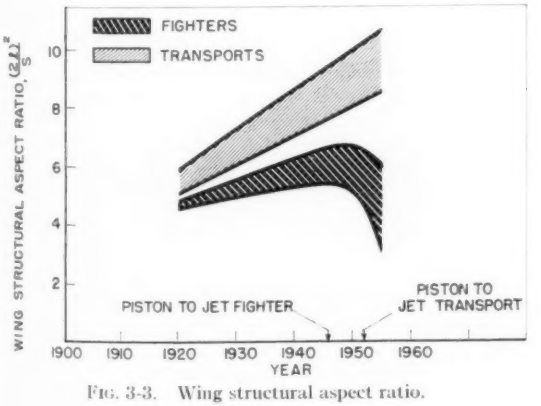

FIG. 3-3. Wing structural aspect ratio.

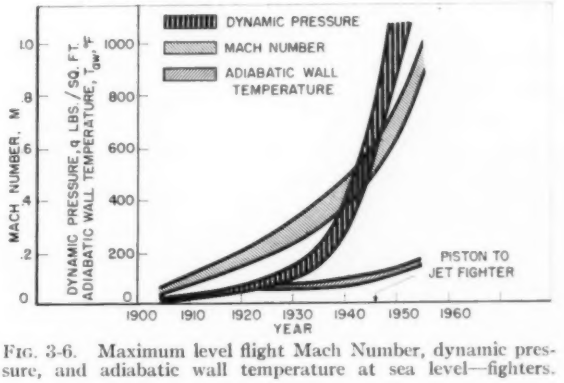

FIG. 3-6. Maximum level flight Mach Number, dynamic pressure, and adiabatic wall temperature at sea level—fighters.

ditions are being met by judicious arrangement of wing mass distribution rather than by increased torsional frequency. It is probable that there is an element of both.

It has been traditional to compare airplanes by their maximum sea-level speeds. Parameters of greater interest to structural engineers are Mach Number, dynamic pressure, and adiabatic wall temperature. Fig. 3-6 shows chronological trends in sea-level values of these parameters for fighters. Here we observe that there has been an extremely sharp rise since 1940 in dynamic pressure, and that aerodynamic heating, as reflected by adiabatic wall temperature, has reached the point where it can no longer be ignored. The adiabatic wall temperature is lower than the stagnation temperature, and it represents a theoretical upper limit of the temperature of the structure if steady flight is sustained and if radiation losses are neglected.

(4) Structural Analysis at Appreciable Supersonic Mach Numbers

The influence of increased dynamic pressure on the response and stability of a structure presents no new fundamental problems. It is true that it may be difficult to find accurate aerodynamic coefficients for a particular configuration and speed range, but the structural problems created by higher dynamic pressures have been solved successfully since 1903. Aerodynamic heating, however, poses new problems which are strangely different from those of the past.

In analyzing the behavior of a deformable body under the simultaneous action of heat and force inputs, the engineer is thrust into the borderland between elasticity and thermodynamics. Fortunately the coupling between the elastic deformation and the heat-transfer parts of the problem is weak and can usually be disregarded. The general problem of analyzing the behavior of an airplane structure functioning in the *elastic range* under the combined influence of aerodynamic pressures and aerodynamic heating can be referred to as an aerothermoelastic problem. It is generally possible to assume that this problem can be separated into an aerothermal problem and an aeroelastic problem. The aerothermal problem deals with thermal equilibrium and heat transfer between the structure and the boundary layer, including the effects of radiation. The aeroelastic problem, on the other hand, deals with equilibrium among the aerodynamic, elastic, and inertial forces.

This division into two separate uncoupled problems rests on two assumptions.

In the first place, thermodynamic coupling between the processes of heat-transfer and elastic deformation is assumed negligible. Justification for this assumption can be found in a memoir by Lord Kelvin[1] written in 1857 and in the later work of Willard Gibbs.[2] The work of these two men forms a foundation for the subject of thermoelasticity. It can be said that when heat and external forces are applied simultaneously to an elastic body, there is a change of internal energy. The latter is a function of the mean position of the molecules under the intermolecular forces and the kinetic energy of the molecules about their mean position. For a unit volume of an isotropic elastic body subject to combined load and heat inputs, the first law of thermodynamics requires that

$$\delta U = \delta Q + \sigma_{ij}\delta\epsilon_{ij} \qquad (i, j = 1, 2, 3) \qquad (4\text{-}1)$$

where δU is the increment in internal energy and δQ is the heat supplied, both in the time interval δt. The quantity $\sigma_{ij}\delta\epsilon_{ij}$* is the work done on the unit volume by the surrounding medium during the time δt. Stresses and strains in the three-dimensional elastic body are represented by σ_{ij} and ϵ_{ij}, respectively, and they are referred to an orthogonal axis system x_1, x_2, x_3. If the change of state is reversible and adiabatic, δQ vanishes, and the function U becomes a perfect differential of the stresses and strains.

$$\delta U = \sigma_{ij}\,\delta\epsilon_{ij} \qquad (4\text{-}2)$$

Thus it can be assumed that there exists a strain energy function, W, representing the potential energy per unit volume with the properties that

$$\sigma_{ij} = \partial W/\partial\epsilon_{ij} \qquad (4\text{-}3)$$

Variations in W, when the body is strained adiabatically, are identical with those of the internal energy. It can also be demonstrated that if the process is reversible and isothermal, the same conclusion is valid.[3] Thus the assumptions of reversible adiabatic or isothermal processes are implicit in the use of a strain energy function. Loads applied very rapidly represent nearly adiabatic conditions, and loads applied very slowly, isothermal conditions. The elastic constants in the function, W, are only slightly different for the two cases. For example, for steel in tension, Young's modulus for adiabatic stretching is only $^1/_2$ of 1 per cent larger than for isothermal stretching. When the second law of thermodynamics is introduced, there is obtained

$$T\delta S = \delta U - \sigma_{ij}\delta\epsilon_{ij} \qquad (4\text{-}4)$$

where the change in entropy during time δt is denoted by δS and T is the absolute temperature. Eq. (4-4) reduces by Gibbs' function and Maxwell's equations[2] to

$$T\delta S = c_\sigma\delta T + l_{ij}\delta\sigma_{ij} \qquad (4\text{-}5)$$

where

c_σ = specific heat per unit volume at constant stress
l_{ij} = latent heat of change of strain at constant stress

The influence of the loading on the temperature can be estimated from Eq. (4-5) by assuming a rapidly applied or nearly adiabatic loading.

$$\delta T = -(l_{ij}/c_\sigma)\delta\sigma_{ij} \qquad (4\text{-}6)$$

* The summation convention is employed so that the quantity $\sigma_{ij}\delta\epsilon_{ij}$ actually represents a sum of six terms.

In practical applications, the temperature change given by Eq. (4-6) for a given loading condition is negligibly small.

The second assumption required to separate the aerothermoelastic problem into separate uncoupled problems is that static and dynamic aerothermoelastic coupling is small. By small static aerothermoelastic coupling we mean that the total elastic deflections are too small to change the flow to the extent that the temperature distribution within the structure, and the thermal deflections due to that temperature distribution, are significantly altered. Small dynamic aerothermoelastic coupling implies that the characteristic times of the aerothermal system are long compared to the periods of the natural modes of the aeroelastic system. Except perhaps in very special cases, the second assumption would appear to be valid for manned aircraft of the near future.

The diagram of Fig. 4-1 represents a possible topical breakdown of the problems of air-frame structural analyses in the presence of elevated temperature. Interrelated topics are connected by lines in the diagram. The dominating influence of the internal temperature distribution on all phases of structural and aeroelastic analyses is apparent by tracing the connecting lines. The discussion of a large part of the subject matter which follows proceeds according to the division of topics in Fig. 4-1.

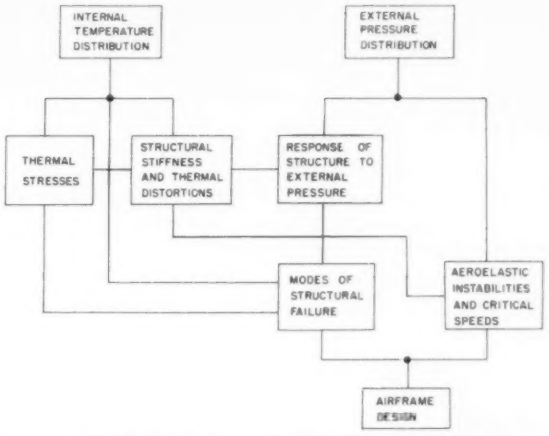

FIG. 4-1. Topical breakdown of the problem of air-frame structural analysis in the presence of elevated temperature.

(5) THE THERMAL ENVIRONMENT

Aircraft structural problems produced by an elevated temperature environment have always been present to some extent in the design of structural components in close proximity, for example, to power plants or to ice prevention systems. However, these problems, because of their localized nature, have been relatively minor compared to the more serious problems expected to be produced by aerodynamic heating.

(5.1) *Convective Heat Transfer from the Boundary Layer*

Since Osborne Reynolds first pointed out in 1874 the analogy between the processes of heat transfer and momentum transfer in a turbulent boundary layer, there has been much experimental and theoretical research on the subject of boundary-layer heat transfer. The resulting fund of knowledge forms a basis from which the thermal environment of high-speed flight can be determined with sufficient precision for purposes of structural analyses. Excellent summaries of results and methods applicable to structural studies are given, for example, by Eckert,[4] Davies and Monaghan,[5] and Bloom.[6]

If the process of velocity reduction in the boundary layer of an ideal gas is assumed to take place in a manner such that the elements of fluid in the boundary layer do not exchange heat with their surroundings, then the temperature at the solid boundary will be equal to the stagnation temperature, T_s, of the flow. This simple assumption is not normally satisfied since there is appreciable conduction away from the solid boundary within the boundary layer. Consequently, the actual temperature attained at the solid boundary is less than the stagnation temperature. If it is assumed that there is no heat flow across the interface between the solid boundary and the gas, the temperature at the solid boundary is called the equilibrium or adiabatic wall temperature, T_{aw}. It is related to the stagnation temperature, T_s, and the ambient temperature, T_a, by the temperature recovery factor, r, defined by

$$r = (T_{aw} - T_a)/(T_s - T_a) \tag{5-1}$$

The temperature recovery factor is primarily a function of the Prandtl Number, Pr. The form of the function depends on the laminar or turbulent nature of the flow. Values of recovery factor are given with sufficient accuracy by $r = (Pr)^{1/2}$ for laminar flow and $r = (Pr)^{1/3}$ for turbulent flow.

The adiabatic wall temperature may be computed by an expression of the form

$$T_{aw} = \left\{1 + r[(\gamma - 1)/2]M^2\right\} T_a \tag{5-2}$$

where M is the local Mach Number outside the boundary layer and γ is the ratio of specific heats. If it is assumed that M is the undisturbed free-stream Mach Number, an average adiabatic wall temperature may be computed at each Mach Number and altitude of an airplane in flight. In order to appreciate the order of magnitude of the quantities being discussed, we can conceive of a hypothetical fighter airplane of the near future—illustrated by the inset of Fig. 5-1—flying the mission profile—also shown by Fig. 5-1. It represents a climb at $M = 0.95$ to 35,000 ft. followed by a level flight full thrust dash to $M = 3.5$. After maintaining level flight at this Mach Number for 2 min., the throttle is closed, a turn is executed, and the airplane descends slowly to sea level. Fig. 5-2 illustrates the average adiabatic wall temperature based on a Prandtl Number of 0.72 and a recovery factor of 0.9, versus time, for this mission. A curve of adiabatic wall

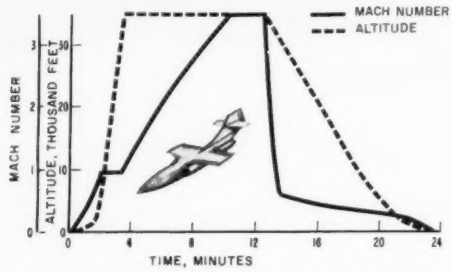

FIG. 5-1. Mission profile of hypothetical fighter.

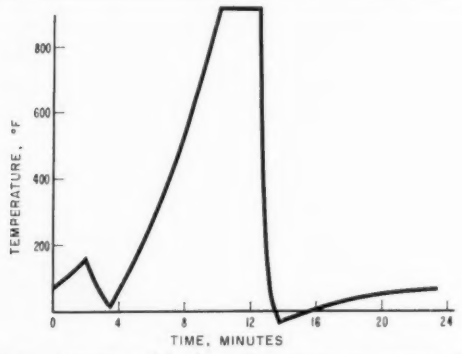

FIG. 5-2. Average adiabatic wall temperature versus time—hypothetical fighter.

temperature versus time serves as a starting point in estimating the actual temperature of the structure.

There is an appreciable exchange of heat between the gas and the solid boundary of an airplane in accelerated flight, and except for sustained periods of steady flight, the adiabatic wall temperature and the actual wall temperature are quite different. Newton's law of cooling can be employed as an approximate framework for computing the rate of heat transfer, q, from the boundary layer to an isothermal boundary with surface temperature, T_w.

$$q = h(T_{aw} - T_w) \tag{5-3}$$

where h is a heat-transfer coefficient. The boundary-layer heat transfer, h, is not a constant but a function of many variables. Experience has shown that reasonably accurate results are obtained for a restricted range of conditions, providing the heat-transfer coefficient, h, as defined by Eq. (5-3), is computed from empirical data measured within this range. Data are already available to define the heat-transfer coefficients of flat plates, cones, cylinders, and parabolic bodies of revolution with sufficient precision for engineering studies in the range of flight speeds likely to be attained by manned aircraft within the next few years. The magnitude of these coefficients depends upon the laminar or turbulent nature of the flow. For laminar boundary-layer flow over an isothermal semi-infinite flat plate, the following approximate formula for heat-transfer coefficient is useful.

$$h = 0.332k_a(U/\nu x)^{1/2}(Pr)^{1/3} \tag{5-4}$$

The interchange of energy is appreciably greater in the case of a turbulent boundary layer, and a corresponding approximate formula is

$$h = 0.0296k_a x^{-1/5}(U/\nu)^{4/5}(Pr)^{1/3}(T_a/T_w)^{0.44} \tag{5-5}$$

In the above formulas, k_a is the thermal conductivity of air, ν is the coefficient of kinetic viscosity of air, and U is the speed of flow. All fluid properties are local static properties evaluated at the outer edge of the boundary layer. In formula (5-4), x is measured from the leading edge of the plate, and in formula (5-5), it is measured from the effective transition point.

When the surface temperature is nonuniform over the plate, the simple "law" expressed by Eq. (5-3) is not strictly applicable since it defines the local heat transfer at a point solely in terms of conditions at that point. Actually, the heat transfer at a point on a non-isothermal surface depends not only on the local surface temperature but also on the distribution of surface temperatures upstream of the point. This phenomenon has been investigated for laminar boundary layer by Chapman and Rubesin,[7] Lighthill,[8] and others. A significant result of Lighthill's work is an approximate solution for a nonisothermal flat plate expressed in terms of a Stieltjes integral.[9]

$$q = -0.332\left(\frac{U}{\nu x}\right)^{1/2}(Pr)^{1/3}k_a\int_{\xi=0}^{\xi=x}\frac{d[T_w(\xi) - T_{aw}]}{[1 - (\xi/x)^{3/4}]^{1/3}} \tag{5-6}$$

It can be verified that Eq. (5-6) reduces to the combination of Eqs. (5-3) and (5-4) when T_w is constant.

The above formulas are based on steady flow, and certain conditions must be satisfied before they can be applied to unsteady flow problems. According to Moore,[10] if the quantities $(x^n/U^{n+1})(d^nU/dt^n)_{\text{laminar}}$, $n = 1, 2, 3, \ldots$, are small compared to unity, the laminar boundary layer can be assumed quasi-steady. These quantites are likely to be quite small for manned aircraft of the near future.[9]

The approximations and difficulties involved in applying results such as summarized above to a complex airplane structure are numerous. The principal difficulty to be mentioned is the prediction of the transition point. This is perhaps the weakest part of the aerodynamic theory, and, at the present time, estimates of transition points on three-dimensional bodies are little better than judicious guesses.[6] Because of the large difference between the heat-transfer coefficients of laminar and turbulent flow, the location of the transition point has a critical effect on the heat input and the severity of the resulting structural problems.

(5.2) *External Radiative Heat Transfer*

When thermal radiant energy impinges on the surface of an airplane, the heat flux, q, absorbed by the skin is defined by

$$q = \alpha\phi_r \cos\theta \tag{5-7}$$

where α is the absorptivity of the skin, ϕ_r is the radia-

tive flux per unit area of surface normal to the line of sight from the airplane to the radiating object, and θ is the angle of incidence between an outward normal to the surface and the incident rays. When the incident radiation is due to solar energy, the flux, ϕ_r, is approximately 440 B.t.u. per sq.ft. per hour above 50,000 ft. This is reduced to about 300 B.t.u. per sq.ft. per hour by the time the radiation reaches ground level on a relatively clear day. Atomic bombs are another source of thermal radiation applied to military aircraft. The luminous fireball of hot gases formed in an atomic explosion radiates thermal energy which propagates through the atmosphere at essentially the speed of light. Data on the direct radiative flux of nominal atomic bombs are given in reference 11.

For relatively high Mach Numbers and altitudes, heat loss by radiation becomes an important factor. The radiative heat flux emitted by a surface of emissivity, ϵ, and absolute wall temperature, T_w, is given by the Stefan-Boltzman law.

$$q = -\epsilon\sigma T_w^4 \tag{5-8}$$

where σ is the Stefan-Boltzman constant. Fig. 5-3, based on data published by Davies and Monaghan,[5] illustrates the influence of Mach Number and altitude on the ratio of equilibrium temperature to adiabatic wall temperature of a flat plate when radiation losses are taken into account. The equilibrium temperature is defined as the temperature attained by the plate after a sufficiently long period of heating such that the inward convective heat transfer from the boundary layer exactly balances the outward radiative heat transfer. The figure illustrates that radiation losses from the structure at high speeds and extreme altitudes can be an important factor in reducing temperature.

(5.3) *Relative Heat Inputs and Losses*

It is of value to compare the relative importance of the various heat inputs and losses for the hypothetical fighter mission of Fig. 5-1. The total heat input due to convective heat transfer from the boundary layer up to the time that the throttle is closed and the turn is executed (t = 12.5 min.) is approximately 1,000 B.t.u./sq.ft. The total radiation loss during this period is approximately 100 B.t.u./sq.ft. based on an emissivity of 0.4, and the solar radiation input is about 30 B.t.u./sq.ft. The total thermal energy absorbed by the airplane from a nominal atomic bomb may be of the order of magnitude of 30 B.t.u./sq.ft. based on an absorptivity of 0.4. However, the latter is applied in a period of less than 5 sec.[11] The maximum rate of convective heat transfer from the boundary layer during the accelerated portion of the mission is nearly 13,000 B.t.u./sq.ft./hr. The peak radiation loss rate is about 1,900 B.t.u./sq.ft./hr. The solar radiation rate of heat transfer is constant at about 160 B.t.u./sq.ft./hr., and the peak atomic bomb rate may approach 50,000 B.t.u./sq.ft./hr. Thus it is seen that, except for the special case of exposure to an atomic bomb, convective heat transfer from the boundary layer is the predominant factor in vehicles of the type that we are considering.

(6) Internal Temperature Distribution

The solution of the aerothermal problem—that is, the prediction of the temperature distribution within the structure—is complicated by the fact that there is coupling between the processes of heat transfer from the outside environment and heat transfer within the structure. The interacting effects are illustrated by the functional diagram of Fig. 6-1. The important elements of the diagram are the structure, the equivalent boundary layer, and the outer radiating surface of the structure. The processes of internal heat transfer are embodied in the structure and the processes of external heat transfer in the equivalent boundary layer and the outer radiating surface. The radiative and convective heat-transfer processes may either heat or cool the structure. If the radiative heat flux

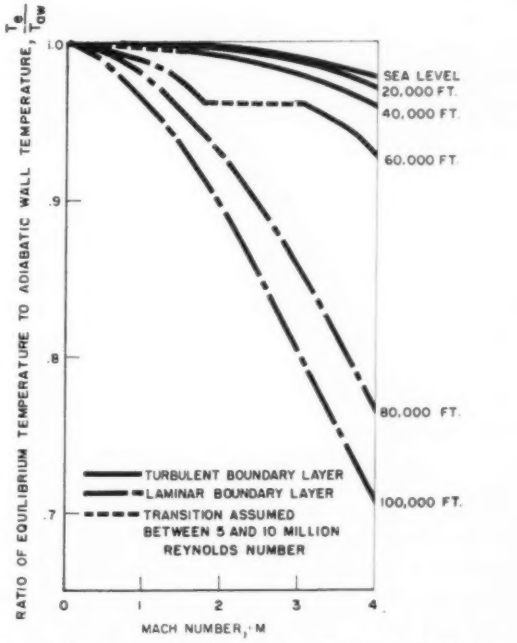

Fig. 5-3. Altitude and Mach Number effects on equilibrium temperature of a flat plate, emissivity = 0.5.

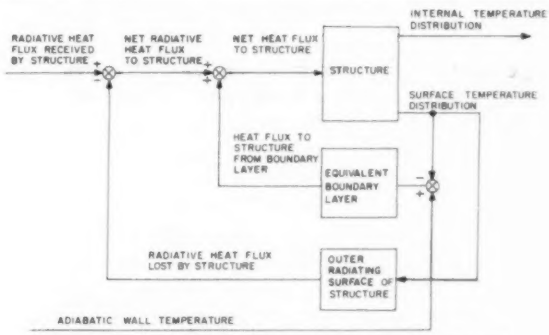
RADIATIVE HEAT FLUX RECEIVED BY STRUCTURE
NET RADIATIVE HEAT FLUX TO STRUCTURE
NET HEAT FLUX TO STRUCTURE
STRUCTURE
INTERNAL TEMPERATURE DISTRIBUTION
SURFACE TEMPERATURE DISTRIBUTION
HEAT FLUX TO STRUCTURE FROM BOUNDARY LAYER
EQUIVALENT BOUNDARY LAYER
RADIATIVE HEAT FLUX LOST BY STRUCTURE
OUTER RADIATING SURFACE OF STRUCTURE
ADIABATIC WALL TEMPERATURE

Fig. 6-1. Functional diagram of heat-transfer process.

lost exceeds that received, there is a net radiative cooling, and if the local surface temperature exceeds the local adiabatic wall temperature, there is net convective cooling.

(6.1) *Heat Transfer Within the Structure*

The internal heat-transfer processes may be conduction, radiation, and free convection. In the case of a solid structure, the heat-transfer process is entirely conduction. For the built-up structures of general interest today, conduction is of primary importance at the lower temperatures with radiation assuming a more important role as temperatures are increased.

(a) *Heat Transfer by Conduction*—The theory of heat transfer by conduction originated with Fourier[12] in 1822. Since that time, the theory has been extensively developed and the aeronautical engineer has at his disposal several comprehensive treatises on basic principles and methods of solution of heat conduction problems.[13] Excellent examples are the books by Jakob[14] and Carslaw and Jaeger.[15]

For a homogeneous isotropic solid with a distribution of temperature at time t given by $T(x_1,x_2,x_3,t)$, the partial differential equation of heat conduction in rectangular coordinates is

$$\partial/\partial x_i[k(\partial T/\partial x_i)] = c\rho(\partial T/\partial t) \qquad (i = 1,2,3) \quad (6\text{-}1)$$

where x_1, x_2, and x_3 are an orthogonal set of axes and k, c, and ρ are, respectively, the thermal conductivity, specific heat per unit mass, and density of the material. If the whole surface of the body is denoted by $S = S_1 + S_2 + S_3$, the boundary conditions may be mixed as follows:

S_1 = boundary where the temperature is prescribed, $T = T_0$
S_2 = insulated boundary, $k(\partial T/\partial n) = 0$
S_3 = boundaries where heat is transferred

$k(\partial T/\partial n) + q = 0$, n is an inwardly drawn normal to the body surface.

Elegant analytical methods of solution of the heat conduction equation have been devised. However, methods such as the Fourier transform, Duhamel's method, and Green's function[15] become almost inapplicable when the body shapes are complicated or when the thermal properties vary from point to point. Some problems yield to rigorous solution in terms of Fourier series, but in a practical case a prohibitively large number of terms must be taken.[16] Relaxation methods such as the one proposed by Emmons[17] can be used to obtain practical solutions for bodies with complicated forms and varying properties. Galerkin's method has been applied by Weiner[18] with some success. A variational principle for the transient heat conduction problem has been suggested by Washizu.[16] This principle, which is analogous to the variational principles of elasticity and dynamics, is applied by choosing modes of temperature distribution. Solutions of Eq. (6-1) for practical structures can usually be obtained by reducing the continuous system to a lumped parameter system. This is equivalent to applying the calculus of finite differences to the space variables.

(b) *Heat Transfer by Radiation*—Radiative heat transfer within a built-up structure depends in a complicated way upon the spectral emissivities of the materials and the geometry of the structure. When radiation emitted from one surface impinges on another, part penetrates into the surface and the rest is reflected in a specular or diffuse manner. The reflected radiation impinges on the original surface as well as other surfaces, and the process of reflection and absorption continues until equilibrium is attained. Radiative heat transfer is thus considerably more complex than conductive heat transfer, and methods of analysis have not yet been developed to the point where they can be used with ease in engineering studies. Assumptions of black and gray bodies, in which the emissivity and absorptivity are independent of wave length, can be used to give reasonable answers. In a recent National Bureau of Standards study, Goodman[19] reported that radiant heat-transfer rates between infinite parallel plates computed from the spectral emissivities were from 2 to 29 per cent higher than the corresponding rates computed from gray body assumptions over a wide range of temperatures and temperature differences.

(c) *Relative Importance of Modes of Internal Heat Transfer*—The relative importance of the various modes of heat transfer within a structure depends upon the temperature level, the materials, and the geometrical configuration. It seems likely that purely conductive heat transfer can be assumed for aluminum-alloy structures up to skin temperatures of about 600°F. However for other materials and higher temperatures, radiation becomes important.

In order to assess the error of assuming purely conductive heat transfer, a test was conducted in a radiant heating facility at M.I.T. A reasonable wing structural design was conceived for the hypothetical fighter of Fig. 5-1. The material chosen is titanium alloy RC-130A. A one-fourth titanium scale model of the six inner cells of the wing was constructed. Three of the cells were filled with insulation and the remainder were left open, as shown by the inset of Fig. 6-2. Heating rates, based upon conductive heat-transfer scaling laws, were applied symmetrically to the top and bottom of the beam to represent approximately the mission profile. Temperature responses in the insulated and uninsulated regions are illustrated by the figure. The skin temperatures in the two regions of the box are nearly the same within experimental error whereas the web temperatures differ considerably. From the standpoint of thermal stresses, the important aspect of Fig. 6-2 is the maximum temperature difference between skin and web. This difference is reduced approximately 30 per cent by the influence of radiation and free convection. It is interesting to observe that calculations assuming conductive and radia-

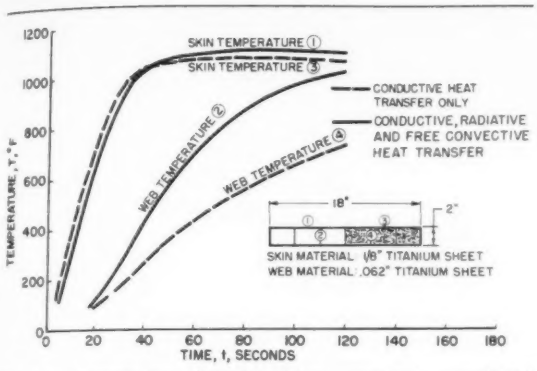

FIG. 6-2. Comparison of modes of heat transfer in a multicell titanium box beam.

tive heat transfer, neglecting convection, agree substantially with these results.

In terms of material properties, the ratio of radiative to conductive heat transfer is large for large values of ϵ/k, the ratio of coefficient of emissivity to coefficient of thermal conductivity. For a given configuration and temperature distribution, it can, therefore, be expected that the ratio of radiative to conductive heat transfer will be much higher for titanium and stainless steel than for aluminum.

(6.2) *Balance of External and Internal Heat Transfer for Thin Skins*

A vast simplification in analysis is obtained if it can be assumed that the skin is thermally thin—that is, there is no appreciable temperature difference across the thickness. For a thermally thin skin, the net heat flux, q, into a unit surface area is related to the space and time variations in skin temperature, T_w, by

$$q = c\rho\delta \frac{\partial T_w}{\partial t} - k \frac{\partial}{\partial x_i}\left(\delta \frac{\partial T_w}{\delta x_i}\right) \qquad (i = 1, 2) \qquad (6\text{-}2)$$

where δ is the skin thickness. A fundamental inconsistency arises when Eq. (6-2) is combined with Eq. (5-3), since the latter is based on the assumption of an isothermal surface. Estimates of the error in temperature distribution obtained by applying heat-transfer coefficients for laminar flow on isothermal surfaces to nonisothermal surfaces have been made by Chapman and Rubesin[7] and Bryson and Edwards.[9] Bryson and Edwards obtained closed form solutions for the equation obtained by substituting Eq. (5-6) into Eq. (6-2) and neglecting the conduction of heat along the skin. Comparison of these solutions with results of analyses based on heat-transfer coefficients for an isothermal surface indicates that the latter approximation leads to relatively little error in temperature distribution.

Assuming that sufficient precision can be obtained by applying isothermal heat-transfer coefficients, the net heat flux into a unit area of skin is given approximately by

$$q = h(T_{aw} - T_w) + \alpha\phi_r \cos\theta - \epsilon\sigma T_w^4 + \phi_i \qquad (6\text{-}3)$$

where ϕ_i is the flux from heat sources within the structure. The problem of balancing the external and internal heat transfer of thin skins is formulated by combining Eqs. (6-2) and (6-3). Numerical solutions to Eqs. (6-2) and (6-3) can be obtained by several of the methods mentioned previously. Reduction of the continuous system to a lumped parameter system by means of a finite difference approximation is a convenient approach in practical problems. Consider, for example, a segment of wing skin having uniform thickness and conductivity in which spanwise heat flow can be neglected. The first finite difference approximation of Eq. (6-2) for one-dimensional heat flow is

$$q_n = c\rho\delta \frac{\partial T_n}{\partial t} - \frac{k}{(\Delta x)^2}(T_{n-1} - 2T_n + T_{n+1}) \qquad (n = 1, 2, \ldots, N) \qquad (6\text{-}4)$$

This equation describes the heat transfer through N equal skin segments of length Δx. The temperature at the nth station is denoted by T_n. When n is given successive values, a set of N simultaneous ordinary differential equations is formed. Digital computing machines may be used to obtain solutions to Eqs. (6-3) and (6-4) when the independent variable, time, is also replaced by its finite difference form, as suggested by Jakob.[14] In order to test the validity of this approach for a simple box beam at moderate temperatures, Schmit and Williams[20] compared experiment with theory for a 2 by 5 in. 63 S-T5 extruded box beam subjected to radiant heating on one side ($q = \alpha\phi_r \cos\theta$). The Whirlwind I automatic digital computer at M.I.T. was used to solve the finite difference equations. The inset of Fig. 6-3 illustrates the 54 station grid used in the temperature distribution analysis. Spanwise heat flow was neglected. The chordwise variation of the absorbed radiant heat energy is illustrated at the top of the box. The calculated and experimentally observed temperature distributions are shown also in Fig. 6-3 for times of 5 and 10 sec. after sudden exposure. The agreement between experiment and theory is seen to be satisfactory in this simple case.

The experiment described above does not include the important effects of joints always present in a built-up structure. Joint thermal resistance in a built-up structure reduces the temperature gradients,

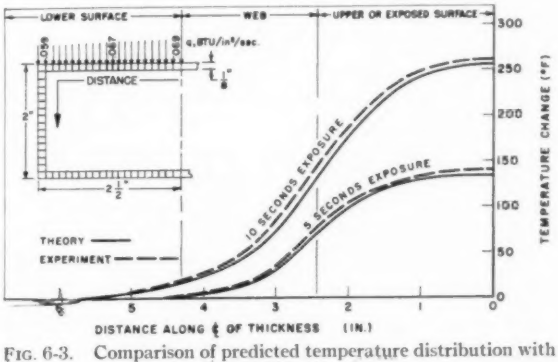

FIG. 6-3. Comparison of predicted temperature distribution with experiment.

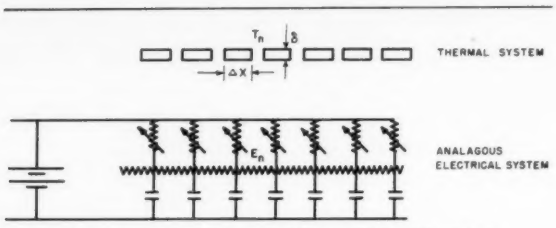

FIG. 6-4. Electrical analog for aerothermal system.

$\partial T/\partial x$, everywhere except at the joints and has a significant effect on temperature distribution which cannot usually be neglected. Experimental studies of joint heat-transfer coefficients have shown that they depend on such factors as assembly technique, temperature, and stress level. A test on the particular joint under consideration is the only reliable way of evaluating these factors.

General purpose analog computers or special analog devices can be employed to solve Eqs. (6-2) and (6-3). Ambrosio, Russell, and MacInnes[21] have demonstrated how to construct special purpose analog devices to solve aircraft structural problems. As an example, for the case of convective aerodynamic heating, $q = h(T_{aw} - T_w)$, Eqs. (6-4) may be represented by an electrical analog consisting of a simple *R-C* mesh, the elements of which are illustrated by the simplified diagram of Fig. 6-4.

(6.3) *Some Practical Aspects of Temperature Distribution Analyses*

A wide variety of simplifying assumptions may be permissible and necessary to obtain practical solutions of Eqs. (6-2) and (6-3). Neglect of radiation leads to a vastly simpler problem. Conduction along the outer skin can often be neglected except in regions of steep temperature gradients such as the leading and trailing edges of wings. It may frequently be possible to calculate outer skin temperatures by neglecting the internal structure and then using the temperature of the outer skin as a temperature boundary condition on the internal structure. Errors introduced by such simplifications can be evaluated only by comparing numerical solutions, one with another, and with experimental data.

An indication of the nature of the temperature time history and its distribution is given by Figs. 6-5 and 6-6 for the hypothetical fighter flying the mission profile of Fig. 5-1. These results are based on a turbulent boundary layer and on conductive heat-transfer calculations neglecting all aspects of radiation. Results are illustrated in Fig. 6-5 for two values of nondimensional joint conductance, θ. They represent extreme values of a range of joint conductances which might be obtained by varying design details in a titanium structure of the type considered here. The important influence of joint detail on temperature distribution is evident. The wing temperature distribution in Fig. 6-6 corresponds to the joint with the lowest nondimensional conductance, $\theta = 5$.

(7) LOADS AT HIGH SUPERSONIC SPEEDS

Any survey of structural problems should include at least a few remarks on the matter of loads. The important structural loads at high supersonic speeds can be classified in the usual manner into the categories of gust and maneuvering loads.

(7.1) *Loads Due to Atmospheric Turbulence*

Two points of view can be stated with respect to the structure of gusts and their resulting loads. The first is the concept of a discrete gust and the second is that of continuous atmospheric turbulence. The former has historical precedence and is firmly imbedded in structural design philosophy. The latter is a new and refreshing point of view, and, although design implications are somewhat vague, it is a useful supplement to the discrete gust concept.

(a) *The Discrete Gust*—Airplane response to discrete gusts of various shapes has been extensively studied at subsonic speeds.[22] The basic ingredients of such studies are the lift growth functions due to gust penetration and to sudden change in angle of attack.[23] The former defines the loads on the wing due to the gust and the latter the loads on the wing due to motion of the airplane in response to the gust. For incompressible flow, the Küssner function defines the lift growth for a sharp edge gust and the Wagner function the lift growth for a sudden change of angle of attack. Similar results are available for high subsonic and supersonic speeds. At the higher supersonic Mach

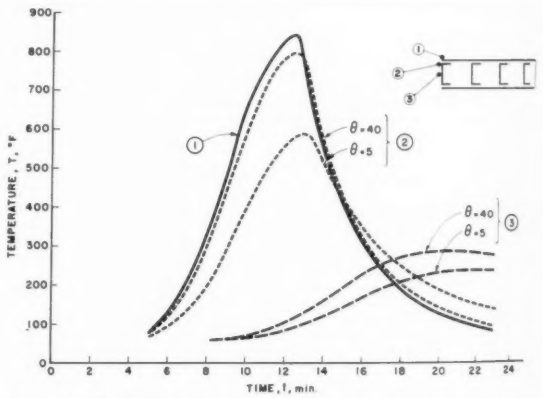

FIG. 6-5. Typical temperature-time histories in a wing section near root-hypothetical fighter.

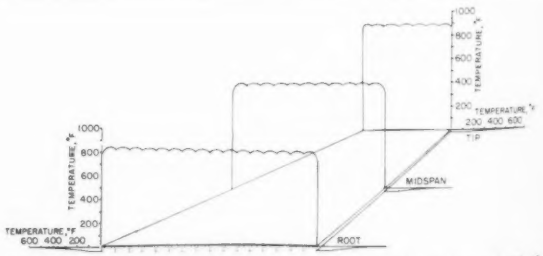

FIG. 6-6. Typical temperature distribution of the hypothetical fighter wing structure, $t = 12.5$ min.

Numbers, piston theory and its various improvements permit a vast simplification in the form of these functions and takes account of certain second-order effects neglected by linearized supersonic wing theory. It has been discussed in papers by Lighthill,[24] Miles,[25] and Landahl,[26] and applied to aeroelastic problems by Landahl, Mollø-Christensen, and Ashley,[27] and Zartarian, Heller, and Ashley.[28] Piston theory is valid for two-dimensional flow past slender bodies whenever any one of the conditions

$$M^2 \gg 1, \quad kM^2 \gg 1, \quad k^2M^2 \gg 1 \tag{7-1}$$

is fulfilled, k being the reduced frequency of unsteady motion based on the semichord. When two-dimensional flow is assumed, an especially simple point-function relation between pressure difference and normal velocity is derived, see reference 28, for the case of a thin airfoil with an initial angle of attack α_0, a symmetrical thickness distribution $2z_\delta(x)$, and a time dependent mean line (cf. Fig. 7-1).

$$\frac{\Delta p_a}{\Delta p_\infty} = -\left[2\gamma + \gamma(\gamma+1)\frac{v_\delta}{a_\infty} + \frac{\gamma(\gamma+1)}{2}\left(\frac{v_\delta}{a_\infty}\right)^2 + \frac{\gamma(\gamma+1)}{2}\left(\frac{U\alpha_0}{a_\infty}\right)^2\right]\frac{v_1}{a_\infty} \tag{7-2}$$

where

Δp_a = pressure difference, positive in z direction, Fig. 7-1
Δp_∞ = pressure in undisturbed medium
γ = $\rho a_\infty / p_\infty$ = ratio of specific heats, c_p/c_v
a_∞ = speed of sound in undisturbed medium
v_δ = $U(dz_\delta/dx)$
v_1 = $(\partial w/\partial t) + U(\partial w/\partial x)$
$w(x,t)$ = displacement of point on the wing surface

A parallel three-dimensional piston theory has been proposed by Landahl, Mollø-Christensen, and Ashley,[27] but the simple point-function relationship between pressure and normal velocity is lost. However, if the conditions, Eq. (7-1), are satisfied and the thickness ratio is not too small for the given Mach Number, it can be shown that Eq. (7-2) holds for all but the immediate tip region of three-dimensional wings.

For an airfoil of zero thickness, a lift growth function analogous to the Küssner function derives from Eq. (7-2) as follows:

$$\left.\begin{aligned}\Psi(s) &= s/2, \quad s \le 2\\ \Psi(s) &= 1(s), \quad s \ge 2\end{aligned}\right\} \tag{7-3}$$

where

$s = (2U/\bar{b})t$ = nondimensional distance travelled by the wing in half chords
$\bar{b}$ = mean semichord of wing

For a sudden change in angle of attack, the lift growth function analogous to the Wagner function, is simply

$$\Phi(s) = 1(s) \tag{7-4}$$

It can easily be verified that the above formulas are close approximations to exact results above Mach Numbers of approximately 2.5.

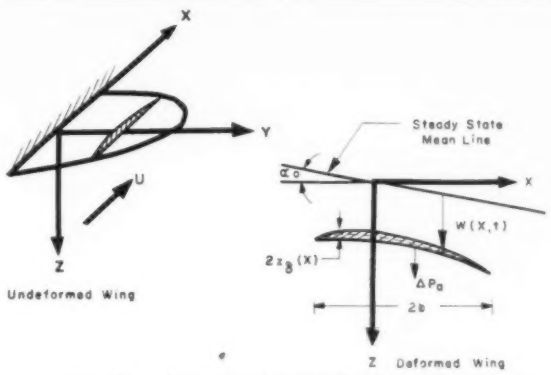

FIG. 7-1. Axis system for aeroelastic problems.

A completely general formulation of the equations of disturbed motion of an elastic airplane in flight involves consideration of a three-dimensional elastic body with six translational and rotational degrees of freedom, in addition to its many elastic degrees of freedom. A simpler mathematical model in which the structure is represented by an unrestrained elastic plate in the x-y plane is often adopted for aeroelastic studies. Assume that the airplane is permitted freedom in vertical translation, pitch, and roll. A disturbance pressure, $\Delta p^D(x,y,t)$, with arbitrary spatial and time dependence, is applied by the gust. As a result of the disturbed displacements, velocities, and accelerations, aerodynamic pressures denoted by $\Delta p^M(x,y,t)$ are brought into play. The equations of equilibrium are

$$\left.\begin{aligned}
&\iint_S \ddot{w}(x,y,t)\rho dxdy + \iint_S (\Delta p^D + \Delta p^M)dxdy = 0\\
&\iint_S \ddot{w}(x,y,t)\rho x dxdy + \iint_S (\Delta p^D + \Delta p^M)x dxdy = 0\\
&\iint_S \ddot{w}(x,y,t)\rho y dxdy + \iint_S (\Delta p^D + \Delta p^M)y dxdy = 0\\
&w(x,y,t) - w(0,0,t) - x\frac{\partial w(0,0,t)}{\partial x} - y\frac{\partial w(0,0,t)}{\partial y} + \iint_S C(x,y;\,\xi,\eta)[\Delta p^D(\xi,\eta,t) + \Delta p^M(\xi,\eta,t) + \rho(\xi,\eta)\ddot{w}(\xi,\eta,t)]d\xi d\eta = 0
\end{aligned}\right\} \tag{7-5}$$

In this system of equations, the unknown quantity, $w(x,y,t)$, represents the small disturbed displacement of the airplane from its original equilibrium configuration. The airplane mass density per unit area is denoted by $\rho(x,y)$, and the influence function corrected for loss of stiffness due to thermal effects is expressed by $C(x,y;\,\xi,\eta)$. The gust disturbance Δp^D is assumed to be defined with respect to both its space and time variations. The aerodynamic pressures, Δp^M, at high supersonic speeds are given explicitly by Eq. (7-2). Solutions of Eqs. (7-5) are usually accomplished by assuming that

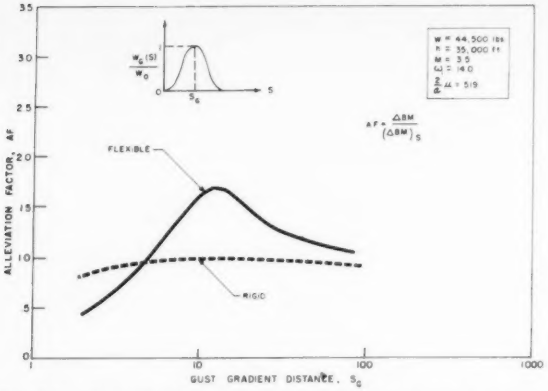

FIG. 7-2. Gust alleviation factor based on discrete gust approach.

the space configuration of the deformed structure, which is actually an infinite degree of freedom system, can be approximated by an equivalent system with a finite number of degrees of freedom. Once this initial step is taken, the equations are reduced to simultaneous ordinary differential equations with time the independent variable. It is well known that the elastic and inertial coupling can be eliminated if displacements of normal modes are chosen as degrees of freedom.

$$w(x,y,t) = \sum_{i=1}^{n} \phi_i(x,y)\xi_i(t) \tag{7-6}$$

where $\phi_i(x,y)$ are natural mode shapes of the unrestrained airplane and $\xi_i(t)$ are normal coordinates.

In order to illustrate gust response phenomena at appreciable supersonic speeds, we can eliminate for simplicity all freedoms except vertical translation and wing bending. It is convenient to express the solution of such a system in terms of a nondimensional quantity called the alleviation factor denoted by the symbol, AF, and defined by

$$\Delta BM = (AF)(\Delta BM)_s \tag{7-7}$$

where

ΔBM = actual maximum increment of wing root bending moment due to gust

$(\Delta BM)_s = (BM)_g \left[\frac{(\rho/2)Uw_0}{W/S}\frac{dC_L}{d\alpha}\right]$

$(BM)_g$ = wing root bending moment in lg flight

$\left[\frac{(\rho/2)Uw_0}{W/S}\frac{dC_L}{d\alpha}\right]$ = sharp-edge gust formula

If it is assumed that the hypothetical fighter encounters a one-minus-cosine gust at $M = 3.5$ and an altitude of 35,000 ft., we can obtain the results plotted in Fig. 7-2. For the case of a rigid airplane, Fig. 7-2 indicates that the alleviation factor is for all practical purposes equal to one over a wide range of gust gradient distance. On the other hand, if the wing is permitted freedom in its fundamental mode of vibration, the alleviation factor is critically dependent upon gust gradient distance with a peak value of nearly 1.7. The ratio of alleviation factors of the elastic to rigid airplane is called the dynamic overstress ratio. It would appear from this simple example that dynamic overstress ratios somewhat in excess of those ordinarily encountered in subsonic flight are possible in flight at appreciable supersonic speeds.

The three-dimensional envelope illustrated by Fig. 7-3 is useful in assessing the relative levels of gust loads at various speeds and altitude. It illustrates incremental gust load factors of the rigid hypothetical fighter based on a one-minus-cosine gust disturbance. A sea-level gust intensity of 50 ft./sec. is assumed with an appropriate reduction in altitude.[29] There is a significant reduction in peak gust load factor with increasing altitude. At the higher altitudes—above 40,000 ft.—increasing the Mach Number has little apparent effect on rigid airplane load factor. Care must be exercised, however, in drawing conclusions from results based on the assumption of a rigid airplane since we have seen from Fig. 7-2 that the influence of elasticity alters the stresses appreciably at high speeds and altitudes.

(b) *Continuous Atmospheric Turbulence*—The artificiality of the discrete gust as a basis for structural design has long been recognized. Since atmospheric turbulence is continuous and random in character, methods of classifying it should be of a statistical nature. One such method, the theory of generalized harmonic analysis, was developed by Wiener[30] and others in connection with communication theory. It has since been applied in studies of small scale turbulence of wind tunnels and in buffeting.[31] The principles of generalized harmonic analysis were applied first to atmospheric turbulence by Clementson[32] who derived a power spectrum of the atmosphere from flight measurements. When piston theory and the principles of generalized harmonic analysis are combined, relatively simple results are obtained. For example, the following explicit result for the mean square incremental root bending moment of a rigid airplane can be derived,

$$\overline{(\Delta BM)_R^2} = \left[\frac{(\Delta BM)_s}{w_0}\right]^2 \overline{w_G^2}\, I_R(\kappa,a) \tag{7-8}$$

where

$$I_R(\kappa,a) = \frac{1}{\pi\kappa^2}\int_0^\infty \frac{(1+3\zeta^2)\sin^2\kappa\zeta}{(1+\zeta^2)^2(a^2+\zeta^2)}\,d\zeta$$

$a = \dfrac{1}{\kappa(M/2)\mu}, \qquad \kappa = \dfrac{\bar{b}}{L}$

$\bar{b}$ = mean semichord of wing

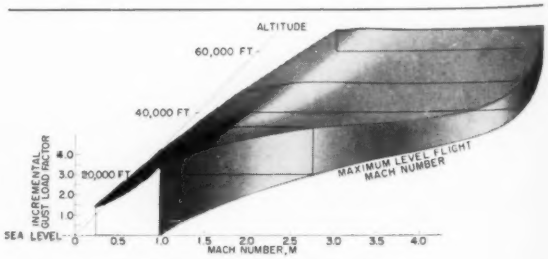

FIG. 7-3. Gust envelope.

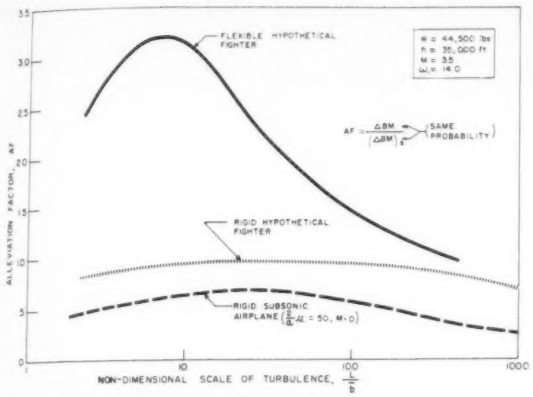

FIG. 7-4. Gust alleviation factor based on power spectrum approach.

M = Mach Number
μ = nondimensional mass parameter
L = integral scale of turbulence

The integral $I_R(\kappa,a)$ can be evaluated explicitly in closed form. If it is assumed that the probability distributions of ΔBM and w_G are of the same type, the rigid airplane alleviation factor at high supersonic speeds is given simply by

$$(AF)_R = \sqrt{I_R} \tag{7-9}$$

Fig. 7-4 illustrates a plot of Eq. (7-9) vs. nondimensional scale of turbulence for the hypothetical fighter at $M = 3.5$ and 35,000 ft. altitude. For purposes of comparison, there is plotted on the same figure an analogous curve due to Fung[33] for a typical subsonic airplane. The generally higher level of alleviation factors at supersonic speeds is evident. By comparing Figs. 7-2 and 7-4, it may be seen that there is no appreciable difference between rigid airplane alleviation factors computed by the discrete gust and the power spectrum approaches.

If it is assumed that the airplane is flexible with a single natural mode of vibration, and if the probability distribution of ΔBM and w_G are of the same type, the flexible airplane alleviation factor is given by

$$(AF)_F = \sqrt{I_F} \tag{7-10}$$

where

$$I_F = \frac{1}{\pi\kappa^2}\int_0^\infty \frac{(1+3\zeta^2)\,|H(\zeta)|^2 \sin^2 \kappa\zeta}{(1+\zeta^2)^2\zeta^2}\,d\zeta$$

$H(\zeta)$ = admittance function of flexible airplane due to unit sinusoidal gust

Eq. (7-10) is also plotted on Fig. 7-5 for the hypothetical fighter. The maximum dynamic overstress ratio of the flexible airplane computed by generalized harmonic analysis is somewhat higher than that computed by the discrete gust approach. When a scale of turbulence, L, of the order of 1,000 is selected, the two methods give results for dynamic overstress ratio which are of the same order of magnitude. It is not entirely clear which approach gives the better result, although some evidence obtained from flight tests at low subsonic speeds indicates that the power spectrum result may be closer to reality.

(7.2) *Maneuver Loads*

The maneuvering envelope of an airplane is defined by aerodynamic and performance limitations as well as strength capabilities. The latter are based on design criteria established by statistical analyses of flight test data. Fig. 7-5 may be used to illustrate these limitations and capabilities for a supersonic airplane. It represents a qualitative picture of the maneuvering envelope of the hypothetical fighter plotted on a load factor, Mach Number, and altitude axis system. The surface comprising the left-hand side of the diagram is defined by aerodynamic limitations—i.e., by maximum lift. In the vicinity of Mach Number 1, a buffeting trough extends parallel to the altitude axis. The form of this trough depends upon the transonic behavior of the airplane. The surface that forms the right-hand side is defined by strength capabilities. It has a downward slope to the right because of the influence of aerodynamic heating on strength. The vertical surface bounding the right-hand side of the figure is defined by either a performance or structural limitation. The latter can be a limiting temperature from material strength consideration or a limiting dynamic pressure. In Fig. 7-5 a limiting adiabatic wall temperature at 900°F. is used to define the right-hand boundary. If such an airplane had the performance capability to reach the right-hand boundary, it would be "flight restricted" for temperature.

(8) Structural and Aeroelastic Problems Introduced by High-Speed Flight

A number of entirely new structural and aeroelastic problems are introduced at high supersonic speeds as a result of the high temperature environment and the nature of the aerodynamic forces.

(8.1) *Deterioration in Mechanical Properties of Materials at Elevated Temperature*

The most obvious and by far the most important effect of elevated temperature is the deterioration in mechanical properties of materials. Fig. 8-1 illustrates

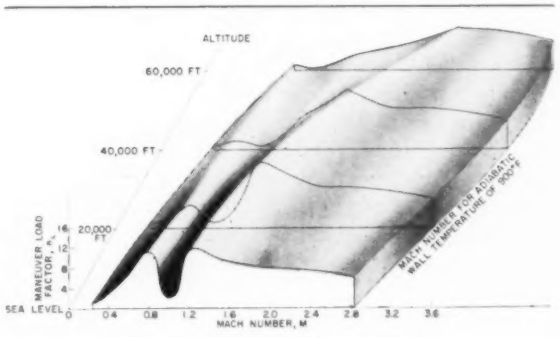

FIG. 7-5. Maneuvering envelope.

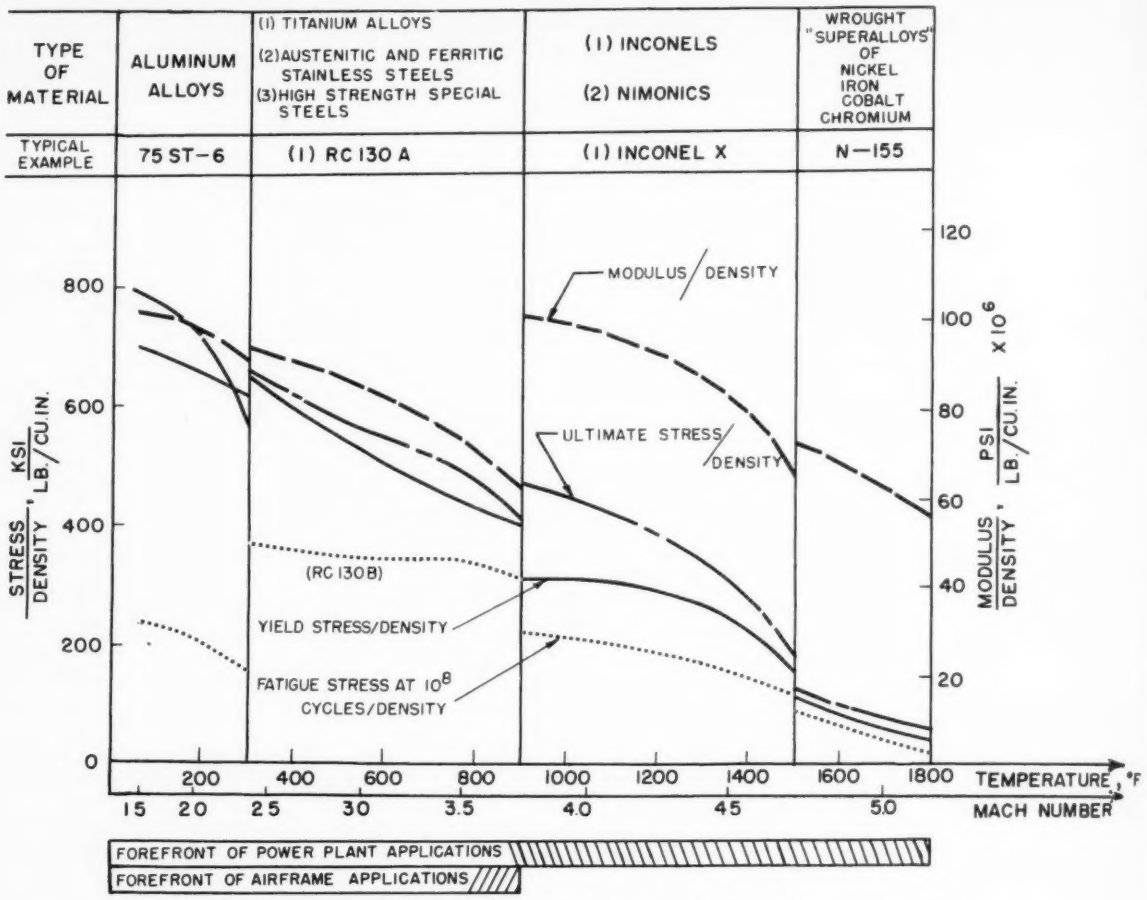

FIG. 8-1. Property variations with temperature of possible alloys for air-frame construction.

a chart of the approximate areas of applicability of four sheet alloys suitable for air-frame construction, together with typical property variations with temperature. The figure illustrates the sharp downward trend in ultimate and yield strength to density ratios with temperature of the four materials. It is interesting to observe that the downward trends in the modulus to density ratios and fatigue strength to density ratios are not nearly so sharp. These curves portend that short time static strength efficiencies of structures at elevated temperature will be rather low at high Mach Numbers compared with present standards.

(8.2) *Thermal Stresses*

Among other undesirable effects that result from an elevated temperature environment, we find thermal stresses. Thermal stresses arise in structures as a result of the fact that most engineering materials expand with increase of temperature. Temperature gradients within a structure produce different degrees of expansion in different parts of the structure. If the structure is statically indeterminate, there is resistance to this expansion, and a self-equilibrating stress system is formed.

(a) *Elastic Thermal Stress Theory*—The earliest contributor to the theory of thermal stresses was Duhamel[34] in 1838. Since Duhamel's original work, there have been numerous additions to the theory, and the aeronautical engineer may obtain statements of the fundamentals with applications from several sources—for example, reference 35.

A direct approach to thermal stress analysis is to employ the ordinary equations of elasticity with modified stress-strain relations.[35] Let the reference axis system be orthogonal and designated by x_1, x_2, x_3, with displacements represented by u_i and stresses and strains by σ_{ij} and ϵ_{ij}, respectively. The temperature above ambient is specified by $\Delta T(x_1,x_2,x_3)$ and the direction cosine between a line normal to a surface and the axis x_j is denoted by l_j. The appropriate equations for a homogeneous isotropic body read as follows:

$$\begin{aligned}
&\text{Equilibrium equations:} && \partial\sigma_{ij}/\partial x_j = 0 \\
&\text{Strain-displacement relations:} && \epsilon_{ij} = \frac{1}{2}\left(\frac{\partial u_i}{\partial x_j} + \frac{\partial u_j}{\partial x_i}\right) \\
&\text{Boundary conditions:} && \sigma_{ij} l_j = 0 \\
&\text{Stress-strain relations:} && \begin{cases} \epsilon = [(1-2\nu)/E]\sigma + \alpha\Delta T \\ \sigma_{ij}' = 2G\epsilon_{ij}' \end{cases}
\end{aligned} \tag{8-1}$$

where i and j go from 1 to 3. The stress-strain relations are divided into two parts. The first part repre-

sents a volume expansion or contraction where $\sigma = (1/3)\sigma_{ii}$ and $\epsilon = (1/3)\epsilon_{ii}$ are the mean stress and strain, respectively. The second part relates the deviatoric stresses and strains, or those stresses and strains which relate to distortions of the material rather than to volume changes. They are defined by $\sigma_{ij}' = \sigma_{ij} - \delta_{ij}\sigma$ and $\epsilon_{ij}' = \epsilon_{ij} - \delta_{ij}\epsilon$, where δ_{ij} is the Kronecker delta. Since thermal expansions and contractions do not distort the material, temperature does not appear in the second stress-strain relation. This system of equations may be solved in the usual manner of theory of elasticity to obtain stresses corresponding to a prescribed rise in temperature $\Delta T(x_1,x_2,x_3)$.

Another approach, which is based on the principle of superposition, expresses the problem in terms of the ordinary stress-strain relations with fictitious body and surface forces.[35] It is interesting to observe that this approach was described by Duhamel in his original paper,[34] and it represents probably the earliest application of superposition in stress analysis.

Energy theorems have always been useful tools in engineering stress analysis since they can often provide approximate solutions when other methods fail. Of the two principal energy theorems, the one relating to complementary energy has found wider application in thermal stress analysis. It may be stated that among all stress states satisfying the equations of equilibrium and the boundary conditions, the actual state of thermal stress—that is, the state which also satisfies compatibility—is the one which makes the complementary energy a minimum.[36] If we designate the complementary energy as U_c, then

$$\delta U_c = 0 \tag{8-2}$$

where

$$U_c = \int_V (U_0 + \alpha \Delta T \sigma_{ii}) dV, \qquad (i = 1, 2, 3)$$

Thus, the theorem of minimum complementary energy can be employed in its usual form, if, instead of the strain energy density, U_0, expressed in terms of stresses, we use a quantity derived from it by adding the term $\alpha \Delta T \sigma_{ii}$. For example, in the important case of plane stress, which applies to thermally thin sheets, the complementary energy in terms of Airy's stress function, ϕ, reads

$$U_c = \frac{1}{2E} \iint_S \left[\left(\frac{\partial^2 \phi}{\partial x_1^2} \right)^2 + \left(\frac{\partial^2 \phi}{\partial x_2^2} \right)^2 - 2\nu \left(\frac{\partial^2 \phi}{\partial x_1^2} \right) \times \left(\frac{\partial^2 \phi}{\partial x_2^2} \right) + 2(1 + \nu) \left(\frac{\partial^2 \phi}{\partial x_1 \partial x_2} \right)^2 + 2E\alpha \Delta T \left(\frac{\partial^2 \phi}{\partial x_1^2} + \frac{\partial^2 \phi}{\partial x_2^2} \right) \right] dx_1 dx_2 \tag{8-3}$$

where

$$\sigma_1 = \partial^2 \phi / \partial x_1^2$$
$$\sigma_2 = \partial^2 \phi / \partial x_2^2$$
$$\sigma_{12} = -(\partial^2 \phi / \partial x_1 \partial x_2)$$

Approximate solutions employing Eq. (8-3) can be obtained in the usual manner of Rayleigh-Ritz analyses by putting $\phi(x_1,x_2) = f(x_1)g(x_2)$ and assuming the form of either $f(x_1)$ or $g(x_2)$.

(b) *Applications of Elastic Thermal Stress Theory*—A simple illustration of interest to the aeronautical engineer is that of thermal stresses in slender beams. When the assumptions of elementary beam theory are introduced, the thermal normal stresses in a uniform beam with temperature rise, $\Delta T(x_1,x_3)$, over its cross-sectional area, A, and uniform spanwise temperature distribution, is[35]

$$\sigma = -E\alpha\Delta T + E \left[\frac{\int_A (E\alpha\Delta T) dA}{\int_A d(EA)} + \frac{x_1 \int_A (E\alpha\Delta T x_1) dA}{\int_A x_1^2 d(EA)} + \frac{x_3 \int_A (E\alpha\Delta T x_3) dA}{\int_A x_3^2 d(EA)} \right] \tag{8-4}$$

where x_1 and x_3 represent distances from the centroidal principal bending axes. Eq. (8-4) is valid only for cross sections remote from the ends and does not, in general, hold if the spanwise temperature distribution is nonuniform. It is analogous to the engineering flexure formula for externally applied bending moments and axial loads. If the distribution of $E\alpha\Delta T$ over the cross section is uniform or linear, the resulting thermal stresses are zero. The result of applying Eq. (8-4) to the extruded box previously introduced by Fig. 6-3 is illustrated by Fig. 8-2. The solid lines in Fig. 8-2 represent the normal stresses computed by Schmit and Williams[30] corresponding to the temperature distribution of Fig. 6-3. The computed results compare satisfactorily with the corresponding experimentally obtained dash lines on the same figure.

Formulas like Eq. (8-4) are referred to as primary stress formulas since they hold only in the absence of structural and temperature discontinuities. Stress perturbations introduced by such discontinuities are sometimes called secondary stresses. Discontinuities are, of course, always present in engineering structures. Structural discontinuities vary widely, and little of a general nature can be said about either their form or

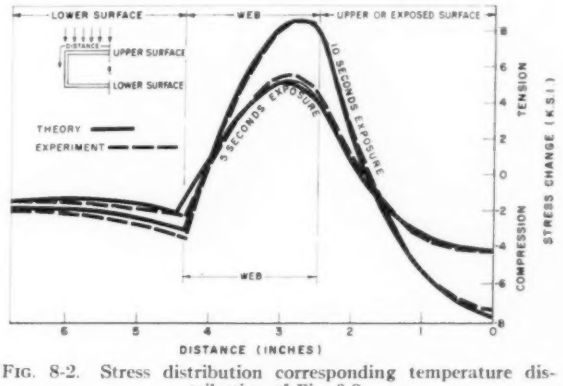

FIG. 8-2. Stress distribution corresponding temperature distribution of Fig. 6-3.

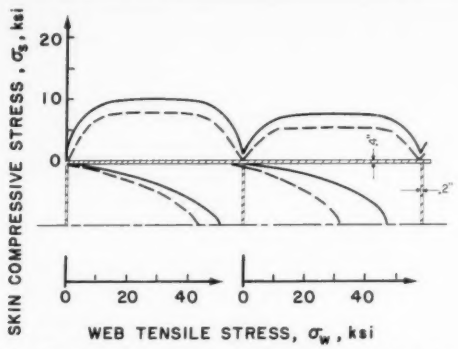

FIG. 8-3. Typical thermal stress distributions in wing structure —hypothetical fighter.

their effect on thermal stresses. Each case requires a separate investigation.

An indication of the magnitude and distribution of elastic thermal stresses due to aerodynamic heating is given by Fig. 8-3. This figure shows the elastic thermal stress distribution in the web and cover of the wing of the hypothetical fighter corresponding to the temperature distribution of Fig. 6-6. The solid lines are obtained from the temperature distribution based on internal conductive heat transfer only. The dash lines represent the estimated thermal stress distribution taking into account internal radiative as well as conductive heat transfer. Stress relief due to the influence of radiation appears to be a significant factor in this case. The web is almost entirely in tension and the cover skin almost entirely in compression at the particular instant of time selected for these calculations. Fig. 8-3 verifies previous statements by other authors—for example, Hoff[37]—that sizeable thermal stresses are possible in accelerated supersonic flight. The stress distribution illustrated by Fig. 8-3 is typical of that obtained when a shell structure is heated externally. The hot exposed cover tends to expand but is restrained by the relatively cooler webs. Thus compressive stresses are induced in the cover and tensile stresses in the webs. A reverse situation arises if the structure originally is hot and the cover suddenly is cooled. The latter corresponds to a sudden reduction in flight speed.

(c) *Inelastic Thermal Stress Theory*—When a material is said to behave elastically, it is meant that all deformation disappears with the removal of applied forces, and it is implied that there is a linear relation between components of stress and strain. This conception of material behavior is nearly correct for many materials at relatively low temperatures and stress levels. However, at higher temperatures and stress levels, the assumption of elasticity is often a poor approximation to real behavior, and the material is said to be inelastic. The fact that thermal stress systems are self-equilibrating makes them more sensitive to the inelastic properties of materials than are stress systems resulting from externally applied loads.

Formulation of a stress-strain law which can describe "in toto" the properties of an engineering material over a wide temperature and stress range would be a formidable task. Even if such a law could be formed, it would be much too cumbersome to be useful in the treatment of engineering problems. For this reason, rather simple laws must be employed which represent only those features essential to the particular problem under consideration. In assessing the influence of inelasticity on thermal stresses, the features of greatest importance are the elastic and creep properties of the material. These features are embodied in a simplified manner in the linear visco-elastic stress-strain relations. Such stress-strain relations, and the idea of representing materials by analogous mechanical models consisting of springs and dampers, originated with Maxwell.[38] A tension test of a material at a specified temperature can be visualized in which a constant stress, σ, is applied from time $t = 0$ to $t = t_1$ and then removed. An idealization of the time history of strain is portrayed by the solid line in Fig. 8-4. The portion O-A of the curve represents the elastic deformation that results when the stress is applied. Curve A-B represents the primary creep deformation which proceeds at a variable strain rate. Line B-C is secondary creep at constant strain rate. When the stress is removed at t_1, there is immediate recovery of the elastic deformation along C-D, followed by partial recovery of deformation along D-E. The features of the elastic-creep behavior portrayed by the solid line in Fig. 8-4 can be approximated in varying degrees by mechanical models consisting of springs and dash-pots. For example, when the step function in stress is applied to a dash-pot and spring in series (Maxwell model), the result obtained is illustrated by the dash line in Fig. 8-4. When the step function is applied to a dash-pot and spring in parallel (Kelvin model), the dotted line response is obtained. Finally if the Maxwell and Kelvin models are put in series (Maxwell-Kelvin model), the solid line is obtained.

In general, the following relation between stress and strain for visco-elastic models can be stated:

$$\mathcal{P}[\sigma] = 2\mathcal{Q}[\epsilon] \tag{8-5}$$

where σ is the total stress and ϵ is the total strain. $\mathcal{P}$ and $\mathcal{Q}$ are linear differential operators. For the Maxwell-Kelvin model they are

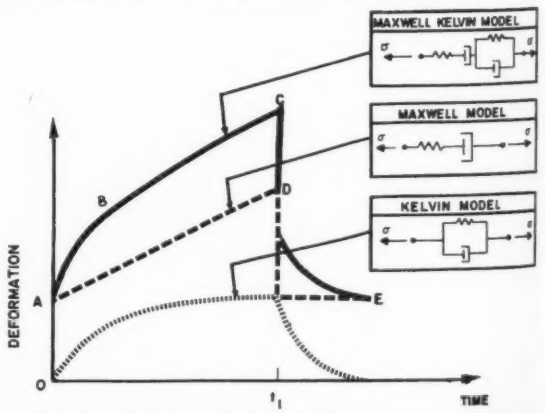

FIG. 8-4. Response of visco-elastic models to step input.

$$\mathcal{P} = \frac{\partial^2}{\partial t^2} + \left(\frac{1}{\tau_1} + \frac{1}{\tau_2}\right)\frac{\partial}{\partial t} + \frac{1}{\tau_1 \tau_2} \tag{8-6}$$

$$\mathcal{Q} = \frac{E}{2}\left(\frac{\partial^2}{\partial t^2} + \frac{1}{\tau_3}\frac{\partial}{\partial t}\right) \tag{8-7}$$

where E is an effective modulus of elasticity and τ_1, τ_2, and τ_3 are characteristic times defining the relaxation and retardation properties of the material.[39] These four constants can be adjusted to fit the creep data for a given material at a specified temperature and stress.

In applying a visco-elastic model to thermal stress problems involving multiaxial stress systems, stress-strain relations must be formed which include the differential operators $\mathcal{P}$ and $\mathcal{Q}$. Experiments involving purely hydrostatic states of stress indicate that, for all practical temperature and stress levels, the behavior of engineering materials is essentially elastic. The creep law is therefore applied to the deviatoric stress-strain relation. The pertinent stress-strain relations are

$$\epsilon = [(1 - 2\nu)/E]\sigma + \alpha \Delta T \tag{8-8}$$

$$\mathcal{P}[\sigma_{ij}'] = 2\mathcal{Q}[\epsilon_{ij}'] \tag{8-9}$$

A theory of thermal stresses with visco-elastic creep is thus obtained by replacing the stress-strain relations in Eqs. (8-1) by those stated above. Serious complications arise in applying such a theory to engineering structures. The relaxation and retardation times of aircraft structural materials are functions of both temperature and stress. As a result, the relation between stress and strain and their time derivatives is nonlinear, and the linear visco-elastic stress-strain relations are not strictly applicable. They may, however, be applied in an incremental process in which the assumption of linearity is made over a small interval of temperature and stress. Hoff[40] has suggested an elastic analog for nonlinear creep and has shown how it can be applied to solutions of practical structures. This approach has the advantage of having a more general law which covers all levels of stress.

The result to be expected when creep effects are included in a thermal stress analysis of the hypothetical fighter during one cycle of its mission is a reduction of peak thermal stress and the formation of a residual thermal stress of opposite sign. However, for the particular structural configuration selected for the hypothetical fighter, the thermal stresses are so low (10 per cent of room temperature F_{tu}) that there is no detectable creep during the time of the mission of Fig. 5-1, and hence no readjustment of the elastic thermal stress distribution. This was verified by a creep test of the wing material. If it is assumed that the wing geometry is altered so that the peak elastic thermal stress in the cover is 30 per cent of room temperature F_{tu}, a simplified visco-elastic thermal stress analysis of the wing structure indicates that the peak thermal stress is reduced by about 5 per cent. Such a high thermal stress would be excessive for other structural reasons. In general, it can probably be concluded that readjustment of elastic thermal stresses due to creep effects will be a minor factor in a vehicle such as the hypothetical fighter.

(8.3) *Stiffness and Vibration Properties of Shell Structures at Elevated Temperatures*

Another undesirable effect of elevated temperature is that of reducing structural stiffness and vibration frequencies. Two phenomena are involved. The first is the reduction in Young's modulus, previously mentioned. All heated structural components are affected by this reduction. For example, Fig. 8-5 illustrates the effect of soaking at elevated temperature on chordwise bending frequencies of a multiweb titanium box beam. The plotted points denote experimental values of the ratio of elevated temperature to room temperature frequencies. They can be compared with the solid line, which represents the square root of the ratio of elevated to room temperature values of Young's modulus.

A second phenomenon is a reduction in stiffness due to thermal stresses. It is well known that the presence of thermal stresses in a structural element, such as a plate, can produce buckling. It is logical, therefore, to expect that a change of stiffness may also result from thermal stresses in certain cases. Loss of stiffness in the presence of thermal stresses can be investigated analytically by the principle of virtual work,[35] which can be stated as follows: If a body is in equilibrium under the action of prescribed forces, the virtual work performed by these forces in a small additional displacement compatible with the geometric constraints (virtual displacement) is equal to the change in strain energy. A mathematical statement is

$$\delta \int_V U_0 dV = \delta \int_V (X_1 u_1 + X_2 u_2 + X_3 u_3) dV + \delta \int_S (\bar{X}_1 u_1 + \bar{X}_2 u_2 + \bar{X}_3 u_3) dS \tag{8-10}$$

where U_0 is the strain energy density expressed in terms of strains, X_i are the body forces per unit volume, $\bar{X}_i$ are surface tractions per unit area, and u_i are displacements along the x_i axes.

In the case of a shell beam, there is no significant effect of thermal stresses on bending stiffness, unless thermal buckling of the outer cover takes place. However, there may be a reduction of torsional stiffness, even in the absence of thermal buckling, for certain chordwise variations of thermal stress.[41] For example, consider a uniform shell beam with self-equilibrating axial thermal stresses $\sigma_2(x_1,x_3)$, as shown by Fig. 8-6. We apply a dummy torque, T, as a means of testing the torsional stiffness. Assuming that the St. Venant torsion theory applies—so that $\partial\sigma_2/\partial x_2 = 0$ and $\partial v/\partial x_2 = 0$, where v is the warping deformation—we obtain from Eq. (8-10) for a unit length of beam,

$$\delta\left[\frac{GJ_0}{2}\left(\frac{d\theta}{dx_2}\right)^2+\frac{1}{2}\left(\frac{d\theta}{dx_2}\right)^2\times\right.$$
$$\left.\iint_A \bar{\sigma}_2(x_1^2+x_3^2)dx_1dx_3\right]=\delta\left(T\frac{d\theta}{dx_2}\right) \quad (8\text{-}11)$$

From Eq. (8-11) the result is obtained that the ratio of effective torsional stiffness, GJ, to torsional stiffness without thermal stress, GJ_0, is

$$\frac{GJ}{GJ_0}=1+\frac{1}{GJ_0}\iint_A \bar{\sigma}_2(x_1^2+x_3^2)dx_1dx_3 \quad (8\text{-}12)$$

The sign and magnitude of the corrective term in Eq. (8-12) depends upon the wing cross-sectional shape and its temperature and thermal stress distributions. For a rectangular box with uniform chordwise distribution of skin temperature, the corrective term is small. If it is assumed that the hypothetical fighter wing beam has essentially the rectangular shape shown by the upper right inset in Fig. 8-7, the reduction in torsional stiffness with time in the mission (including reduction in G) is illustrated by the solid curve. On the other hand, if the leading- and trailing-edge sections of the wing are part of the spanwise load carrying box—as illustrated by the lower left inset in Fig. 8-7—the reduction in torsional stiffness is more pronounced—as illustrated by the dash curve.

The bending stiffness and frequencies of a thermally thin flat plate are influenced by self-equilibrating mid-plane thermal stresses. The inset of Fig. 8-8 illustrates a thin flat plate attached to stiffeners with a thermal stress distribution $\bar{\sigma}_{11}$, $\bar{\sigma}_{22}$, and $\bar{\sigma}_{12}$. The plate is subjected to a lateral pressure, p, and is vibrating at a natural frequency, ω. The appropriate virtual work expression, derived from Eq. (8-10), reads

$$\delta\left[\iint_S U_0dx_1dx_2+\frac{t}{4}\iint_S \bar{\sigma}_{ij}\left(\frac{\partial u_i}{\partial x_j}+\frac{\partial u_j}{\partial x_i}+\right.\right.$$
$$\left.\left.\frac{\partial u_3}{\partial x_i}+\frac{\partial u_3}{\partial x_j}\right)dx_1dx_2\right]=\delta\left[\rho\omega^2\iint_S u_3^2dx_1dx_2+\right.$$
$$\left.\iint_S pu_3dx_1dx_2\right] \qquad (i,j=1,2) \quad (8\text{-}13)$$

where

U_0 = strain energy per unit area of plate due to lateral deformation (cf. reference 42, p. 391)
ρ = mass per unit area of plate
t = plate thickness

The first integral represents the total strain energy in the plate due to lateral deformation. In general, this expression includes both the strain energy of stretching of the mid-plane and the strain energy of bending. The second integral represents the strain energy due to mid-plane thermal stresses. The third and fourth integrals represent the contributions of the inertial forces and the applied pressures, respectively.

The conditions for thermal buckling and the influence of thermal stresses on stiffness and natural frequencies can be derived from Eq. (8-13). For example, the deformation properties of a thin high aspect ratio plate with nonyielding supports varies with $\Delta T/\Delta T_{cr}$ as shown by Fig. 8-8. ΔT is the actual increase in plate temperature, and ΔT_{cr} is the increase in plate temperature required to produce thermal buckling. p is the value of the normal pressure on the plate, and dp/du_3 is the normal pressure per unit deflection of the mid-point. Stretching of the mid-plane of the plate has been included in the calculations upon which Fig. 8-8 is based. This feature of the theory brings out the fact that the effective plate stiffness increases after thermal buckling occurs and that it is markedly affected by the level of normal pressure on the plate.

When the thermal buckling mode and the fundamental vibration mode of the plate can be assumed identical, the reduction in plate frequency, ω, assuming small amplitudes of vibration is given by

$$\frac{\omega}{\omega_0}=\sqrt{\frac{E}{E_0}}\sqrt{1-\frac{\Delta T}{\Delta T_{cr}}} \quad (8\text{-}14)$$

where

ω_0 = frequency of the plate at room temperature
E/E_0 = ratio of modulus of elasticity of the plate at elevated temperature to that at room temperature

The result given by Eq. (8-14) is valid only for small values of $\Delta T/\Delta T_{cr}$.

(8.4) *Aeroelastic Instabilities and Critical Speeds*

The reduction in structural stiffness and frequencies produced by the deterioration of Young's modulus and the presence of thermal stresses has a primary effect on all aeroelastic behavior. This effect can usually be evaluated by introducing appropriate stiffness properties in the existing aeroelastic theories. There are also complicating aerodynamic features at the higher supersonic speeds. It has been demonstrated that there are many cases where linearized supersonic aerodynamic theory is unsatisfactory. Piston theory, and its various improvements, appear to be meeting the new requirements, at least up to the hypersonic speed range, where no longer $M\delta \ll 1$. (δ = thickness ratio or angle of attack.)

(a) *Flutter*—Lifting surface flutter, analogous to the bending-torsion flutter of slender wings, is a distinct possibility which cannot be ignored at high supersonic Mach Numbers. Two new factors must be taken into consideration. They are the influence of wing thickness and angle of attack on aerodynamic forces and the influence of aerodynamic heating on structural stiffness. The possibility of aerothermoelastic coupling in the flutter problem is remote since the thermal transient times are long compared to the natural periods of the lifting surface.

A flutter analysis of an unrestrained elastic surface can be expressed in terms of the homogeneous form of the equilibrium Eqs. (7-5). That is, the form obtained

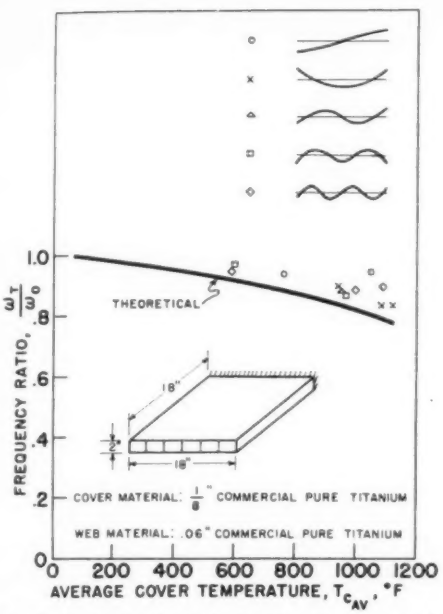

FIG. 8-5. Reduction in chordwise bending frequencies with temperature.

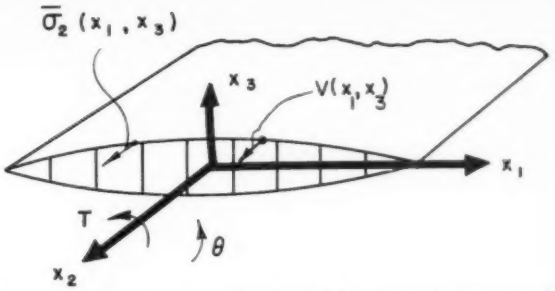

FIG. 8-6. Beam cross section loaded by thermal stresses and external torque.

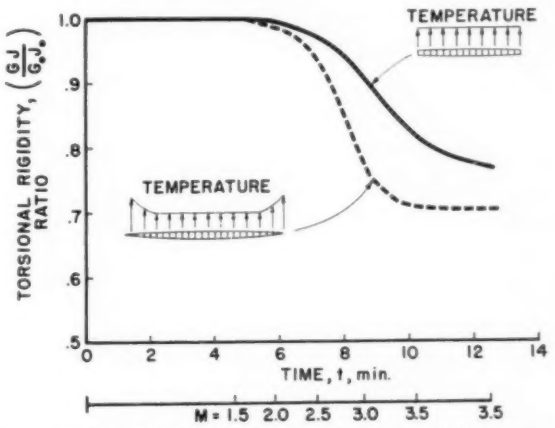

FIG. 8-7. Loss in torsional stiffness for two types of wing beams.

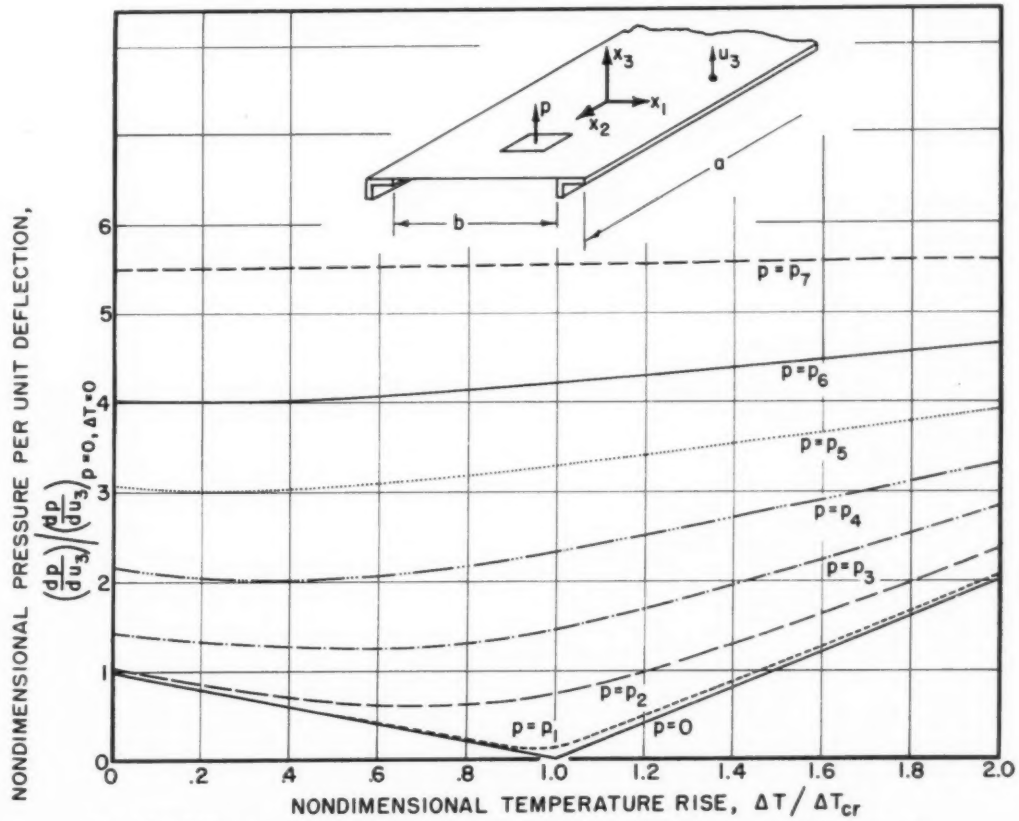

FIG. 8-8. Stiffness properties of high aspect ratio simply supported plate on nonyielding supports.

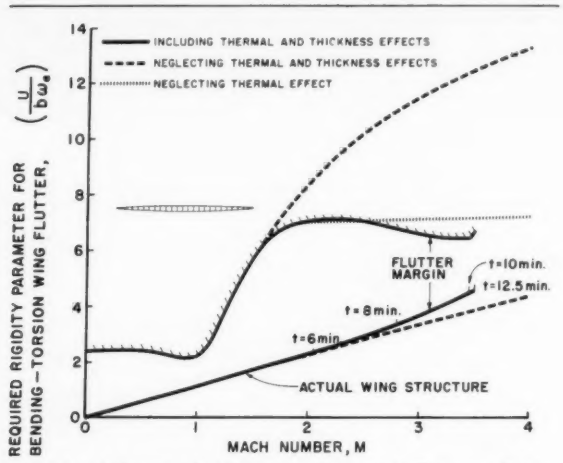

FIG. 8-9. Influence of thickness and thermal effects on flutter margin.

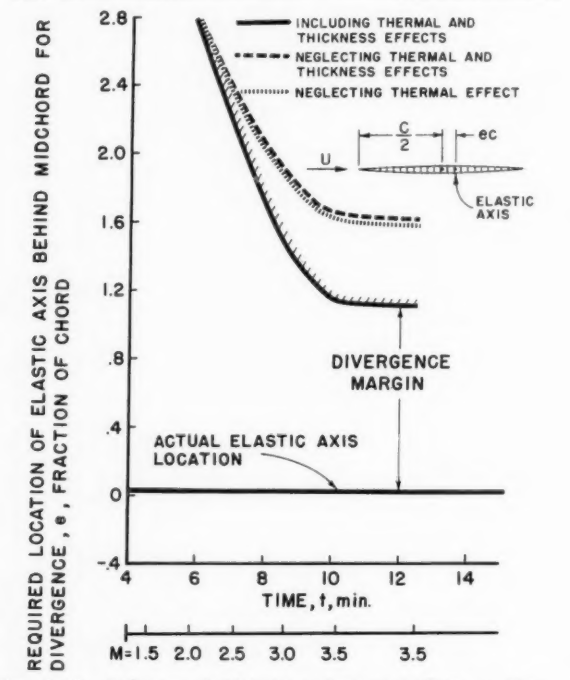

FIG. 8-10. Influence of thickness and thermal effects on divergence margin.

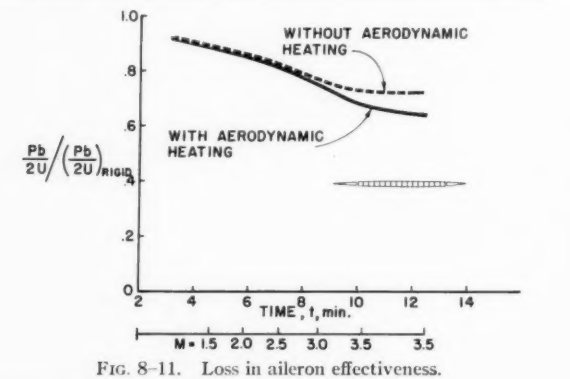

FIG. 8-11. Loss in aileron effectiveness.

when Δp^D is put equal to zero. The flutter speed and flutter frequency are defined respectively as the lowest air-speed and the corresponding circular frequency at which the structure will exhibit sustained simple harmonic oscillations.

$$\omega(x,y,t) = \bar{w}(x,y)e^{i\omega t} \tag{8-15}$$

An additional equation relating the aerodynamic loading and the deformation is required. It can be expressed symbolically by

$$i\omega\bar{w} + U\frac{\partial\bar{w}}{\partial x} = \frac{1}{4\pi\rho}\iint_S \Delta p_a(\xi,\eta)K(x,y;\,\xi,\eta)d\xi d\eta \tag{8-16}$$

or by the inverted form of this expression which can be readily obtained by supersonic linearized theory. In Eq. (8-16), $K(x,y;\,\xi,\eta)$ or its inverse is an aerodynamic influence function, usually of very complicated form.[23] The problem generated when Eqs. (7-5), (8-15), and (8-16) are combined is a difficult one, and methods of obtaining approximate numerical solutions have been the subject of a large part of the theoretical research on supersonic flutter. For example, the method of supersonic influence coefficients[13] is the most recent numerical technique developed for this purpose. At the higher Mach Numbers, piston theory permits a vast simplification in the form of Eq. (8-16) and takes account of second-order effects neglected by linearized supersonic wing theory. Eqs. (7-2), (7-5), and (8-15) can be combined to yield a remarkably simple flutter theory valid above Mach Numbers of approximately 2.5.

Fig. 8-9 illustrates the calculated influence of wing thickness and thermal effects on the bending-torsion flutter margin of the wing of the hypothetical fighter flying its assigned mission. The figure indicates that, if these effects are neglected, a minimum flutter margin exists near $M = 1$, and the margin widens thereafter. This is the basis for the belief that a lifting surface which is satisfactory from the standpoint of transonic flutter will be satisfactory at higher speeds. However, the combined thickness and thermal effects narrow the margin at high supersonic speeds. The upper line, representing the flutter boundary, is lowered by thickness effects and by the increase in ratio of bending to torsional frequency, which results from thermal effects. The lower line, which is a plot of actual reduced flight speed, $U/b\omega\alpha$, vs. M at 35,000 ft., is raised because of the reduction in torsional frequency with Mach Number.

Control surface and skin panel flutter must also be considered as possibilities at appreciable supersonic speeds. The former is influenced by thickness and thermal effects in a manner similar to that of bending-torsion flutter. In addition, the impedance properties of both open and closed loop control systems must be mentioned as having an influence on control surface flutter. These properties may also be affected by an elevated temperature environment.

Panel flutter is apparently possible at supersonic speeds, and it is believed to have been observed on V-2 rockets as well as in the wind tunnel. Panel flutter theory is in a state of transition and uncertainty at the present time. One theoretical result which seems to be established is that linearized aerodynamic theory and small deflection plate theory, when combined, indicate that flutter of unbuckled panels cannot occur at high supersonic Mach Numbers.[44] It must therefore be concluded that if panel flutter does in fact exist at high supersonic Mach Numbers, factors beyond those included in the ordinary linearized flutter theory are responsible.

(b) *Static Aeroelastic Phenomena*—All of the common static aeroelastic phenomena exist at high supersonic Mach Numbers and, like flutter, they are influenced by the factors of wing thickness, initial angle of attack, and aerodynamic heating.

(i) *Static aeroelastic phenomena in the presence of reduced stiffness:* A statement of the problem of static aeroelastic behavior of a lifting surface is embodied in the equations of equilibrium, (7-5), with the acceleration terms, $\ddot{w}(x,y,t)$, put equal to zero A solution of these equations becomes possible when we supply an additional relationship connecting the steady-state aerodynamic loading and the deformation. If the assumptions of piston theory are admissible, Eq. (7-2) supplies the additional relationship with $v_1 = U\partial w/\partial x$ for steady flow. This combination of equations forms a simple theoretical basis for estimating divergence speed, air load distribution, and control effectiveness above Mach Numbers of about 2.5.

Fig. 8-10 illustrates wing torsional divergence trends for the hypothetical fighter. Although divergence is usually not a critical design consideration, it nevertheless typifies static aeroelastic phenomena. The ordinate in Fig. 8-10 represents the elastic axis location, aft of the mid-chord, required to produce divergence at the corresponding Mach Number on the abscissa. The destabilizing effects of both finite thickness and aerodynamic heating are evident. A relatively smaller influence of thickness on divergence than on flutter is apparent by comparing Figs. 8-9 and 8-10.

Fig. 8-11 illustrates the estimated loss of aileron effectiveness, with and without aerodynamic heating, for the hypothetical fighter flying its assigned mission. The wing structure is assumed to consist of a rectangular box. The influence of wing thickness ratio on aerodynamic forces is included. Loss of aileron effectiveness due to aerodynamic heating does not appear to be unduly severe for this configuration.

(ii) *Aerothermoelastic phenomena:* A possible mechanism of aerothermoelastic coupling is suggested by the simple model of a wing leading edge—illustrated in Fig. 8-12(a). In flight at constant Mach Number and small finite angle of attack, there is a relatively small difference in wall temperature between the upper and lower surfaces of the model, as illustrated qualitatively in Fig. 8-12(b) by the time region A-B. However, in a transient state at finite angle of attack, such as region B-C, there can be a significant difference in heat flux into the upper and lower surfaces which varies with time. The temperatures of the upper and lower surfaces would have time histories of the form shown qualitatively in the figure. If the Mach Number is near the divergence condition, it is possible that the resulting curling up due to thermal deflections will induce aerodynamic loads larger than the structure is capable of resisting.

A creep chordwise divergence phenomenon is also possible in steady supersonic flight at finite angle of attack. This is analogous to the phenomenon of creep buckling, and the governing differential equations are of the same form.

(8.5) *Modes of Structural Failure*

For many years mechanical engineers have been confronted with the problem of predicting modes of failure under combined thermal and heat inputs. An example of an important problem is that of gas turbine blade design. Here the structure is exposed to nearly uniform temperature and load for long periods of time, and creep and stress rupture become modes of failure of importance. An airplane structure poses a somewhat more difficult problem since the structure is more complicated and since it is subjected to a spectrum of load and heat inputs that are rarely constant for long periods of time.

(a) *Elastic and Plastic Buckling*—Because of the possibility of obtaining high compressive thermal stresses, short time buckling will continue to be a mode of failure of primary importance in shell structures of supersonic aircraft. The short time buckling strength of structural elements at elevated temperature can be computed by the same techniques employed in room temperature predictions. The appropriate stress-strain relations at the corresponding temperature and exposure time must be introduced.

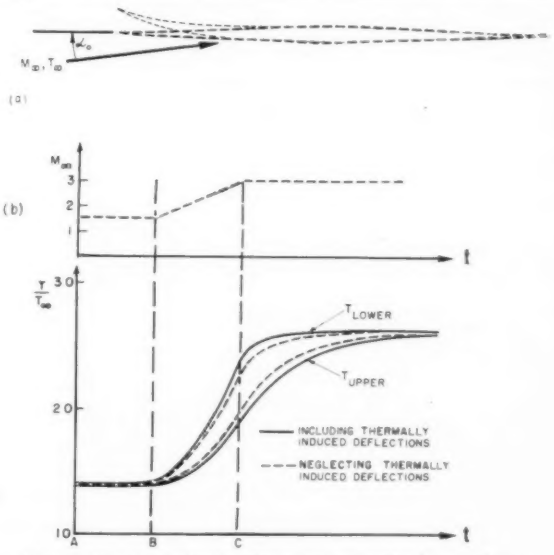

FIG. 8-12. A mechanism for aerothermoelastic coupling.

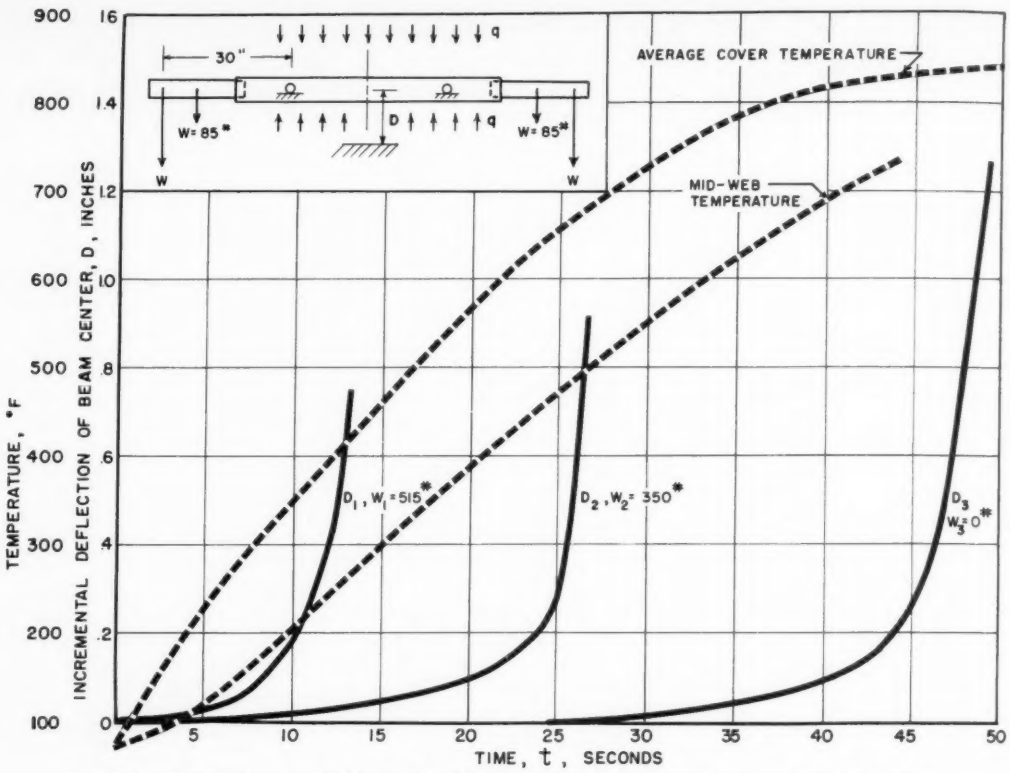

FIG. 8-13. Temperature and deflection time histories of beams under combined load and heat inputs.

Elastic thermal buckling of thin plates can be produced by a temperature gradient over the surface of the plate or by a difference in temperature between the plate and its supports. For example, elastic thermal buckling of a thin plate of thickness t and width b, stiffened in one direction, will occur when the difference between skin and stiffener temperatures, ΔT, is given by

$$\Delta T_{cr} = \frac{\pi^2(t/b)^2}{3(1-\nu^2)\alpha\left[\dfrac{1}{1+(E_p bt/E_s A_s)}\right]} \tag{8-17}$$

where E_p and E_s are, respectively, the moduli of elas-

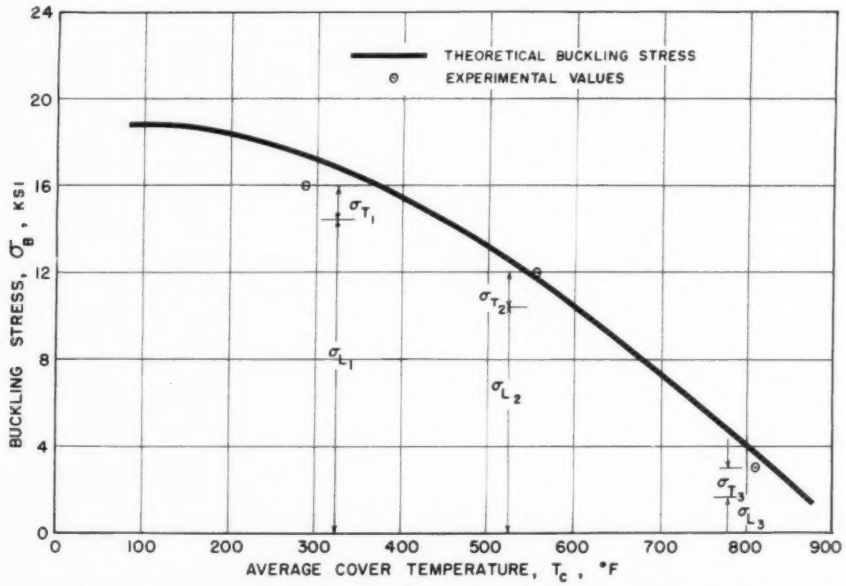

FIG. 8-14. Theoretical and experimental comparison of beam buckling boundary.

ticity of the plate and stiffener, A_s is the stiffener area, and α is the coefficient of thermal expansion of the plate and stiffener material. It is interesting to observe in Eq. (8-17) that the plate modulus of elasticity appears only as a ratio to the stiffener modulus of elasticity. In the event that elastic buckling is permitted within the flight range, there are important questions concerning the aeroelastic stability of the skin, the depth of buckle to be permitted, and the possibility that any buckling—even though it is nominally elastic—may result in permanent deformations in the presence of a high temperature environment.

Wings designed for supersonic airplanes will normally have heavy cover plates which buckle in the plastic range. Plastic buckling and ultimate failure will occur almost simultaneously. NACA results published by Heldenfels, Mathauser, and Brooks[45] indicate that a criterion for failure of a simply supported plate can be expressed by the empirical relation

$$1.60\ (E_{sec}\ \sigma_{cy})^{1/2}(t/b) = \sigma_L + \sigma_T \qquad (8\text{-}18)$$

where σ_L and σ_T are, respectively, the compressive stresses due to load and temperature, E_{sec} is the secant modulus corresponding to the failure stress, and σ_{cy} is the 0.2 per cent offset compressive yield stress. The latter material properties must correspond to the appropriate temperature and exposure time.

Results of tests conducted at M.I.T. to study modes of shell beam failure under the combined effects of external loads and heating are shown in Figs. 8-13, 8-14, and 8-15. Symmetrical transient radiant heat inputs were applied to three 63ST-6 simply supported rectangular beams under different levels of external bending moment. Fig. 8-13 illustrates the time histories of the cover and web temperatures and the time histories of deflection of the mid-points of the beams. The beam deflection is governed by the reduction in modulus of elasticity with rise in temperature until buckling commences, after which the beam stiffness deteriorates rapidly. Fig. 8-14 is a plot of Eq. (8-18) as a function of temperature showing the agreement of the experimental points. Fig. 8-15 illustrates a square buckle pattern typical of the results obtained in these tests.

In Fig. 8-16, Eq. (8-18) has been applied to the hypothetical fighter. It illustrates a comparison of the buckling strength of the cover with the actual compressive stress, including thermal and load stresses, at various times in the mission. The buckling strength of the cover is reduced as the airplane proceeds through its mission. The maneuvering condition at the end of the supersonic dash is a 6g turn. It is evident that if the conventional factor of safety of 1.5 is applied to the maneuvering condition at the end of the supersonic dash, the low-speed factor of safety for the same maneuver will be excessively large—of the order of 3.

In assessing the strength of structures at elevated temperature under rapidly applied loads, the effect of strain rate on allowable stress is more important than at room temperature. Fig. 8-17 illustrates the effect of strain rate on the buckling boundary, estimated from experimental data on an annealed 7 per cent manganese titanium base alloy.[46] The time history of the design gust stress at 35,000 ft., superimposed upon the thermal stress, is also shown. Fig. 8-17 would indicate that the margin of safety for high altitude gust loads is more than ample for the hypothetical fighter airplane.

(b) *Creep*—It has been mentioned previously that creep may affect the intensity of stresses in self-equilibrating thermal stress systems. The important aspect of creep insofar as external forces are concerned is that the structure is slowly and permanently distorted with time. The criterion to be applied in determining when the structure must be discarded as a consequence of these distortions is a matter to be decided in each individual case. The permanent distortions may become so large that the structure is unsatisfactory from the standpoint of aerodynamic drag, stability, or control. Local stress rupture or creep buckling may occur before the distortions become objectionable. In evaluating the creep life of a supersonic airplane, a stress-temperature spectrum must be employed in much the same way that a load spectrum is used in fatigue analyses. That is, we require not only the per cent of total time spent at

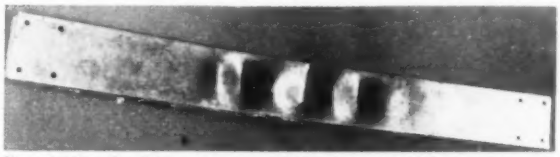

FIG. 8-15. Buckle pattern resulting from combined load and heat inputs.

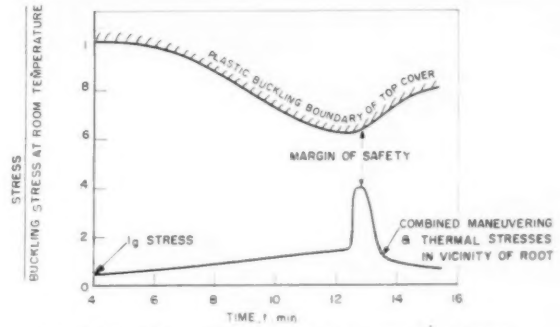
BUCKLING STRESS AT ROOM TEMPERATURE
STRESS
PLASTIC BUCKLING BOUNDARY OF TOP COVER
MARGIN OF SAFETY
1g STRESS
COMBINED MANEUVERING & THERMAL STRESSES IN VICINITY OF ROOT
TIME, t, min

FIG. 8-16. Maneuvering margin of hypothetical fighter.

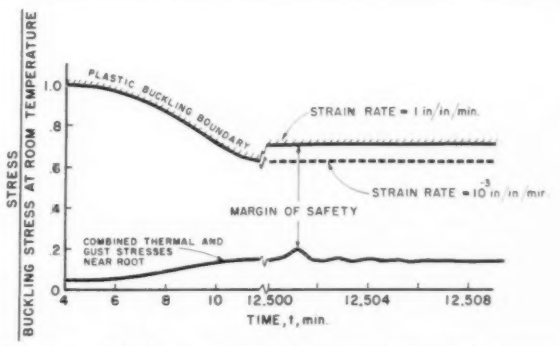
BUCKLING STRESS AT ROOM TEMPERATURE
STRESS
PLASTIC BUCKLING BOUNDARY
STRAIN RATE = 1 in./in./min.
STRAIN RATE = 10⁻³ in./in./min.
MARGIN OF SAFETY
COMBINED THERMAL AND GUST STRESSES NEAR ROOT
TIME, t, min.

FIG. 8-17. Margin of safety under combined gust and thermal stresses.

each stress level, but also the per cent of total time spent at each temperature level. These may, in principle, be correlated to form a single three-dimensional spectrum, the shape of which will depend on service experience.

There is very little fundamental knowledge concerning the creep behavior of materials under varying levels of stress and temperature. Gerard[47] has suggested that the total cumulative creep be taken as the sum of the creep increments due to the time spent at each stress and temperature level. He assumes that the stresses and temperatures may be applied at random and that the order of application is immaterial. Limited experimental evidence indicates that such an hypothesis may be taken as a first approximation.

In the absence of probability data on stress and temperature, an estimate may be made of the creep incurred during a specified mission. The total permanent creep strain per mission is

$$\epsilon = \int_0^{t_1} \dot{\epsilon}(\sigma,T)dt \qquad (8\text{-}19)$$

where t_1 is the total mission time and $\dot{\epsilon}(\sigma,T)$ is the minimum creep rate of the material. The latter is a function of the stress and temperature variations throughout the mission. The hypothetical fighter may be taken as an example. If the titanium RC-130A skin is designed so that the normal stress at limit load is one quarter of room temperature ultimate strength, the creep strain per mission is only about 7.5 by 10^{-6} in./in. On the other hand, if the stress level at limit load is two thirds of room temperature ultimate strength, the creep strain per mission is about 1000 by 10^{-6} in./in. If 5 per cent creep is taken as a failure criterion, the lower working stress would permit about 6,700 missions whereas the upper working stress would permit only 50 missions. Creep would obviously be an important limiting factor on structural life at the higher working stress.

(c) *Fatigue*—In any discussion of aircraft structural modes of failure, the question of fatigue must be mentioned. A number of recent outstanding technical papers have appeared on this subject, and in particular, the 18th Wright Brothers Lecture by Lundberg[48] should be mentioned. Most discussions of the aircraft fatigue problem have naturally been devoted to room temperature and relatively low stress-high cycle fatigue. Fatigue of built-up structures has proved to be such a difficult problem at room temperature that the complexities introduced by adding temperature as a variable seem so great as to discourage speculation. There are, however, a few experimentally established phenomenological trends that can be mentioned.

In assessing the behavior of materials under load, two of the most important variables are temperature and strain rate. It is natural to expect then that changes of these variables can influence the results of fatigue tests. The primary effect of elevated temperatures on fatigue is a lowering of the *S-N* curve with increase in temperature. Although there is a general reduction in fatigue strength with temperature, this reduction is not as great as the reduction of ultimate and yield strength. Rate of cycling has also been shown experimentally to have an effect on fatigue life.

(d) *Interaction Between Creep and Fatigue*—The dependence of both creep and fatigue on temperature and strain rate suggests the possibility of an interaction between the two.. Dolan[49] has pointed out that fracture at high temperature may result from either creep or fatigue or a combination of the two. The rate of progressive damage resulting from the interaction between creep and fatigue may be different from that predicted by simple superposition of effects obtained in separate tests.

Grover, Gordon, and Jackson[50] have suggested that a loading in which the stress is completely reversed during each cycle can be considered, for engineering purposes, independent of creep phenomena. However, when the cycling is about a mean stress, the interaction effects may be appreciable. In evaluating interaction effects, Tapsell[51] has recommended an elliptical interaction curve.

(9) Attacking Structural and Aeroelastic Problems by Design and Development

In the previous section, some of the structural and aeroelastic problems which are likely to be encountered in high-speed flight have been outlined. In common with most discussions of this subject, more questions have been raised than can be satisfactorily answered. However, some reasonably well-defined lines of attack are evident.

(9.1) *Attenuation of Heat Input*

In attacking the structural problems which result from aerodynamic heating, it is logical to consider first how the total heat input or the rate of heat input can be reduced.

The planning of a mission, in particular as it determines the rate at which the airplane is accelerated, can have a significant influence on the rate of heat input and the resulting time history of thermal stresses. For example, Fig. 9-1 compares the effects of finite and infinite accelerations on the time history of web and cover thermal stresses in the wing of the hypothetical fighter. The finite acceleration result is for the mission of Fig. 5-1, whereas the infinite acceleration result is for an instantaneous jump in airplane speed to Mach Number 3.5. The relief in maximum stress due to finite acceleration is small in this case, although the general character of the time histories is quite different. It cannot be concluded, in general, that the maximum stresses due to instantaneous acceleration are always only slightly conservative compared with those for finite acceleration. The result is strongly dependent upon the thermal conductivity of the structural material as well as other factors such as joint conductivity and geometry. For example, if the hypothetical wing were aluminum alloy, then even if the air-

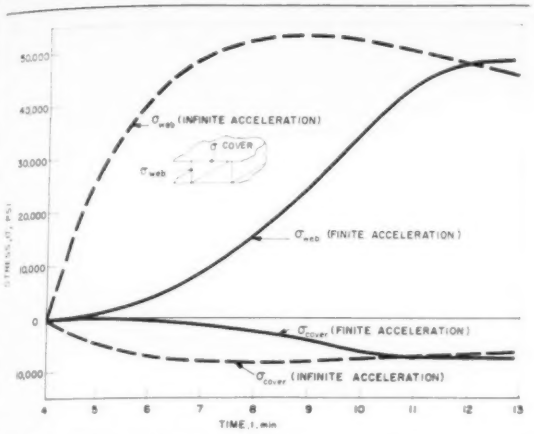

FIG. 9-1. Effects of finite and infinite accelerations on thermal stress response.

plane were accelerated to Mach Number 2.5 instead of 3.5, the relief in maximum stress due to finite acceleration would be of the order of 50 per cent.

A direct method of attenuating the heat input is to insert a thin layer of insulation between the boundary layer and the structure. Fig. 9-2 illustrates the relief in both thermal stress and temperature that can be expected for the hypothetical fighter when a 0.05-in. layer of insulation, of conductivity $k = 0.03$ B.t.u./ft. hr. °F, is placed on the top and bottom of the wing surface. A turbulent boundary layer is assumed. Insulation is highly effective in attenuating both thermal stress and temperature in the present example. The calculations leading to Fig. 9-2 assume that the heat capacity of the insulation is negligibly small compared with that of the structure. The analysis thus simplifies to a problem in which an effective heat-transfer coefficient, h_e, is employed.

$$h_e = \frac{h}{(t_i/k_i)h + 1} \tag{9-1}$$

where t_i is the thickness and k_i is the thermal conductivity of the insulation coating, and h is the heat-transfer coefficient of the boundary layer. Insulation is most effective for short periods of heating. For appreciably longer periods, insulation combined with cooling can be an effective combination.

Maintenance of a laminar boundary layer over the primary structure is an extremely effective way of minimizing the heat flow into the structure. For example, for the hypothetical fighter, laminar boundary-layer heat-transfer coefficients are of the same order of magnitude as those of the turbulent boundary layer with insulation. Thus the influence of laminar boundary layer in reducing temperature and stress is approximately as shown by Fig. 9-2 for the case of insulation. The influence of surface cooling on boundary-layer stability can be mentioned as providing one approach to the problem of delaying the transition from laminar to turbulent boundary layer.

Cooling the structure by passing a gas or liquid into the boundary layer can be an effective method of cooling hot areas of the structure such as wing leading edges and nose cones. One such application is a transpiration system in which a gas or liquid passes through the pores of the material to be cooled, maintaining a continuously regenerated protective film on the surface.[52]

(9.2) *Structural Design Considerations*

Structural design and development of air frames for penetration far into the supersonic range will require a many-sided attack. A purely empirical approach with large margins of safety is impractical because of sacri-

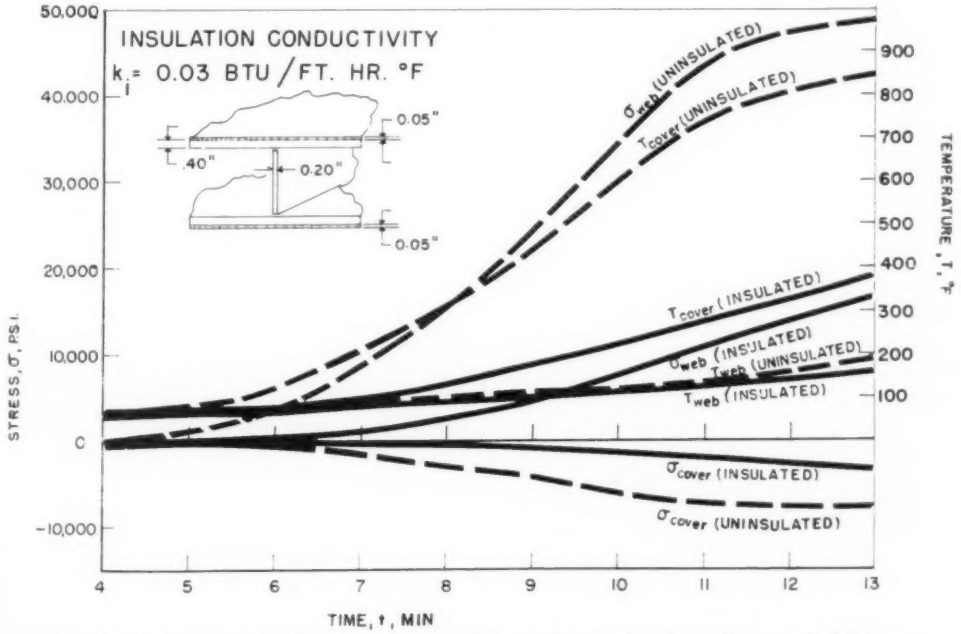

FIG. 9-2. The effect of insulation on the temperatures and thermal stresses of hypothetical fighter.

	ARBITRARY BODY	PLATE	WIDE FLANGED I BEAM
	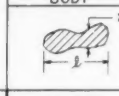	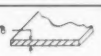	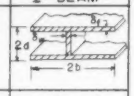
NON-DIMENSIONAL STRESS	$\frac{\sigma(1-2\nu)}{E\alpha(T_f-T_0)}$	$\frac{\sigma(1-\nu)}{E\alpha(T_f-T_0)}$	$\frac{\sigma(1-\nu)}{E\alpha(T_f-T_0)}$
BIOT NUMBER	$\frac{h\ell}{k}$	$\frac{h\delta}{k}$	$\frac{hd^2}{k\delta_f}$
NON-DIMENSIONAL LENGTH	$\frac{x}{\ell}$	$\frac{x}{\delta}$	$\frac{x}{d}$
FOURIER NUMBER	$\frac{kt}{c\ell^2}$	$\frac{kt}{c\delta^2}$	$\frac{kt}{cd^2}$
NON-DIMENSIONAL EQUIVALENCE OF MECHANICAL AND THERMAL ENERGY	$\frac{E\alpha}{c}$	$\frac{E\alpha}{c}$	$\frac{E\alpha}{c}$

TABLE 9-1. Nondimensional parameters in thermal stress analysis.

fice in performance. A purely analytical approach is impossible at present because of lack of adequate analytical tools. Combinations of the two will be required with an increased volume of development testing in order to make up for inadequacies of analytical methods.

(a) *Alleviation of Thermal Effects*—There are innumerable possibilities of alleviating thermal effects by ingenious structural design. The object is to arrange primary structural members and select structural materials so that there will be a minimum temperature rise and a minimum temperature gradient. One obvious example is heterogeneous construction in which the loads are carried by an internal structure surrounded by a refractory shell.

Numerous arts and subterfuges can be employed to reduce the intensity of thermal stresses. These resolve essentially into three lines of attack: (1) selecting materials and structural arrangement such that thermal gradients are as small as possible, (2) selecting materials with low values of $E\alpha/(1-2\nu)$, and (3) selecting a structural arrangement that is thermally nonredundant.

The influence of material choice on thermal stresses can be evaluated by considering the dimensionless parameters upon which thermal stresses depend in a thermoelastic system. Table 9-1 illustrates these parameters for an arbitrary homogeneous isotropic body, a plate, and a wide flange I-beam. All are assumed initially at the temperature T_0. The arbitrary body is surrounded by a fluid at temperature T_f, the plate is exposed to a temperature T_f on one side and insulated on the other, and the I-beam is exposed to a temperature T_f on the outer faces of the upper and lower flanges. The important parameters involving material properties are the nondimensional stress, the Biot number, and the Fourier number. The last parameter in the table, which represents the equivalence of mechanical and thermal energy, is negligibly small. In general, the larger the Biot number and the smaller the Fourier number, the larger the temperature gradient and hence the larger the thermal stress. The larger the value of the fictitious thermal stress $E\alpha/(1-2\nu)$, the larger the thermal stress. Thus materials with high values of k and low values of $E\alpha$ are desirable from a thermal stress point of view. The influence of material choice can be illustrated quantitatively by considering the thermal stresses in a flat plate with four completely restrained edges and with one side exposed to the air stream. Fig. 9-3, based on results due to Isakson,[53] illustrates the ratio of maximum thermal stress to elevated temperature yield strength for four different materials as a function of plate thickness. The plate is assumed to be on a vehicle which takes off at sea level and achieves instantly a Mach Number of 3.0 at 50,000 ft. altitude. The favorable position occupied by titanium relative to magnesium, aluminum, and steel is evident. Between Mach Numbers of 3 and 4, the titanium maintains its favorable position, while the aluminum and magnesium alloys lose strength rapidly and the thermal stresses in the steel become excessive.

For a wide flange I-beam, the Biot number has the form $h/k(d/\delta_f)d$. Thus, in addition to a low value of h/k, a small ratio of depth to cover thickness, d/δ_f, is desirable. The additional factor, d, is a scale factor which indicates that thermal stresses will become more critical as structures increase in size.

Parkes[54] has suggested that composite construction in which the skin and webs are made of different materials offers relief from thermal stresses. Titanium skin with aluminum-alloy webs would provide a desirable combination. Increasing the area ratio of flange to web or reducing the degree of mutual restraint between web and flange are other methods of alleviating thermal stresses. The ideal internal structure is one that stabilizes the outer skin against buckling yet provides a minimum restraint against thermal expansion of the skin. "Thermally nonredundant" construction such as a Warren truss web (as suggested by Parkes[54]), post stiffening, or a honeycomb core are examples.

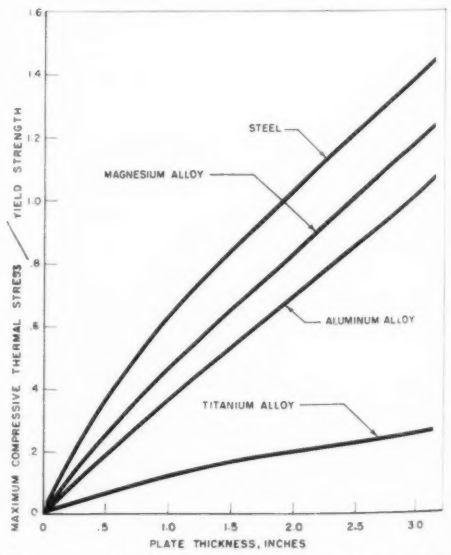

FIG. 9-3. Thermal stress to yield strength ratio for aerodynamic heating of a flat plate, $M = 3$.

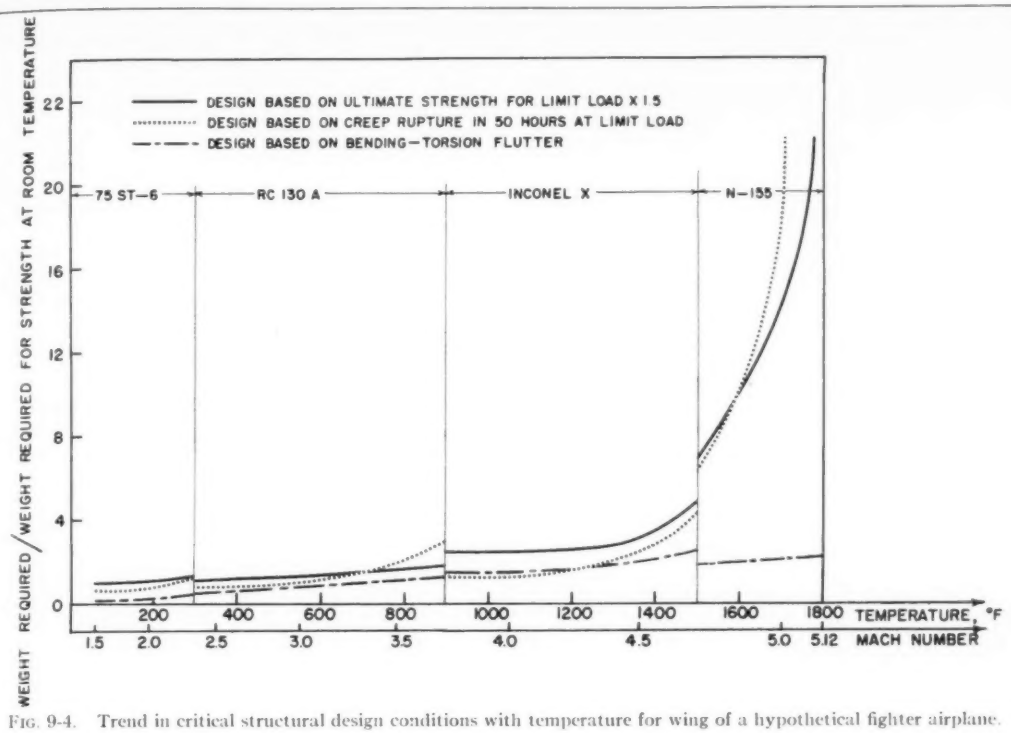

FIG. 9-4. Trend in critical structural design conditions with temperature for wing of a hypothetical fighter airplane.

(9.3) *Design to Minimize Aeroelastic Phenomena*

It is relatively easy to state the factors required for minimization of aeroelastic phenomena, but it is quite another matter to put them into effect in a design of minimum weight. Practically every aeroelastic phenomenon can be cured or avoided by liberal additions of mass, stiffness, or damping, all of which involve additions in weight. The original selection of lifting surface configuration is the most important design decision. In general, it can be said that low aspect ratio wings have a minimum, whereas slender high aspect ratio wings have a maximum of aeroelastic problems.

Once the configuration is established, the design problem is one of attempting to make the airplane satisfactory from an aeroelastic standpoint without adding stiffness or mass over and above that which is incorporated in the original design based on strength and other operational considerations. Design to minimize aeroelastic phenomena and, in particular, to prevent flutter is unfortunately not a process which can be reduced to simple rules. If optimum design is to be achieved, three general lines of attack must be pursued: (1) theoretical methods aided by automatic computing machinery are used to investigate a number of mass and stiffness configurations with the object of selecting the configuration of minimum weight, (2) dynamic tests of models are conducted in wind tunnels or in free flight for the purpose of establishing quantitative data such as critical speeds, and (3) exploratory proof tests of the full-scale airplane are conducted in flight.

(9.4) *Critical Structural Design Conditions*

A matter of fundamental importance in selecting structural arrangements and materials is that of determining which of the factors of strength, stiffness, or creep will be critical in design. Which factor will dominate depends upon many factors peculiar to each new design, and it is difficult to generalize with any degree of certainty. Trends based upon an analysis of specific airplanes can be obtained. Fig. 9-4 is a plot of wing weight ratio of the hypothetical fighter as a function of temperature. Wing weight ratio is defined as the design wing weight at the corresponding temperature level divided by the design wing weight at room temperature. The design wing weight at room temperature is the weight of a multiweb 75S-T6 wing required to support an ultimate bending moment based on a limit load factor of 6 and a factor of safety of 1.5. Three wing weight ratio curves are shown. The solid lines represent the wing weight required to support the same ultimate bending moment at various temperature levels. It is assumed that the structure is soaked for $^1/_2$ hour at the elevated temperature. The influence of elevated temperature on the tension, compression, and shear load carrying elements is taken into consideration. The dash lines represent the weight of a wing designed to support the limit bending moment for 50 hours without creep rupture. The dash dot lines represent the weight of a wing designed on a basis of the stiffness required to prevent bending-torsion flutter at the corresponding Mach Number given on the abscissa.

From this approximate analysis, it would appear that ultimate strength is the dominant design condition

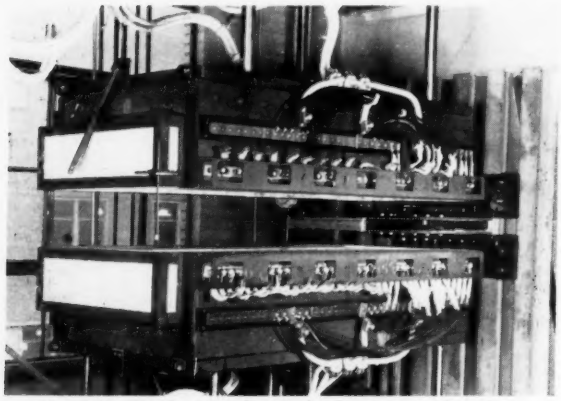

FIG. 9-5. Radiant heating device for structural testing.

over a large part of the practical flight range. Creep becomes important in the temperature range from 700°F. to 900°F. for the titanium RC-130A material and above 1,600°F. for N-155. Of course, if the time to creep rupture were raised to a higher number, creep would appear to be of greater importance. The relatively low structural weight required to prevent bending-torsion flutter, compared with that required to meet the strength and creep requirement, is due to two principal reasons. In the first place, the reduction in Young's modulus with temperature is not so pronounced as the reduction in strength properties. Secondly, the increase in wing solidity at the higher Mach Numbers and temperatures increases the relative density parameter, μ. An increase in μ has a favorable effect in raising flutter speed. In the flutter analyses upon which these curves are based, the distance from the elastic axis to the wing center of gravity, x_α, was assumed constant for all wing designs.

(9.5) *Development Testing; an Aid to Structural Design*

In order to achieve efficient structures under high temperature conditions, an unusually large amount of model and component development testing will be required. Model tests are useful in developing optimum configurations and in supplementing and confirming analytical results. Structural component testing may consist of both "stretch" and "proof" tests.

In assessing the tests that are necessary and feasible in developing high temperature structures, it is apparent that complete simulation by true models operating in a supersonic air stream is very complex and can be achieved only by models which approach the prototype in size. It thus becomes necessary to think in terms of a number of "restricted" purpose models, each tested in a different type of facility. Three types may be mentioned. They are models which study the heat transfer from the boundary layer, models which study structural behavior in the presence of elevated temperature, and models which study aeroelastic behavior.

(a) *Heat-Transfer Models*—Information on the heat input to the structure is a basic ingredient of design. A continuous flow supersonic wind tunnel is an ideal facility for studies of simple heat-transfer models such as plates, cones, or cylinders. Six nondimensional similarity conditions must be satisfied in order to achieve complete similarity between a prototype and its corresponding wind-tunnel model for the case of laminar flow and taking account of the interacting heat transfer between the boundary layer and the body.[35] Complete similarity is generally not feasible. Various degrees of approximation may be obtained by adjusting the four variables of wind tunnel pressure and temperature and model length and material.

(b) *Structural Model, Component, and Assembly Tests*—The task of providing facilities for this purpose will prove to be one of the most formidable laboratory equipment problems yet faced by aeronautical engineers. Three problems must be overcome. The first is that of delivering the required *heat input* to the surface of the structure. The second is the application of the required *load input* at the same time that the heat input is applied. The third is that of measuring the *response* of the structure.

Of the various methods that can be devised for producing heat inputs, few of them satisfy all the special conditions that must be imposed on a practical laboratory system. Radiant heaters provide probably the most convenient solution at the present time. Fig. 9-5 illustrates a radiant heating device built at M.I.T. under Air Force sponsorship. This apparatus, which has a total radiation area of 14 sq.ft., employs silicon

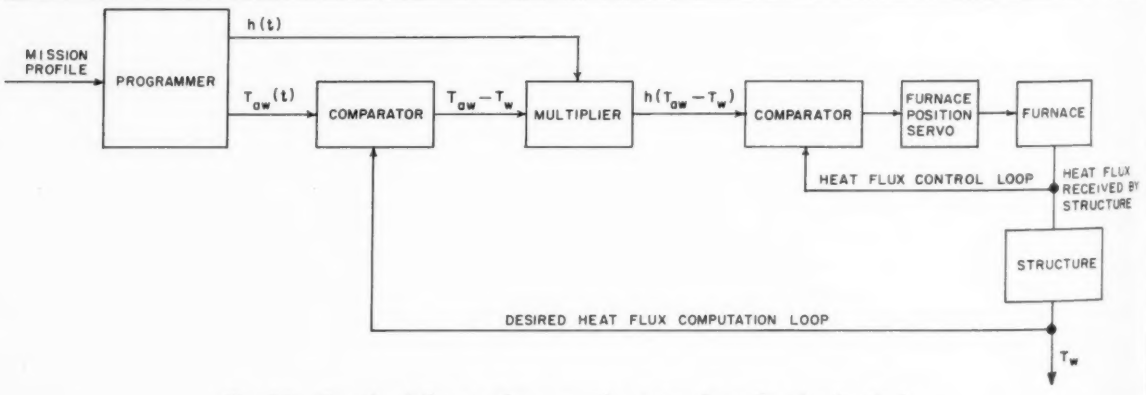

FIG. 9-6. Functional diagram of programming system for radiant heating device.

carbide heating elements mounted in a bed of firebrick. The time history of thermal input to the model is programmed by mechanically moving the heat source with respect to the model. A functional diagram of a system for programming the motion to simulate the aerodynamic heating in a prescribed mission is illustrated by Fig. 9-6. A scheme of controlling the power input to the heating elements would, of course, be necessary in a larger facility, and elaborate electronic control devices would be required in addition to low thermal inertia heating elements. Several other radiant heating sources may be used besides silicon carbide elements. Among these may be mentioned nichrome wire elements, carbon elements, gas-fired radiant panels, tungsten filament lamps, flash tubes, burning combustibles, and solar sources.[56]

In estimating the power requirements of radiant heating facilities, an appreciation is obtained of the effectiveness of a supersonic airplane as a generator of heat. For example, for the hypothetical fighter mission of the present paper, a peak thermal density of 3.8 kw. per sq.ft. is reached. Taking account of average radiation losses and assuming a polished skin with an absorptivity of 0.2, electric power of about 40 kw. per sq.ft. must be delivered to a radiant heating facility in testing a full scale structure. If the skin surface is coated with a black substance so that its absorptivity is raised to 0.8, the power requirement is reduced to about 10 kw. per sq.ft. It is apparent that if large structural components are to be tested, the power requirements will be of the same order of magnitude as those of large supersonic wind tunnels.

A great deal of ingenuity will be required to devise schemes of applying flight loads and heat input simultaneously. Since strain rate is an important parameter in elevated temperature testing, it will be desirable for loading devices to simulate rates of loading as well as peak intensity.

Measurement of structural response involves the parameters of temperature and strain. The thermocouple principle provides a means of reliably measuring temperatures over a wide range. However, the electrical-resistance strain gage, so widely used in room temperature experimental stress analysis, unfortunately does not provide the same degree of reliability, even with recent improvements intended for high temperature applications. New developments in strain gage techniques are necessary before high temperature strains can be conveniently and reliably measured.

Two types of structural tests in the laboratory may be of interest. In the first, a relatively small model can be used in conjunction with a radiant heating device to obtain information on temperature distribution, thermal stresses, and elevated temperature influence coefficients. A model operating entirely in the elastic range could conceivably be subjected to the time varying heat input of the airplane mission several times so that the several kinds of data of interest could be measured. In a thermoelastic model, the nondimensional temperature distribution, $(T - T_0)/(T_{aw} - T_0)$, stress distribution, σ/E, and deformation distribution, δ/L, are functions of the dimensionless loading parameter, P/El^2, in addition to the five parameters listed in Table 9-1. Neglecting the parameter, $E\alpha/c$, complete similarity can be achieved by making the model geometrically similar to the prototype and using the same material. If the test is conducted at a high enough temperature so that there are important variations in the elastic constants with temperature, use of the same material in model and prototype is mandatory. A practical testing difficulty is encountered in model tests, since the time scale of the model t_M is reduced according to the inverse square of the scale ratio, l_M/l_P.

$$t_M/t_P = (l_M/l_P)^2 \tag{9-2}$$

For turbojet aircraft, this reduction of model time scale can probably be accommodated in model tests with radiant heating devices since the heat input rates of the prototype will be relatively low.

A second type of laboratory structural test may be required to obtain modes of failure of structural components or even complete assemblies under combined heat and force inputs. These tests can assume a wide variety of forms. Model tests to obtain modes of failure of prototype structural elements under conditions of constant temperature and short time loading are an example. If model and prototype are geometrically similar, made of the same material, and tested at the same temperature, the nondimensional stress, $\sigma l^2/P$, and deformation distribution, $\delta\ l$, are functions of the single loading parameter, P/l^2. Thus, if these functions are obtained from a model test, they will be identical for the prototype. Tests of "restricted" purpose models, as discussed by Sandorff,[57] and proof tests of complete structural assemblies at elevated temperature, are other examples of laboratory tests to obtain modes of failure.

The similarity laws stated above are valid only if there is a single mode of internal conductive heat transfer. If internal radiative heat transfer is also important, complete similarity is not possible and certain compromises must be accepted.

(c) *Aeroelastic Models*—Testing "restricted" purpose aeroelastic models and, in particular, flutter models has emerged as an indispensable aid in designing structures to avoid aeroelastic phenomena. There are two basically different approaches to the use of models in aeroelastic development work. In one, the model tests are designed to evaluate coefficients to be inserted into the theory. In the other, the model test is designed as an analog of the full-scale problem.

A supersonic blowdown tunnel is an example of a device for flutter development testing at supersonic Mach Numbers. Fig. 9-7 illustrates a variable Mach Number supersonic test section designed for use in conjunction with a blowdown tunnel at M.I.T.[58] The nozzle is of the asymmetric sliding block type and the Mach Number can be varied through the complete range of the tunnel (M = 1.25 to 2.10) during a run by

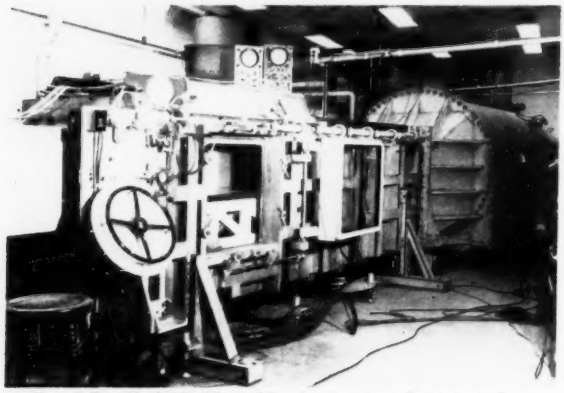

FIG. 9-7. Variable Mach Number supersonic test section

moving the sliding block through its travel without any change in the dimensions of the test section. A running time of approximately 35 sec. is available. A model of a lifting surface is injected into the air stream after supersonic flow is established, and the nozzle configuration is varied until flutter is obtained.

Supersonic flutter model tests have heretofore been conducted, for the most part, at Mach Numbers below those at which appreciable aerodynamic heating is encountered. We have seen previously that heating effects may alter the picture considerably in the simple case of bending-torsion flutter. Other flutter modes heretofore nonexistent may appear. For example, a chordwise "flag waving" type of flutter of a multiweb wing has been reported by Dryden and Duberg.[59] A true flutter model simulating all the elastic, inertial, unsteady aerodynamics and heat-transfer properties of a prototype is virtually out of the question, except for geometric scale ratios of nearly one. It thus becomes apparent again that "restricted" purpose models must be employed. Each model is designed to investigate a particular flutter mode that must be recognized in advance. The object is to design a model that satisfies the flutter similarity laws[23] and at the same time incorporates the loss of stiffness due to aerodynamic heating. This can in principle be accomplished by building the stiffness which exists at one or more points along the mission profile—as calculated or as determined by testing a scaled structural model in a heating device—into a series of room temperature flutter models. Each model can be injected into the established air stream of a continuous flow or blowdown tunnel operating at the Mach Number corresponding to the model stiffness.

(10) Attacking Structural and Aeroelastic Problems by Fundamental Research

Fundamental research is another key element in attacking structural and aeroelastic problems at high supersonic speeds. Design and development teams, however capable, must be supplied fundamental knowledge in the same way that they are supplied materials of construction.

The foremost objective of fundamental research should be the improvement of high temperature materials and a more complete understanding of the behavior of all materials at elevated temperature. The former is a metallurgical problem with obvious limitations on the results that can be achieved. Regardless of our efforts in mixing alloying ingredients to raise the strength level of metals at elevated temperature, we are always confronted with a barrier in the melting points of the principal metallic elements. The melting point of the staple metallic element, iron, is only 2,800°F. Most refractory metals with melting points in excess of 3,000°F. are poor from the standpoint of air-frame construction because of brittleness and susceptibility to rapid oxidation. Cermets offer some hope of achieving significantly higher melting points in the future. However, there is no certainty that substantial strides will be made in the development of new high temperature sheet materials, and the aeronautical engineer must prepare to use more effectively the materials that are now available.

Rational design requires fundamental knowledge of the mechanics of deformable bodies in the presence of elevated temperature—a mechanics that encompasses not only the classical theory of elasticity but also plasticity as well as the parameters of time and temperature. The present position of the structural engineer is similar to that of the aerodynamicist 15 years ago who was forced to abandon his incompressible fluid theory in favor of an aerodynamic theory in which temperature is an important parameter. Fundamental research had already supplied him with a well-established equation of state. Here the similarity ends for the structural engineer has no such equation of state, at least for engineering materials. The materials problem is much more complex than the fluid problem. A theory of plasticity has been extensively developed based on perfectly plastic materials, but aeronautical engineers have so far made very little use of it because of its restrictive simplifications. The stockpile of knowledge in this whole area is very low indeed. I would therefore make a special plea for faster accumulation of fundamental knowledge of the behavior of materials and the analyses of engineering structures in the inelastic range.

Design of complex structures at elevated temperature requires an understanding of the processes of heat transfer within the structure. Because of the nature of its governing physical laws, conductive heat transfer lends itself to analyses, and tools are available for obtaining engineering solutions. On the other hand, the physics of radiative heat transfer, although well understood, is more involved, and the engineer does not now have tools for analyzing complex structures.

The behavior of shell structures in the presence of a combined load and temperature environment requires fundamental study. Particular emphasis should be placed on achieving a better understanding of modes of failure and losses in structural stiffness.

In aeroelasticity, we are concerned with the growing list of phenomena not explainable in terms of classical linearized theories. Nonlinearities in both the structural and aerodynamic ingredients of aeroelastic theories must clearly be included in certain problems. Application of the classical Rayleigh-Ritz or Galerkin approach to the solution of nonself-adjoint aeroelastic problems, such as flutter, is not rigorously correct. Development of new approaches will require research in applied mechanics at the highest level. Panel flutter is a notable example where a higher level theoretical approach is required. Questions concerning the intensity and distribution of unsteady air forces arise continually in the solution of new aeroelastic problems. In the past, each aerodynamic speed range required intensive study before questions of aerodynamic coefficients could be resolved. The hypersonic speed range presents the newest challenge.

Response of structures to random aerodynamic inputs is another area in which the supply of fundamental knowledge is meager. During high-speed flight, airplane structures are exposed to a wide spectrum of random disturbances ranging from atmospheric turbulence to high intensity noise. The theory of generalized harmonic analysis provides a promising line of attack. However, research has not yet progressed to the point where a design tool can clearly be formulated.

In high-speed flight, all features of boundary-layer heat-transfer phenomena assume importance to the structural engineer. Uncertainty in the location of the transition point must be mentioned as the weakest aspect of the present state of the art.

Finally, flight experience by research vehicles is urgently needed in order to provide practical verification of all aspects of our fundamental knowledge.

(11) Conclusions

Today's assessments of the structural problems which will be encountered in high-speed flight are based largely on analytical and laboratory studies. Until flight experience can be gained, such studies provide the only basis for research and development planning. The results of some of these studies have been described by the present paper.

Even at this early stage in our experience, a few conclusions and predictions can and should be ventured. In the first place, design ingenuity will play a tremendously important role in overcoming structural problems at high supersonic speeds. Temperature levels of structural members will be controllable to a considerable extent by insulation, combined insulation and cooling, and ingenious design using heterogeneous structures. Temperature gradients and thermal stresses can be reduced by the use of thermally nonredundant structures, careful selection of materials, and by flight restrictions on fore and aft accelerations.

With regard to the question of loads, maneuvering loads at maximum speeds will require restriction to avoid excessive weight. Large dynamic response effects at high speeds and altitudes will result in moderately severe gust loads in clear air and jet stream turbulence. However, serious structural design problems are not expected.

The influence of aeroelasticity does not appear to be greater relative to the other structural design conditions than at present. In evaluating this conclusion, it must of course be recalled that the influence of aeroelasticity on structural design at any speed depends upon the airplane configuration and the level of strength set for maneuvering flight.

Based on available materials, the dominant factor for aircraft designed for appreciable maneuvering load factors will continue to be the short time static strength properties. There is reason to believe that fatigue of primary structural elements should be relatively less important at high temperatures than at present. Creep is a new factor which will require consideration, especially in the sustained flight of low load factor airplanes. For structures designed by creep, a more rational design philosophy is needed—one which is not tied to an arbitrary factor of safety but is rather based on a stress-temperature spectrum. Questions of when a shell structure must be discarded due to creep damage cannot yet be answered.

In the absence of insulation and cooling devices, weight penalties due to loss in strength of existing materials would appear to limit sustained flight in the isothermal atmosphere to Mach Numbers of the order of 3.5.

Although there will naturally be differences of opinion on technical details, one general conclusion can be stated with reasonable certainty. If we wish to fly fast for sustained periods within the earth's atmosphere, an expanded technological effort in the areas of materials and structures will be required. By its very nature, the so-called "thermal barrier" is not likely to be penetrated very far by a single discovery. It must either be hurdled by flying beyond the earth's atmosphere or it must be penetrated step by step—each succeeding step requiring more effort to achieve than the previous one. In a contest such as this, coordinated effort by research, development, and design teams is the key. New and unique structural testing facilities will be required before substantial progress can be made. They will be expensive with large power requirements.

Even more important than facilities are the needs for new fundamental knowledge and engineers trained to apply this knowledge. One of the perplexing questions of our time is how to foster these elements. There is unfortunately not a simple answer; it is, at least, not one that can be stated in terms of more appropriations. The answer is more likely to be found in terms of the quality of the young engineers and research scientists who will be attracted by the challenge.

(12) Acknowledgment

Assistance and advice was received from many of the author's colleagues in the Department of Aeronautical

Engineering at M.I.T. The author is deeply indebted to Dr. Hua Lin who ably assisted him in every phase of the preparation of the paper. The author also wishes to acknowledge especially the help of Lucien Schmit, Timothy O'Brien, Kenneth Foss, Alphonse Kirsch, Alfred Heller, Thomas Parsons, and William Blackstock, without whose aid the paper could not have been prepared.

References

[1] Thomson, Sir William (Lord Kelvin), *Mathematical and Physical Papers*, p. 291, Vol. 1; Cambridge University Press, 1882.

[2] *A Commentary on the Scientific Writings of J. Willard Gibbs, Vol I;* Yale University Press, 1936.

[3] Love, A. E. H., *Mathematical Theory of Elasticity;* Dover Publications, 1944.

[4] Eckert, E. R. G., *Survey on Heat Transfer at High Speeds*, WADC T.R. 54–70, April, 1954.

[5] Davies, F. V., and Monaghan, R. J., *The Determination of Skin Temperatures Attained in High Speed Flight*, Royal Aircraft Establishment Report No. Aero 2454, February, 1952.

[6] Bloom, M., *Thermal Conditions Associated with Aircraft in Flight*, PIBAL Report No. 241, Dept. Aero. Engrg. and Appl. Mech., Polytechnic Institute of Brooklyn, January, 1954.

[7] Chapman, D. R., and Rubesin, M. W., *Temperature and Velocity Profiles in the Compressible Laminar Boundary Layer with Arbitrary Distribution of Surface Temperature*, Journal of the Aeronautical Sciences, Vol. 16, No. 9, p. 547, September, 1949.

[8] Lighthill, M. J., *Contributions to the Theory of Heat Transfer Through a Laminar Boundary Layer*, Proc. Royal Society A, Vol. 202, No. 1070, p. 359, August, 1950.

[9] Bryson, A. E., and Edwards, R. H., *The Effect of Nonuniform Surface Temperature on the Transient Aerodynamic Heating of Thin-Skinned Bodies*, Journal of the Aeronautical Sciences, Vol. 19, No. 7, p. 471, July, 1952.

[10] Moore, F. K., *Unsteady Laminar Boundary Layer Flow*, NACA T.N. 2471, September, 1951.

[11] *The Effects of Atomic Weapons*, Los Alamos Scientific Laboratory, Los Alamos, New Mexico, September, 1950.

[12] Fourier, J., *Théorie Analytique de la Chaleur*, Paris, France, 1822.

[13] Hoff, N. J., *The Structural Effects of Aerodynamic Heating*, Paper read before the Third General Assembly of AGARD, London, England, September, 1953.

[14] Jakob, Max, *Heat Transfer*, Vol. I; John Wiley and Sons, Inc., New York, 1949.

[15] Carslaw, H. S., and Jaeger, J. C., *Conduction of Heat in Solids*, First Ed.; Clarendon Press, Oxford, 1950.

[16] Washizu, K., *Application of the Variational Method to Transient Heat Conduction Problems*, M.I.T. Aeroelastic and Structures Research Laboratory Report No. 25-17 for The Office of Naval Research, March, 1955.

[17] Emmons, H. W., *Numerical Solution of Heat Conduction Problems*, Trans. A.S.M.E., Vol. 65, p. 607, 1943.

[18] Weiner, J. H., *A Method for the Approximate Solution of the Heat Equation*, Technical Report No. 5, Contract No. AF 33(616)-2071, Columbia Univ., New York, March, 1955.

[19] Goodman, S., *Radiant Heat Transfer Between Infinite Parallel Plates*, National Bureau of Standards Report No. 4239, August, 1955.

[20] Schmit, L. A., and Williams, F. L., *The Effects of Thermal Radiation on Aircraft Structures, Part II—The Response of a Simple Structure to Radiant Heating*, Air Force Technical Report 54-384, Part II, February, 1955.

[21] Ambrosio, Alphonso, Russell, Bertram, and MacInnes, W. F., *Temperature Distribution in a Typical Aircraft Structure due to Transient External Heating, Vol. I, T-33 Airplane*, WADC Technical Report No. 52-216, April, 1953.

[22] Rhode, R. V., and Donely, Phillip, *Frequency of Occurrence of Atmospheric Gusts and of Related Loads on Airplane Structures*, NACA ARR No. L4I21 (Unclassified), November, 1944.

[23] Bisplinghoff, R. L., Ashley, H., and Halfman, R. L., *Aeroelasticity;* Addison Wesley Publishing Co., Inc., Cambridge, Mass., 1955.

[24] Lighthill, M. J., *Oscillating Airfoils at High Mach Numbers*, Journal of the Aeronautical Sciences, Vol. 20, No. 6, p. 402, June, 1953.

[25] Miles, J. W., *Unsteady Supersonic Theory*, Report for the *ARDC*, USAF, Contract AF18(600)-432, March, 1955.

[26] Landahl, M. T., *Unsteady Flow Around Thin Wings at High Mach Numbers*, M.I.T. Fluid Dynamics Research Group Report for the Office of Scientific Research, USAF, Contract AF18(600)-961, June, 1955.

[27] Landahl, M., Mollø-Christensen, E., and Ashley, H., *Parametric Studies of Viscous and Nonviscous Unsteady Flows*, USAF O.S.R. Technical Report No. 55-13, April, 1955.

[28] Zartarian, G., Heller, A., and Ashley, H., *Application of Piston Theory to Certain Elementary Aeroelastic Problems*, Paper presented at the Midwestern Conference on Solid and Fluid Mechanics, Purdue Univ., September, 1955.

[29] Tolefson, Harold B., and Press, Harry, *A Review of Flight Data on Atmospheric Turbulence*, Paper presented at the NACA Conference on Some Problems of Aircraft Operation, Cleveland, Ohio, November, 1954.

[30] Wiener, Norbert, *Generalized Harmonic Analysis*, Acta Mathematica, Vol. 55, p. 117, 1930.

[31] Liepmann, H. W., *On the Application of Statistical Concepts to the Buffeting Problems*, Journal of the Aeronautical Sciences, Vol. 19, No. 12, p. 793, December, 1952.

[32] Clementson, G. C., *An Investigation of the Power Spectral Density of Atmospheric Turbulence*, Sc.D. Thesis, M.I.T., 1950.

[33] Fung, Y. C., *Statistical Aspects of Dynamic Loads*, Journal of the Aeronautical Sciences, Vol. 20, No. 5, p. 317, May, 1953.

[34] Duhamel, J. M. C., *Mémoir sur le calcu des actions moléculaires développées par les changements du température dans les corps solides*, Mém. Acad. sci. savants étrangers, Vol. 5, p. 440, 1838.

[35] Timoshenko, S. P., and Goodier, J. N., *Theory of Elasticity*, Second Ed.; McGraw-Hill Book Company, Inc., New York, 1951.

[36] Sokolnikoff, I. S., *Mathematical Theory of Elasticity;* McGraw-Hill Book Company, Inc., New York, 1946.

[37] Hoff, N. J., *Structural Problems of Future Aircraft*, Third Anglo-American Aeronautical Conference at Brighton, England, The Royal Aeronautical Society, p. 77, 1951.

[38] Maxwell, J., *On the Dynamical Theory of Gases*, Phil. Mag., Vol. 4, 1868.

[39] Freudenthal, A. M., *The Inelastic Behavior of Engineering Materials and Structures;* John Wiley and Sons, Inc., New York, 1950.

[40] Hoff, N. J., *Approximate Analysis of Structures in the Presence of Moderately Large Creep Deformations*, Quart. Appl. Math., Vol. 12, No. 1, p. 49, April, 1954.

[41] Vosteen, L. F., and Fuller, K. E., *Behavior of a Cantilever Plate Under Rapid Heating Conditions*, NACA Research Memorandum, RM L55E20C, July, 1955.

[42] Timoshenko, S., *Theory of Elastic Stability;* McGraw-Hill Book Company, Inc., New York, 1936.

[43] Pines, S., Dugundji, J., and Neuringer, J., *Aerodynamic Flutter Derivatives for a Flexible Wing with Supersonic and Subsonic Edges*, Journal of the Aeronautical Sciences, Vol. 22, No. 10, p. 693, October, 1955.

[44] Goland, Martin, and Luke, Y. L., *An Exact Solution for Two Dimensional Linear Panel Flutter at Supersonic Speeds*, Reader's Forum, Journal of the Aeronautical Sciences, Vol. 21, No. 4, p. 275, April, 1954.

[45] Heldenfels, R. R., Mathauser, E. E., and Brooks, W. A., *Some Structural Effects of Aerodynamic Heating*, NACA-University Conference on Aerodynamics, Construction, and Propul-

sion, Vol. I, Aircraft Structures and Materials, October, 1954.

[46] Luster, D. R., Wentz, W. W., and Catlin, J. P., *Effect of Strain Rate on the Mechanical Properties of Titanium Base Materials*, WADC Technical Report 53-71, *ARDC*, USAF, Wright-Patterson Air Force Base, September, 1953.

[47] Gerard, George, *Some Structural Aspects of Thermal Flight*, Paper presented at the Aviation Division of the ASME Symposium on the Thermal Barrier, November 28–December 3, 1954.

[48] Lundberg, B. O., *Fatigue Life of Airplane Structures*, The Eighteenth Wright Brothers Lecture, Journal of the Aeronautical Sciences, Vol. 22, No. 6, p. 349, June, 1955.

[49] Dolan, T. J., *How Can We Appraise Metals for High Temperature Service*, Metals Progress, Vol. 61, p. 56, March, 1952.

[50] Grover, H. J., Gordon, S. A., and Jackson, L. R., *Fatigue of Metals and Structures*, NAVAER 00-25-534, Prepared for Bureau of Aeronautics, Department of the Navy, 1954.

[51] Tapsell, H. J., *Fatigue at High Temperatures*, Symposium on High Temperature Steels and Alloys for Gas Turbines, Iron and Steel Institute, 4 Grosvenor Gardens, London, S. W. 1, p. 169, 1950.

[52] Rubesin, Morris W., *An Analytical Estimation of the Effect of Transpiration Cooling on the Heat-Transfer and Skin-Friction Characteristics of a Compressible, Turbulent Boundary Layer*, NACA Technical Note 3341, December, 1954.

[53] Isakson, Gabriel, *A Study of Thermal Stresses in Aircraft Structures due to Aerodynamic Heating*, Sc.D. Thesis, M.I.T., June, 1953.

[54] Parkes, E. W., *The Design of Wings for Minimum Thermal Stress*, Summary of Paper Read at a Conference on Thermal Stress, University of Bristol, Aircraft Engineering, Vol. XXVI, No. 300, p. 52, February, 1954.

[55] Mahoney, J. J., *Some Aspects of Similarity Conditions for Supersonic Flows with Heat Transfer*, S.M. Thesis, Dept. of Aero. Engrg., M.I.T., June, 1954.

[56] Horton, W. H., *Laboratory Simulation of Kinetic Heating*, Aircraft Engineering, Vol. XXVI, No. 302, p. 138, April, 1954.

[57] Sandorff, P. E., *Design of Structural Models, with Application to Stiffened Panels Under Combined Shear and Compression*, Paper presented at the 23rd Annual Meeting of Institute of Aeronautical Sciences, January, 1955.

[58] McCarthy, J. F., and Halfman, R. L., *The Design and Testing of Supersonic Flutter Models*, Paper presented at the 23rd Annual Meeting of the Institute of Aeronautical Sciences, January, 1955.

[59] Dryden, H. L., and Duberg, J. E., *Aeroelastic Effects of Aerodynamic Heating*, Paper presented to Fifth General Assembly AGARD, Ottawa, Canada, June, 1955.

Discussion of the Lecture

John E. Duberg, Chief, Structures Research Division, NACA, Langley Field: If one considers the subject matter of the recent Wright Brothers Lectures, he is impressed with the fact that what seems a large share of them have been concerned with the problems of the construction of the air frame. The presentation we have heard this afternoon has continued that trend and by its broad coverage of the construction problem has given us the reasons. It should be clear from the presentation by Professor Bisplinghoff that the modern aircraft structures designer cannot look about him and find such a ready solution to his structure problems as did the Wright Brothers when they borrowed the bridge truss from the civil engineers. The time has long passed in the development of aircraft when he could go off by himself with a few static loading criteria and build a satisfactory structure within a high-performance aerodynamic form. And now, after he has gained a firmer appreciation of the interaction of aerodynamic forces and the elasticity of the structure, he is confronted with the fact that if man is to fly faster, he must design an air frame that can perform satisfactorily when surrounded by a boundary layer of enormous thermal potential.

When one ponders on the multitude of problems with which our speaker has confronted us, and he has made no mention of power plants or stability and control, it is possible that a feeling of pessimism may be engendered in the listener. It may therefore be in order to see if one can find some reasons to be optimistic about the future. Because optimism thrives on the knowledge and the feeling that the situation is under control, it might be well to review briefly some of the things we do know.

The gravest aspect of flying at ever-increasing speeds is the heating of the air frame. It is convenient to consider its effects on the air frame in two parts—the first, when the air frame is at uniform temperatures, and the second, when the temperature distribution varies throughout the structure. Sufficient evidence exists to indicate we can predict, within usual engineering accuracy, the strength and stiffness of the air frame at any uniform temperature level. These predictions are based on properties over a wide range of temperatures and heating histories. While this is no small task, it can be done and is being done on a large scale. It is in this part of the heating problem that lies the so-called thermal barrier. It is a barrier not on speed but on the temperatures that materials can stand. But, while the aircraft equilibrium temperature is strongly dependent on speed, it also depends on altitude. At high altitude there can be a considerable amount of cooling by radiation. This cooling is sufficient to enable us to use not too unusual materials beyond the Mach Number of 6 which Professor Bisplinghoff has set as the range of immediate interest. Therefore, when we fly faster, we will fly higher.

The second aspect of the heating problem—that is, the possibility of the existence of wide variations of temperature in the air frame—is the one on which the least amount of firm knowledge exists. This situation is rapidly changing in that experimental equipment now exists for the simultaneous heating and loading under realistic conditions of air frame components. The M.I.T. equipment has been described today by Professor Bisplinghoff and that of the NACA has been described by this reviewer on other occasions. The test results that have been obtained from the NACA equipment indicate that, for redundant structures, the thermal stresses which arise from the nonuniform temperatures

can lead to significant reductions in stiffness and, when combined with the stresses due to external loading, can cause wrinkling of the plate elements. These effects are extremely deleterious to the integrity of the structure but fortunately are under considerable control of the designer. Therefore, much of the design for high temperatures will be concerned with devising clever methods of avoiding thermal stressing while still retaining the efficient structural form which is the modern airplane. Such structures may undergo considerable thermal stress-free distortion, but their strength and stiffness will be as predictable as that of the air frame at uniform temperature. On this point I have considerable confidence in the inventiveness of the American engineer and research man.

If there is any cause to be concerned by the broad presentation made by Professor Bisplinghoff, it does not lie among the many technical problems but rather in the final figure of his paper which shows that in this time of great technical challenge to the young of this country there seem to be few acceptors. None of them need fear the challenge if they prepare for it by associating with professors of the caliber of our speaker, and I do recommend they associate with him.

Y. C. Fung, Associate Professor, California Institute of Technology: Professor Bisplinghoff is to be congratulated for his excellent presentation of a comprehensive picture of the thermal and aeroelastic problems of high-speed flight. Clear statements of these problems are offered. By means of an example of a future supersonic fighter, he indicated how the practical importance of these problems can be assessed. As is well known to all engineers and research workers, a clear formulation of a problem is always the most decisive step toward its successful solution. In this respect Professor Bisplinghoff has been uniquely successful. He has undoubtedly made a most timely contribution to aeronautics.

One could not have listened to the lecture without being impressed by the richness of the field of aerothermoelasticity. As a field of research, it offers nice problems for people of all caliber and inclination. To a mathematically inclined mind, here is the basic eigenvalue problem of nonselfadjoint differential systems or integral equations with unsymmetric kernels. To a person interested in nonlinear mechanics, here are the problems involving large deflection of plates and shells and such nonlinear oscillations as the flutter of buckled panels. For a man well versed in special functions, here are the ideal problems of oscillating airfoils, variable thickness plates, and shells of special forms. For one who likes fundamental physical problems, here are the problems of thermal radiation, the theory of strength of solids at elevated temperature, and the basic problem of fatigue of metals. For one who likes statistics, here are the problems of random loading—some may be treated as stationary stochastic processes and others must be considered as nonstationary. Finally, for an inventive mind, here are innumerable chances of invention.

There is no question about the practical importance of these studies, for a success in solving any of these problems cannot but result in more efficient and lighter structures. In fact, the reward of research in structures field is almost always felt immediately. A saving of structural weight reduces the inertia loading, the power and fuel required, and, finally, the wing area, aerodynamic loading, and structural cross section. The reduction proceeds in such a closed loop that, at present, the growth factor may be as high as 15 or 20 for high-performance machines. In other words, 1 lb. of structural weight saved may result in a reduction of 15 to 20 lbs. of gross weight. Thus the importance of accurate structural analysis is readily apparent.

Professor Bisplinghoff's lecture demonstrates most dramatically the expanding domain of aircraft structures in the last decade. Most of the problems discussed in this lecture would not be regarded as belonging to the proper field of structures a few years ago, yet they now form a necessary part of a structural engineer's knowledge.

Would the broadness of the structures field, the challenge of many fundamental and difficult problems, the richness in the possibilities of research and invention, and the practical importance of any success in this field be enough to attract young engineers of the future to this field? Could it be that the most important contribution of the Nineteenth Wright Brothers Lecture lies in telling more people about how the structures engineers are having a good time these days?

E. Z. Gray, Stress Unit Chief, Boeing Airplane Company, Seattle Division: It is always an honor to be asked to take part in the Wright Brothers Lecture. It is doubly so when our lecturer is as notable as Professor Bisplinghoff. His discussion of the structural problems associated with high-speed flight is most valuable in the comprehensive summation of the problems associated with high supersonic speeds.

Since Professor Bisplinghoff's discussion concerns primarily the problems associated with short-range airplanes, I would like to supplement his lecture with a look at some of these design factors as applied to longer range airplanes. Certain conclusions resulting from Mr. Bisplinghoff's investigation will be modified when one considers airplanes which fly for longer periods of time. Let us therefore consider a typical multiengine airplane which could be either a transport or bombardment type.

Fig. 1 shows a hypothetical airplane of this type. It will be noted that the airplane has a swept wing with several engines mounted along the wing. On the left-hand wing is shown the typical subsonic load distribution. The distribution has been modified to account for the effects of the nacelle on the wing loads. It will be noted that the center of pressure of this load lies along

the quarter chord. It is apparent that there are no sharp discontinuities in the spanwise loading. On the right-hand wing is shown the air loading for a supersonic condition of approximately Mach 2. The very marked difference in the distribution of loading from the subsonic case will be noted. The shock pattern caused by the inboard nacelle is shown superimposed on the normal wing load. Additional shock effects, not shown, will be caused by the inboard power-plant installation as well as fuselage wing intersections, etc. The complexity of the loads resulting from these many discontinuities makes it evident that a very ambitious test program involving both models and full-scale flight will be required to determine accurately the summation of these effects. This only bears out Professor Bisplinghoff's comments that a much enlarged effort in the field of air loads will be required for airplanes of a supersonic type. It is believed that this represents at least a threefold increase over the present loads analysis, and probably even greater than that.

Fig. 2 shows the spanwise aeroelastic load distribution on the wing of the hypothetical airplane shown in Fig. 1. The chart in the upper right-hand corner shows three design points selected for this airplane. The low Mach Number design point occurs near sea level and near the rough air speed of the airplane. The transonic case was selected to be the minimum flight condition possible in the transonic speed regime. The supersonic case was selected to be the maximum combination of Mach Number and equivalent air speed. From the main chart, it is readily apparent that the most outboard center of pressure occurs in the subsonic case. However, since the transonic loading has a further aft center of pressure, and since the bending axis of the wing is not at right angles to the centerline of the fuselage, the transonic case actually produces higher bending moments on the wing. The chart shows that the supersonic center of pressure is far inboard of either of the other two flight conditions. This effect can compensate for the reduction in wing strength resulting from aerodynamic heating in determining the requirements for bending material in the wing, provided the proper choice of material is made.

Fig. 2 also shows the effect of engine thrust on span loading. Since a very large thrust will be required to fly to high supersonic speeds and since the wings will be extremely thin, engine thrust can cause very marked deflections of the wing. The curve shown is for a thrust ratio of two, between the subsonic and supersonic cases. It is also readily apparent that such large changes in span loading will have a considerable effect on the airplane flight characteristics.

Professor Bisplinghoff mentioned that greatly expanded flight tests will be required to check both air loads and thermal effects on airplanes which will fly the high Mach Numbers. We are in complete agreement with him on this score. It is our belief that the scope of such flight testing will increase many times that of the present structural programs and complicate the instrumentation requirements exceedingly.

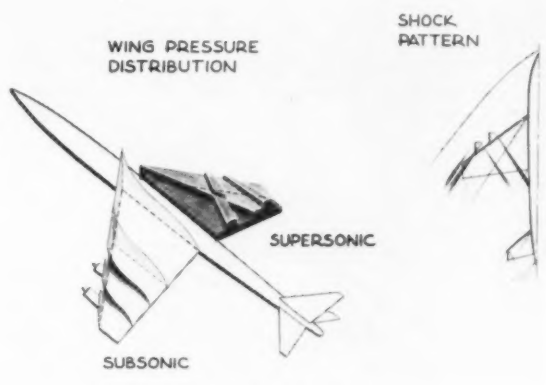

FIG. 1. Air load distribution.

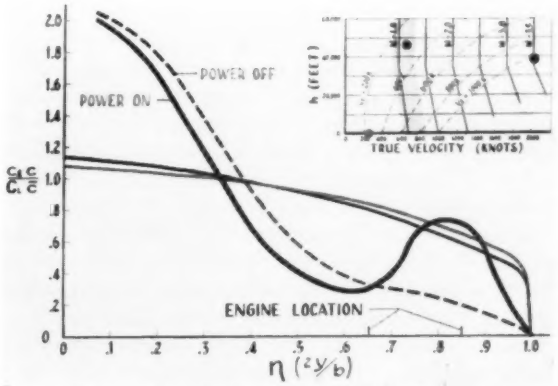

FIG. 2. Aeroelastic spanwise load distribution.

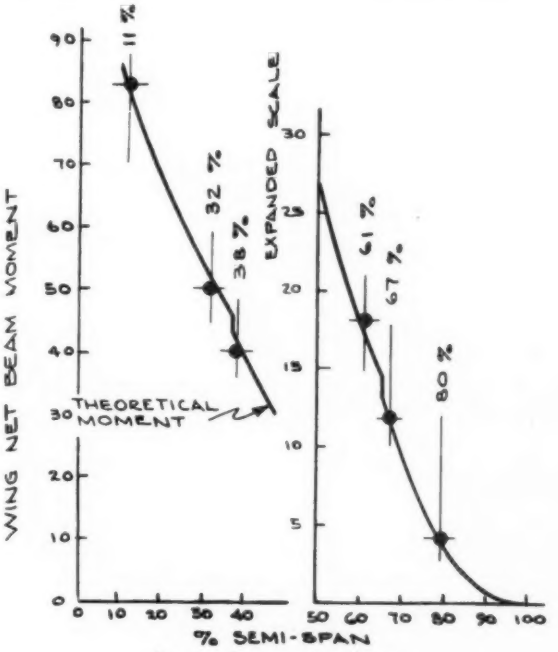

FIG. 3. Low-speed pull-up.

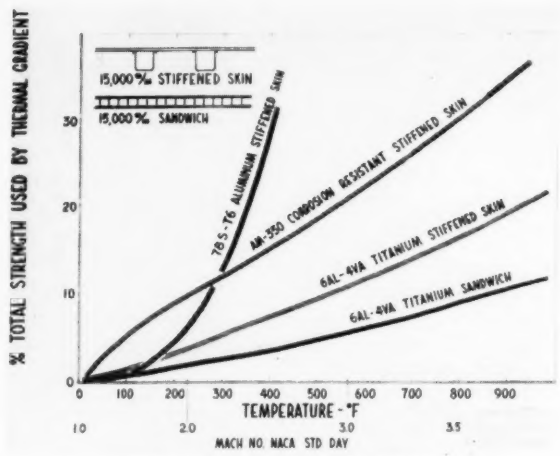
% TOTAL STRENGTH USED BY THERMAL GRADIENT
15,000% STIFFENED SKIN
15,000% SANDWICH
75-T6 ALUMINUM STIFFENED SKIN
MN-350 CORROSION RESISTANT STIFFENED SKIN
6AL-4VA TITANIUM STIFFENED SKIN
6AL-4VA TITANIUM SANDWICH
TEMPERATURE - °F
MACH NO. NACA STD DAY

FIG. 4. Effect of thermal gradient.

Fig. 3 is presented to show that we are already engaged in flight-test programs of this type. The curve shown is the bending moment for a wing of one of our airplanes as determined by a combination of wind-tunnel testing and theoretical analysis. The dots shown are the flight-test results obtained to check the computed air loads. The close agreement shown gives us confidence that present flight-test techniques can be expanded to include subsonic and supersonic flight demonstrations. It is realized that aerodynamic heating is going to affect materially the procedures necessary to measure flight loads on airplanes of the high supersonic speed class. It may require several different techniques to handle the many environmental problems involved in such a program.

Professor Bisplinghoff presented information showing the relative effect of thermal heating on different materials. He presented information which showed the induced stresses on a plate of various materials supported on all edges and subjected to a very rapid rate of heating. It will be recalled that titanium alloy was shown to be the least affected.

Fig. 4 presents additional information on this subject for typical aircraft construction. The curve plots the per cent of total strength used by the thermal gradient for different materials which may be used for a typical airplane wing. This effect was computed for a condition occurring during acceleration up to the Mach Number shown along the ordinate. Our data confirms the conclusions reached by Professor Bisplinghoff since a wing constructed of titanium is least affected by the transient effects of aerodynamic heat. For instance, up to 500°, only 3 per cent of the total strength available in titanium is used by the thermal induced stress. It is readily apparent also that titanium sandwich construction is very superior to the typical stiffened skin structure in this regard. If the wing is made of steel, a much larger per cent of its strength is lost to these induced stresses. This curve confirms again the need for ingenious methods of construction to minimize the thermal problems in high-speed aircraft.

Finally, the structural designer realizes that, even though a much larger effort will be required to solve the many added problems to produce a successful high supersonic airplane, the time at his disposal will be quite comparable to the development time for past airplanes. Since his manpower is limited, it will therefore require judicious use of fundamental theory and practical evaluation of the relative importance of these problems to meet the time goals. It follows then that more reliance will be required on flight tests to develop fully the potential of aircraft of this type.

L. M. Hitchcock, Staff Engineer, Boeing Airplane Company, Seattle Division: First, I would like to compliment Professor Bisplinghoff on an excellent summary of the structural aspects of high-speed flight. It is gratifying to have a first-hand realization of the contribution that M.I.T. is making to the advancement of technical knowledge in this field.

Professor Bisplinghoff has discussed a number of the structural problems which must be considered in the design of high-speed airplanes. As a supplement to his paper, I believe Figs. 1 and 2 will be of interest.

Fig. 1 is an indication of the structural efficiency of various materials. The vertical scale is weight-strength ratio with aluminum alloy at a base point of 1, and the horizontal scale is temperature and Mach Number. These data are based on the ultimate strength characteristics of these various materials.

This figure illustrates that in the range of temperatures being considered, titanium alloys have the optimum or most efficient weight-strength characteristics in comparison with the other materials. In addition to this factor, titanium has a further advantage over steel from a structural efficiency standpoint in areas which are critical in compression and subject to crippling, buckling, and column strength considerations. Since titanium is lighter and has lower allowable stresses, a given structure will have more thickness in titanium than in steel and, therefore, will have better characteristics from the standpoint of the above mentioned compression considerations. It is also believed that titanium may have even a further advantage over steel in the higher temperature ranges since its melting point is higher than steel. From this consideration, it would appear that titanium alloys have a development potential which would further improve the strength characteristics at a higher temperature as compared with steel.

From the standpoint of development of high-speed airplanes, particularly in the military, it is believed that significant gains performancewise will be realized with the utilization of titanium alloys within the temperature and speed ranges illustrated in Fig. 1 because of the structural weight saving which can be realized. We are optimistic in the consideration of using titanium alloys but realize that certain problems must be solved. Considerable improvement will have to be made by the material manufacturers relative to quality and quan-

tity of the higher strength alloys in titanium. In addition, for large airplanes of the bombardment type, there is a requirement for relatively large sheet sizes as compared to fighter-type aircraft. Facilities must be acquired by the titanium producers to enable them to roll large sheet sizes and also to heat-treat these large sheets. Considerable work must also be done to provide extrusions of relatively long lengths and of satisfactory gages and tolerances. There is also much work to be done in establishing design and manufacturing know-how for airplanes constructed of titanium.

Fig. 2 is a plot of wing beam deflection versus wing semispan which illustrates on the lower curve wing deflection of a large airplane under level flight conditions. The upper curve represents wing deflection in level flight plus an incremental deflection due to 0.2 of 1 per cent permanent deformation in the bending material. The 0.2 of 1 per cent happens to be the value of permanent deformation which we structural engineers have used for years in establishing yield points of materials.

Fig. 2 is purely for illustrative purposes, but it indicates the significance of creep in a large airplane if we were to use the same criteria in establishing the upper limit of working stress for some temperature and time period with the same criteria used for establishing yield point. We believe that creep may be a very important factor for large bombardment-type airplanes in which the operating stress level is three to four times that of a fighter-type airplane and where the time at temperature per mission is very much longer in a fighter-type airplane. A considerable amount of investigation must be done to determine creep criteria especially for low load factor airplanes. It is also believed that creep data must be obtained with considerably greater accuracy than is currently being obtained. We visualize that structural materials and full-scale fitting and joints will have to be cycled under various conditions of alternating stresses and temperature cycling. Creep testing of this nature may well be more critical for bombardment-type airplanes than the considerations of structural fatigue.

I would like to thank Professor Bisplinghoff for his very excellent presentation because it has indicated to the audience the fact that we structures engineers really have our work cut out for us.

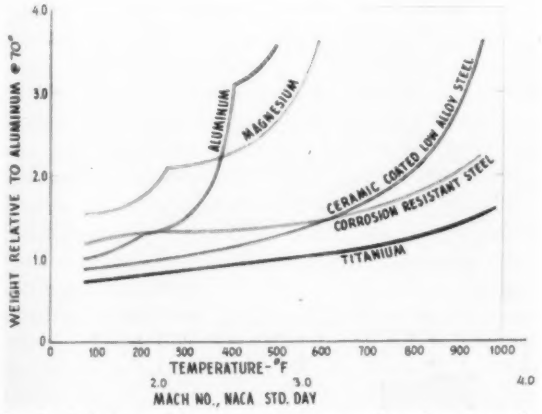

FIG. 1. Relative weight versus temperature based on strength.

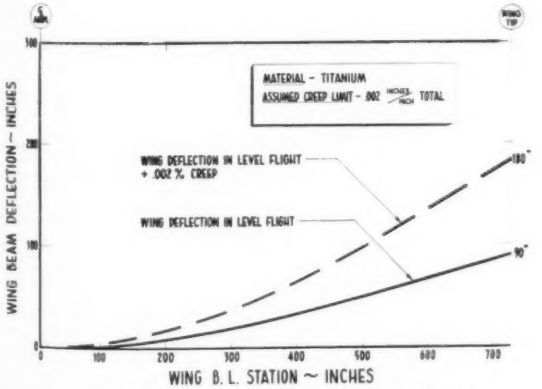
WING BEAM DEFLECTION ~ INCHES
WING TIP
MATERIAL - TITANIUM
ASSUMED CREEP LIMIT - .002 INCHES/INCH TOTAL
WING DEFLECTION IN LEVEL FLIGHT + .002 % CREEP
WING DEFLECTION IN LEVEL FLIGHT
180°
90°
0 100 200 300 400 500 600 700
WING B. L. STATION ~ INCHES

FIG. 2. Effect of structural creep on wing deflection.

N. J. Hoff, Head, Department of Aeronautical Engineering & Applied Mechanics, Polytechnic Institute of Brooklyn: Probably the most important function of the Wright Brothers Lecture is to tear outstanding scientists and engineers away from their everyday duties and detail problems and compel them to find time for a review—from a broad standpoint—of their own work, of that of their associates, and of the literature on their subject all over the world. The result is a review paper of the highest caliber which, without this compulsion, would probably never have been written. I believe that everyone agrees that such papers are badly needed by the profession. We should be grateful therefore to those who made the Wright Brothers Lecture series possible; we should also be thankful for the selection of Ray Bisplinghoff as this year's lecturer because in this manner we were given a most authoritative record of the state of the art of aerothermoelastic analysis.

It is particularly fortunate that this year's lecturer should be a man whose lifework has been aeroelasticity. This makes him capable of talking with equal authority on problems of structural analysis and aerodynamics. Before the last war, these fields were essentially independent, and men working in them very often did not even understand one another's language. In today's and tomorrow's supersonic airplanes and hypersonic missiles, the former clearly defined boundaries merge, and an extreme specialization is accompanied simultaneously by the development of aerophysicists who must understand the behavior of rarefied gases, phase changes in alloys of metals, thermodynamics, and heat transfer, as well as aerodynamics and stress analysis. It was a great pleasure to listen to a review of the interrelation of all these fields of study.

It is obvious that all details cannot be treated in a single lecture, or in its written version, even with the amount of space allotted to the Wright Brothers Lecture. For this reason one should not accuse a Wright Brothers Lecturer of omissions. Nevertheless, I would

like to add one item to the topics discussed. Professor Bisplinghoff has shown in an example that creep is not likely to alter significantly the thermal stresses in aircraft structures. He has also mentioned that creep must be considered as a possible cause of fracture and that the magnitude of the creep deformations accumulating during the lifetime of the aircraft will have to be checked in the future. It seems to me that another effect of creep may be even more important than the ones mentioned. As every aircraft structure is statically indeterminate, the stress distribution in it under given loads cannot be calculated from the equations of equilibrium alone. It is governed in an equal measure by the conditions of compatibility of deformations and by the load-deflection relations. The latter are the generalized expressions of Hooke's linear law when the structure is assumed perfectly elastic; this assumption was practically always made in stress analyses performed in the past. In the presence of creep, Hooke's law must be replaced by the creep law which is highly nonlinear for our structural metals. Consequently, when high temperatures cause noticeable creep deformations in the structure of a supersonic airplane or missile, the stresses are distributed entirely differently than they are when Hooke's law is valid.

I would like to close by emphasizing once more how much interesting and up-to-date information was presented to us in this lecture. Professor Bisplinghoff brought out the fundamental concepts of the new problems, and, at the same time, he never forgot the practical implications. It was particularly valuable that he devoted space to the methods of avoiding high temperature effects by ingenious design. I would like to congratulate him on a most successful performance of a very difficult task.

Alexander Kartveli, Vice-President, Republic Aviation Corporation: Professor Bisplinghoff's paper comes at a very opportune time and is most welcome to an engineering audience. Most of the research and creative engineering work in the last decade has been devoted to refinements of aerodynamic design and problems of stability, control, power plant, equipment, etc. In recent years, however, the advent of supersonic aircraft and the anticipation of much higher speeds in the near future have drastically changed the situation with the result that problems of structural engineering now assume fundamental importance.

This lecture, in my opinion, is an outstanding piece of work on today's status of our knowledge of aircraft structural problems with a scientific outlook for future possibilities. In a very concise way, Professor Bisplinghoff has systematically organized this material in good logical sequence giving us a clear picture of what we know, where we stand, and what lies ahead of us. To the data already published, he has added valuable results of his own experience and that of M.I.T. Available information and known mathematical approaches are described in a clear way and are supplemented by suggestions and some definite ideas for further improvement of our knowledge.

Professor Bisplinghoff's lecture encompasses so many interesting subjects that it is impossible in the short time allotted to me to comment on the entire scope of this outstanding paper. I, therefore, shall confine my remarks to aspects of the paper which appeal to me as the most novel and interesting in aircraft design. These are the effects of heat on the structure of the hypothetical fighter referred to in Professor Bisplinghoff's lecture.

While thermal stresses (stresses due to temperature gradients) and methods for their computation are very comprehensively discussed by Professor Bisplinghoff, it must be realized that temperature stresses resulting from use of different materials and their coupling with thermal stresses very often occur in a design with consequent complications and must, therefore, be given equal emphasis.

In the type of fighter considered, sources of heat are twofold; outside, due to aerodynamic heating, and inside, due to power plant and various accessories. In many instances the inside heat has more pronounced effects than outside heating. A fuselage bulkhead, for instance, may be subjected to 900°F. on an inner flange and only 500°F. on the outer flange under steady-state conditions. For efficient design, different materials, such as titanium and steel, should be used in the same structural element, thus introducing different coefficients of thermal expansion in the presence of a temperature gradient. Complex stress patterns will then arise which belong to both the thermal and temperature category. Cases of this kind are often encountered, and it is believed that for practical aircraft design such cases should be given more consideration and study.

Regarding methods for computing thermal stresses, the subject is very well covered in Professor Bisplinghoff's paper. It is felt, however, that from a practical engineering point of view, the application of energy solutions presents advantages over purely analytical methods of the theory of elasticity. Although less rigorous, energy methods are sufficiently accurate for engineering needs and are more flexible when combined with the use of high-speed electronic computers.

Professor Bisplinghoff very justly emphasizes the complex nature of stress flow in an aircraft structure and advises very careful analysis with particular attention to structural discontinuities so as not to invalidate the main theory. Engineering experience shows that the validity of any stress computing method should be checked by tests at elevated temperature. Such tests are necessary primarily because the numerical calculations ignore effects of slippage in riveted and bolted joints and local plastic yielding of the material. Unfortunately, the technique for such tests is not yet well developed and much must be learned in this field. In this connection, it will be of interest to give some figures obtained in actual design practice. Calculations have shown that the largest values of thermal stress occur in the main fuselage bulkheads and in the leading

edge of the wing. These stresses may increase the stresses due to aerodynamic loads by as much as 30 per cent. It has also been found that, in the wing box cover, the effect of thermal stress is of the order of 15 per cent. A study of various missions shows that wing thermal stresses are not much affected by the actual rate of aircraft acceleration.

Failure due to creep, a type of failure phenomenon associated with thermal effects, is discussed in Professor Bisplinghoff's paper, and a brief outline of this complex problem and a possible method of approach is given. I feel that establishing a criterion for creep is a very important phase of structural design for supersonic aircraft, and, as this is a relatively new problem, more elaboration on the subject would be desirable. While I agree with the general approach suggested by Professor Bisplinghoff, I should like to emphasize the fact that unless a practical criterion for creep is established on statistical data, severe unnecessary penalties in weight may be incurred. Such a criterion should give the period of time during which the aircraft, in the course of its life, would be subjected to various levels of stress and temperature. To do this, it is necessary in the same analysis to combine the type of mission of the aircraft, its life expectancy, total time at maximum temperature, and frequency of application of the load factor. A high-speed fighter airplane is not designed to fly at its maximum or near maximum Mach Number during the entire mission, nor does it experience its maximum load factor continuously over the whole flight regime. As a matter of fact, the time at maximum load factor is very short as compared to the time of the whole mission. Knowing the desired life expectancy and a definite operational mission, it is possible to predict the cumulative temperature cycle for each mission. Statistical data on duration and frequency of load factor can then be used to compute for each value of temperature the total time during which the aircraft will be subjected to a given stress level. A combination of these results will give the creep criterion as described above.

Some studies of this type have shown that a supersonic-type fighter aircraft will be at maximum stress level and maximum temperature for approximately $\frac{1}{2}$ hour for each 1,000 hours of its life. Several other studies of practical supersonic design have brought to evidence that creep in general is not critical for normally accepted types of missions and required load factors. It has been found that short-time material properties still govern most of the structural design, and, in many instances, design will be critical for cold temperature conditions at low Mach Numbers since loading patterns are generally more severe in the transonic regime than at high supersonic speeds. Of course, if for some tactical reason an excessively long period of time is required at high temperature for a mission, the situation will then change and creep may become a critical factor. However, a mission should be carefully evaluated so that undue weight penalty is not incurred. Also, proper emphasis should be given to the economics of the airplane as compared to the importance of the mission.

Professor Bisplinghoff's final analysis of fundamental research requirements is very true and enlightening, and I wholeheartedly agree with him. I think, however, that some emphasis should have been put on the great value and utility of flight-test methods whereby measurements of strains could be performed under the proper environment of combined temperature and load conditions. Further consideration should also be given to obtaining and analyzing service experience on structures subjected to intermittent periods of various temperature and stress levels. Present day fighter aircraft equipped with accelerometers and thermocouples afford the pilot knowledge of load and temperature levels attained in maneuvering flight.

Considering the wealth of information that Professor Bisplinghoff has brought to us, this lecture will be long remembered by design engineers and will often be consulted for data, general information, and last, but not least, for inspiration.

Jerome F. McBrearty, Chief Structural Engineer, Lockheed Aircraft Corporation: It is an honor indeed to be asked to comment on this Wright Brothers Lecture, and I would like to show my appreciation by being brief. First, I think we are all deeply indebted to Professor Bisplinghoff for putting together this monumental work on aerothermoelastic considerations and for his appraisal of the developments and gaps in this field. This paper will be used as a reference by aircraft engineers for a long time to come. Second, I am grateful for the effort he has made to separate the complete problem as much as possible into manageable parts. Perhaps the most perplexing aspect of this subject is the interdependence of aerodynamics, thermodynamics, and elasticity, and there has been little success in carving it up into pieces that could be attacked either analytically or experimentally. The lecturer has succeeded in this to a marked degree, and I regard that a significant contribution in itself.

Third, Professor Bisplinghoff has not neglected experimental techniques, although I must say that the methods at hand look pretty grim. The development of the high-temperature structure by analytical means alone appears most unlikely, as evidenced by the great dependence on testing in the engine field. Consequently, I think we are in great need of more testing methods that are practical for air-frame companies to use for development work. In this regard, I can report the successful use of a battery-operated radiant-heating device at Lockheed. This facility uses a large number of commercial 6-volt batteries, provides some heat programming by switching, and precludes a high peak power demand. In this respect, it is analogous to a blowdown wind tunnel since the batteries can be recharged for another run.

Lastly, I think it is significant that once again the Wright Brothers Lecture has been devoted to aircraft

structures. In recent years, we have heard the P. B. Walker and Bo Lundberg lectures on structures and William Littlewood's which dealt considerably with structural matters. I believe this illustrates the growing importance of the structural design in determining what the aircraft of the future can and cannot do. Professor Bisplinghoff has done much in the 1955 Wright Brothers Lecture to advance the state of the art in the field of high-speed structures by organizing and analyzing the work done and sharpening up the direction for the work ahead.

C. H. Stevenson, Chief of Strength and Weights, Douglas Aircraft Company, El Segundo Division: I would like to make one comment on Professor Bisplinghoff's unusually complete lecture. It concerns the solution of the heat conduction equation.

It is relatively simple to solve this equation on an analog computer—in fact, this method was first given in 1942 by Paschkis and Baker.[1] I would like to outline very briefly the method of solution on an analog computer. In order to prevent complications, I will consider heat flow in only one direction.

Suppose we have a slab of material having dimensions ΔX, ΔY, and ΔZ, of specific heat C, thermal conductivity K, and density ρ. Let Q_X be the rate of heat flow per unit time across one face and let T_X be the temperature of that face. We know that the rate of heat storage in the slab is the product of thermal capacity and rate of increase of temperature—that is, Eq. (1). We also know that the flow of heat is in the direction of greatest temperature drop and proportional to the rate of change of temperature with space—that is, Eq. (2).

If we now consider the resistor capacitor network on the right and its Eqs. (3) and (4), we see that by a happy coincidence the two sets of equations are analogous. Thus the analogy between the mechanical and electrical systems is complete if we note the following correspondence:

$$Q_X \leftrightarrow I_X$$
$$T_X \leftrightarrow E_X$$
$$(\Delta X\, \Delta Y\, \Delta Z)c\rho \leftrightarrow C$$
$$(\Delta Y\, \Delta Z/\Delta X)K \leftrightarrow (1/R)$$

This analog method has certain definite advantages due largely to the fact that a network of resistors and capacitors is trouble-free and inexpensive even when a large number is used as in heat conduction in three dimensions. Moreover, complicated body shapes can be readily handled in this way thus eliminating a serious disadvantage of some of the analytical methods as pointed out by Professor Bisplinghoff. A very fine analysis of the inherent errors in an analog solution are given in a paper by Guile and Carne.[2]

Finally, cases where the thermal properties vary from point to point can be approximated quite well by an analog computer. Very recently, D. R. Otis[3] has treated thermal properties of the conducting medium that are arbitrary functions of the temperature by using photoformers and servodriven resistors.

References

[1] Paschkis, V., and Baker, H. D., *A Method for Determining Unsteady-State Heat Transfer by Means of an Electrical Analogy*, Trans. ASME, Vol. 64, No. 2, February, 1942.

[2] Guile, A. E., and Carne, E. B., *An Analysis of an Analog Solution Applied to the Heat Conduction Problem in a Cartridge Fuse*, AIEE, Communication and Electronics, January, 1954.

[3] Otis, D. R., *Electric Analogy to Transient Heat Conduction in a Medium with Variable Thermal Properties*, to be presented at the National Simulation Conference sponsored by IRE, on January 19, 1956.

M. J. Turner, Structural Dynamics Unit Chief, Boeing Airplane Company, Seattle Division: Professor Bisplinghoff has presented some very interesting data showing the historical trend of speed capability in relation to wing torsional frequency for fighter airplanes. From this it may be inferred that closer attention to distributions of mass and stiffness is now required in order to achieve adequate flutter margins with minimum structural weight. A similar trend has been apparent in the large bomber field during recent years. However, the wing flutter problem for the large bomber with engines supported elastically from the wing is considerably more complex, largely due to the greater number of different types of wing flutter that can occur. For this reason, there is no single parameter which can be used as an index of the relative gravity of the flutter problem. Nevertheless, it is quite evident from our investigations on specific projects that the problem of wing flutter has become more acute and that requirements for flutter prevention will have an effect on airplane configurations and possibly on structural stiffness requirements of future designs.

Professor Bisplinghoff has indicated that thermal effects on structural stiffness and certain non-linear effects due to wing thickness are likely to create a critical flutter situation at supersonic speeds. In this connection, it may also be noted that the airplane characteristics which are required for supersonic speed capabilities also tend to produce a configuration for which the transonic flutter problem is more critical. Hence we

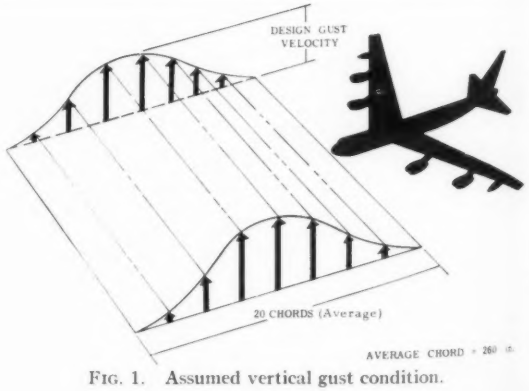

Fig. 1. Assumed vertical gust condition.

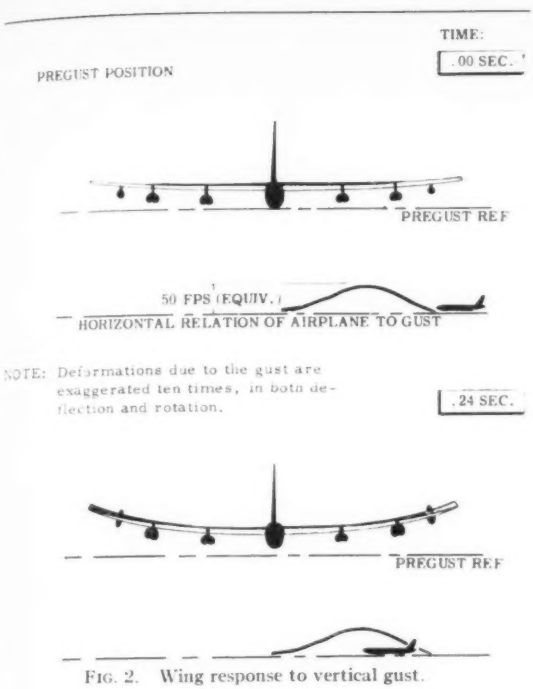

FIG. 2. Wing response to vertical gust.

feel that flutter in the high subsonic and transonic speed ranges still presents a very substantial problem.

The lecturer has also emphasized the important point that nonuniform structural heating may produce reductions in stiffness and in the natural frequencies of some structural components and that these changes may tend to promote new types of flutter and to reduce the critical speeds of other modes which can also occur at lower speeds. It appears that the new phenomena which must be guarded against are generally associated with conditions where compressive stresses induced by nonuniform heating tend to induce buckling of some portion of the structure. It is hoped that the structural designer will be able to evolve configurations which are not actually subject to thermal buckles. However, as the lecturer has pointed out, the presence of compressive stresses due to heating can produce a substantial reduction in natural frequencies of structural components even though the temperature is well below the critical value. For example, we may consider the case of a wing with heated edges having a relatively light trailing-edge structure which is incapable of influencing the torsional frequency of the wing as a whole. When heated to a sufficiently high temperature relative to the main wing structure, it will buckle into spanwise waves, and at temperatures less than critical, it will exhibit a substantially reduced natural frequency in a mode of vibration which is closely similar to the buckling mode. There appears to be a possibility that this trailing-edge mode could couple with one of the primary wing modes to produce a flutter condition closely related to wing-aileron flutter. It is to be expected that phenomena of this nature will be quite nonlinear; presumably they can be avoided by providing some sort of expansion

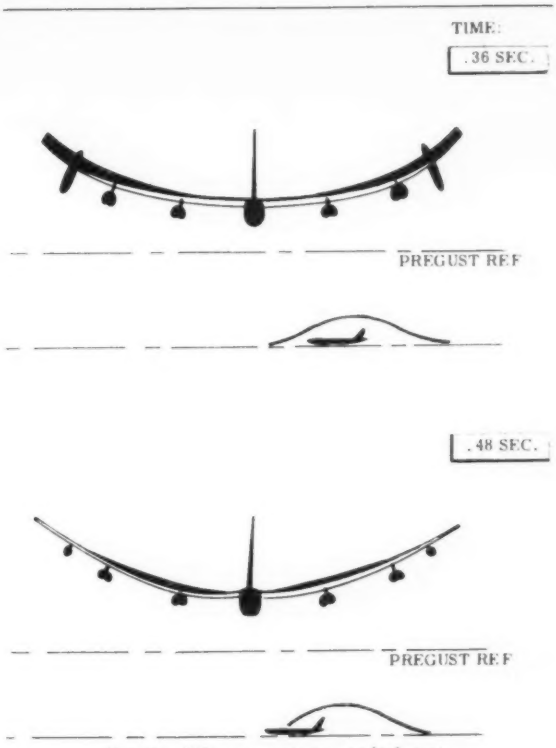

FIG. 3. Wing response to vertical gust.

joints in the leading and trailing edge.

It has been clearly established by the lecturer that there is a need for dynamic gust load analysis, including effects of structural vibration, on fighter aircraft which

(*Continued on page 367*)

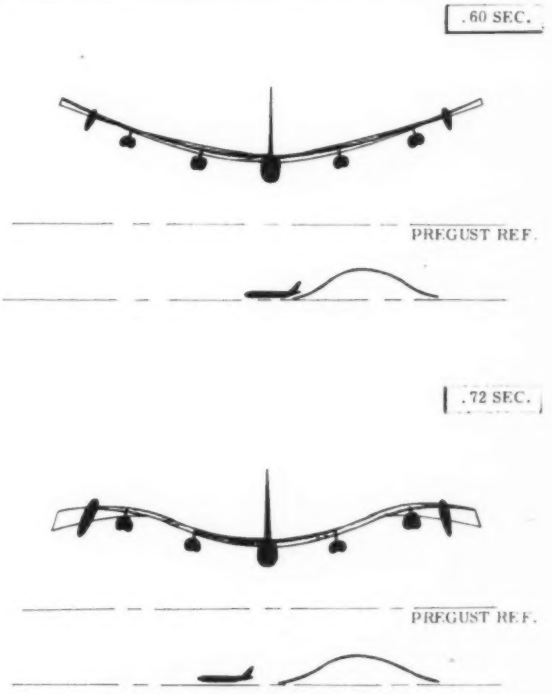

FIG. 4. Wing response to vertical gust.

A Method for Predicting Lift Effectiveness of Spoilers at Subsonic Speeds*

ARTHUR L. JONES,† OWEN P. LAMB,‡ AND ALFRED E. CRONK**

FluiDyne Engineering Corporation

Summary

As part of an investigation concerning gust alleviation controls, it was necessary to develop a means for predicting the lift effectiveness of spoilers. Methods for estimating the lift effectiveness of ordinary flap-type control devices can usually be developed by application of thin airfoil theory. However, control devices depending on flow separation for their effectiveness, such as spoilers, have not proved amenable to analyses based solely on potential flow considerations. In the case of plain spoilers, a semiempirical approach utilizing both lifting-surface theory and experimental data has provided a satisfactory basis for analyzing variations in spoiler lift effectiveness. The method for prediction which evolved proved to be applicable at subsonic Mach Numbers up to approximately 0.95 for an angle-of-attack range restricted to an upper limit of about 6°. The method takes into account the effects of the following parameters: aspect ratio, taper ratio, sweepback, airfoil thickness ratio, chordwise location and spanwise location of the control, and spanwise extent of the control. A design chart presentation has been used to show the relative effects of variations in each parameter and to provide for a rapid, straightforward prediction procedure.

Symbols

A = aspect ratio

C_{L_ζ} = rate of change of lift coefficient with spoiler projection for symmetrically deflected spoilers on each semispan

M = free stream Mach Number

c = wing chord measured normal to the quarter-chord line, ft.

c' = streamwise wing chord, ft.

h = spoiler projection, ft.

r = ratio of spoiler lift effectiveness at a given value of a parameter to the effectiveness at the basic value

t = maximum airfoil profile thickness, ft.

x = chordwise location measured from leading edge along profile normal to quarter-chord line, ft.

Λ = sweepback angle of the quarter-chord line

ζ = spoiler projection in terms of streamwise chord, (h/c'), positive downward

η_e = spanwise extent of spoiler, measured in semispans

η_m = spanwise location of mid-span point of spoiler, measured in semispans

λ = ratio of tip chord to root chord

Presented at the Aerodynamics Session, Twenty-Third Annual Meeting, IAS, New York, January 24–27, 1955.

* The investigation reported in this paper is a portion of the work performed under Contract AF 33(616)-2094 with the United States Air Force, Wright Air Development Center, Aircraft Laboratory, in order to evaluate various aerodynamic control devices for gust alleviation.

† Senior Project Engineer.

‡ Senior Development Engineer.

** Associate Professor, Dept. of Aeronautical Engineering, University of Minnesota; Consultant, FluiDyne Engineering Corp.

Introduction

THE TERM SPOILER has been used to designate almost any device which can be installed on a wing and operated to spoil the flow on the upper surface, thereby decreasing the lift. If a spoiler is projected from the lower surface of a wing, it will also spoil the flow and to some extent will increase the lift; the magnitude of the lift increase being somewhat sensitive to spoiler configuration and to other conditions. The degree to which a spoiler, operated as both an upper and lower surface device, will provide symmetrical lift increments has not been satisfactorily determined as yet. Symmetry of lift effectiveness is an important factor in the consideration of spoilers as gust alleviation devices. Further research in regard to the feasibility of lower surface spoiler operation has been scheduled by the Air Force. At present, however, the lift effectiveness results derived and presented herein must be considered as representative of upper surface spoilers in particular, since the derivation was based on upper-surface spoiler data. Moreover, the results are indicative of the lift effectiveness that can be obtained using an unperforated spoiler projected perpendicular to the airfoil surface, or very nearly so. Configurations such as this are often referred to as plain spoilers and that nomenclature has been adopted herein. It is probable that the effectiveness of similar mechanical devices such as flap-type spoilers, slot-lip ailerons, and plug-type ailerons could be predicted by small modifications to the plain spoiler results. No attempt will be made, however, to include such modifications in this analysis.

The values of lift effectiveness presented herein can be considered representative of the variation of lift with spoiler projection between projection limits of 0.01 c' and 0.10 c' where c' refers to the streamwise chord. It is well known that for spoiler projections of 0.01 c' or less, a loss or perhaps a reversal in effectiveness often occurs. Moreover, beyond approximately a 0.1 c' projection the effectiveness usually begins to decrease. Thus the lift increments predicted herein will tend to be somewhat high outside the range of projections from 0.01 c' to 0.1 c'.

Method of Analysis

Recognition of the fact that spoiler operation results in a separated flow condition, leads to the conclusion that an analysis based on thin-airfoil potential-flow

theory, exclusively, would not be satisfactory. On the other hand, the experimental data on spoilers which have been compiled to date, do not contain a sufficiently comprehensive survey of the effects of all pertinent wing plan form and profile characteristics to permit the establishment of a strictly empirical procedure for predicting C_{L_ζ}, the lift effectiveness. Thus a semiempirical technique was indicated which would combine the available theoretical estimates of the effects of variations in plan form parameters such as aspect ratio, taper ratio, sweep, the spanwise location, and spanwise extent of the device with the experimentally determined effects of section parameters such as airfoil thickness ratio, angle of attack, and the chordwise location of the device. It was felt that the technique to be developed should show directly, insofar as possible, the effects on C_{L_ζ} of variations of the parameters and at the same time provide a reliable, rapid, and straightforward procedure for the calculation of predicted values.

The method that evolved, finally, was developed around certain selected basic values of the parameters. These values are tabulated in Fig. 1 along with the somewhat restrictive range of parameter values this method was intended to cover. There is no particular significance to be attached to the basic values listed in Fig. 1 except that they appeared to be either fairly average values in terms of conventional wing-spoiler configurations or reasonable starting points from which the effects of variations could be ascertained. No basic value of Mach Number was selected because it was felt that the effects of variations in the rest of the parameters could be determined throughout the range of Mach Numbers investigated, namely, 0 to 0.95, and that Mach Number, therefore, could be treated as an autonomous variable.

The plan was to determine the values of C_{L_ζ} for a wing-spoiler configuration corresponding to the combination of basic parameter values and, in addition, to determine the modifications to C_{L_ζ} which would occur when the parameters were changed to other than their basic values. In order to accomplish this, the available spoiler lift-effectiveness data on various finite-span models had to be modified to correspond to the basic configuration. Thus, initially, it was necessary to make some assumption about the manner in which these modifications could be accomplished. The assumption made was that the effect on C_{L_ζ} of a change in any one

Parameter		Basic Value	Range of Values Considered
Aspect Ratio,	A	6	$4 \leq A \leq 10$
Taper Ratio,	λ	0.5	$0.25 \leq \lambda \leq 1.00$
Sweepback,	Λ	0°	$0^\circ \leq \Lambda \leq 60^\circ$
Spanwise Location,	η_m	0.83	$0.17 \leq \eta_m \leq 0.833$
Spanwise Extent,	η_o	0.33	$0 \leq \eta_o \leq 1.00$
Chordwise Location,	x/c	0.7	$0.5 \leq x/c \leq 0.90$
Thickness Ratio,	t/c	0.09	$0.04 \leq t/c \leq 0.20$
Angle of Attack,	α	2°	$-2^\circ \leq \alpha \leq 6^\circ$

FIG. 1. Variable parameters, basic values, and ranges of valves considered in the development of the method.

$$C_{L_\zeta} = (C_{L_\zeta})_{basic} (r_A)(r_\lambda)(r_A)(r_{t/c})(r_{x/c})(r_{\eta_m})(r_{\eta_o})(r_\alpha) K$$

where $(C_{L_\zeta})_{basic} = C_{L_\zeta}$ for the configuration specified by the basic values of the parameters

$$r_A = \frac{(C_{L_\zeta})_A}{(C_{L_\zeta})_{A=6}} \qquad r_{x/c} = \frac{(C_{L_\zeta})_{x/c}}{(C_{L_\zeta})_{x/c=0.7}}$$

$$r_\lambda = \frac{(C_{L_\zeta})_\lambda}{(C_{L_\zeta})_{\lambda=0.5}} \qquad r_{\eta_m} = \frac{(C_{L_\zeta})_{\eta_m}}{(C_{L_\zeta})_{\eta_m=0.83}}$$

$$r_A = \frac{(C_{L_\zeta})_A}{(C_{L_\zeta})_{A=0^\circ}} \qquad r_{\eta_o} = \frac{(C_{L_\zeta})_{\eta_o}}{(C_{L_\zeta})_{\eta_o=0.33}}$$

$$r_{t/c} = \frac{(C_{L_\zeta})_{t/c}}{(C_{L_\zeta})_{t/c=0.09}} \qquad r_\alpha = \frac{(C_{L_\zeta})_\alpha}{(C_{L_\zeta})_{\alpha=2^\circ}}$$

$$K = f(M, A, \Lambda, \eta_m)$$

FIG. 2. Formula for predicting spoiler lift effectiveness.

parameter could be accounted for independently of changes in the other parameters by application of a correction factor. It was felt that the proper choice of the basic parameter values and the restrictions placed on the ranges of the parameters would materially assist in achieving this independence of parameter effects. The correction factor would be the ratio of spoiler lift effectiveness at the arbitrary value of the parameter being varied to the spoiler lift effectiveness at the basic value, with all other parameters remaining fixed.

Providing this technique worked and well-defined basic values of C_{L_ζ} were obtained throughout the Mach Number range investigated, the procedure could then be reversed for prediction purposes. That is, the basic value of C_{L_ζ} at a given Mach Number could be taken as a starting point and modified, using the correction factors, to fit any other combination of parameter values, within the limits specified, for which a prediction of C_{L_ζ} might be desired. The expression that would apply for prediction purposes is shown in Fig. 2.

The method was checked and proved feasible by preparation of graphs of the type illustrated in Fig. 3, showing prediction curves for Mach Numbers of 0.2, 0.5, 0.7, 0.8, 0.9, and 0.95 and reduced data points for Mach Numbers of 0.2 and 0.7. On each graph the data points shown were obtained by modifying data from the fairly abundant but uncorrelated supply that exists for three-dimensional wing-spoiler configurations. These data on Fig. 3 were modified to correspond to the basic value of all the parameters except the one used as the abscissa variable. The initial correction factors required for this operation were based on the best preliminary estimates that could be made of the influence on C_{L_ζ} of changes in each parameter. These initial estimates were obtained primarily from two-dimensional experimental data for the section parameters and for the rest of the parameters primarily from the wing theory for symmetrically deflected controls in NACA TR 1071 by DeYoung. It was realized from the outset that the initial estimates of the correction factors based on these sources might not be completely satisfactory. By applying them to the three-dimensional data, however, in the manner just described and comparing the

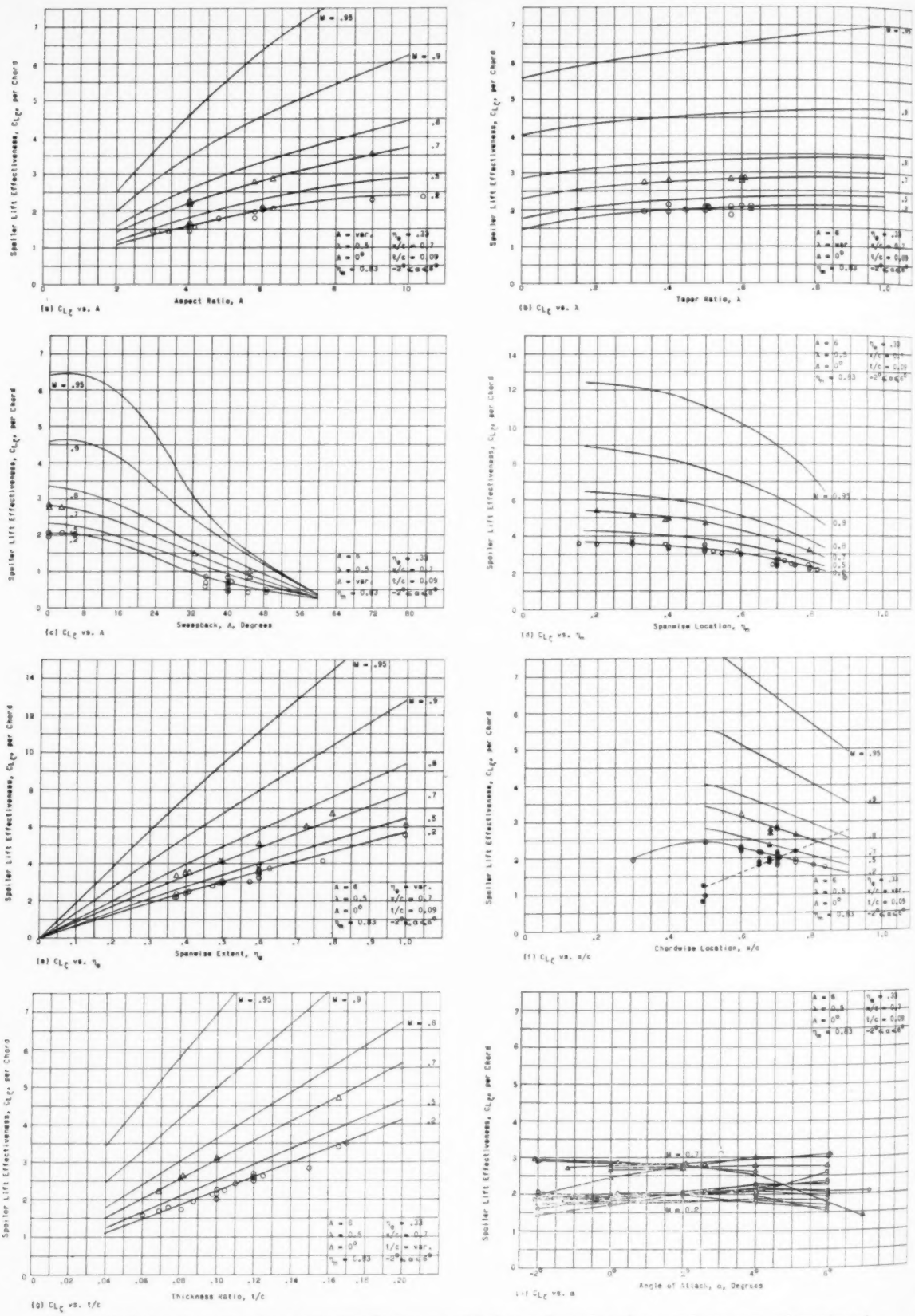

FIG. 3. Variation of upper-surface spoiler lift effectiveness with the aerodynamic and geometric parameters investigated.

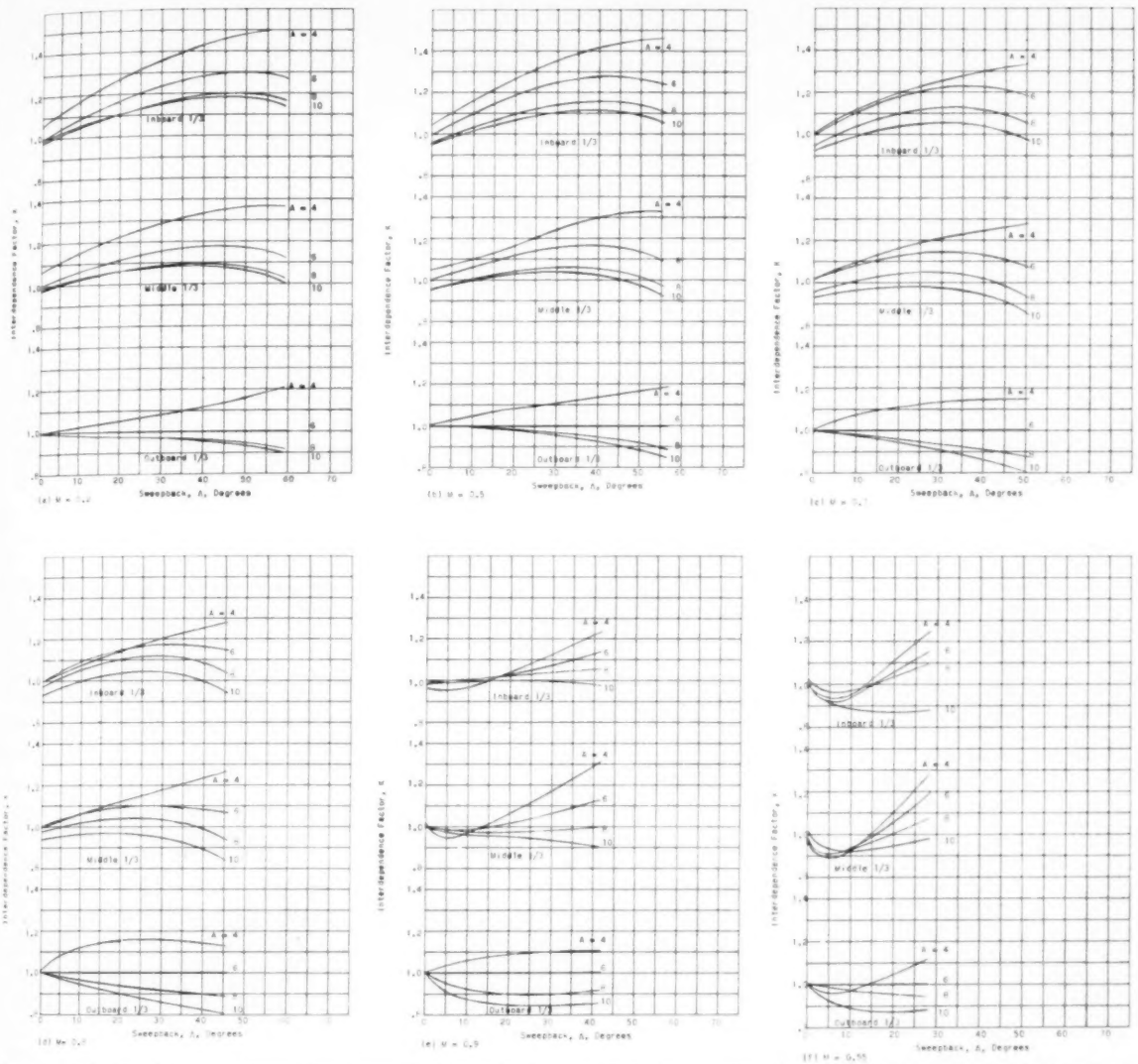

FIG. 4. Variation of the interdependence factor K with angle of sweep for various aspect ratios and spanwise locations of the control.

reduced data points with the variations initially estimated, an indication of how to revise the initial correction factors was obtained. Then, wherever necessary, modifications to the correction factors were made and the whole procedure repeated until a given set of curves yielding correction ratios were in good agreement with the resulting reduced data points. In addition to being the source for the correction ratios, the prediction curves provide a very graphic illustration of the relative importance of each variable, a feature which was felt to be almost a prerequisite.

It should be pointed out that no prediction curves have been included in Fig. 3 for the effect of angle of attack. The reduced data points plotted in Fig. 3 on the graph indicating the results of angle of attack variations showed some scatter. The trend indicated by the data, however, was that no particular variation in lift effectiveness with changes in angle of attack existed in the range from $-2°$ to $6°$. Consequently, it was assumed that the predicted values of spoiler lift effectiveness would be reasonably uniform throughout this range and that no correction ratios would be necessary for angle of attack.

Another item of importance in regard to the prediction curves concerns the apparent influence of sweep on the variation of C_{l_δ} with chordwise location. The variations shown by solid lines in the chordwise location graph of Fig. 3 were established from data available on unswept wings. For sweptback wings, data on diverse chordwise locations were available only in the low Mach Number range. These data points, shown blacked in, were used to construct the dotted line shown on this chordwise location graph. This line indicates a trend opposite to the variations established for unswept wings. There have been a number of spoiler tests made on sweptback wings at high Mach Numbers but, unfortunately, all the spoilers in these tests were located very close to the 0.7 c position. Thus no estimation of

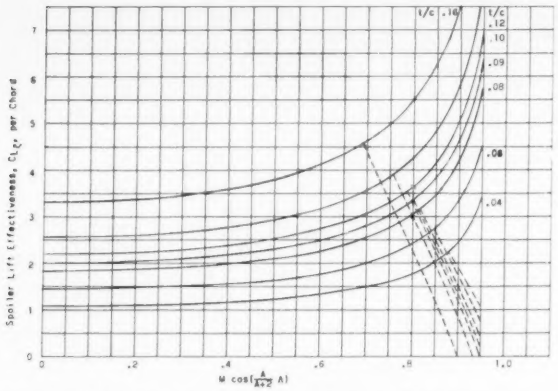

FIG. 5. Variation of spoiler lift effectiveness with a lift-divergence parameter $M \cos [A/(A+2)]\Lambda$ for various thickness ratios.

the variations with chordwise location could be made. An experimental investigation to clarify this situation is under way. Until more data pertinent to the effect of chordwise locations on swept wings become available, however, the prediction of spoiler lift effectiveness on sweptback wings is apparently restricted to chordwise locations of 0.7 c, at least for Mach Numbers greater than 0.2.

A further imperfection in the complete independence hoped for between parameter effects was noted. In order to satisfactorily minimize the scatter that occurred in the reduced experimental data, a correction factor was needed to account for what proved to be an irrepressible interdependence between aspect ratio, sweep, and spanwise location. This interdependence factor was computed using the theoretical results in NACA TR 1071 by DeYoung. Graphs showing the variation of this factor with sweepback for various aspect ratios and span locations are presented in Fig. 4 for Mach Numbers of 0.2, 0.5, 0.7, 0.8, 0.9, and 0.95. The interdependence factor is applied in the same manner as the correction ratios as shown in the formula on Fig. 2. It should be emphasized that although complete independence between parameter effects was not achieved, this did not impair the accuracy of the method nor the celerity with which predictions could be made. The interdependence affects only the degree to which the relative importance of each parameter's effects can be illustrated in a graphical presentation like that of Fig. 3.

The variations of C_{L_ζ} with Mach Number shown in Fig. 3 are based on the well-known Prandtl-Glauert rule. This is a very convenient means for estimating Mach Number effects and it is usually quite reliable up to a certain point, which might be set as low, generally speaking, as a Mach Number of 0.7. Beyond this point, however, discrepancies begin to show up between predicted values based on the Prandtl-Glauert rule and the experimental results. In the case of spoiler lift effectiveness, the experimental values tended to fall below the predicted values. It was found that the Mach Number at which theory and experiment began to diverge in this case was primarily a function of thickness ratio, aspect ratio, and sweepback. Consequently, an investigation was undertaken to ascertain the manner in which these parameters affected this divergence Mach Number. Two-dimensional experimental data on spoilers were examined for the effects of thickness ratio and the point at which lift effectiveness started to drop off was noted. It was observed incidentally, that the variation of lift-divergence Mach Number with thickness ratio obtained in this manner closely paralleled the critical Mach Number variation with thickness for flapped airfoils. To account for the effect of sweepback, a straight cosine correction was tried but did not work so satisfactorily as might be expected. It was felt that the tip and root influences, which reduce the beneficial influence of sweep in delaying the onset of adverse compressibility effects, might be the factors invalidating the cosine rule. Consequently, a simple aspect ratio correction often used in predicting lift-curve slope, $(A/A+2)$, was used to modify the sweep angle in the cosine correction. The result was satisfactory and a means for obtaining a reasonably accurate prediction of the Mach Number for lift-effectiveness divergence was assured. All that remained then was the problem of estimating the variation in lift-effectiveness with Mach Number beyond this point. In view of the fact that mixed sub- and supersonic flow conditions prevail in this high subsonic Mach Number range, these variations were estimated by a procedure involving primarily an inspection of experimental data. The results are shown in Fig. 5. Their use is not mandatory in the prediction procedure but is recommended as a means of obtaining a rational or at least more conservative estimate of spoiler lift effectiveness once the Mach Number of lift divergence has been exceeded. The simplest and most reasonable way of applying this result is to take the value of C_{L_ζ} obtained using the formula previously established and reduce it by the ratio of C_{L_ζ} given by the appropriate dotted line in Fig. 5 to C_{L_ζ} given by the appropriate solid line. This operation amounts to another simple ratio correction which can be readily incorporated into the overall prediction procedure just by including it as a multiplying factor.

CONCLUSION

By considering the effects of each parameter individually and by developing a semiempirical method of combining these effects, a simple straightforward procedure for predicting spoiler lift effectiveness at subsonic speeds has been developed. The method makes use of correction ratios picked off prediction curves which indicate the variation of lift effectiveness with a given parameter. A total of eight parameters in addition to Mach Number were taken into account. For Mach Numbers beyond the point of lift-effectiveness divergence, a means is suggested for modifying the results predicted on the basis of the Prandtl-Glauert rule.

As developed, the method is applicable to plain spoilers located along a constant per cent chord line. With no alterations the method probably is applicable

(*Continued on page 376*)

An Investigation of the Flutter Characteristics of Compressor and Turbine Blade Systems†

CHI-TEH WANG,‡ FRANK LANE,†† AND ROBERT J. VACCARO‡‡
New York University

ABSTRACT

As a first phase of a general research program, theoretical and experimental investigations have been carried out on the flutter characteristics of compressor and turbine blade systems in incompressible flow at low incidence. It was found that, in the theoretical treatment of fluttering blade systems, the prohibitively large number of the degrees of freedom necessary to analyze a multiblade system can be greatly reduced by recognizing the existence of a single equivalent blade, thus permitting the actual carrying out of a flutter calculation. As examples, numerical calculations are made on two-dimensional unstaggered, as well as staggered, cascades. From these calculations, several interesting results are obtained. First, for unstaggered cascades, the calculation shows this flutter occurs with adjacent blades oscillating 180° out of phase, thus confirming the experimental observations by Lilley. Second, it was found that for staggered cascades a very small change in blade inertial properties may cause a complete change of the blade flutter mode from one in which bending predominates to one in which torsion predominates. To check the theoretical results, an experimental program is carried out at the same time. A flutter mechanism with two degrees of freedom was designed and constructed for the testing of a two-dimensional cascade at low speed. The experimental results obtained checked very well with the theoretical findings.

LIST OF SYMBOLS

b	= semi-chord length
c	= chord length
I'	= blade mass polar moment of inertia about elastic axis$/2\rho b^4$
$K(x, \xi)$	= kernel function for aerodynamic integral equation
k	= reduced frequency of flutter $= \omega b/V$
m'	= blade mass per unit span length$/2\rho b^2$
N	= number of blades in row
p	= degrees of freedom per blade
P	= configuration parameter $= (\pi b/s)\cos\beta^* e^{i\beta*}$
q	= generalized-coordinate vector
q^j	= generalized-coordinate vector for jth blade
$\bar{q}^2$	= dimensionless flexural amplitude = bending deflection$/b$
$\bar{q}^\alpha$	= torsional deflection amplitude, radians
s	= normal distance between blades
S'	= nose-down blade mass unbalance about elastic axis$/2\rho b^3$
V	= velocity of stream relative to blade row
w	= upwash velocity
x, ξ	= chordwise coordinates, dimensionless with respect to b
x_e'	= distance of elastic axis aft of mid-chord$/b$
β^*	= stagger angle
ρ	= air density
σ	= interblade phase angle
τ	= vortex density amplitude
ω	= flutter (circular) frequency
ω_α	= natural (circular) frequency of blades in torsion alone
ω_h	= natural (circular) frequency of blades in flexure alone

(I) INTRODUCTION

THE FATIGUE FAILURE of the blades of aircraft jet engine compressors has been of considerable concern for some time. It is generally conceded that the loading causing this failure is of aerodynamic origin. The trend in blade design seems to aggravate the situation even further, since the blade shapes used are those with a high susceptibility to either forced or self-excited oscillation at large amplitude. One of the recognized possibilities is that blade flutter may be responsible for a portion of the structural failures observed to date and may become a problem of serious magnitude in future blade designs.

The study of the flutter phenomenon as it may occur in compressor blade rows involves several problems that do not arise in the investigation of flutter of conventional aircraft wings. During the past two and one-half years, a combined theoretical-experimental research program has been carried out at New York University aimed at exploring some of the peculiarities inherent in the flutter of compressor and possibly turbine blade systems. The present paper constitutes a brief summary of the theoretical and experimental results obtained to date under this program. The work is reported in detail in references 1, 3, and 9.

Outstanding among the problems peculiar to the understanding, analysis, prediction, and control of flutter in compressor blade rows is the complication introduced by the presence and the simultaneous oscillation of many blades. Another problem characteristic of compressor blade systems is the necessity of the study of high-incidence or stalling flutter. The program of investigation reported herein was directed toward the analytical study of the effects of multiple blade interaction, the experimental verification of theoretical findings, experimental surveys of classical cascade flutter in general, and a study of stall flutter. Since the investigation on stall flutter is still in its

Presented at the Aeroelasticity Session, Twenty-Third Annual Meeting, IAS, New York, January 24–27, 1955.

† This work was sponsored by the Fluid Dynamic Branch, Aeronautical Research Laboratory, WADC, USAF, under Contract No. AF 33(616)-25. The project was carried out under the direction of the first author. Theoretical work reported herein was performed by F. Lane, while experimental work was carried out by R. J. Vaccaro.

‡ Professor of Aeronautical Engineering. Now deceased.

†† Research Associate Professor of Aeronautical Engineering.

‡‡ Research Associate in Aeronautical Engineering.

initial stages, this phenomenon will not be discussed here. The problem of rotating stall is recognized as a critical possibility in causing the failure of blades but falls in the category of a forced oscillation relative to the blade row structure and, as such, is not treated under the present program.

(II) Blade System Mode Shapes

If any attempt is to be made at the inclusion in a flutter or vibration analysis of coupling effects between blades, be they aerodynamic, elastic, inertial, or all three, then the major problem to be solved is the determination of the relative motions of different blades during oscillation. Previous investigations[4-6] have either avoided this issue by neglecting coupling effects or have made initial restrictive assumptions concerning relative blade motions without ultimately justifying these assumptions in the light of the resulting analysis. Lilley[5] found experimentally that alternate airfoils in a fluttering cascade model, with or without stagger, oscillated nearly in phase with one another, adjacent airfoils appearing nearly 180° out of phase. In the particular case of zero stagger and zero incidence, for an infinite cascade, this corresponds to the single-wing oscillating between parallel walls, a phenomenon that has received some attention for its tunnel-wall interference aspects. Sisto[4] performed an oscillatory aerodynamic analysis for a two-dimensional cascade at zero incidence under the less restrictive assumption that all blades oscillate with equal amplitude and identical blade mode, but with some undetermined phase angle between blades. He obtained numerically the oscillatory aerodynamic forces and moments acting on unstaggered cascades. No criterion was advanced for the determination of this phase angle nor for the ultimate justification of the original assumed form of motion. Others have made various assumptions of more or less restrictive nature prior to proceeding with an aerodynamic analysis of the blade row or cascade oscillation phenomenon.

In view of the fact that the critical flutter velocity for a blade row may be severely influenced, particularly at high solidities by the nature of the system flutter mode, a theoretical investigation was performed to determine whether or not certain information could be developed to determine in advance the form of the flutter or vibration system mode shapes without resort to restrictive assumptions. This study proved successful in limiting the system mode shape, without loss of generality, to a particularly simple form while permitting at the same time a tremendous simplification in the flutter analysis of a multibladed system in which coupling between blades is of sufficient magnitude to warrant consideration.

The method was developed first for the case of a rotor of infinite inertia and consists in the representation of the blade system deflection amplitudes as a vector consisting of sub-vectors, each constituting the amplitude vector for a single blade.

$$q = \begin{pmatrix} q^1 \\ q^2 \\ \cdot \\ \cdot \\ \cdot \\ q^N \end{pmatrix} \tag{1}$$

for a system with N blades. Each q^j is a vector (say, of order p) of deflection amplitudes for the jth blade. Now the complete flutter problem may be represented in the form

$$Aq = 0 \tag{2}$$

wherein the matrix A includes elastic, inertial, and aerodynamic effects. Recognizing the fact that the blades are spaced equally about a common rotor and that the Nth blade affects the first in the same way that the first affects the second, and so on, we see that A is of cyclic form with respect to its pth order submatrices.

$$A = \begin{pmatrix} A_1 & A_2 & A_3 \ldots A_N \\ A_N & A_1 & A_2 \ldots A_{N-1} \\ A_{N-1} & A_N & A_1 \ldots \\ & & \cdot \\ & & \cdot \\ A_2 & A_3 & A_4 \ldots A_1 \end{pmatrix} \tag{3}$$

where each A_N is a pth order submatrix.

It is important to note at this point that the form (3) of A holds true under all forms of linear analysis and under all forms of interblade coupling. Thus the system mode analysis, as explained herein, holds in any flow régime in which the assumption of a linear relation between deflections and pressures is permissible. The investigation of $|A|$ may be simplified tremendously by recognizing the fact that A may be factored as follows:

$$|A| = \prod_{n=1}^{N} \alpha_n \tag{4}$$

each $|\alpha_n|$, in turn, being expressible as a pth order determinant. In fact, if we let α_n denote a pth order matrix whose determinant is $|\alpha_n|$, then we find

$$\alpha_n = A_1 + \omega_n A_2 + \omega_n{}^2 A_3 + \ldots + \omega_n{}^{N-1} A_N \tag{5}$$

where ω_n is the nth of the Nth roots of unity. The annihilation of $|A|$ is thus reduced to the far simpler problem of the annihilation of one or more of the pth order determinants $|\alpha_n|$.

It may then be shown that the entire system oscillation mode which corresponds to the vanishing of any particular $|\alpha_n|$ is one in which all blades oscillate with identical amplitude, in the same blade mode, and in which each blade leads the preceding blade by a phase angle given by ω_n.

$$q^m = q^{m-1}\omega_n \tag{6}$$

Moreover, the common blade deflection-amplitude vector q^m corresponding to the velocity and frequency that annihilate $|\alpha_n|$ is simply the (nontrivial) solution

vector of the pth order equation:

$$\alpha_n q = 0 \tag{7}$$

This immediately indicates that we need merely study the flutter of a single blade under a particular form of influence from the other blades—namely, the influence corresponding to the system motion described by Eq. (6). In other words, the blade-row flutter problem may be attacked, in all generality, in terms of a single equivalent blade. Now the critical conditions for flutter correspond simply to the subdeterminant $|\alpha_n|$ with minimum annihilating velocity and to the frequency and blade-mode vector associated therewith. As the number of blades becomes large, the roots of unity approach a condition of density about the unit circle, and, as is justified in references 1 and 9, we may replace the problem of choosing from among N combinations a combination (V_n, ω_n) having minimum velocity by the problem of minimizing the velocity with respect to an interblade phase angle, denoted by σ and assumed to vary continuously between 0 and 2π. In other words, we may annihilate a general pth order determinant $|\alpha_\sigma|$ depending upon the phase angle σ at a small (relative to N) number of values, plot the resulting annihilating velocity against σ, and pick the critical value of σ as that admissible value, $(2\pi m \div N)$, closest to the minimum point in the curve (m is same integer less than N). Thus the blade row flutter problem resolves itself into the study of a single oscillating blade under a particular type of influence from other blades characterized by the interblade phase-lag angle σ and the subsequent minimization of velocity with respect to σ. Finally, the minimizing value of σ is replaced by the nearest admissible value.

In the above discussion it is assumed that rotor inertia is infinite and the flutter determinant is simply degenerate. The extension to the case of finite rotor inertia and to the possibility of multiple degeneracy can be found in references 1 and 9.

(III) Aerodynamics of the Oscillating Cascade

In order to perform a complete flutter analysis, it is necessary to carry out the numerical determination of the oscillatory aerodynamic forces and moments on a cascade of airfoils. Sisto[4] has treated the oscillatory aerodynamics of unstaggered two-dimensional cascades under assumed system modes which prove to be the same as those characterized by Eq. (6). The more general case of the aerodynamics for an oscillating cascade with non-zero stagger will now be developed.

The problem of determining oscillatory lift and moment in terms of flexural and torsional deflections was formulated for the case of an infinite, two-dimensional cascade at zero incidence and for arbitrary stagger angle and gap-chord ratio. The formulation rests heavily upon the fact, developed in Section (II), that all blades must oscillate with identical blade mode, at identical amplitude, and with some undetermined interblade phase angle σ characterizing the system-mode shape. Thus, in addition to the usual frequency and velocity parameters that must be left open in single-wing flutter analysis, the additional parameter σ must be introduced with freedom to vary continuously between 0 and 2π.

The aerodynamics problem was expressed in the form of an integral equation, the kernel of which appears initially in infinite-series form in order to account for aerodynamic effects of all blades. It was found[1] that this kernel could be expressed in closed form, leading to the equation

$$w(x) = \int_{-1}^{\infty} \tau(\xi)\, K(x, \xi) d\xi \qquad -1 \leqslant x \leqslant 1 \tag{8}$$

where x is chordwise coordinate made dimensionless with respect to blade semichord, b, $w(x)$ is the downwash amplitude distribution along the blade, expressible in a linear combination of the blade deflection amplitudes, $\tau(\xi)$ is the vorticity amplitude distribution over the blade and its semi-infinite wake, and $K(x, \xi)$ is the kernel function, expressible in closed form as

$$K(x, \xi) = \frac{1}{4\pi} \left\{ \frac{P e^{(\xi - x) P [1 - (\sigma/\pi)]}}{\sinh P(\xi - x)} + \frac{\bar{P} e^{-(\xi - x) \bar{P} [1 - (\sigma/\pi)]}}{\sinh \bar{P}(\xi - x)} \right\} \tag{9}$$

with

$$P = (\pi b/s) \cos \beta^* e^{i\beta^*} \tag{10}$$

where β^* is stagger angle and s is distance between blades normal to blades.

The usual condition of zero pressure jump across the blade wakes permits expression of the wake vortex density in terms of the trailing-edge value of the bound or blade vortex density. This, in turn, must be expressed in terms of a chordwise integral of bound vorticity in order to make the problem determinate. Thus the integral equation is expressed completely in terms of the unknown vortex density $\tau(x)$ between the chordwise limits $x = -1$ and $x = 1$,

$$w(x) = \int_{-1}^{1} \tau(\xi) K(x, \xi) d\xi - ike^{ik} \int_{-1}^{1} \tau(\xi) d\xi \times \int_{1}^{\infty} e^{-ik\eta} K(x, \eta) d\eta \tag{11}$$

k being the usual reduced frequency, $\omega b/V$.

Solution of Eq. (11) for the bound vortex-density amplitude, and consequently the oscillatory lift and moment amplitudes which are easily expressible in terms of τ and weighted integrals thereof, was accomplished by transformation to trigonometric variables and expansion of τ in a sine series augmented by a term providing the correct form of leading-edge singularity. This corresponds closely to Kussner's approach[7] for single wings. A form of Galerkin technique for integral equations such as that noted by Hildebrand[2] was then utilized in solving for the coefficients in the expansion for τ. Actual execution of this solution involved the evaluation of three classes of integrals for numerous values of parameters involved. One class was found

to be expressible in terms of modified Bessel functions of the second kind, while the remaining two types of integrals required numerical evaluation. This was performed upon high-speed electronic computers after limiting the configuration to the particular case of unit gap-chord ratio and 45° stagger angle. It was felt that the information so derived, together with results obtained using Sisto's zero-stagger air forces, would serve to provide an adequate picture of the nature of the effects to be expected. The details of the analysis appear in reference 1. Actually, the coefficients in the expansion for vortex-density τ were found through the intermediate use of a set of influence coefficients for the system of algebraic equations involving the τ-coefficients. Use of these influence coefficients facilitates the introduction of various elastic axis location values into the expressions for oscillatory lift and moment at a late stage of the analysis. In fact, the use of influence coefficients makes it possible, at the expense of only minor additional effort, to introduce chordwise deformation into the problem in addition to the usual flexural and torsional deformations. Tables of the aforementioned influence coefficients appear in reference 1, valid for all elastic axis locations, together with oscillatory lift and moment values for the particular elastic-axis location of $32^1/_2$ per cent of chord from the blade leading edge, this being the value for which Sisto's unstaggered air forces and moments are tabulated.[4,1]

(IV) Application of Theory to Flutter Analysis of Simplified Configurations

The system-mode analysis described in Section (II), together with the oscillatory air forces described in Section (III) and tabulated in reference 1, was utilized in the performance of a series of flutter calculations for a simple two-dimensional cascade at zero incidence, permitting freedom in pitching and translation (normal-to-chord) to each blade. Computations were performed for unstaggered cascades at gap-chord ratios of 1.0 and 0.5 utilizing Sisto's air force data[4, 1] and for cascades of unit gap-chord ratio and −45° stagger utilizing the air force data of reference 1. All calculations were performed for an elastic axis location of $32^1/_2$ per cent of chord from the blade leading edge. Other pertinent parameter values for the unstaggered case were taken as follows:

m' = blade mass$/2\rho b^2 = 79.47$
I' = blade mass polar moment of inertia about elastic axis$/2\rho b^4 = 18.00$
S' = nose-down blade mass unbalance about elastic axis$/2\rho b^3 = -14.12$
ω_u/ω_α = bending-torsion natural frequency ratio = 0.60

All values specified for unit spanwise blade length.

For the condition of zero stagger the usual approach described by Scanlan and Rosenbaum[8] as Theodorsen's Method was followed. At each value of interblade phase angle σ for which Sisto's air forces were available, successive values of reduced frequency k were inserted into the single-equivalent-blade flutter determinant until a velocity appeared which annihilated simultaneously the real and imaginary parts of the determinant. This pair $[k(\sigma), V(\sigma)]$ then constituted the combination appropriate to the corresponding value of σ. The procedure was repeated for all available σ-values, and the results were plotted versus the phase angle σ. In view of the symmetry of configuration represented by zero stagger and incidence, it was necessary to plot values for σ varying only between zero and π. The plots from π to 2π would be simple reflections.

Figs. 1 and 2 show the behavior of frequency and velocity as well as blade mode with varying interblade phase angle σ. The definite minimum in the velocity curve at the antiphase condition ($\sigma = \pi$) is evident, and this accordingly represents the critical flutter point. For purposes of comparison, the isolated-blade values of critical flutter parameters are shown in Figs. 1 and 2. Similar results were obtained for a gap-chord ratio of 0.5. These appear in Figs. 3 and 4.

A second series of calculations for an unstaggered infinite cascade at zero incidence and unit gap-chord ratio was made at different mass and frequency-ratio values and for a range of mass unbalance values. These new parameter values were chosen to facilitate experimental duplication. They were as follows:

m' = 86.79
I' = 18.00
S' = (this parameter is left open since results are desired for a range of mass-unbalance values)
ω_u/ω_α = 0.45

The air force coefficients used in this computation were again those calculated by Sisto. For these zero stagger and incidence calculations however, since the interblade phase angle is known (experimentally and theoretically) to be 180°, this value is assumed *a priori*, and no minimization with respect to σ was performed. With the mass unbalance parameter S' left open, it was unnecessary to use successive trial values of reduced frequency k. To every value of k within a certain range, the values of velocity and mass unbalance which caused simultaneous annihilation of real and imaginary parts of the flutter determinant were found. This permitted a survey-type analysis with respect to the mass unbalance S'. Results of these calculations appear in Figs. 11, 12, 13, and 14, together with values measured experimentally. As noted earlier, all calculations and experimental values are for the antiphase condition, and mass unbalance serves as abscissa for the curves.

For the condition of −45° stagger and unit gap-chord ratio, parameters were the same as those for the first set of unstaggered calculations with the exception of mass unbalance. For purposes of performing a survey-type analysis this was left as an open parameter. In the staggered condition no advance assumption of antiphase motion was permitted, and the minimization

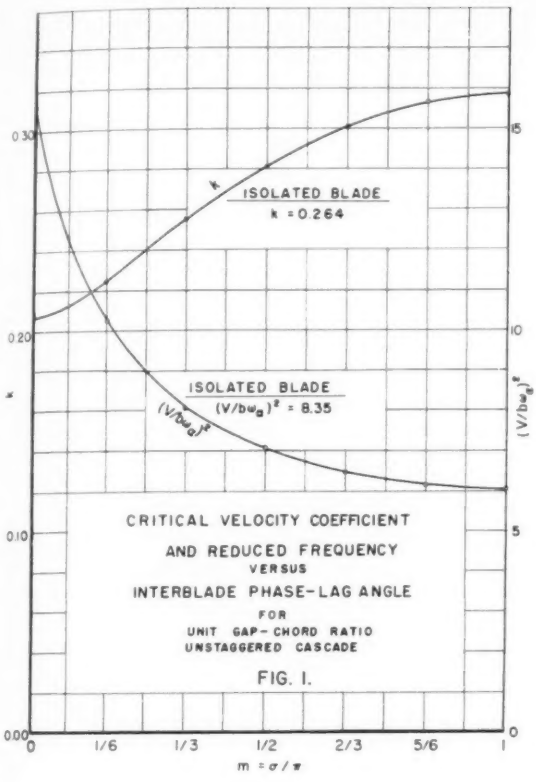

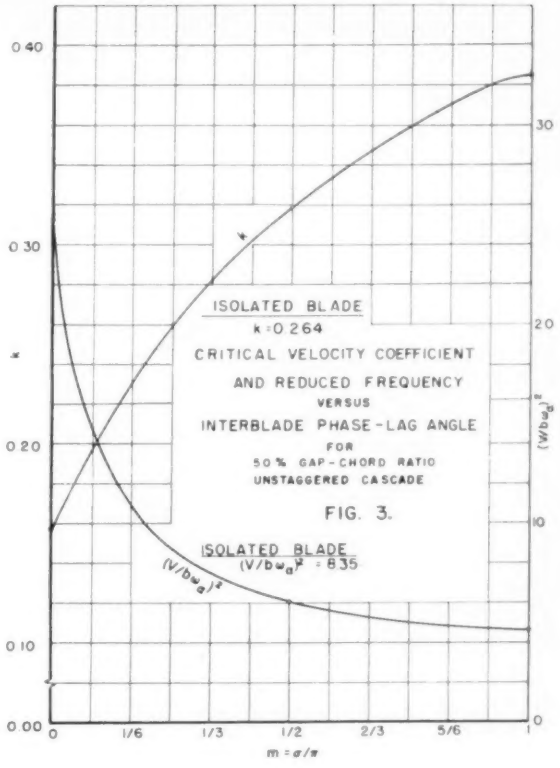

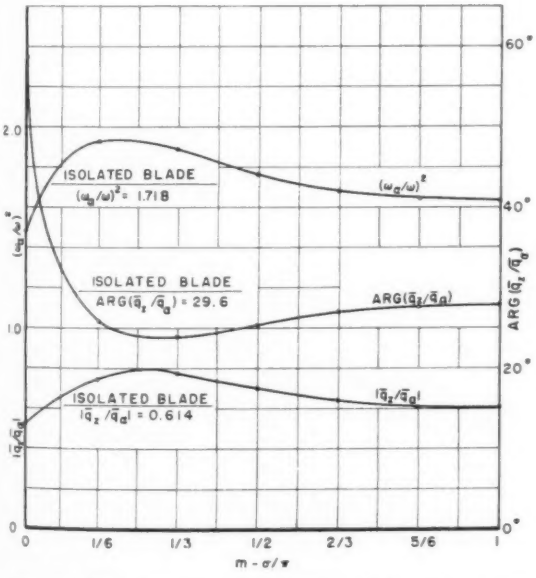

FIG. 2. Critical frequency ratio and blade mode versus interblade phase-lag angle for unit gap-chord ratio, unstaggered cascade.

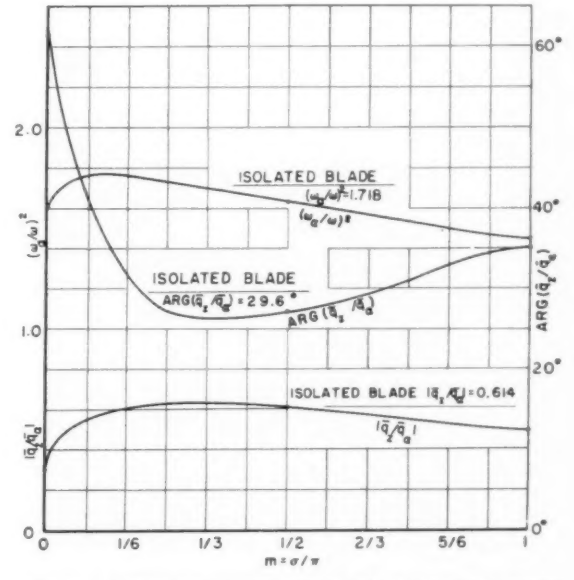

FIG. 4. Critical frequency ratio and blade mode versus interblade phase-lag angle for 50 per cent gap-chord ratio, unstaggered cascade.

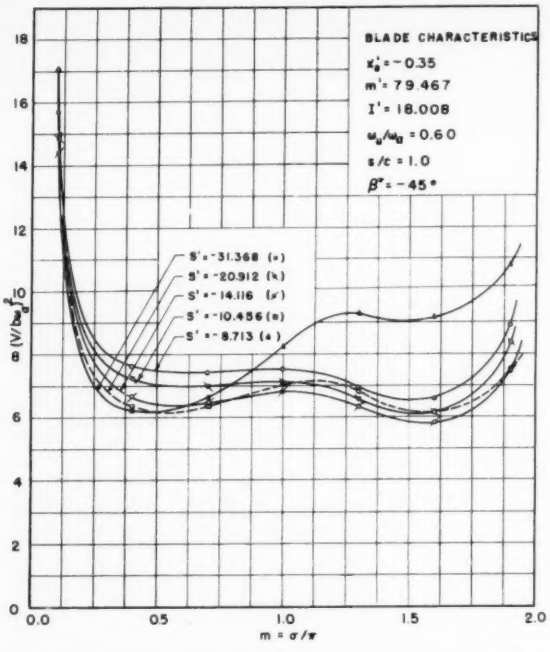

FIG. 5. Contours of velocity coefficient versus interblade phase-lag angle, σ, for various values of mass unbalance, S'.

procedure with respect to σ was carried out at each of a set of discrete values of mass unbalance.

Figs. 5, 6, 7, and 8 present dimensionless critical values of flutter velocity, frequency, and blade mode versus interblade phase angle for various values of mass unbalance. As may be seen from an inspection of Fig. 5, predicted values of critical interblade phase angle σ (minimum values on the curves) no longer fall at 180° but may be either in the vicinity of 90° or in the vicinity of 290°. No experimental verification of these curves is yet available, but the necessary apparatus is presently under construction.

One of the most significant features of the curves of Figs. 5–8 is the fact that two σ-regions of minimum velocity occur, depending upon the value of mass unbalance. Moreover, the lower σ-values correspond to predominantly flexural motion, while the higher σ-values are associated with highly torsional oscillation. The indications are, therefore, that a region of values of mass unbalance exists in which a small variation in mass unbalance may alter completely the blade flutter mode (though not the flutter velocity). It is thus most likely that the same phenomenon must occur with respect to the other physical parameters of the system.

(V) Experimental Apparatus and Procedure

Cascade flutter tests at zero incidence and stagger were performed in the 7- by 10-ft. wind tunnel in the Daniel Guggenheim School of Aeronautics at New York University. The Reynolds Number of the tests based on blade chord varied from approximately 0.2 to 0.4 × 10^6. The tests were two-dimensional and surveyed the effects of changing blade inertial and elastic properties.

The major portion of the testing utilized a cascade composed of five oscillating blades. However, since the stagger angle was zero, another model of an infinite cascade—i.e., a single blade oscillating between parallel walls—was also employed for a limited amount of testing.

The flutter apparatus is composed of individually supported blades each with two degrees of freedom. Every blade is permitted to translate vertically and to rotate about a prescribed elastic axis. Both the translatory or flexural motion and the rotary or torsional motion are restrained by calibrated springs. Hence, the elasticity of the blade system is well defined. Identical spring systems called the flutter mechanism support the blades from both ends and are especially designed to eliminate any tendency for the blade to roll. A composite drawing of the flutter mechanism is shown in Fig. 9. The blades are mounted in a two-dimensional air passage provided by two large wings or end plates† which are placed one foot apart and span the wind-tunnel test section from floor to ceiling. The cascade is mounted between the end plates, and the flutter mechanism is concealed inside them. Fig. 10 is a photograph, taken downstream, of the end plates in the test section with the cascade installed. To permit observation of the cascade during testing, one end plate is equipped with a plastic window on its exterior side while on its interior side, that part of the end plates adjacent to the blade tips is composed of a series of plastic plates, one plate forming the endwall of each blade.

Physical characteristics of the individual blades, such as moment of inertia and mass unbalance about

† These end plates were originally designed and constructed by Prof. G. H. Strom for another purpose and were modified for the present series of experiments.

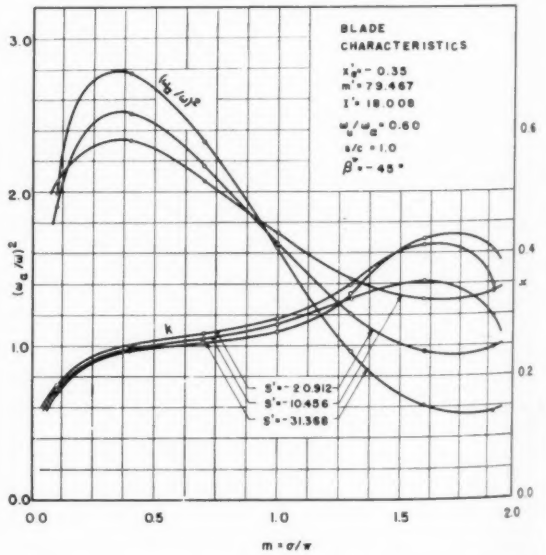

FIG. 6. Contours of inverse-square frequency ratio and reduced frequency versus interblade phase-lag angle, σ, for various values of mass unbalance.

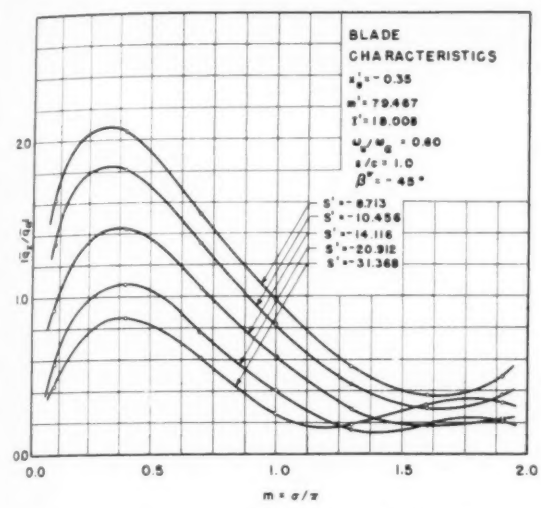

FIG. 7. Contours of bending-torsion amplitude ratio versus interblade phase-lag angle, σ, for various values of mass unbalance, S'.

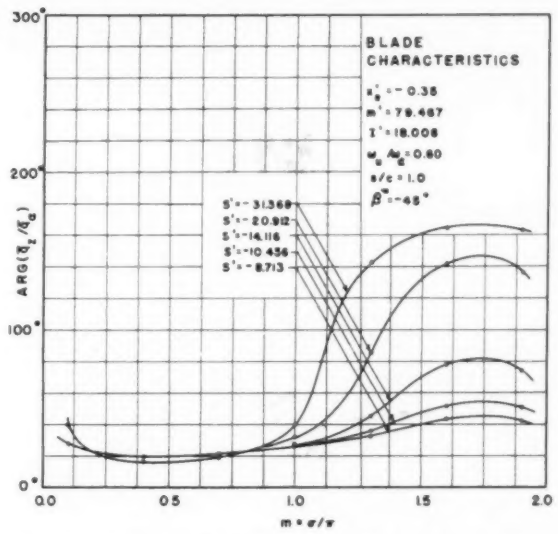

FIG. 8. Contours of bending-torsion phase-lag angle versus interblade phase-lag angle, σ, for various values of mass unbalance, S'.

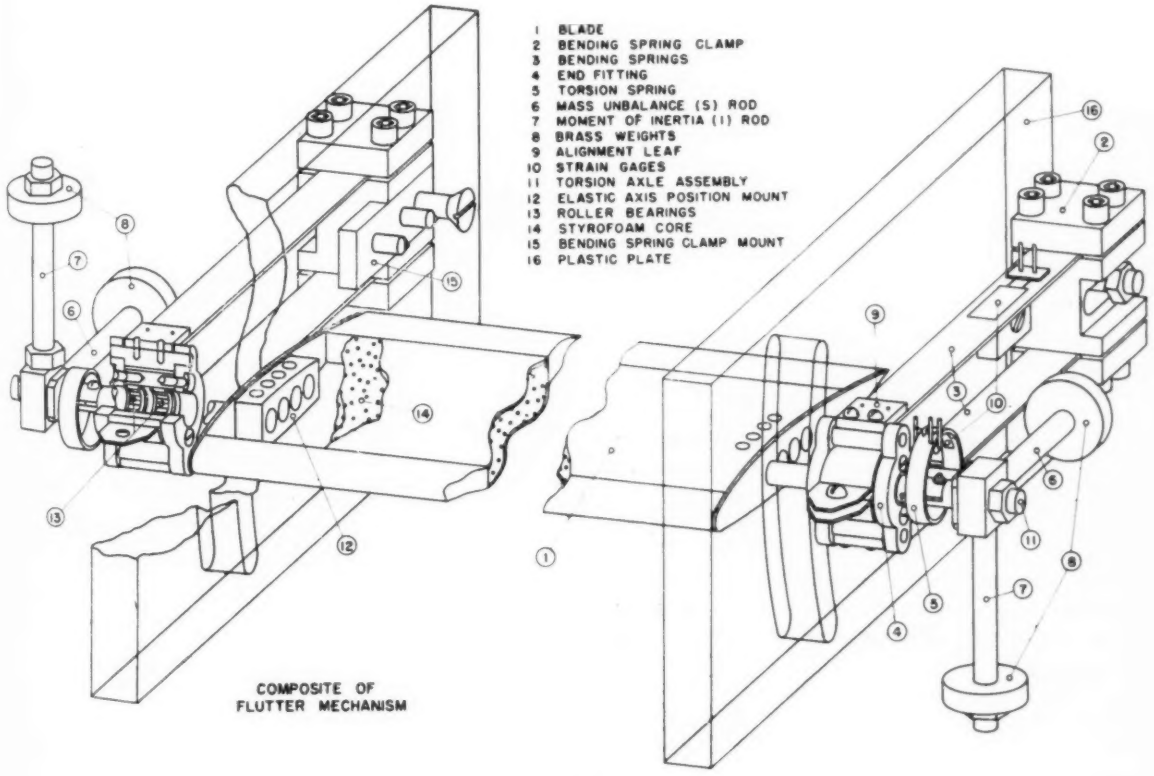

FIG. 9.

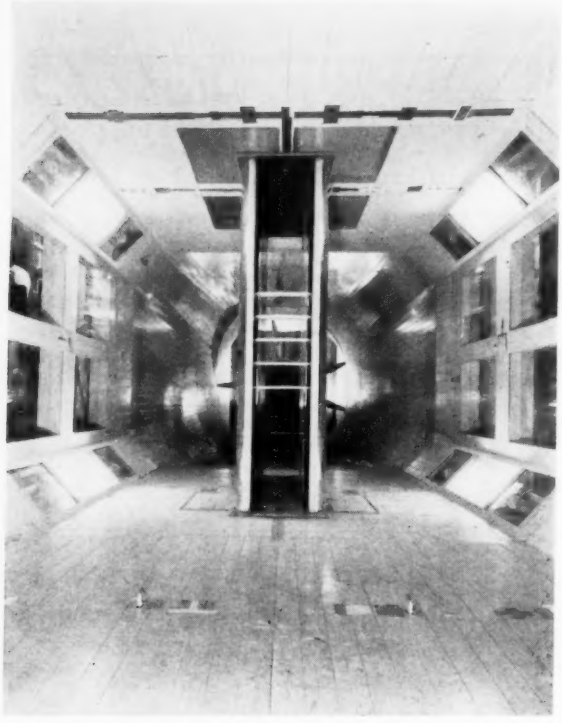

FIG. 10. View of test section looking downstream.

the elastic axis, may be varied by adjusting four brass weights which form a part of the flutter mechanism. Two weights may be adjusted in the chordwise direction, while the other two adjust in a direction normal to the chord. The overall oscillating mass of the system may be altered by changing the brass weights or by adding weight to the elastic axis. The natural frequency of the flexural and torsional motions may be varied by changing the springs that restrain these motions. Four possible attachment points for the torsion axle of the flutter mechanism are provided on each blade to permit four elastic axis positions.

The flutter mechanism is instrumented on one side so that the flexural and torsional motions during flutter may be separately recorded. The transducers consist of two strain gages cemented to the springs and two fixed resistors all connected to form a Wheatstone bridge. This system is self temperature compensating, and the output signal is of sufficient strength to be recorded without amplification. A Consolidated Bridge Balance is used as a control link between the transducers and a recording oscillograph to provide voltage adjustment, balancing, and calibration of each channel. Only 12 of the 18 channels available in the recording oscillograph were necessary to record the air speed and the motions of each degree of freedom of each blade and to monitor the supply voltage to the Eridge Balance. The velocity of the flow in the two-dimensional channel was obtained from a pitot static system installed in the end plates and was read from an inclined manometer and later checked by the air-speed trace on the oscillogram.

The uncoupled natural frequencies in flexure and in torsion were obtained after the flutter mechanisms were installed in the end plates. A maximum variation of one per cent was allowed between highest and lowest frequency readings of the five blades. Damping in both the flexure and torsion modes was low, with average measured values of 17.0 and 11.0 cycles required to damp to half amplitude, respectively. The incidence angle for all blades was set at zero, and the necessary tunnel calibration was accomplished. The testing proceeded as follows: The tunnel speed was raised rapidly until the blades in the cascade began to exhibit damped oscillation. From this point on, the tunnel velocity was raised very slowly. Proximity to the flutter speed was indicated by increasingly poor damping. Upon reaching the flutter speed, which was very well defined, the recording oscillograph was switched on and simultaneously the velocity was read on an inclined manometer. The tunnel velocity was then lowered as rapidly as possible. The manometer air speed was employed as a check on the value obtained from the oscillogram, and the two usually agreed to within two per cent. Flutter was observed as a constant amplitude oscillation usually of greater magnitude than the damped oscillations. The amplitude distribution for the cascade as a whole was parabolic with the maximum at the center blade, this being a direct consequence of the finite blade number. However, the flexure-torsion amplitude ratio was approximately constant for the five blades. Extreme caution had to be exercised in order not to raise the tunnel speed any further once flutter began, since the amplitudes usually grew until the blade stalled at the top and bottom of the cycle. Since the stall flutter speed is lower than the zero incidence flutter speed, the condition was very often disastrous. A complete discussion of the experimental apparatus, as well as testing and calibration procedures, is given in reference 3.

(VI) Experimental Results

The experimental program reported herein was limited to zero angle of attack and zero stagger. This limitation was imposed by the end plates that were

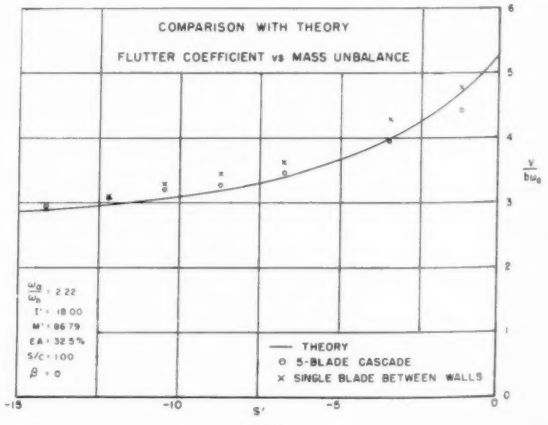

FIG. 11.

available at the beginning of the program. In choosing the ranges of the parameters to be investigated, three criteria were considered. First, in order that any general results be considered applicable to practical compressor configurations, parameters could not depart too severely from realistic values. Second, in view of the fact that oscillatory aerodynamic interaction between blades was the primary feature under investigation, it would not do to suppress this effect by employing too high a value of blade-air mass ratio. Third, critical flutter velocities should fall within the wind-tunnel speed range. The parameter ranges finally agreed upon constituted an attempt at compromise between these requirements. Among the variables investigated were blade flexure-torsion, natural frequency ratio, overall mass, mass unbalance or static moment about the elastic axis, moment of inertia about the elastic axis, and elastic axis location. Since the flutter mode for an unstaggered cascade at zero incidence was found to be antiphase from the five-blade tests as well as from the theory discussed previously, the testing of a single blade between parallel walls is justified as a means of obtaining unstaggered cascade data. Therefore, the effect of varying the elastic axis location was surveyed by this method of test.

The results obtained from the oscillograms included flutter velocity, frequency, amplitude ratio, intrablade phase angle or the phase angle between the flexural and the torsional motions, and the interblade phase angle (for the five-bladed cascade). Special techniques were devised in reducing the data to account for finite-blade-number effects in the five-bladed cascade. The data reduction techniques as well as the experimental results are presented in detail in reference 3.

A series of tests was run which duplicated the conditions employed in the theoretical calculations for a two-dimensional unstaggered cascade at zero incidence. The results of these tests are plotted as the circled and crossed points on Figs. 11 through 14. The experimental values shown in these figures were obtained from tests in which five blades were used and from tests on a single blade between parallel walls corresponding

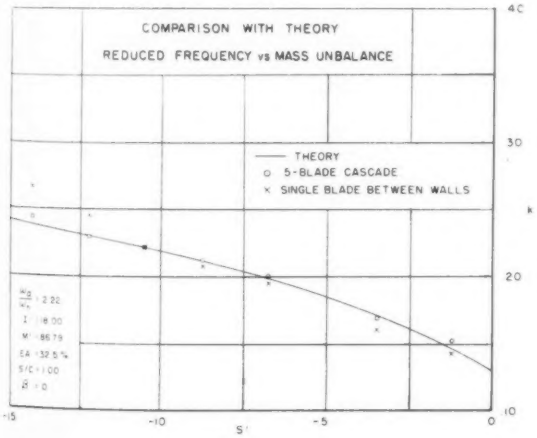

FIG. 12.

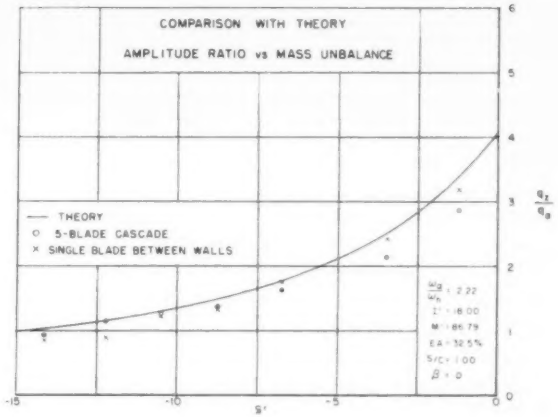

FIG. 13.

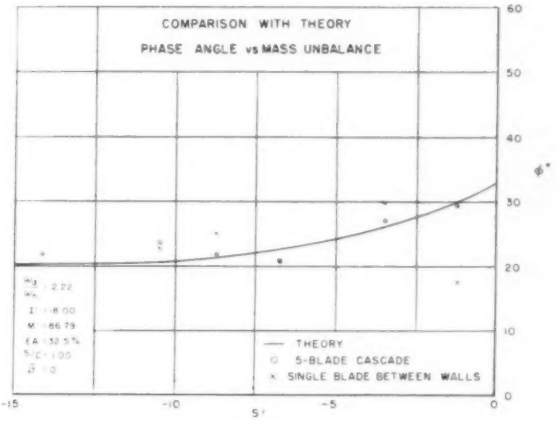

FIG. 14.

to a condition in which interblade phase angle is restricted to 180°. The experimental critical velocity has been corrected to standard density. In general, the agreement between theory and experiment is very satisfactory. It is interesting to note that points obtained from the five-bladed cascade tests are, in most instances, closer to the theoretical curves than the points given by the single-blade-between-walls tests which should in fact be more representative of an infinite cascade. One reason is perhaps that small errors in setting the physical characteristics of the single blade are effectively duplicated throughout the infinite cascade, while in the five-blade cascade, the inconsistencies in the settings tend to be averaged and thus minimized by the remainder of the blades. On the other hand, the single-blade points seem to follow the trend of the theoretical curves more closely. This is more obvious at the lower value of S' for the flutter coefficient and amplitude ratio curves. Possible reasons for the differences between theory and experiment may be summarized as follows.

(1) The theory for the unstaggered case relies upon the use of Sisto's oscillatory air force calculations,[4] and these calculations were performed on the basis of an approximation to the true kernel in the aerodynamic integral equation.

(2) The discrepancy in the critical flutter velocity (flutter coefficient) was not totally unexpected since the theory was developed for an infinite cascade, whereas, in one case, the experimental cascade model consisted of only five blades. Since the isolated blade critical flutter velocity is considerably higher than that of the infinite cascade, it is not suprising that the experimental flutter velocity for the five-blade cascade generally exceeded the theoretical values. Furthermore, the unavoidable presence of mechanical friction in the flutter mechanism accounts for at least a portion of the discrepancy in critical velocity and probably plays the major role in the single blade tests.

(3) In some regions of the variables investigated the blades showed an extreme proclivity toward stall flutter even when initially oriented at zero incidence. This is a direct result of the large torsional amplitudes that build up immediately after the inception of flutter. This type of stall flutter is of necessity predominantly torsional and occurs with a frequency that is close to the natural frequency in torsion. When the flutter remains unstalled, the frequency usually lies roughly midway between the bending and torsion natural frequencies and is therefore lower than the stall flutter frequency. It is reasonable to expect, therefore, that the frequencies obtained experimentally (where the amplitudes are finite) will be somewhat higher than those predicted by theory, since the theoretical predictions are based upon the usual assumptions that the disturbance velocities are small relative to the free-stream velocity. This in turn implies the assumption of small flutter amplitudes. That this is indeed the case is evidenced by the reduced frequency curve. Although the critical velocities are generally higher than the theoretical predictions, the reduced frequencies agree very well, indicating that the experimental frequencies must also have been high to compensate for the velocities. In those cases where the experimental points fall above the curve by a considerable amount, it was observed that the amplitudes were larger than usual though still unstalled.

(4) The discrepancy between predicted and observed amplitude ratios, $|\bar{q}_t/\bar{q}_a|$, may be attributed in part to the large amplitude, recalling the fact that the theory is derived for small disturbance velocities. Furthermore, spill-over through the side-wall slots would tend to decrease the bending amplitude while leaving the torsional amplitude unaffected since these slots are located at the elastic axis. As might be expected, this situation is aggravated as the flutter becomes predominantly bending and is more serious for the five-blade than for the single-blade tests.

(5) Inaccuracies inherent in the measurements of experimental bending-torsion phase angles are too great to permit significant interpretation of the discrepancies observed in this quantity. In general, more consistent values of the phase angle were obtained from the five-blade cascade than were obtained from the single-blade tests, probably because of the averaging effect of the cascade.

(6) The theory predicts a value for the interblade phase angle $\sigma = 180°$. This value is automatically imposed on the single-blade tests, and, since the single-blade results and the cascade results agree rather well, the mode of the cascade must have been approximately antiphase. Subject to the data reduction technique discussed in reference 3, the following is a tabulation of the interblade phase angle results obtained from the cascade tests:

S'	σ
−14.12	174°
−12.20	153°
−10.47	175°
− 8.71	180°
− 6.73	185°
− 3.49	168°
− 1.22	188°

Although the experimental results display a certain amount of scatter, the antiphase relation for the test series as a whole is clearly indicated.

The experimental apparatus for the flutter tests with stagger and the stall flutter program is in the preliminary stages of construction at the time of this writing. The equipment will permit investigation of stagger angles up to 55° and incidence angles well into the static stall region. The flutter mechanism will be the same as that described herein; however, complete redesign of the wall configurations was necessary.

References

[1] Lane, F., and Wang, C. T., *A Theoretical Investigation of the Flutter Characteristics of Compressor and Turbine Blade Systems*, W.A.D.C., Technical Report 54-449.

[2] Hildebrand, F. B., *Methods of Applied Mathematics*, First Ed., pp. 451, 452, New York, Prentice-Hall, Inc., 1952.

[3] Vaccaro, R. J., and Wang, C. T., *Experimental Investigation of Flutter in Cascade with Zero Incidence and Stagger*, W.A.D.C., Technical Report 54-507.

[4] Sisto, F., *Flutter of Airfoils in Cascade*, Doctoral Dissertation, Massachusetts Institute of Technology, 1952.

[5] Lilley, G. M., *An Investigation of the Flexure-Torsion Flutter Characteristics of Airfoils in Cascade*, Report No. 60, The College of Aeronautics, Cranfield, May, 1952.

[6] Meller, M. G., *Étude Preliminare sur le Flutter des aubes de Compresseur*, France, ONERA N.T. 18, 1953.

[7] Kussner, H. G., *Zusammenfassender Bericht uber den instationaren Auftrieb von Flugeln*, Luftfahrtforschung, Vol. 13, pp 410–424, 1936.

[8] Scanlan, R. H., and Rosenbaum, R., *Introduction to the Study of Aircraft Vibration and Flutter*, First Ed., p. 266, New York, The Macmillan Company, 1951.

[9] Lane, F., *System Mode Shapes in the Flutter of Compressor Blade Rows*, Journal of the Aeronautical Sciences, Vol. 23, No. 1, pp. 54–66, January, 1956.

An Investigation of Helicopter Descent and Landing Characteristics Following Power Failure

E. F. KATZENBERGER* AND M. J. RICH†

Sikorsky Aircraft Division, United Aircraft Corporation

SUMMARY

The paper is primarily concerned with an analytical investigation of helicopter descent and landing characteristics following partial or complete power failure on take-off.

An analysis is made of the time history of descent velocity following power failure for the critical case of vertical take-off.

The investigation includes the determination of the time rate of change of descent velocity and velocity at ground contact employing pilot control inputs representative of pilot capabilities and helicopter characteristics representative of current helicopters.

The special case of steady-state autorotative descent and landing is treated separately, and an index for comparing helicopter designs as to autorotative landing capabilities is derived.

SYMBOLS

A	= area of rotor disc, sq.ft.
a	= lift slope, $dC_L/d\alpha$, the value of 5.73 used as the constant
B	= tip loss factor
b	= number of rotor blades
c_e	= rotor blade chord width, ft.; subscript refers to effective chord, if the chord is not constant
C_1, C_2, etc.	= arbitrary constants
C_Q	= nondimensional torque coefficient, equals $Q \div A\rho(\Omega R)^2R$
C_{Qa}	= subscript refers to available torque
C_{Q0}	= subscript refers to profile torque
C_T	= nondimensional thrust coefficient, equals $T \div A\rho(\Omega R)^2$
C_{D_0}	= section profile drag coefficient, expressed in power series as a function of α_r; $C_{D_0} = \delta_0 + \delta_1\alpha_r + \delta_2\alpha_r{}^2$
D_v	= vertical drag, lbs.
E	= energy, ft.lbs.
f	= nondimensional thrust coefficient defined as $1/f = 2A\rho\dot{y}^2/T$
F	= nondimensional thrust coefficient defined as $1/F = 2A\rho\bar{U}^2/T$
g	= gravitational acceleration, 32.2 ft. per sec.^{2} in this report
h	= altitude, ft.
HP	= horsepower
I_R	= moment of inertia of rotor system about the axis of rotation, slug-ft.^{2}
K	= constant defined for vertical drag
K_1, K_2, etc.	= constants defined by boundary conditions of rotor flow as shown in Fig. 4
L	= rotor lift, lbs.
M	= mass of aircraft, W/g, lbs.-sec.^{2} per ft.
N	= a unit value of rotor r.p.m. used in computor programming
n	= instant of time considered
$n-1$	= immediate previous instant of time that is being considered, where Δt seconds separates time (n) from time $(n-1)$
Q	= torque, wherein a positive torque causes positive acceleration of the rotor, ft.lbs.
Q_E	= engine torque at the rotor, equals torque at engine × gear ratio of rotor to engine × mechanical efficiency of system
q	= dynamic pressure, lbs. per sq.ft.
R	= rotor radius, ft.
r	= radius of rotor blade element, ft.
T	= rotor thrust, lbs.
t	= time, sec. (general)
$\bar{U}$	= total average flow through rotor disc; positive when directed upwards through rotor, ft. per sec. $\bar{U} = \dot{y} - \bar{v}$
$\bar{v}$	= average induced velocity, always positive and acting downward, ft. per sec.
W	= gross weight of helicopter system, lbs.
x	= nondimensional ratio of r/R
y	= displacement of aircraft, ft.
$\dot{y}$	= first time derivative, sinking velocity, ft. per sec.
$\ddot{y}$	= second time derivative, acceleration, ft. per sec.^{2}
α_r	= blade element angle of attack, radians
γ_1	= ratio of $bc_e a\rho R^4/I_R$ or $\sigma_e a\rho AR^3/I_R$ and is comparable to Lock Number and approximately equivalent to latter if centerlines of rotation and flapping axis coincide
δ_0, δ_1, δ_2	= coefficients in power series expressing C_{D_0}
θ	= blade pitch setting, radians; $\theta = \theta_0 + x\theta_1$
θ_0	= blade pitch setting at root, radians
$\theta_{(3/4BR)}$	= blade pitch setting at $^3/_4$ effective radius, radians
θ_1	= blade twist, radians; positive when hub angle is smaller than tip angle
λ	= ratio of total average flow to tip speed, $\bar{U}/\Omega R$, nondimensional
ρ	= air density, lb.-ft.$^{-4}$ sec.^{2}
σ	= solidity ratio of rotor, ratio of blade area to disc area, $bc/(\pi R)$, nondimensional
ϕ	= induced angle of attack, radians
Δt	= time increment separating instants (n) and $(n-1)$
μ	= advance ratio, $V\cos\alpha/(\Omega R)$, where α is the rotor angle of attack
η	= mechanical efficiency of a helicopter defined as a ratio of the rotor shaft horsepower to the engine brake horsepower; $\eta = HP/BHP$

Presented at the Helicopter Design Session, Twenty-Third Annual Meeting, IAS, New York, January 24–27, 1955.

* Chief Development Engineer—General Design.

† Senior Engineer.

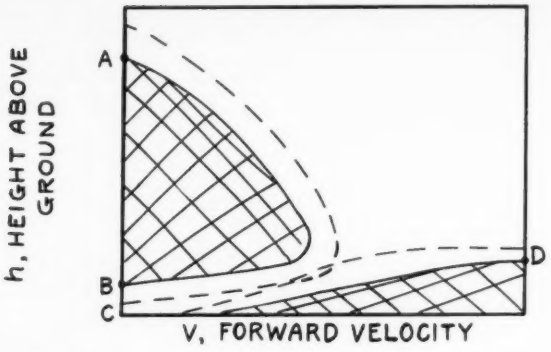

FIG. 1 HEIGHT-VELOCITY ENVELOPE DIAGRAM

INTRODUCTION

A PRINCIPAL ADVANTAGE of the helicopter, as compared to present conventional fixed-wing aircraft, is the ability to operate at low to zero forward speeds. However, there are definite limitations to this advantage. These limitations are best illustrated by the well-known height-velocity diagram[18] such as illustrated in Fig. 1.

The shaded regions indicate the flight regimes that are to be avoided for continuous flight. This is due to the near impossibility of landing the helicopter, in the event of a power failure, within the design ground contact sinking speed designated for the landing gear, usually 8 ft. per sec. for the low forward speed range. While the shaded regions may vary for the particular aircraft, the diagram is generally characteristic for autorotative landings following power failure.

The inability to make a normally "safe" landing in the upper shaded region is due to the rotor characteristics; the rotor may not have sufficient energy to reduce the sinking speed of the helicopter to a value within the designated limit and/or the rapid loss of rotor speed may require that the landing maneuver be accomplished with a precision beyond the normal capabilities of the pilot.

The dotted lines in Fig. 1 indicate a more critical helicopter, for which every take-off or landing requires some operation in the "hazardous" region if exceeding the design limit sinking speed on ground contact following power failure is to be avoided.

Fig. 2(a) shows a limited landing area, such as might be required to obtain maximum utility of the aircraft. The most critical flight condition would then arise. In the event of a power failure at some ground height off the heliport less than the height of the boundary obstacles, the helicopter would then have to make a vertical or near-vertical descent.

A power failure that occurs during a full powered vertical take-off obviously results in the critical combination of conditions, particularly if it is assumed that, for economic reasons, the aircraft is operated at its maximum safe gross weight. This combination results in the largest selection of collective pitch causing the most rapid initial loss of rotor speed following power failure.

Following power failure the aircraft would have a resultant ground contact velocity the magnitude of which is dependent on (1) the height at time of engine failure, (2) the rotor performance in vertical flight, and (3) the pilot's ability to make corrective action. A possible height-ground contact velocity characteristic is shown in Fig. 2(b).

As seen in Fig. 2(b), there are two ground contact velocity limitations—that for aircraft damage and that for safety of the occupants of the helicopter.

Since the helicopter would be landing without any appreciable forward velocity, the danger to the occupants is reduced by virtue of the attitude of the aircraft upon ground contact. In general, passenger injury is due to (1) the large forward deceleration of conventional aircraft moving with great forward speed upon striking an obstacle in an emergency landing, (2) the position of the passengers in relation to the crash loads, resulting in the passengers' being thrown forward, and (3) the destruction of the passenger area of the aircraft.[12–15] The maximum vertical ground contact velocity must be limited to a value that precludes passenger injury.

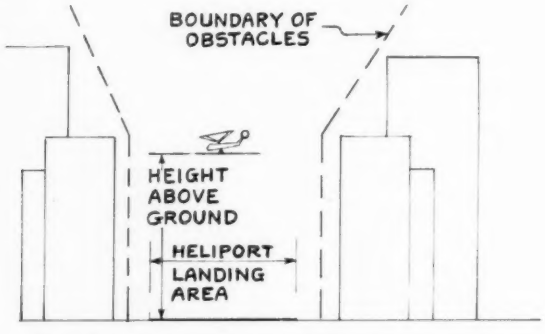

FIG. 2(a)— A LIMITED LANDING AREA REQUIRING VERTICAL TAKE OFF AND LANDING OPERATION

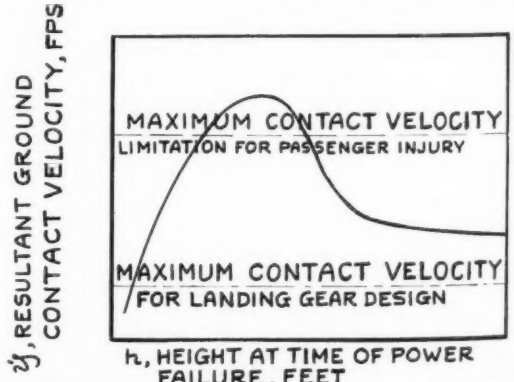
ẏ, RESULTANT GROUND CONTACT VELOCITY, FPS
MAXIMUM CONTACT VELOCITY LIMITATION FOR PASSENGER INJURY
MAXIMUM CONTACT VELOCITY FOR LANDING GEAR DESIGN
h, HEIGHT AT TIME OF POWER FAILURE, FEET

FIG. 2(b)—HEIGHT-GROUND CONTACT VELOCITY DIAGRAM

It then remains to ascertain the value of a ground contact velocity that can be considered "safe." For an established value of a "hard" landing, reference is made to an inadvertent landing that occurred[17] while conducting flight tests to determine the Sikorsky Model 52 height-velocity diagram. This landing resulted in vertical ground contact velocity of 22.7 ft. per sec. in combination with a forward ground velocity of 72.8 ft. per sec. While there are many cases of "hard" landings without occupant injury, the case cited was one in which the aircraft was instrumented and the values referred to are recorded ones. The "hard" vertical contact caused the failure of the landing gear and moderate aircraft damage, but without occupant injury. For the present a maximum vertical ground contact velocity of 25 ft. per sec. will be considered as emergency safe until further data can become available.

The assumption would then be to use the following criteria:

(a) For single-engine powered helicopters: The maximum vertical ground contact velocity is to be limited to a "safe" value as determined by landing gear capabilities.

(b) For multiengine helicopters: In the event of a single engine failure, the remaining power can be used during descent and flare-up to reduce the ground contact velocity. The maximum vertical ground contact velocity is to be limited to a "safe" value as determined by landing gear capabilities.

For a total power failure the maximum vertical ground contact velocity is to be limited to that velocity that precludes passenger injury (considered to be 25 ft. per sec.).

It is not the purpose of this paper to argue the validity of the approach that considers valid a distinction between a ground contact velocity acceptable for complete integrity of structure and one acceptable from the standpoint of the probability of avoiding personnel injury, though experience has shown the latter to be substantially greater. This question involves problems as much matters of policy as of engineering, and it is doubtful whether, even though safety equivalent to that of fixed-wing operations could be demonstrated, the approach of permitting the possibility of exceeding the design limit sinking speed would be seriously considered. The purpose here is only to show how the resulting contact velocity may be related on a rational basis to the design characteristics of the helicopter. The design of helicopter structures adequate to the higher contact velocities may well be considerably less of an economic penalty than the alternatives of providing hovering capability with one engine inoperative or the larger heliport dictated by the lower design limit sinking speeds presently in use.

Method of Analysis

The analysis is divided into two portions, these being (1) flight time history of a vertical powered take-off and (2) vertical flight time history after power failure. The flight time history of (1) will provide the initial conditions for part (2) by selecting a given altitude for the time of power failure.

The solution of both portions will be made on the conservative assumption of quasi-static conditions. In investigating the effects of rapid increase of collective pitch, it was found that the rotor lift would be increased from the value expected for steady-state use of collective pitch. In addition, the normal stall limitations of the rotor would be extended so as to allow higher values of maximum lift. These magnitudes of the dynamic lift increases are dependent upon the rapidity of the increase of collective pitch and are maintained for only a short duration. But at the rates of change of collective pitch to be considered, it was estimated[20] that only a $6^1/_2$ per cent increase of maximum rotor lift could be expected. However, since only a small portion of the flight time history encounters rapid change of collective pitch and large decelerations of the aircraft, it was decided that the dynamic lift increment would be neglected, considering the accuracy of the empirical data to be used. Also the ground effect was conservatively neglected since the combination of acceleration and possible ground obstacles tend to decrease this effect.

Flight Time History During Vertical Powered Take-Off[22]

The aircraft is initially considered to be hovering just prior to full powered vertical take-off with a ground height of zero feet. The available rotor shaft horsepower for a rotor mechanical efficiency, η, and engine brake horsepower, *BHP*, is:

$$HP_a = \eta\, BHP \tag{1}$$

For a given rotor r.p.m. the available rotor torque is:

$$Q_a = HP_a\, 5250/(\text{r.p.m.}) \tag{2}$$

From the relationship[25] of

$$Q_a = C_{q_a} A \rho (\Omega R)^2 R \tag{3}$$

the available torque coefficient is then:

$$C_{q_a} = HP_a\, 5250/[(\text{r.p.m.}) A \rho (\Omega R)^2 R] \tag{4}$$

Using the modified Euler notation that n represents the instantaneous time and Δt is the time increment separating n from the previous instant n-1, the relationship of inflow ratio λ, thrust coefficient C_T, and torque coefficient is:[23]

$$\lambda_n C_{T_n} = C_{q_n} = (C_{q_0} - C_{q_a})_n \tag{5}$$

where the instantaneous value of the thrust for zero advance ratio $\mu = 0$ is:

$$T = C_{T_n} A \rho (\Omega R)_n{}^2;\ C_{T_n} = \frac{\sigma a}{2}\left(\frac{\theta_0 B^3}{3} + \frac{\theta_1 B^4}{4} + \frac{\lambda B^2}{2}\right)_n \tag{6}$$

Since the profile power, for rotors employing blade twist, varies only slightly in climb from the hovering value, it may be assumed that changes in C_{q_0} are small

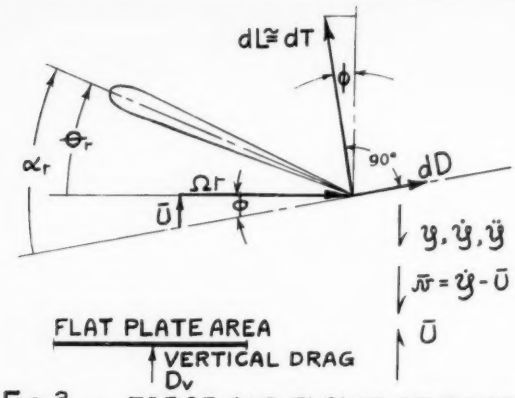

FIG. 3 — FORCE AND FLOWS AT ROTOR AND FLAT PLATE ELEMENTS

in comparison to C_q and that it will be sufficient to use C_{q_0} as determined from hovering as a constant value. This simplifies the problem without any appreciable loss of accuracy. The vertical rate of climb is then:[23]

$$V_{cn} = -\dot{y}_n \cong -\{\lambda - [C_T/(2\lambda B^2)]\}_n \Omega_n R \quad (7)$$

For the vertical powered take-off a constant value of collective pitch and rotor speed will be used for all practical purposes, the rotor speed being selected and collective pitch being found for the condition of steady-state climb.

The collective pitch at the 3/4 effective radius is:[23]

$$\theta_{3/4B\cdot R} = (3/B^3)\,(2C_T/\sigma a) - (1.5\,\lambda/B) \quad (8)$$

where the collective pitch at the blade root for a blade twisted θ_1 radians is:

$$\theta_0 = \theta_{3/4B\cdot R} - (3/4)B\theta_1 \quad (9)$$

The direction of forces and flows as considered in this analysis are shown in Fig. 3. The net flow $\bar{U}$ through the rotor is considered positive when directed up through the rotor.

The equilibrium of forces then becomes, where ϕ is a small angle:

$$M\ddot{y} = W - T - D_v \quad (10)$$

The vertical drag caused by the rotor net flow is the major component of drag, and, since the drag for the other portions of the aircraft not beneath the rotor is relatively small, the latter is neglected.

The vertical drag will be for an equivalent flat plate drag area:

$$D_v = C_{D_F} S_F q = C_{D_F} S_F (\rho/2) \bar{U}^2$$

Letting $K = C_{D_F} S_F (\rho/2)$,

$$D_v = K\bar{U}^2 \quad (11)$$

Since the vector direction of the vertical drag cannot be found from Eq. (11), the algebraic sign of D_v must be that of the average rotor flow $\bar{U}$, or

$$D_v = K\bar{U}^2(\bar{U}/|\bar{U}|) \quad (12)$$

The following finite difference nomenclature will be used to express the displacement, velocity, and acceleration of the aircraft:

$$y_n = y_{n-1} + (\dot{y}_{n-1} + \dot{y}_n)\,(\Delta t/2) \quad (13)$$

$$\dot{y}_n = \dot{y}_{n-1} + (\ddot{y}_{n-1} + \ddot{y}_n)\,(\Delta t/2) \quad (14)$$

For small values of Δt used to solve the equations of motion, the third and higher-order effects are neglected.

To solve the value of the instantaneous inflow ratio λ_n, the combination of Eqs. (7), (13), and (14) resolve to cubic equation of the form:

$$-A_1\lambda_n^3 + (1 + A_2A_{3n})\lambda_n^2 + [-(A_2/2B^2) - A_{4n} + A_{3n}A_{5n}]\lambda_n - (A_{5n}/2B^2) = 0 \quad (15)$$

where the coefficients are:

$$A_{1_n} = K\Omega R\Delta t/(2M)$$

$$A_2 = \sigma\, aB^2/4$$

$$A_{3n} = A\,\rho\Omega R\Delta t/(2M)$$

$$A_{4_n} = [1/(\Omega_n R)]\,[\dot{y}_{n-1} + (\ddot{y}_{n-1} + g)\,(\Delta t/2)]$$

$$A_{5_n} = (\sigma a/2)\,[(\theta_0 B^3/3) + (\theta_1 B^4/4)]_n$$

Since the average flow is down through the rotor disc, the negative and real root of Eq. (15) is used.

The solution of the vertical powered flight history can now be solved by an increment method. The procedure is as follows:

(1) For a stated rotor speed and engine power find C_{q_a} from Eq. (4).

(2) Find value of C_{q_0} for hovering; this may be conveniently found from Fig. 4.9 of reference 25.

(3) Solve inflow λ for steady-state condition $\ddot{y} = 0$ by combining Eqs. (5), (6), and (10).

$$[-K(\Omega R)^2\,(\bar{U}/|\bar{U}|)]\lambda^3 + W\lambda - C_q A\rho\,(\Omega R)^2 = 0$$

Solve for negative and real root.

(4) Using value of λ from (3) find steady-state value of C_T from Eq. (5).

(5) Find value of collective pitch from Eqs. (8) and (9) using steady-state values of λ and C_T.

(6) Solve λ_n from Eq. (15).

(7) Calculate C_{T_n} from Eq. (5).

(8) Calculate T_n from Eq. (6).

(9) Calculate $\ddot{y}_n$ from Eq. (10).

(10) Calculate $\dot{y}_n$ from Eq. (14).

(11) Calculate y_n from Eq. (13).

Using these values for new initial conditions (at time $n - 1$), repeat steps from (6) to (10).

Vertical Flight Time History Following a Power Failure During Powered Vertical Flight

Knowing the initial conditions at the time of a partial or complete power failure, the equation of motion would be:

$$\dot{y}_n = \dot{y}_0 + \int_{t=0}^{t=n} \left[\frac{W - T - K\,\bar{U}^2(\bar{U}/|\bar{U}|)}{M}\right] dt \quad (16)$$

The integral could be solved directly only if the thrust could be considered as being a constant term so that the vertical drag alone would be a function of the flow condition. This would result in an answer that would be untrustworthy due to the method of prestating the problem without any check on the original assumption of being able to maintain a given thrust.

Rotor Thrust

Unfortunately the rotor thrust in the region of vertical descent is complicated by the fact that the energy that goes into providing a given thrust consists of not only the normal drag energy but also of large recirculation losses. This is due to the nature of the flow through the rotor.

Normally the rotor thrust in vertical flight can be stated by the simple propeller momentum theory. The nondimensional thrust coefficients are related in the flow states as:[24]

$$f = F/(1 \pm F)^2 \tag{17}$$

where the positive sign is used for the windmill state where the flow is upwards through rotor and the negative sign is used for the ascent state where the flow is downward through rotor. The coefficients are defined in the following thrust equations as:

$$T = 2 f A \rho \dot{y}^2 \tag{18}$$

$$T = 2 F A \rho \bar{U}^2 \tag{19}$$

In the limited region where the simple momentum theory will not apply, the relationship shown in Fig. 4 has been found empirically or from test.

The three flow states in this region are classically[24] known as:

(A to B) Turbulent windmill brake state where the average flow is up through the rotor disc when the aircraft is descending. Some small recirculation is present, causing an energy loss to the system.

(B to C) Vortex ring state where the average flow is down through the rotor disc when the aircraft is descending. Large recirculation is present, causing roughness of flight and large energy losses to the system.

(C to D) Vertical climb state, in which the average flow is directed down through the rotor when the aircraft is ascending. In this state the simple momentum theory can be shown to apply if correction is made for blade tip losses (contraction of vortex stream due to a finite loading on rotor disc).

Having shown the relationship of the thrust coefficients in this limited flight region, the following relationships are considered to meet the actual conditions with reasonable accuracy.

For the turbulent windmill brake and vertical climb states, a linear relationship is considered with the boundaries shown in Fig. 4.

$$(1/f) + (K_1/F) = K_2 \tag{20}$$

For the vortex ring state a cubic relationship is considered.

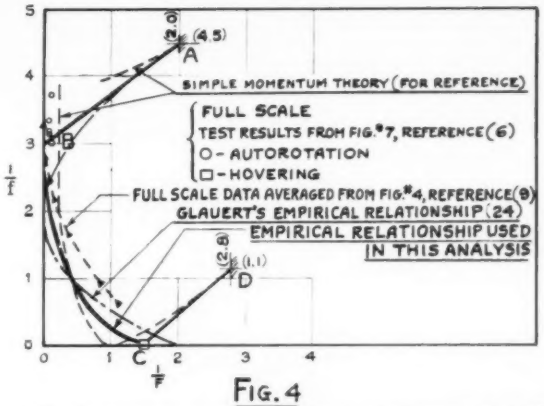

FIG. 4

RELATIONSHIP OF NON DIMENSIONAL COEFFICIENTS f AND F

$$1/F = K_4 [K_3 - (1/f)]^3 \tag{21}$$

The value of the constants being derived from Fig. 4 are:

	Vertical constant for		
Constant	Turbulent windmill brake state	Vortex ring state	Vertical climb state
K_1	−0.750		−0.785
K_2	3.00		−1.10
K_3		3.00	
K_4		0.0518	

Combining the thrust coefficient relationships of Eqs. (20) and (21) to the basic definition of the thrust equations, Eqs. (18) and (19).

$$T = (2A\rho/K_2)(\dot{y}^2 + K_1 \bar{U}^2) \tag{22}$$

for turbulent windmill brake and vertical climb state and

$$T = 2A\rho \bar{U}^2 / \{K_4[K_3 - (\dot{y}/\bar{U})^2(1/F)]^3\} \tag{23}$$

for vortex ring state.

Having empirically defined the thrust in terms of sinking velocity and flow for the particular states of flow, the thrust is now also known for the input condition from Eq. (6) if the value of the flow state for vertical flight is related by:

$$\lambda = \bar{U}/(\Omega R) \tag{24}$$

Rotor Angular Velocity

To find the thrust at a particular time, it is necessary to know the instantaneous value of the rotor speed. This is found by finding the angular acceleration of a rotor at the given time.

The total net accelerating torque input to the rotor is the algebraic sum of the aerodynamic and the engine torque to the rotor; thus, at a particular time n,

$$\dot{\Omega}_n = \frac{Q_{An} + Q_{En}}{I_R} = \frac{C_{q_n} A \rho (\Omega_n R)^2 + Q_{En}}{I_R}$$

where Q_E = engine torque × gear ratio of rotor to en-

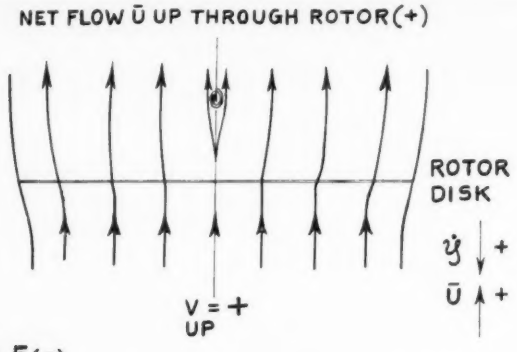

FIG. 5(a)

PICTORIAL VIEW OF TURBULENT WINDMILL BRAKE STATE

gine × mechanical efficiency of system)

$$\Omega_n = [\gamma_1 \Omega_n^2/(2a)]\,(C_1\lambda^2 + C_2\lambda - C_3)_n + \dot{\Omega}_{En} \quad (25)$$

where $\dot{\Omega}_{En} = Q_{En}/I_R$ where[25] for an advance ratio of $\mu = 0$

$$C_1 = [(B^2/2)a] - (\delta_2/2)$$

$$C_2 = \theta_0\left(\frac{B^3}{3}a - \frac{2}{3}\delta_2\right) + \theta_1\left(\frac{B^4}{4}a - \frac{\delta_2}{2}\right) - \frac{\delta_1}{3}$$

$$C_3 = \frac{\delta_0}{4} + \delta_1\left(\frac{\theta_0}{4} + \frac{\theta_1}{5}\right) + \delta_2\left(\frac{\theta_0^2}{4} + \frac{2}{5}\theta_0\theta_1 + \frac{\theta_1^2}{6}\right)$$

The instantaneous angular velocity is:

$$\Omega_n = \Omega_{n-1} + (\dot{\Omega}_{n-1} + \dot{\Omega}_n)\,(\Delta t/2) \quad (26)$$

Combining Eq. (26) with Eq. (25) results in a quadratic of:

$$\Omega_n = [1 \pm \sqrt{1 - 4\,C_{4n}C_{5n}}]/(2\,C_{4n}) \quad (27)$$

where only the negative sign before the square root results in a positive answer and

$$C_{4n} = [\Delta t/(4a)]\gamma_1\,(C_1\lambda^2 + C_2\lambda - C_3)_n$$

$$C_{5n} = \dot{\Omega}_{n-1}(\Delta t/2) + \Omega_{n-1} + (\dot{\Omega}_{En}\,\Delta t/2)$$

For small values of Δt the approximation may be made that

$$\Omega_n \cong C_{5n} + \Omega_{n-1}^2\,C_{4n} \quad (28)$$

Since the available engine torque to rotor may be a function of both r.p.m. and torque requirements, the solution of this part may require the use of charts and/or an auxiliary equation.

The solution of the time history may now be made in the following steps:

(1) Using the conditions at time of power failure as t_{n-1}, the values of y_{n-1}, $\dot{y}_{n-1}$, $\ddot{y}_{n-1}$, Ω_{n-1}, $\dot{\Omega}_{n-1}$, θ_{0n-1} are known.

(2) Select θ_{0n}.

For trial values of λ_n:

(3) Calculate Ω_n from Eqs. (27) or Eq. (28).

(4) Calculate rotor flow $\bar{U}$ from Eqs. (24).

(5) Calculate vertical drag from Eq. (12).

(6) Calculate thrust from Eq. (6) using θ_{0n}.

(7) Calculate $\ddot{y}_n$ from Eq. (10).

(8) Calculate $\dot{y}_n$ from Eq. (14).

(9) Calculate thrust from flow state, $\dot{y}$ and $\bar{U}$ from Eq. (22) or Eq. (23).

(10) Let $\Delta T = T_n$ [step (6)] $- T_n$ [step (9)].

For $\Delta T = 0$, the value of the inflow that results is used to calculate the time history at time, n, and the process is repeated for increasing values of time.

This step process is not difficult but is very laborious. The solutions for both portions of flight time histories in the studies made in this analysis were accomplished in a very quick and economical manner on an IBM 701 Digital Computor. The method of using a digital computor allowed some scanning of the different types of collective pitch control in order to arrive at some analytically optimum control.

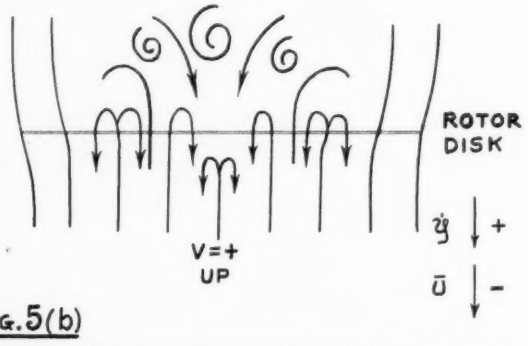

FIG. 5(b)

PICTORIAL VIEW OF VORTEX RING STATE

Relative Autorotative Landing Index

When the time available for investigating a new or revised helicopter design is very limited, a quick, readily available index for evaluation of autorotative landing characteristics is valuable. For this purpose a relative index is developed which may be used but which requires some judgment on the limitations of the value of the index.

The indices of helicopters of known autorotational landing characteristics are compared with the index of a proposed helicopter. The comparison yields a preliminary estimate of the capabilities of the proposed aircraft as compared to known values.

The basic factors affecting the autorotative landing are:

(a) Energy factor: This is the ratio of the kinetic energy of the rotor to the energy of the falling aircraft. The kinetic energy of the rotor is all that is available to the rotor at low to zero forward speeds in autorotation.

(b) Time factor: The rate of loss of the rotor speed is the second factor since this is related to the amount of time for pilot control correction and to the rate of loss of the rotor energy being used.

For an illustrative example, Fig. 6 shows two rotors,

both able to retard the aircraft sinking velocity, but with definitely different time factors. Thus, while Rotor No. 1 may be satisfactory, Rotor No. 2 loses rotor speed too rapidly to allow the pilot to make a normal "safe" landing.

Let the relative autorotative landing index be the following:

$$\text{Index} = \text{Energy factor}/\text{Time factor} \tag{29}$$

where the kinetic energy of rotor is:

$$(\text{K.E.})_R = (1/2)I_R\Omega^2 \tag{30}$$

Kinetic energy of the descending aircraft is:

$$(\text{K.E.})_A = (1/2)M\dot{y}^2 \tag{31}$$

where $\dot{y}$ is empirically $\cong K_5\sqrt{W/A}$ so that

$$(\text{K.E.})_A \cong (1/2)M\,K_5^2(W/A) \tag{32}$$

The previous analysis has shown that the rate of loss of rotor speed without engine power available is:

$$\dot{\Omega} \sim \gamma_1\Omega^2 \tag{33}$$

Dropping constants for the relative index, then:

$$\text{Relative Autorotative Index} = (I_R/W) \div (W/A)\gamma_1 \tag{34}$$

An inspection shows the terms are compatible:

I_R/W = ratio of rotor inertia to weight of aircraft. For a given rotor rotational speed, this value results in a value of kinetic energy per pound of aircraft. The greater this value the better the landing characteristics.

W/A = disc loading, indicative of sinking velocity. The lower this value the less the sinking velocity and resultant aircraft energy required to be dissipated.

γ_1 = rotor mass factor, which is the ratio of the air to mass forces. The lower this value for a given rotor speed, the less the rotor tends to decelerate.

As stated, the index assumes all other factors are the same, such as collective pitch requirements and rotor airfoil characteristics.

A comparison of two helicopter indices is shown in Fig. 7.

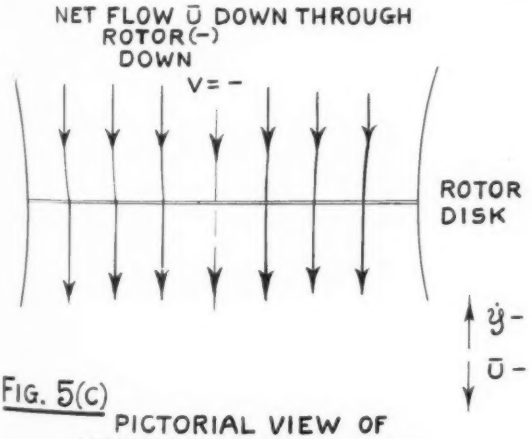

FIG. 5(C) PICTORIAL VIEW OF VERTICAL CLIMB STATE

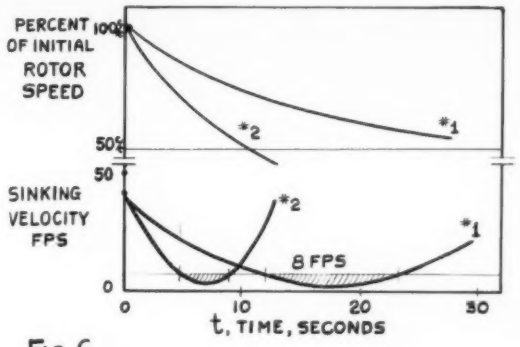

FIG. 6 COMPARISON TIME HISTORIES OF FLARE UPS

While both aircraft have comparable disc loadings, the index value of the S-51 is much higher than that of the S-52. Consequently it can be expected that the autorotative landing characteristics of the S-51 will be appreciably better than for the S-52.

Flight experience with both aircraft has shown that the S-51 has the superior autorotative landing characteristics and performance, in comparison with the S-52.

In addition, some model test data[5] are available, and time histories of power-off flare-ups from steady-state autorotation are shown in Fig. 8. Both test models have an 8-ft. rotor diameter, solidity ratio of 0.08, and blades have NACA 0015 airfoil sections. The collective pitch was increased from 0° to 12½° for the flare-up.

The disc loadings of the rotors are comparable and show the effect of increasing the rotor inertia and reducing the rotor blade mass factor.

Comparison of Theory with Experimental Test and Flight Data

Comparison with controlled experimental test data is limited to the tests made with rotor models tested for the power-off conditions.

Flare-Up Without Power from Steady-State Autorotation

The model rotors shown in Fig. 9 were tested[5] in a fully enclosed tower, which permitted a one rotor diameter clearance to minimize wall interference.

The model rotors were guided in their fall by a wire to ensure vertical descent.[5] Upon reaching a steady rate of autorotative descent, the collective pitch was increased so as to retard the descent of the rotors (flare-ups).

The physical data for the model rotors were:

Model	Disc loading	γ_1
"C"	0.573	2.8
"D"	0.789	5.3

For the analysis the following constants were used: Drag coefficients: $\delta_0 = 0.0097$, $\delta_1 = 0$, $\delta_2 = 0.90$, $\rho = 0.002378$, $a = 5.73$, $B = 0.94$, $\theta_1 = 0$ radians, $K = 0$.

SIKORSKY HELICOPTER AIRCRAFT DATA	S-51*	S-52*
GROSS WEIGHT, LBS (W)	5300	2700
ROTOR DISK LOADING PSF (W/A)	2.81	3.16
ROTOR INERTIA PER LB OF HELICOPTER FEET-SEC^2 (I_R/W)	.396	.100
ROTOR MASS FACTOR (γ_1)	9.55	9.59
RELATIVE MINIMUM SINKING SPEED, FPM	1320	1430
INDEX VALUE $[(I_R/W) \div (W/A)\gamma_1] \times 1000$	14.8	3.3

*ROTOR BLADES ARE ALL METAL OF NACA 0012 AIR FOIL SECTION

FIG. 7 COMPARISON OF AUTOROTATIVE LANDING INDICES

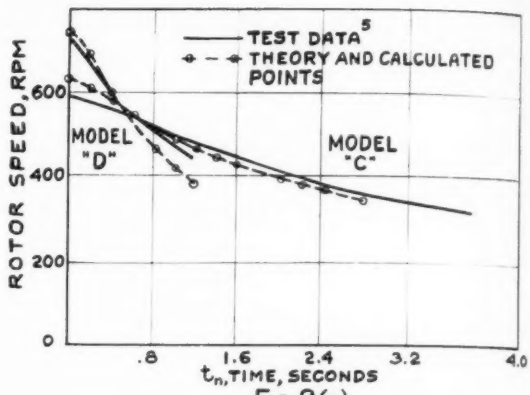

FIG. 9(a) COMPARISON OF TEST AND THEORY FOR POWER-OFF FLARE UPS OF MODEL ROTORS

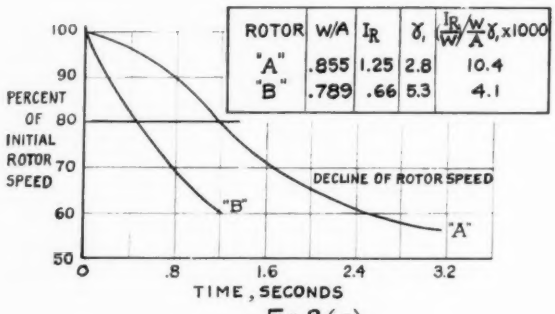

FIG. 8(a) EFFECT OF ROTOR INERTIA AND MASS FACTOR UPON VERTICAL PERFMORMANCE

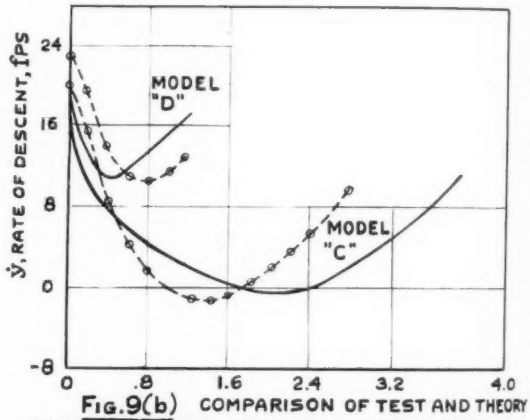

FIG. 9(b) COMPARISON OF TEST AND THEORY FOR POWER-OFF FLARE UPS OF MODEL ROTORS

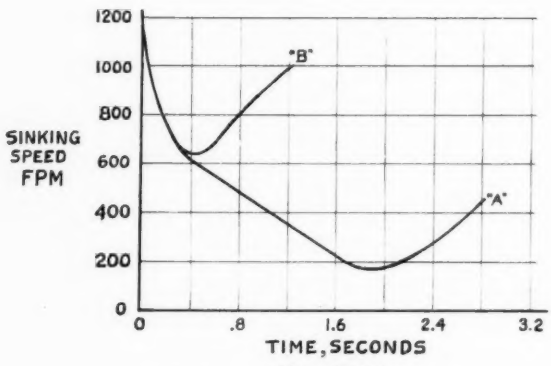

FIG. 8(b) EFFECT OF ROTOR INERTIA AND MASS FACTOR UPON VERTICAL PERFORMANCE

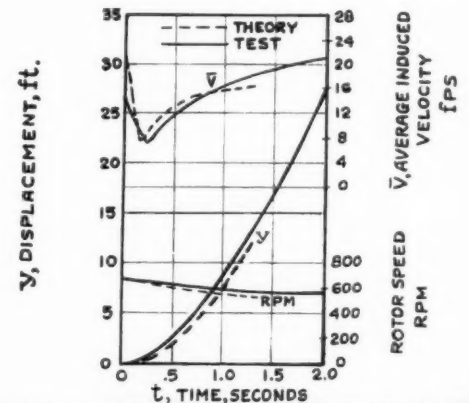

FIG. 10 COMPARISON OF TEST AND OF THEORY FOR THE TRANSITION FROM HOVERING TO VERTICAL AUTOROTATION FOR A MODEL ROTOR

The collective pitch was initially 0° and was increased for the flare-up to 12½° in 0.2 sec.

In Fig. 9 the initial conditions of rotor speed and rate of steady-state descent differ slightly for the theoretical calculations as compared to the recorded values of the test models. This is due to using the present available full-scale empirical $1/f$ vs. $1/F$ data of Fig. 4. No attempt was made to use the actual values of model test data (other than collective pitch) in the theoretical calculations since reference 4 has indicated the rotor flow may be somewhat altered in the vertical test tunnel due to wall effect.

The calculated theoretical time histories are in close correlation with the decline of rotor speed and the minimum sinking speed during the flare-up. There is a difference between theory and test of the time at which the minimum sinking speed occurs, but in investigating a large number of cases it was found that the loss of altitude for a minimum sinking speed was in reasonably close correlation. The discrepancy is on the conservative side and is primarily due to original conservative assumptions contained in basic analysis.

Transition from Hovering to Vertical Autorotation

The model rotor was tested[4] in the same test equipment used for flare-up tests.

The model data were: disc loading of 0.50 lb. per sq.ft., $\gamma_1 = 5.3$, and all other rotor parameters were the same as listed for the flare-up test models.

The same drag coefficients and air density are used as for the flare-up tests.

The model rotor[4] was gradually speeded up (r.p.m.) to a hovering condition, then released, at which time the collective pitch was reduced from 10° to 4° in 0.1 sec

The calculated theoretical time history shown in Fig. 10 is in close correlation with the test data for both decline of rotor speed and loss of altitude. The percentage variation between test and theory is within the accuracy of the rotor blade section airfoil characteristics used for analysis.

Comparison with Full-Scale Test Data

Because of the nature of the problem, little data are available from full-scale instrumented flight. However, there was a test instrumented helicopter that had an inadvertent power failure while hovering at low altitude (1,760 ft.).[11]

During a series of flight tests at the National Lochtvaant Laboratory in Holland, an S-51 helicopter had a complete power failure while hovering. Since the airspeed indicator cannot be considered as accurate in that aircraft at low air speeds, we can only presume that the aircraft was flying at a very low forward speed in the first few seconds after power failure. Records of the collective pitch control indicate that the pilot made no control changes for about a second after power failure and thereupon reduced the collective pitch from the hovering control to a low pitch. Since no data are available on the accuracy of the calibration of the collective pitch control, the calculated results were based upon known Sikorsky data which reduced the collective pitch from 11° hovering to 2° low. Only a trend can be expected since the test records indicate a scatter of 0 to 20 m.p.h. air speed in the immediate time following the power failure.

The 11° initial collective pitch estimate was evidently also made in other investigations of this flight by Stewart and Sissingh,[5] but, as can be expected, the trend at the decline of the rotor speed is similar but not within the accuracy found with the model test rotors.

For the analysis of this flight condition the following data were used: $\delta_0 = 0.010$, $\delta_1 = -0.0216$, $\delta_2 = 0.400$, $\rho = 0.002378$, $\sigma_r = 0.067$, $b = 3$, $W/A = 2.7$ lbs. per sq.ft. $\gamma_1 = 11.41$.

In Fig. 11 the maximum decline of the rotor speed is found to be 68 per cent from the test data, and the theory for a true vertical flight calculates this decline to be 57 per cent. Again, while agreement is not established, the discrepancy is small and on the conservative side.

Example of Analytical Height-Ground Contact Velocity Solution

The aircraft analyzed is a Sikorsky S-55 type helicopter, and the following aircraft and physical values are used:

W = 6,835 lbs.
R = 26.5 ft.
b = 3,
σ = 0.0493
W/A = 3.098 lbs. per sq. ft.
I_R = 2,860 slug ft.^{2}
γ_1 = 9.63
Engine brake horsepower at take-off = 600
η = 0.82 (conservative)
Gear ratio, engine to rotor = 11.315:1
θ_1 = −0.1396 radian
a = 5.73
ρ = 0.002378
B = 0.97
δ_0 = 0.0087
δ_1 = −0.0216
δ_2 = 0.400
$K \cong 0$, no engine power available after power failure

Time History During Full Powered Take-Off

The rotor tip speed was 550 ft. per sec. during the powered take-off. From the method presented in steps (1) to (11) in the powered take-off analysis, the take-off flight time history in Fig. 12 was calculated. It is to be noted that the steady-state climb value is in good agreement with the test data of reference 19.

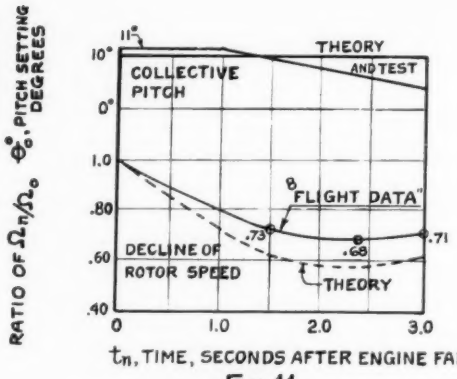

FIG. 11

COMPARISON OF FLIGHT DATA AND THEORY FOR THE BEHAVIOR OF ROTOR AFTER ENGINE FAILURE DURING HOVERING

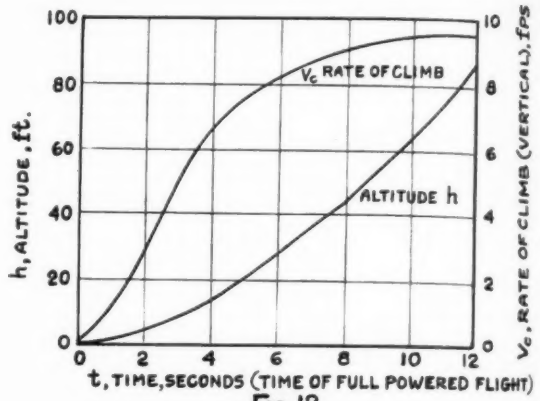

FIG. 12

RATE OF ASCENT AND GAIN OF ALTITUDE DURING FULL POWERED TAKE OFF

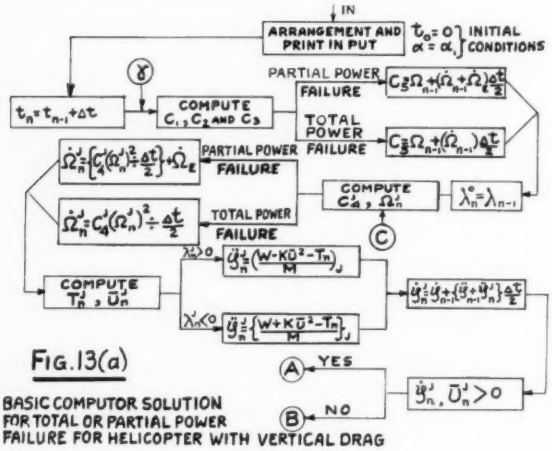

FIG. 13(a)

BASIC COMPUTOR SOLUTION FOR TOTAL OR PARTIAL POWER FAILURE FOR HELICOPTER WITH VERTICAL DRAG

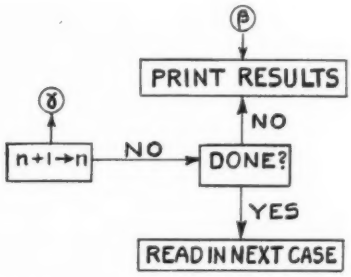

FIG. 13(c)

BASIC COMPUTOR SOLUTION FOR TOTAL OR PARTIAL POWER FAILURE FOR HELICOPTER WITH VERTICAL DRAG

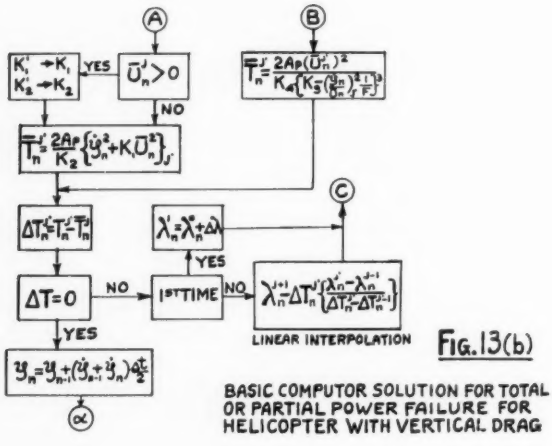

FIG. 13(b)

BASIC COMPUTOR SOLUTION FOR TOTAL OR PARTIAL POWER FAILURE FOR HELICOPTER WITH VERTICAL DRAG

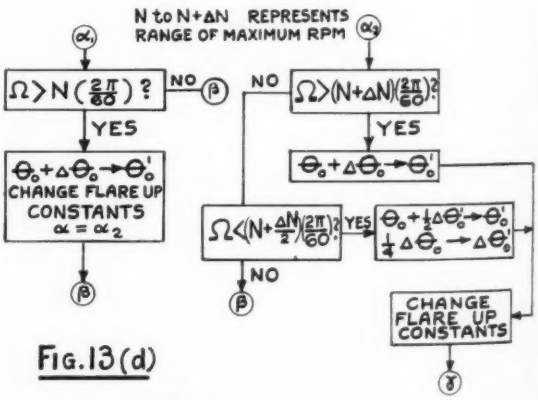

FIG. 13(d)

RPM LIMIT CONTROL

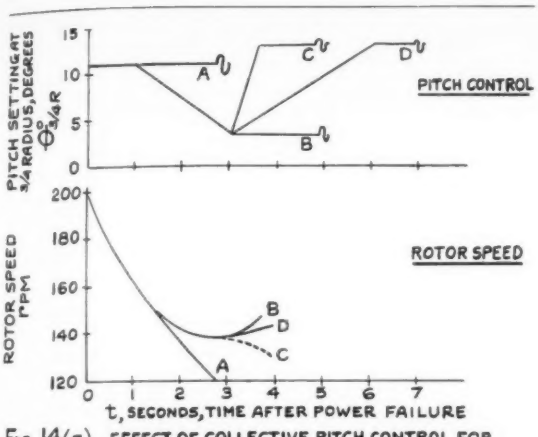

FIG. 14(a) EFFECT OF COLLECTIVE PITCH CONTROL FOR ENGINE FAILURE AT 50 FOOT ALTITUDE

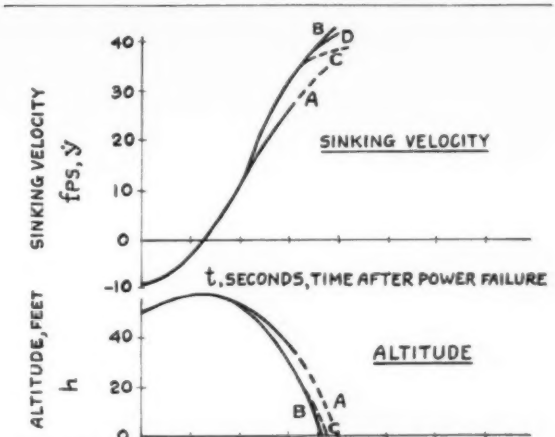

FIG. 14(b) EFFECT OF COLLECTIVE PITCH CONTROL FOR ENGINE FAILURE AT 50 FOOT ALTITUDE

Time History After Power Failure

While the flight time history for powered take-off may be solved by hand calculations, it was found that the use of a digital computor was mandatory for an economical solution of the time histories following a power failure. This also allowed some scanning of the problem in order to find values of collective pitch inputs that resulted in reasonable rotor behavior within the limits of allowable rotor speeds.

The inputs for conditions at time of power failure were found from the time history of powered vertical take-off. The general procedure used is shown in Fig. 13.

Various types of collective pitch control were used in computing the time histories following a power failure. A 1-sec. delay in pilot control was used before any reduction of collective pitch and then reduced to a low setting in a linear manner in 2 secs. In increasing the collective pitch for a flare-up, two rates were used: (1) a fast flare-up from low to high pitch in 0.6 sec. and (2) a moderate flare-up from low to high pitch in 2 secs. The calculated time history following an engine failure at 50 ft. altitude is shown in Fig. 14 and is indicative of calculated histories following engine failure at altitudes of 10 ft. up to 450 ft. Flight experience has shown that this analysis for the Sikorsky S-55 is conservative. The Flight Manual for this aircraft indicates the height-velocity diagram upper limit for zero forward speed is 400 ft. Thus, at an altitude of 400 ft. and zero forward speed, the pilot has evidently been able to land within the design contact velocity of 8 ft. per sec. if forward flight maneuver was used. In actual practice some forward maneuver would normally be available.

The dotted lines in Fig. 14 indicate the beginning of rotor stall. The stall is estimated to start at a blade section angle of attack at 12° at the 0.4 radius of the blade. This criterion appears to be conservative since the model rotor test data do not exhibit this effect when the rotor kinetic energy is used during the flare-up. The criterion is probably conservative because of the assumption of a constant induced angle of attack (ϕ) which is the result of using an average net flow through the rotor disc ($\bar{U}$).

By combining the time histories of power failures occurring at 10 to 450 ft., a height-ground contact velocity relationship can be constructed. This is shown in Fig. 15 for this aircraft.

The rotor system of this aircraft was unable to reduce sufficiently the maximum value of ground contact velocity. By adding 60 lbs. to the rotor for rotating inertia, the maximum contact speed would reduce to 20 ft. per sec.

If this aircraft had two engines each of 300 hp, then the maximum contact speed could be reduced to 25 ft. per sec. for a single-engine descent. Then by adding 60 lbs. to the rotor system, the maximum contact velocity would be further reduced so as to be within the landing gear limitations for this aircraft (8 ft. per sec.).

Conclusions

(1) By proper combination of rotor parameters, both the utility and inherent safety of the helicopter can be improved. The rotor inertia is the most effective means for improving the autorotative and partial powered

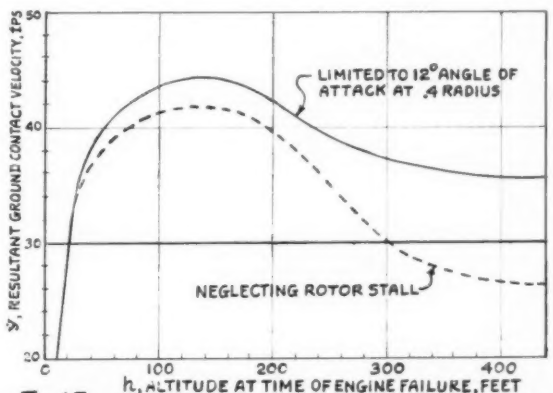
ẏ, RESULTANT GROUND CONTACT VELOCITY, fps
LIMITED TO 12° ANGLE OF ATTACK AT .4 RADIUS
NEGLECTING ROTOR STALL
h, ALTITUDE AT TIME OF ENGINE FAILURE, FEET

FIG. 15 HEIGHT GROUND CONTACT VELOCITY CHARACTERISTICS CHART FOR S-55 HELICOPTER WITH GROSS WEIGHT OF 6835 POUNDS

landing characteristics. The use of a low disc loading by itself does not ensure against marginal autorotative landing characteristics.

(2) The index method provides a means for preventing marginal autorotative landing characteristics from being incorporated in the initial design stage but for proper use requires an element of judgment based on experience. The index is not an absolute criterion and is used only to compare new designs, or modifications of existing designs, with helicopters of known autorotative landing characteristics. The general method of analysis used in this paper provides a more rigorous criterion.

(3) By (a) improving the rotor performance in autorotative landing (which may generally be accomplished at a very small weight cost by increasing the rotor inertia) and (b) permitting the use of, or designing for, higher vertical ground-contact velocities than existing limit sinking speeds of 8 to 10 ft. per sec., safe landings may be accomplished with representative pilot technique following power failure where the entire maneuver is conducted without the benefit of any forward velocity.

(4) These conclusions suggest the possibility of greatly increasing the economic utility of the helicopter by a reduction of heliport size and hence a considerably increased freedom in the selection of heliport sites. They point up the desirability of re-assessing present design requirements to compare this potential economic gain with the possible penalty in terms of operating cost resulting from the increased rotor weight to improve vertical performance and/or the additional structural weight necessary to permit higher contact speeds.

References

[1] Gessow, A., *Flight Investigation of Rotor Blade Twist on Helicopter Performance in the High Speed and Vertical-Autorotative Descent*, NACA TN No. 1666.

[2] Nikolsky, A. A., and Seckel, E., *Analytical Study of the Steady State Vertical Descent in Autorotation of Single Rotor Helicopters*, NACA TN No. 1906.

[3] Nikolsky, A. A., and Seckel, E., *An Analysis of the Transition of a Helicopter from Hovering to Steady State Vertical Descent*, NACA TN No. 1907.

[4] Slaymaker, S. E., Lynn, R. R., and Gray, R. B., *Experimental Investigation of Transition of a Model Helicopter from Hovering to Vertical Autorotation*, NACA TN No. 2648.

[5] Slaymaker, S. E., and Gray, R. B., *Power-Off Flare-Up Tests of a Model Helicopter Rotor in Vertical Autorotation*, NACA TN No. 2870.

[6] Castles, W., Jr., and Gray, R. B., *Empirical Relationship Between Induced Velocity, Thrust and Rate of Descent of a Helicopter Rotor as Determined by Wind Tunnel Tests on Four Model Rotors*, NACA TN No. 2474.

[7] Stewart, W., *Helicopter Behavior in the Vortex Ring Conditions*, ARC TN No. Aero 2131 (Great Britain), November, 1951.

[8] Stewart, W., and Sissingh, G., *Notes on Helicopter Rotor Behavior After Engine Failure in Hovering Flight*, Royal Aircraft Establishment TN Aero 1997 (Great Britain), May, 1949.

[9] Brotherhood, P., *Flow Through Helicopter Rotor in Vertical Descent*, Royal Aircraft Establishment Report Aero 2272 (Great Britain), July, 1948.

[10] Brotherhood, P., *An Investigation of the Induced Velocity Distribution Under a Helicopter When Hovering*, Royal Aircraft Establishment Report No. Aero 2212 (Great Britain).

[11] Lucassen, L., Drees, J., and Senger, E., *Emergency Landing After Power Failure with a Sikorsky S-51 Helicopter*, Report V. 1463 (Holland).

[12] DeHaven, H., *Semi-Annual Progress Report*, Crash Injury Research, Cornell University Medical College, January, 1951.

[13] DeHaven, H., *The Site, Frequency and Dangerousness of Injury Sustained by 800 Survivors of Light-Plane Accidents*, Cornell University Medical College, July, 1952.

[14] DeHaven, H., *Development of Crash-Survival Design in Personal, Executive and Agricultural Aircraft*, Cornell University Medical College, May, 1953.

[15] Hasbrook, A., *Crash Survival Study: National Airlines DC-6 Accident at Elizabeth, New Jersey, on February 11, 1952*, Cornell University Medical College.

[16] Smith, H., and D'Ostilio, P., *An Experimental Investigation of the Drop Test Load Factors of a Hovering Helicopter*, Sikorsky Engineering Report No. SER-1826, May, 1950.

[17] Sherry, M., Macomb, J., and Gartsu, G., *"Structural Demonstration of the HO5S-1 Helicopter for the Bureau of Aeronautics*, Sikorsky Engineering Report No. SER-1862, December, 1952.

[18] Sherry, M., Macomb, J., and Gartsu, G., *Aerodynamic Demonstration of the HO5S-1 Helicotper for the Bureau of Aeronautics*, Sikorsky Engineering Report No. SER-1863, December, 1952.

[19] Hunter, H., and Sullivan, R., *Preliminary Flight Test Report of the YH-19 Helicopter*, Sikorsky Engineering Report No. SER-2018, May, 1950.

[20] Rich, M. J., *A Study of the Effects of Flapping, Cyclic Pitch, and Rapid Increase of Collective Pitch of a Rotor System Upon the Rotor Blade Element Airfoil Characteristics*, Sikorsky Engineering Report No. SER-2531, September, 1953.

[21] Rich, M. J., *Analysis of Vertical Descent Performance for the Purpose of Determining Height-Velocity Limitation Characteristics*, Sikorsky Engineering Report No. SER-2528, September, 1953.

[22] Rich, M. J., *Flight Time History for Partial Powered Vertical Flight for Purpose of Determining Height-Velocity Relationship*, Sikorsky Engineering Report No. SER-3019, December, 1954.

[23] Sikorsky, I. A., *International Handbook of Aeronautical Engineering*, Section 39, Part II (Helicopter Performance), Klemin, A., ed., 1949, unpublished. (Material used is now contained in *Aerodynamics and Performance of Helicopters* by A. Klemin and I. A. Sikorsky, edited by A. Gessow, 1954, distributed by U.S. Dept. of Commerce (PB 111390).)

[24] Durand, W., *Aerodynamic Theory*, Vol. IV, Chapter X, Helicopter Airscrews.

[25] Gessow and Meyers, *Aerodynamics of the Helicopter*, The MacMillan Co., New York, 1952.

Dynamic Derivatives in Yaw and Sideslip of Thin Wings at Supersonic Speeds*

THEODORE R. GOODMAN†
Cornell Aeronautical Laboratory, Inc.

Introduction

The Flight Research Department of the Cornell Aeronautical Laboratory has undertaken a program for the Air Force to compute the stability derivatives of certain specific aircraft and missiles. In connection with this program, the Aerodynamic Research Department of the Laboratory has been assigned the task of computing stability derivatives for a large variety of wings. Many of these derivatives are obtainable directly from the analysis of perturbations from a uniform, steady flow directed parallel to the plane of symmetry of the wing; these offer no particular conceptual difficulties. Others (for example, the rolling wing) may be obtained by introducing the characteristic parameter of the motion into the boundary condition only and by using the same differential equation as for uniform rectilinear motion. The forces and moments induced by these dynamic attitudes are readily obtainable, at least to the first order in the characteristic parameter.

As the program progressed it was found that there are two dynamic attitudes that do not fall into the categories as given above. For these two cases it is necessary to introduce the characteristic parameter into the differential equation and boundary condition simultaneously. These two motions are the rate of change of yaw and the rate of change of sideslip.

Lest there be confusion between them, the two motions will now be described. If a wing in a horizontal attitude moves in a circular path in the horizontal plane such that the angle between the plane of symmetry of the wing and the velocity vector is a constant, then β (the angle of yaw) is a constant, $\dot{\beta}$ (the rate of change of sideslip) is zero, and the wing is undergoing a pure yawing motion. If the radius of the turn is C, the flight speed is U, and the angular velocity of the turn is r, then clearly $r = U/C$. It may be seen that for each revolution about the center of the turn, the wing undergoes one rotation about some central point (the moon revolving about the earth). This rotation induces sidewash and backwash on the wing proportional to r and proportional respectively to the longitudinal and lateral distances of the points on the wing from the central point.

A motion consisting of only a rate of change of sideslip is one for which the sidewash and backwash induced is the same for every point on the wing. There would, therefore, be no rotation and no central point. To imagine this, picture a wing moving at flight speed U while gradually a side velocity V is introduced such that the angle β is changing with time. It is inconvenient to consider this motion *per se*, and instead the wing will be supposed to move forward with constant velocity U at the same time that it rotates with angular velocity $\dot{\beta}$ about a central point. Hence, not only will sidewash and backwash be induced as in the case of pure yawing motion, but also the orientation of the leading edge with respect to the free-stream velocity vector will also change from instant to instant. This is the case for which $r = \dot{\beta}$.

The remainder of this paper will be divided into three parts. Part I deals with the case $\dot{\beta} = 0$; Part II deals with the case $\dot{\beta} = r$; and Part III correlates the work contained in Parts I and II and compares it with the results of other investigators.

Part I—The Curved Flight Path, Zero Rate of Change of Sideslip

Consider a set of Cartesian coordinates ξ, η, ζ fixed in space. If a is the velocity of sound, then the linearized velocity potential obeys the wave equation:

$$(\partial^2\phi/\partial\xi^2) + (\partial^2\phi/\partial\eta^2) + (\partial^2\phi/\partial\zeta^2) = (1/a^2)\,(\partial^2\phi/\partial\tau^2) \quad (1)$$

where τ is the time. The pressure is given by

$$p = \rho(\partial\phi/\partial\tau) \quad (2)$$

Let a wing be revolving counterclockwise with angular velocity r about the origin of coordinates; and let it rotate once for each revolution. Then, if the radius of the turn is $C\ (= U/r)$ and if the center of rotation is the origin of the ξ, η, ζ system, the following transformation of coordinates may be made to axes fixed in the wing, and in this new set the motion will be steady (see Fig. 1)

$$\left.\begin{aligned} y &= \xi\cos r\tau - \eta\sin r\tau - U/r \\ x &= \xi\sin r\tau + \eta\cos r\tau \\ t &= \tau \\ z &= \zeta \end{aligned}\right\} \quad (3)$$

Here x is in the direction opposing the motion, and consequently the x, y, z axes are the so-called wind axes.

Presented at the Aerodynamics Session, Twenty-Third Annual Meeting, IAS, New York, January 24–27, 1955.

* This paper is based upon research carried out under Contract No. W33-038-ac-18517 administered by the Structures Branch of the Aircraft Laboratory of the Wright Air Development Center.

† Principal Engineer.

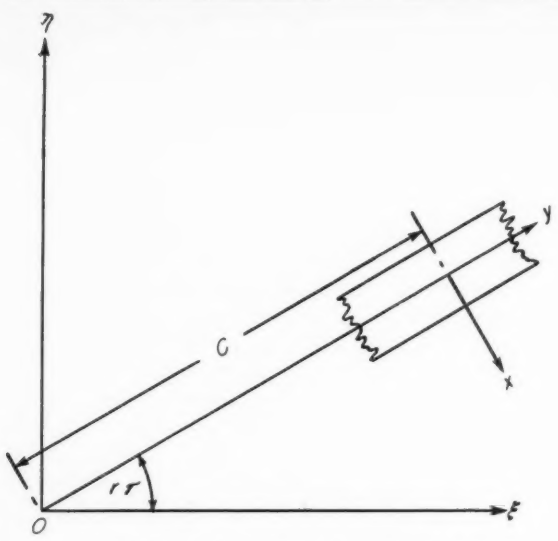

FIGURE 1—A WING IN A CIRCULAR PATH

Applying the transformation (3) to Eq. (1) and retaining terms of order r, there is obtained

$$-B^2\frac{\partial^2\phi}{\partial x^2}+\frac{\partial^2\phi}{\partial y^2}+\frac{\partial^2\phi}{\partial z^2}= b\left(2y\frac{\partial^2\phi}{\partial x^2}-\frac{\partial\phi}{\partial y}-2x\frac{\partial^2\phi}{\partial x\partial y}\right) \quad (4)$$

where $B^2 = M^2 - 1$, M is the free-stream Mach Number, and $b = M^2r/U$. With similar substitutions Eq. (2) becomes

$$p=\rho\{[U(\partial\phi/\partial x)]+[ry(\partial\phi/\partial x)]-[rx(\partial\phi/\partial y)]\} \quad (5)$$

If, in the stationary coordinate system the equation of the surface is given by $g(\xi, \eta, \zeta, \tau) = 0$, then the boundary condition is $g_\tau + \phi_\xi g_\xi + \phi_\eta g_\eta + \phi_\zeta g_\zeta = 0$ at the surface, where the subscripts denote differentiation. Applying Eqs. (3), the boundary condition becomes $g_x(ry + U) - g_y rx + \phi_x g_x + \phi_y g_y + \phi_z g_z = 0$, where it has been assumed that in the new coordinate system g is independent of time. Now express the equation of the surface explicitly such that $z = f(x, y)$ or $g = z - f(x, y)$. The boundary condition becomes

$$-(ry+U)f_x+rxf_y-\phi_x f_x-\phi_y f_y+\phi_z=0 \quad (6)$$

The terms $\phi_x f_x + \phi_y f_y$ are of second order and may be ignored; moreover, consistent with the linearization, the boundary condition may be applied at $z = 0$. The linearized boundary condition for this motion is

$$\partial\phi/\partial z = Uf_x + r(yf_x - xf_y)|_{z=0} \quad (7)$$

The boundary-value problem given by the differential Eq. (4) and the boundary condition (7) will be solved to the first order in r by expanding the potential in powers of r. Let $\phi = \varphi + \psi$ where φ is of zeroth order in r and ψ of first order. Substituting into Eqs. (4), (5), and (7) and equating like orders of r, there is obtained for the zeroth order the equations for straight forward flight which will not be reproduced. For the first order in r, however, there is obtained

$$-B^2\psi_{xx}+\psi_{yy}+\psi_{zz}=b(2y\varphi_{xx}-\varphi_y-2x\varphi_{xy}) \quad (8)$$

$$P=\rho(U\psi_x+ry\varphi_x-rx\varphi_y) \quad (9)$$

$$\psi_z|_{z=0}=r(yf_x-xf_y) \quad (10)$$

The Boundary Condition at the Foremost Surface of Discontinuity*

Jumps in the solution for supersonic flow may occur at the boundary and also on characteristic surfaces or envelopes of these characteristics. The fundamental property of the latter type of discontinuity is that across those surfaces where the jump occurs, the components of velocity tangential to the surface are continuous. Hence, if the equation of such a surface is given by $G(x, y, z) = 0$, and if q_1 and q_2 represent the velocity vector on either side of the surface, then the condition $q_1 \times \nabla G = q_2 \times \nabla G$ ensures the continuity of the tangential velocity. In the special case when the perturbation velocities are zero upstream of such a surface, the condition becomes $\delta q \times \nabla G = 0$ where δq is the perturbation velocity vector. In terms of the perturbation rectilinear velocity components, u, v, w, this vector equation gives the following:

$$u(\partial G/\partial z) = w(\partial G/\partial x); \quad v(\partial G/\partial z) = w(\partial G/\partial y) \quad (11)$$

The third component yields a redundant relationship.

If Eq. (8) were the basic differential equation of the flow, then the characteristic surfaces of the differential equation would be the same as those for uniform flow, and the foremost surface of discontinuity (being the envelope of those characteristic surfaces which passes through the leading edge of the wing) would be the same as that for uniform flow. But the basic equation of the flow is Eq. (4), and the characteristic surfaces of this equation are not the usual Mach cones, but distortions of them. Likewise, the foremost surface of discontinuity (whose equation is $G = 0$) is a distortion of the same surface in a uniform flow. As a result of this distortion Eq. (11) becomes a nonhomogeneous boundary condition. By an argument using the Taylor expansion, it can be shown that to the first order in b this boundary condition at the foremost discontinuity may be applied at the undistorted (uniform flow) location of the discontinuity.

In order that Eqs. (11) be satisfied to order b, the equation $G = 0$ must be found to this order. To do this it is necessary to revert to the fundamental equation of the problem, Eq. (4), and find the characteristic surfaces of this equation. This may be done by the method outlined in reference 1, for example. To order b, the resulting characteristic surfaces are:

* Subsequent to the development of this method it was discovered that Martin and Gerber had developed an alternative procedure for deriving this boundary condition (see references 9 and 10).

$$-(x - x_0)^2 + B^2(y - y_0)^2 + B^2(z - z_0)^2 + b(x - x_0)\,[(x - x_0)\,(y + y_0)/B^2 + (y - y_0)(x + x_0)] = 0 \quad (12)$$

where the apex of the conoid is located at the point x_0, y_0, z_0.

For any particular wing problem with a supersonic leading edge, the foremost discontinuity, G, will be an envelope of the characteristic conoids whose apexes form the locus that is the leading edge. For example, if the equation of the leading edge is $z_0 = 0$, $x_0 = ky_0 (k < B)$, then this represents an infinite sweptback wing with a supersonic leading edge (see Fig. 2). Substitute these into Eq. (12), differentiate with respect to y_0, and eliminate y_0 from the equation thus obtained and Eq. (12). This standard procedure for finding an envelope gives the following equation for G (to order b):

$$G = 0 = (x - ky)^2 - \lambda^2 z^2 - (b/\lambda^4)(x - ky)^2\,[(2B^2 - k^2 + k^2B^2)y - (2k^2 - B^2 + 1)kx] \quad (13)$$

where $$\lambda = \sqrt{B^2 - k^2}$$

The subject of the boundary condition along the foremost surface of discontinuity will be pursued further later on.

The Particular Integral

It is easily verified by substitution that a particular integral of Eq. (8) is

$$\bar{\psi} = (b/B^2)\,[-xy\varphi_x + (M^2 - 2)x^2\varphi_y/2B^2 - y\varphi/2] \quad (14)$$

Hence the complete solution, ψ, will be

$$\psi = \psi' + \bar{\psi} \quad (15)$$

where ψ' satisfies the homogeneous equation

$$-B^2\psi_{xx}' + \psi_{yy}' + \psi_{zz}' = 0 \quad (16)$$

and the boundary condition

$$\psi_z'|_{z=0} = -\bar{\psi}|_{z=0} + r(yf_x - xf_y) \quad (17)$$

together with the proper condition at the foremost surface of discontinuity.

The Infinite Sweptback Wing

Only a flat plate will be considered which, in effect, means that angle of attack will be taken into account, but the thickness of the wing will be ignored. Eventually, this will permit a determination of the rolling moment due to rate of yaw (proportional to angle of attack, α, and r) but not yawing moment due to rate of yaw (proportional to αr and thickness parameter).

The zeroth order solution for a flat plate is given by

$$\varphi = -(u\alpha/\lambda)\,(x - ky - \lambda z) \quad (18)$$

The particular integral associated with this solution is found from Eq. (14):

$$\bar{\psi} = (bU\alpha/B^2\lambda)\,[3xy/2 + k(M^2 - 2)x^2/2B^2 - ky^2/2 - \lambda zy/2] \quad (19)$$

The complementary solution must be of the form of a polynomial of the second degree

$$\psi' = bU\alpha(Ax^2 + B'y^2 + Cz^2 + Dxy + Exz + Fyz) \quad (20)$$

In order that this satisfy Eq. (16), it is necessary that $C = B^2A - B'$. Then, incorporating certain of the constants of the particular integral into the arbitrary constants of the complementary function, there is obtained

$$\psi = (bu\alpha/B^2\lambda)\,\{[A + k(M^2 - 2)/2B^2]x^2 + (B' - k/2)y^2 + (B^2A - B')z^2 + Dxy + Exz + Fyz\} \quad (21)$$

If the boundary condition at the wing is applied—viz., $\psi_z|_{z=0} = ry\alpha$—it is found that $E = 0$, $F = B^2\lambda/M^2$. The remaining unknown constants A, B', D must be determined from the conditions at the Mach sheet. There are really two Mach sheets involved in Eq. (13), one above the $z = 0$ plane and one below. Only the solution above will be considered, and the solution below will be determined by considerations of symmetry. For b equal to zero, Eq. (13) becomes $(x - ky - \lambda z)\,(x - ky + \lambda z) = 0$. The solution $x - ky - \lambda z = 0$ corresponds to the Mach sheet above the $z = 0$ plane. Hence, to obtain this Mach sheet for the case when $b \neq 0$ let $x = ky + \lambda z + b\,\Delta x$, substitute into Eq. (13), and equate coefficients of like powers of b. This special surface G, becomes

$$G = 0 = x - ky - \lambda z - (bz/2\lambda^3) \times [(2B^2 - k^2 + k^2B^2)y - (2k^2 - B^2 + 1)k(ky + \lambda z)] \quad (22)$$

Now the boundary condition at the Mach sheet may be determined explicitly for the problem at hand.

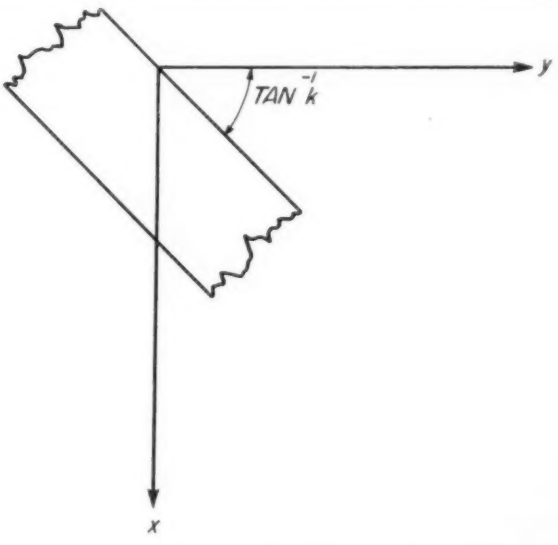

FIGURE 2—THE SWEPT BACK WING

Let $u = u_0 + u_1$; $v = v_0 + v_1$; $w = w_0 + w_1$; where $u_0 = \varphi_x$, $u_1 = \psi_x$, etc. Then, substituting into Eq. (11) there is obtained, upon equating like orders,

$$\left.\begin{aligned} w_1 &= (u_0 b/\lambda^2)\,[kz(2k^2 - B^2 + 1) - \lambda(1 + k^2)y] - \lambda u_1 \\ v_0 b[kz(2k^2 - B^2 + 1) - \lambda(1 + k^2)y]\lambda^{-2} - \lambda v_1 &= w_1 k - w_0 b z \lambda^{-2}(1 + k^2) \end{aligned}\right\} \quad (23)$$

From Eq. (18) the zeroth order velocity components are found to be

$$\left.\begin{aligned} \varphi_x &= u_0 = -U\alpha/\lambda \\ \varphi_y &= v_0 = U\alpha k/\lambda \\ \varphi_z &= w_0 = U\alpha \end{aligned}\right\} \quad (24)$$

From Eq. (21), the first-order velocity components are

$$\left.\begin{aligned} \psi_x = u_1 &= (bU\alpha/B^2\lambda)\,\{Dy + [2A + k(M^2 - 2)/B^2]x\} \\ \psi_y = v_1 &= (bU\alpha/B^2\lambda)\,[Dx + (2B' - k)y + B^2\lambda z/M^2] \\ \psi_z = w_1 &= (bU\alpha/B^2\lambda)\,[2z(B^2 A - B') + B^2\lambda y/M^2] \end{aligned}\right\} \quad (25)$$

Substitute Eqs. (24) and (25) into Eqs. (23) and evaluate at $x = ky + \lambda z$. Then, since the equations must hold true for all y and z, the coefficients in each of Eqs. (23) are set equal. The result is four conditions at the Mach sheet [two from each of Eqs. (23)]. It is readily ascertained that one of the equations is redundant, and consequently there are three equations for the three unknowns A, B', D. Solving for these constants it is found that

$$A + k(B^2 - 1)/2B^2 = -(kB^2/4\lambda^4) \times (5k^2 + 3 - 2B^2) + B^2 k/2\lambda^2 M^2 \quad (26)$$

$$D = (B^2/2\lambda^4)\,(2B^2 + k^2 + 3k^4) - B^4/\lambda^2 M^2 \quad (27)$$

$$B' - k/2 = -(kB^2/4\lambda^4)\,(4B^2 - k^2 + 2B^2k^2 + k^4) + B^2 k(B^2 + \lambda^2)/2\lambda^2 M^2 \quad (28)$$

The pressure is readily ascertained to be

$$p = [\rho U r\alpha(1 + k^2)/2\lambda^5]\,[2\lambda^2(y + kx) - 3M^2 k(x - ky)] + (\rho U r\alpha/\lambda^3)\,(-B^2 y + kx) \quad (29)$$

If the wing is unswept, $k = 0$, and Eq. (29) becomes

$$p = \rho U r\alpha(2 - M^2)y/B^3 \quad (30)$$

A discussion of this result, along with a comparison with the investigations of Harmon,[2] Westley,[3] and Lomax, Heaslet, and Fuller[4] will be found in Part III.

The rolling moment is given by

$$L = -\iint 2pydS \quad (31)$$

where the integration is to extend over the entire wing area, and the factor 2 takes into account the underside of the wing. The rolling moment coefficient is defined to be

$$C_{lr\alpha} = L \div (1/2)\rho U^2(rs/U)S2s\alpha \quad (32)$$

where S is the wing area and s is the semispan. The result of this calculation is

$$C_{lr\alpha} = -2[(1 + k^2)^2 - B^2]/3\lambda^3 + 0(1/B\mathbf{R}) \quad (33)$$

This formula is charted in Fig. 3. It should be noted that this result is correct for a two panel sweptback wing with supersonic leading edges provided the aspect ratio, $\mathbf{R}$, is large enough. It is significant that $C_{lr\alpha}$ changes sign. Sweepback clearly delays this change by increasing the Mach Number at which the change occurs.

Slender Wings

At this point a different type of wing will be studied—namely, the slender wing. It can be seen by examining Eq. (8) that for slender wings the right-hand side is dominated by the term φ_y. The other terms on the right-hand side are of higher order in slenderness since they are differentiated with respect to x. Hence, the

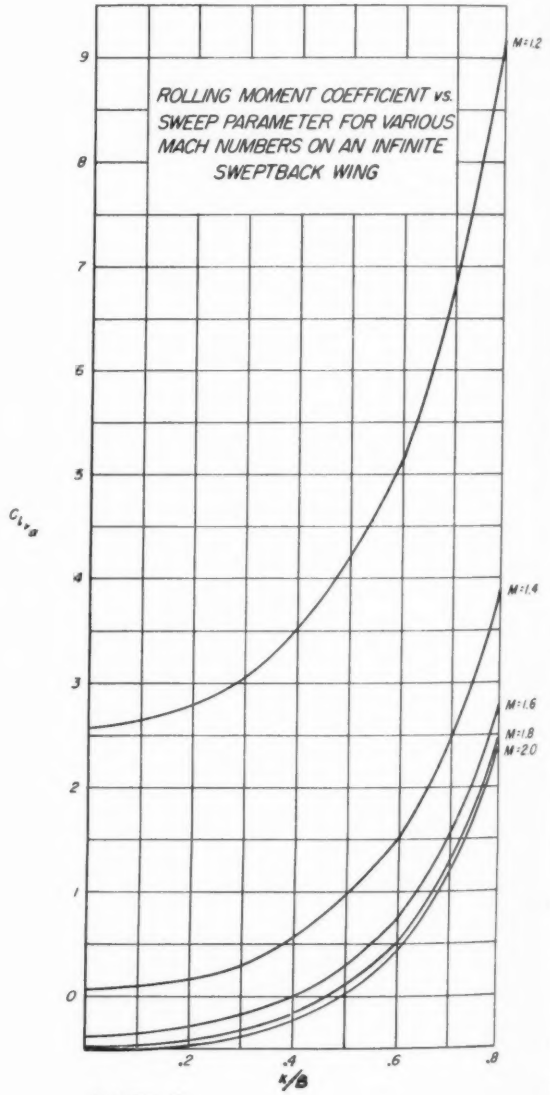

FIGURE 3

solution for ψ will be of the same order in slenderness as φ. Armed with this knowledge, the pressure formula, Eq. (9), can be attacked, and it is seen that the first two terms are of higher order in slenderness than the last term because they involve derivatives with respect to x. Hence, for slender wings, the pressure formula becomes

$$p = -\rho r x \varphi_y \tag{34}$$

Insofar as the linearized pressure formula is correct, this result is valid for any slender configuration and not merely planar ones. It can be seen that it is not necessary to obtain ψ at all, but, rather, the zeroth order solution is sufficient for obtaining the pressure. Ribner[5] has used this result successfully to obtain rolling moment due to rate of yaw of slender wings.

Part II—The Straight Flight Path, Rate of Change of Sideslip Equals Rate of Yaw

In the previous problem of the curved flight path the equations of motion involved the parameter r, and the solution, to the first order in r, was obtained by first linearizing the boundary value problem with respect to r and then attempting to find the solution. Only the infinite sweptback wing was considered, and even this very simple plan-form shape offered considerable mathematical complexity.

For the problem of the straight flight path ($\dot{\beta} = r$), a different method of attack will be used. Fortunately, a method exists for obtaining the complete solution for general classes of plan forms without linearizing with respect to $\dot{\beta}$. Hence, in theory at least, the solution could be obtained first, and the linearizations effected afterwards. In practice, however, it is found convenient to perform the linearization as the solution is developed. The method that will be used is a modification of that given by Gardner[6] who has shown how to solve for the potential of a planar wing in supersonic flow when the disturbances are small nonsteady perturbations from a uniform rectilinear motion.

Chapter I—The Theory of Wings with Supersonic Edges

The Gardner Method for Solving Nonsteady Wing Problems

Consider a wing lying in the $z = 0$ plane and flying in the x direction with velocity U. If x, y, z are rectilinear coordinates fixed in the wing, then for a thin wing the velocity potential obeys the following partial differential equation for flows depending on time, t.

$$(M^2 - 1)\phi_{xx} - \phi_{yy} - \phi_{zz} + (2M/a)\phi_{xt} + (1/a^2)\phi_{tt} = 0 \tag{1}$$

If $z = F(x, y, t)$ describes the surface of the wing and $W(x, y)$ is the projection of the wing in the x, y-plane, then the boundary condition is

$$\text{for } (x, y) \text{ in } W \quad \lim_{z \to 0^+} \phi_z = \lim_{z \to 0^-} \phi_z = UF_x(x, y, t) + F_t(x, y, t) \tag{2}$$

The spatial "initial" condition is

$$\text{for } x < x_0, \ \phi \equiv 0 \tag{3}$$

Gardner[6] has presented a method for attacking the above problem. The chief points will be briefly described. First, transform the variables x and t to the variables x' and t', where

$$\left.\begin{aligned} x' &= x/B \\ t' &= (Mx - B^2at)/B \end{aligned}\right\} \tag{4}$$

Let $h = UF_x + F_t$. Now drop the primes on the transformed variables x' and t'. All subsequent equations will be given in terms of the transformed variables unless it is specifically stated to the contrary. Eqs. (1), (2), and (3) become

$$\text{for } (x, y) \text{ in } W, \ \lim_{z \to 0^+} \phi_z = \lim_{z \to 0^-} \phi_z = h(x, y, t) \tag{5}$$

$$\text{for } x < x_0, \quad \phi \equiv 0 \tag{6}$$

$$\text{for } x > x_0, \quad \phi_{xx} - \phi_{yy} - \phi_{zz} - \phi_{tt} = 0 \tag{7}$$

Gardner's method consists in introducing the variable ξ and the quantities ψ and χ and in reducing this four-dimensional problem to two three-dimensional ones. χ satisfies the following boundary-value problem

$$\text{for } \xi \geq 0, \ \chi_{xx} - \chi_{tt} - \chi_{\xi\xi} = 0 \tag{8}$$

$$\text{for } \xi = 0, \ \chi = h(x, y, t) \tag{9}$$

$$\text{for } x < x_0, \ \chi = 0 \tag{10}$$

Having found x, one then proceeds to find ψ, which satisfies the following boundary-value problem:

$$\psi_{\xi\xi} - \psi_{yy} - \psi_{zz} = 0 \tag{11}$$

$$\lim_{z \to 0^+} \psi_z = \lim_{z \to 0^-} \psi_z = \chi(\xi, x, y, t) \tag{12}$$

$$\text{for } \xi > x - x_0, \quad \psi \equiv 0 \tag{13}$$

The velocity potential itself is then found by setting $\xi = 0$ in ψ—viz.,

$$\phi(x, y, z, t) = \psi(0, x, y, z, t) \tag{14}$$

The pressure in terms of physical x, t variables is given by

$$p = \rho(\phi_t + U\phi_x) \tag{15}$$

This presents Gardner's method as he himself has given it. A slight modification is required in order to apply it to the problem at hand. For the wing undergoing a rate of change of yaw, the projection of the wing in the x,y-plane is dependent upon the time. Hence, let W_1 be this projection and let W be independent of time, where $W_1 \subset W$. Then $h(x, y, t)$ can be taken as zero for x, y in $(W - W_1)$. Now the problem can be reformulated so that h will be independent of time and W_1 will depend on it.

The spacial "initial" point x_0 is chosen far ahead of the wing, and so, whereas Eq. (13) is certainly true, it is not of any value in determining the "leading edge" of the "wing" to be analyzed in determining ψ. The

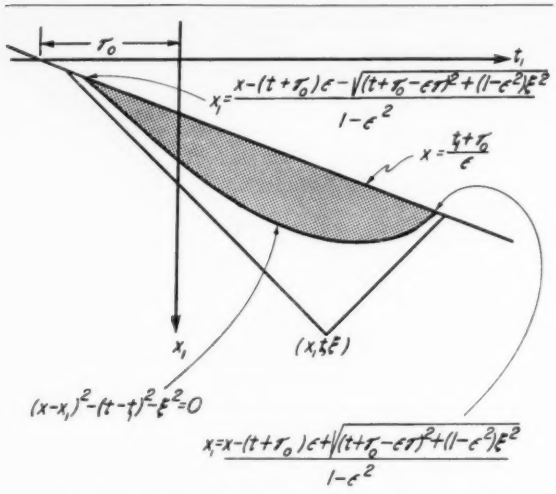

FIGURE 4—THE "WING" OF THE FIRST PROBLEM

equation of this leading edge will be found from the solution for χ.

The Wing Undergoing a Rate of Change of Yaw

It will be assumed that the leading and trailing edges of the wing are supersonic, and that the amount of yawing which occurs is not sufficient to change the character of any edge. Later on the restriction of supersonic leading edges will be removed. Assume the equation of the leading edge is given by

$$x = g(y) \tag{16}$$

Let the central point be the origin; then if the equation of the leading edge is transformed into polar coordinates, r and θ, this becomes

$$r \cos \theta = g(r \sin \theta) \tag{17}$$

If the wing rotates counterclockwise with angular velocity $\dot{\beta}$, then θ must be replaced by $\theta - \dot{\beta}t$.

Reconverting to rectangular coordinates and considering $\dot{\beta}t$ to be small, Eq. (17) becomes

$$x + \dot{\beta}ty = g(y) - g'(y)\dot{\beta}tx \tag{18}$$

Introducing the transformed variables, Eq. (41), there is obtained

$$x\epsilon - \tau_0 = t \tag{19}$$

where

$$\left.\begin{aligned} \epsilon &= (1 + M\gamma)/\nu \\ \gamma &= \dot{\beta}\, G(y)/aB^2 \\ G(y) &= y + g(y)g'(y) \\ \tau_0 &= g(y)/\gamma B \end{aligned}\right\} \tag{20}$$

The First Problem

The quantity h which appears in Eq. (9) is the upwash on the wing and is equal to $w(x, y)$ provided $x > x_{LE}$; h is zero for $x < x_{LE}$. It is convenient to define a quantity σ such that

$$\partial\sigma/\partial\xi = \chi \tag{21}$$

σ satisfies the wave equation, Eq. (8), and Eq. (9) becomes in terms of transformed variables

$$\partial\sigma/\partial\xi = w(Bx, y) \tag{22}$$

The boundary value problem in $xt\xi$ space can be thought of as a wing problem with Eq. (19) defining the leading edge. But Eq. (19) is a straight line since the coordinate y is merely a parameter. The solution for σ may be obtained by integrating simple sources over the shaded area as shown in Fig. 4. If the result is carried out to the first order in γ (i.e., $\dot{\beta}$) there is obtained

$$\partial\sigma/\partial\xi = \chi = w\,[B(x - \xi), y] \tag{23}$$

But this result is true only aft of the leading edge "Mach sheet." Ahead of this sheet $x = 0$. In order to find the equation of the sheet consider the general characteristic cone:

$$(x - x_0)^2 - (t - t_0)^2 - (\xi - \xi_0)^2 = 0 \tag{24}$$

where x_0, t_0, ξ_0, is the location of the apex. The leading edge "Mach sheet" will be the envelope of such cones, the apexes of which form the locus that is the leading edge. From Eq. (19), put $\xi_0 = 0$, $t_0 = x_0\epsilon - \tau_0$ into Eq. (24). Differentiate with respect to x_0, and eliminate x_0 between the original and the differentiated equations. To the first order in γ(i.e., $\dot{\beta}$) there is obtained

$$\xi = x - g(y)/B - \gamma[t - Mg(y)/B] \tag{25}$$

Recapitulating the results of the first problem: for $\xi \leqq x - g(y)/B - \gamma[t - Mg(y)/B]$

$$\chi = \begin{cases} w[B(x - \xi), y] \\ 0 \end{cases} \tag{26}$$

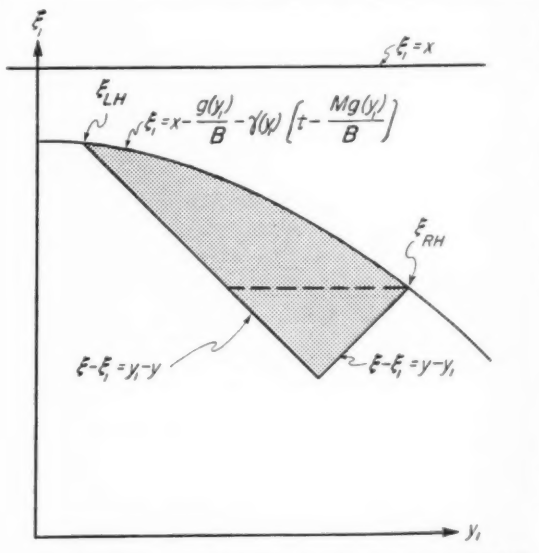

FIGURE 5—THE "WING" OF THE SECOND PROBLEM

The Second Problem

Eq. (25) becomes the equation of the leading edge of the "wing" as shown in Fig. 5. If $\dot{\beta}$ were zero, then the leading-edge equation would be $\xi_1 = x - g(y_1)\,B$; but the function $g(y_1)$ has been so specified that this is a supersonic edge. It will be assumed that, although the leading-edge equation is given by $\xi_1 = x - g(y_1)\,B - \gamma(y_1)\,[t - Mg(y_1)/B]_1$, nevertheless, the leading edge remains supersonic. The function ψ will be obtained for $z \to 0$ so that finally, when ξ is put equal to zero, the potential, ϕ will have been obtained only on the wing.

The leading-edge equation, Eq. (25), is a relation between ξ_1 and y_1 (x is merely a parameter in the second problem). It is convenient to have an explicit expression for y_1 in terms of ξ_1. Let the inverse of the equation $x = g(y)$ be given by $y = f(x)$. Then, to the first order in $\dot{\beta}$, the leading-edge equation becomes

$$y_{LE} = f[B(x - \xi_1)] - \dot{\beta}F[B(x - \xi_1)] \times [t - M(x - \xi_1)]\,aB \quad (27)$$

where $F(x) = f(x)f'(x) + x$.

The solution for ψ is obtained by integrating sources over the shaded region shown in Fig. 5.

$$\psi = -\frac{1}{\pi}\int_{\xi}^{\xi_{RH}} d\xi_1 \int_{y+\xi-\xi_1}^{y-\xi+\xi_1} \frac{w[B(x-\xi_1),\, y_1]dy_1}{\sqrt{(\xi-\xi_1)^2 - (y-y_1)^2}} - \frac{1}{\pi}\int_{\xi_{RH}}^{\xi_{LH}} d\xi_1 \int_{y+\xi-\xi_1}^{y_{LE}(\xi_1)} \frac{w[B(x-\xi_1),\, y_1]\,dy_1}{\sqrt{(\xi-\xi_1)^2 - (y-y_1)^2}} \quad (28)$$

Let $\xi_{RH} = \xi_{RH}^{(0)} + \dot{\beta}\xi_{RH}^{(1)}$; $\xi_{LH} = \xi_{LH}^{(0)} + \dot{\beta}\,\xi_{LH}^{(1)}$; $y_{LE} = y_{LE}^{(0)} + \dot{\beta}y_{LE}^{(1)}$; where $\xi_{RH}^{(0)}$, $\xi_{RH}^{(1)}$, $\xi_{LH}^{(0)}$, $\xi_{LH}^{(1)}$, $y_{LE}^{(0)}$, $y_{LE}^{(1)}$ are all independent of $\dot{\beta}$. In order to obtain that portion of ψ which is proportional to $\dot{\beta}$, differentiate Eq. (28) with respect to $\dot{\beta}$ and take lim $\dot{\beta}\to 0$. If it is observed from Fig. 5 that $y_{LE}^{(0)}(\xi_{LH}^{(0)}) = y + \xi - \xi_{LH}^{(0)}$, and $y_{LE}^{(0)}(\xi_{RH}^{(0)}) = y - \xi + \xi_{RH}^{(0)}$, then a number of simplifications can be effected, and the result is

$$\frac{\partial\psi}{\partial\dot{\beta}} = \frac{1}{\pi}\int_{\xi_{RH}^{(0)}}^{\xi_{LH}^{(0)}} \frac{w[B(x-\xi_1),\, y_{LE}^{(0)}]d\xi_1}{\sqrt{(\xi-\xi_1)^2 - (y-y_{LE}^{(0)})^2}} \quad (29)$$

From Eq. (27), it is determined that

$$y_{LE}^{(0)} = f[B(x - \xi_1)] \quad (30)$$

$$y_{LE}^{(1)} = -F[B(x - \xi_1)]\,[t - M(x - \xi_1)]/aB \quad (31)$$

When $\xi = 0$, $\psi = \phi$. Then if the variable of integration is changed such that $x_1 = B(x - \xi_1)$ and if the function $F(x_1)$ is expressed explicitly [see Eq. (27)], then in terms of the physical xt variables, the potential may be written as a line integral along the leading edge of the wing (see Fig. 6).

$$\phi = \frac{-\dot{\beta}}{aB^2\pi}\int_{A_1}^{B_1} \frac{w(x_1, y_1)\,(y_1dy_1 + x_1dx_1)[M(x - x_1) - B^2at]}{\sqrt{(x - x_1)^2 - B^2(y - y_1)^2}} \quad (32)$$

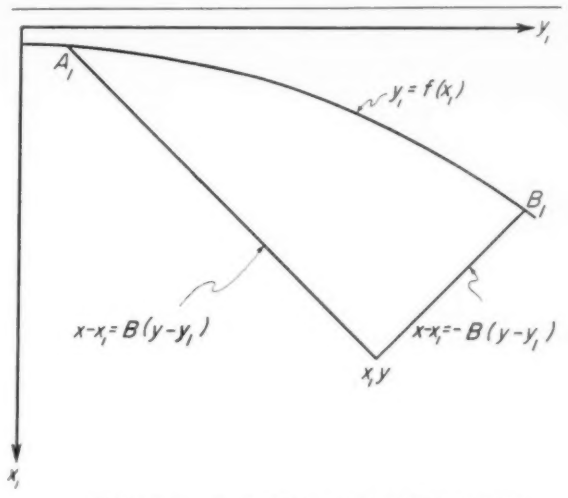

FIGURE 6 – THE WING IN PHYSICAL SPACE

The Formula for the Pressure

Eq. (32) may be substituted into the formula for the pressure, Eq. (15), provided the finite part of the integral is taken when the integrals are differentiated.[7] The pressure may be written as two terms; the first is proportional to $\dot{\beta}t$, the other proportional to $\dot{\beta}$ alone. But the quantity $\dot{\beta}t$ for small $\dot{\beta}$ and small t is merely the angle of yaw, β. It can, in fact, be shown that the term proportional to $\dot{\beta}t$ is precisely that which would have been obtained for the pressure due to a small angle of yaw of amount $\dot{\beta}t$ if steady flow considerations were used. The pressure, therefore, splits up into two parts—that part which is proportional to $\dot{\beta}$ and that part which is proportional to β. Specifically, if the xy axes represent unyawed coordinates, then

$$\frac{\partial p}{\partial\dot{\beta}} = \frac{\rho}{\pi}\left[\int_{A_1}^{B_1} \frac{(y_1dy_1 + x_1dx_1)\,[(x - x_1)^2 + (y - y_1)^2]w(x_1, y_1)}{[(x - x_1)^2 - B^2(y - y_1)^2]^{3/2}}\right] \quad (33)$$

$$\frac{\partial P}{\partial\beta} = \frac{\rho U}{\pi}\left[\int_{A_1}^{B_1} \frac{(y_1dy_1 + x_1dx_1)\,(x - x_1)w(x_1, y_1)}{[(x - x_1)^2 - B^2(y - y_1)^2]^{3/2}}\right] \quad (34)$$

CHAPTER II—APPLICATIONS TO WINGS WITH SUPERSONIC EDGES

(1) The Infinite Sweptback Wing

For the wing under consideration the leading-edge equation is given by $y_1 = x_1/k$ (see Fig. 7). It will be assumed that the wing is a flat plate so that w is constant. Then the integration is readily performed along the leading edge, and the final result is

$$p = [w\dot{\beta}\rho(1 + k^2)/\lambda^5]\,[-y(M^2 - 1 + 3k^2M^2 - k^2) + kx(1 + k^2 + 2M^2)] \quad (35)$$

For $k = 0$ (unswept wing)

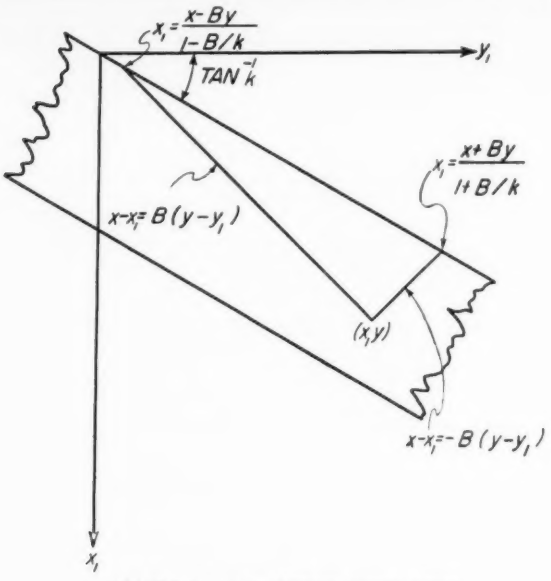

FIGURE 7—THE SWEPT BACK WING

$$P = -w\dot{\beta}\rho y/B^3 \tag{36}$$

(2) *The Wide Delta Wing*

The wing to be considered is a flat plate, so that w is a constant. The central point is chosen to be the apex of the wing. Then (see Fig. 8) in regions I and II the solution for the sweptback wing is used. In region III the integrations may be performed along the leading edge. The result is

$$p_{III} = \frac{-w\dot{\beta}\rho(1 + k^2)}{\pi\lambda^5}\left\{[(kx + B^2y)(1 + k^2) + 2M^2k(ky + x)]\cos^{-1}\frac{kx + B^2y}{B(ky + x)} + [(-kx + B^2y)(1 + k^2) + 2M^2k(ky - x)] \times \cos^{-1} - \frac{kx + B^2y}{B(ky - x)}\right\} \tag{37}$$

(3) *The Rolling Moment on the Wide Delta Wing*

The rolling moment is given by

$$L = -2\iint_s py\,dS \tag{38}$$

where the integration is to be performed over the entire wing area, S, and the factor 2 takes into account the underside of the wing. The result is obtained after a great deal of calculation in a very simple form:

$$L = 4w\dot{\beta}\rho(1 + k^2)c^4/B^3k^3 \tag{39}$$

where c is the root chord.

Define the dimensionless coefficient of this rolling moment to be

$$L \div (1/2)\rho U^2(\dot{\beta}s/U)2sS = C_{lr} + C_{l\dot{\beta}} \tag{40}$$

If C_{lr} is the partial derivative of the rolling moment coefficient with respect to rate of yaw and $C_{l\dot{\beta}}$ is the partial derivative of the rolling moment coefficient with respect to rate of change of sideslip, then for the motion under consideration ($r = \dot{\beta}$) the coefficient defined by Eq. (40) is the sum $C_{lr} + C_{l\dot{\beta}}$. The result for the wide delta wing is

$$C_{lr} + C_{l\dot{\beta}} = \alpha(1 + k^2)/3B^3 \tag{41}$$

where α ($= w/U$) is the angle of attack.

Chapter III—Wings for Which a Subsonic Edge Adjoins a Supersonic Edge

Although it is by no means necessary to do so, wings that have a subsonic edge will be restricted to flat plates, so that w is constant. It is easily seen that the first problem in the Gardner method remains identically the same as before. The method of Evvard[5] will be applied to solve the new configuration that manifests itself in the second problem. For a flat plate the solution is obtained by integrating sources over the region S_1 (shown shaded in Fig. 9). By expanding for small $\dot{\beta}$ in a manner similar to that used in the previous problem, one is led finally to the result that

$$\psi = -\frac{w\dot{\beta}}{\pi}\int_{\xi_{LH}^{(0)}}^{\xi_P^{(0)}} \frac{y_{LE}^{(1)}(\xi_1)d\xi_1}{\sqrt{(\xi - \xi_1)^2 - (y - y_{LE}^{(0)})^2}} - \frac{w\dot{\beta}}{\pi}\int_{\xi_{RH}^{(0)}}^{\xi_P^{(0)}} \frac{d\xi_1(y_{RH}^{(1)} + \xi_{RH}^{(1)})}{\sqrt{(\xi - \xi_1)^2 - (y - y_{RH}^{(0)} - \xi_{RH}^{(0)} + \xi_1)^2}} \tag{42}$$

If it is observed that $y_{RH}^{(1)} + \xi_{RH}^{(1)}$ is independent of ξ_1, then the second integral may be evaluated. The first term in Eq. (42) will reduce in the final analysis to Eq. (32) with B_1 replaced by B_1' (see Fig. 10). Concentrate attention on the second term of Eq. (42). If the integration is performed, there is obtained

$$\Delta\psi = -(w\dot{\beta}/\pi)(y_{RH}^{(1)} + \xi_{RH}^{(1)}) \times \sqrt{(\xi_P^{(0)} - \xi_{RH}^{(0)})/(\xi_{RH}^{(0)} - \xi)} \tag{43}$$

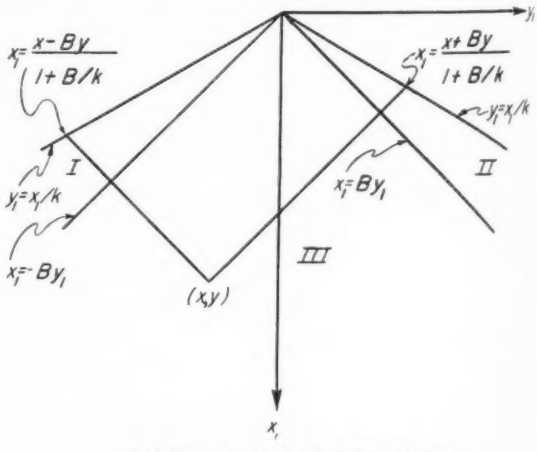

FIGURE 8—THE WIDE DELTA WING

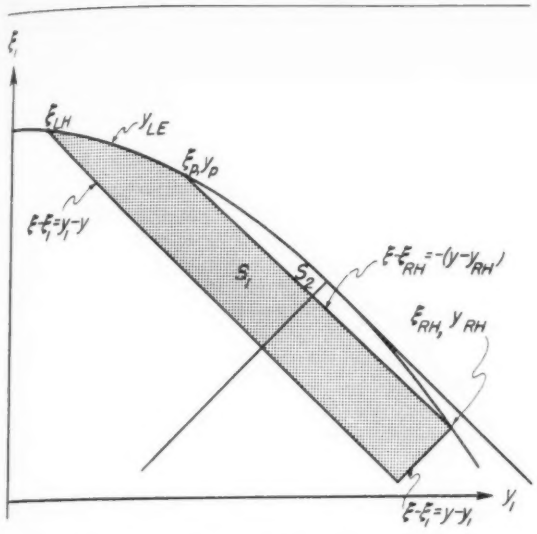

FIGURE 9—THE "WING" OF THE SECOND PROBLEM WITH AN ADJACENT SUBSONIC EDGE

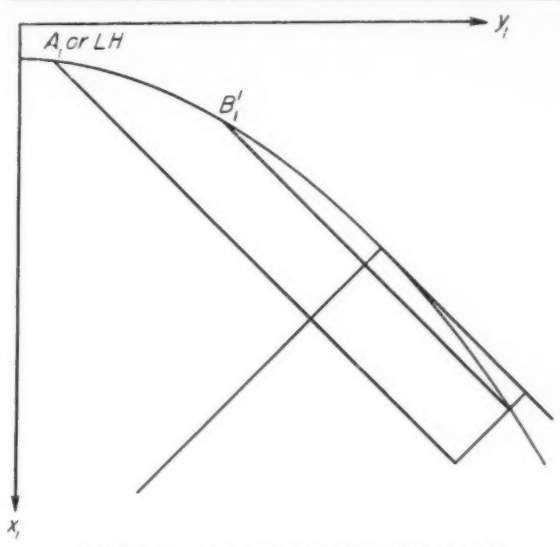

FIGURE 10—THE WING IN PHYSICAL SPACE WITH AN ADJACENT SUBSONIC EDGE

where use has been made of the identity $y_{RH}^{(0)} = y + \xi_{RH}^{(0)} - \xi$. Let $\eta = B(x - \xi)$. Then $\eta_{RH} = B(x - \xi_{RH})$, etc. Replace the variable ξ by η throughout Eq. (43); there is then obtained

$$\Delta\psi = -(w\dot{\beta}/\pi)\,(y_{RH}^{(1)} - \eta_{RH}^{(1)}/B)\,\sqrt{(\eta_{RH}^{(0)} - \eta_p^{(0)})/(\eta - \eta_{RH}^{(0)})} \quad (44)$$

In order to obtain the potential, ξ must be set equal to zero. In this case $\eta = Bx$, where x is the transformed variable. In terms of the physical variable $\eta = x$ when $\xi = 0$. The various quantities involved in Eq. (44) can be explicitly stated in terms of variables on the physical wing if recourse is made to the so-called Mach coordinates. Let

$$\left.\begin{aligned} \eta/B &= v + u \\ y &= v - u \\ \eta_1/B &= v_1 + u_1 \\ y_1 &= v_1 - u_1 \end{aligned}\right\} \quad (45)$$

The pertinent lines are all labeled in Mach coordinates in Fig. 11. The quantity under the radical in Eq. (44) is readily transformed into $[v - v_3(u_2)]/[u - u_2(v)]$. It is necessary to obtain the transformation of the quantity $(y_{RH}^{(1)} - \eta_{RH}^{(1)}/B)$. The Mach line that passes through the points u,v and *RII* is expressed by

$$\eta/B + y = \eta_1/B + y_1 \quad (46)$$

Let $y_1 = y^{(0)} + \dot{\beta}y^{(1)}$; $\eta_1 = \eta^{(0)} + \dot{\beta}\eta^{(1)}$. Substitute into Eq. (46) and equate coefficients of like powers of $\dot{\beta}$. Then there is obtained

$$y^{(0)} + \eta^{(0)}/B = y + \eta/B; \qquad y^{(1)} + \eta^{(1)}/B = 0 \quad (47)$$

Hence the quantity $(y_{RH}^{(1)} - \eta_{RH}^{(1)}/B)$ becomes $2y_{RH}^{(1)}$.

The equation of the leading edge, as determined from Eq. (27), becomes when expressed in terms of the variable η

$$y_1 = f(\eta_1) - (\dot{\beta}/aB)\,[f(\eta_1)f'(\eta_1) + \eta_1] \times (t - M\eta_1/B) \quad (48)$$

Once again, let $y_1 = y^{(0)} + \dot{\beta}y^{(1)}$; $\eta_1 = \eta^{(0)} + \dot{\beta}\eta^{(1)}$, substitute into Eq. (48), and equate coefficients of like powers of $\dot{\beta}$. There is then obtained

$$\left.\begin{aligned} y^{(0)} &= f(\eta^0) \\ y^{(1)} &= \eta^{(1)}f'(\eta^{(0)}) - B^{-1}[f(\eta^{(0)})f'(\eta^{(0)}) + \eta^{(0)}] \times (t - M\eta^{(0)}/B) \end{aligned}\right\} \quad (49)$$

Eliminating $\eta^{(1)}$ from the second of Eqs. (47) and the second of Eqs. (49) and solving for $y_{RH}^{(1)}$, there is obtained

$$y_{RH}^{(1)} = -(1/aB)\,[f(\eta^{(0)})f'(\eta^{(0)}) + \eta^{(0)}] \times (t - M\eta^{(0)}/B)/[1 + Bf'(\eta^0)] \quad (50)$$

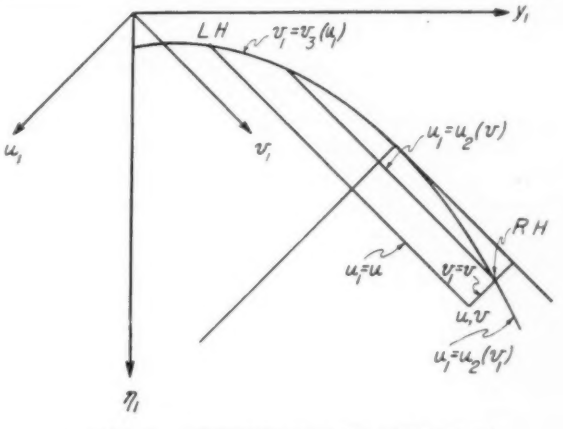

FIGURE 11—PERTINENT LINES LABELED IN MACH COORDINATES

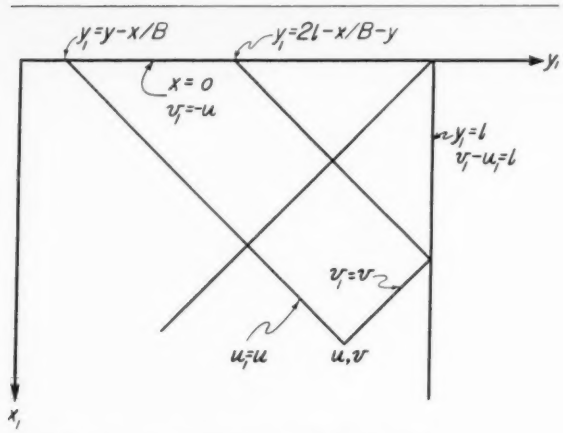

FIGURE 12—THE RECTANGULAR WING TIP

Change to Mach coordinates. Then, along the leading edge

$$\left.\begin{aligned} f(\eta_1) &= v_1 - u_2(v_1) \\ f'(\eta_1) &= [1 - u_2'(v_1)]/B[1 + u_2'(v_1)] \end{aligned}\right\} \quad (51)$$

At the point *RII*, since $v_1 = v$, these equations become

$$\left.\begin{aligned} f(\eta^{(0)}) &= v - u_2(v) \\ f'(\eta^{(0)}) &= [1 - u_2'(v)]/B[1 + u_2'(v)] \end{aligned}\right\} \quad (52)$$

These quantities may be substituted into Eq. (50), which in turn implies the explicit expression for $\Delta\psi$. If the entire formula is then expressed in terms of physical variables, the final expression for the potential may be written

$$\begin{aligned} \phi = &- \frac{w\dot{\beta}}{\pi aB^2}\int_{A_1}^{B_1'} \frac{(y_1dy_1 + x_1dx_1)\,[M(x - x_1) - B^2at]}{\sqrt{(x - x_1)^2 - B^2(y - y_1)^2}} - \\ &\frac{2w\dot{\beta}}{\pi aB^2}\left[u_2 - vu_2' - \frac{M^2}{2}(u_2 + v)(1 + u_2')\right]\times \\ &[M(u - u_2) - Bat]\sqrt{\frac{v - v_3(u_2)}{u - u_2}} \end{aligned} \quad (53)$$

where the first term is given in terms of rectilinear coordinates and the second in terms of Mach coordinates: $x/B = v + u$; $y = v - u$. This is the most convenient way to express the potential. The corresponding expression for the pressure is found to be very cumbersome, and it is simpler to find the pressure for any particular case after the potential is found for that case.

Chapter IV—Application to the Rectangular Wing

The method of Evvard used in Chapter III is applicable to subsonic leading edges. For subsonic trailing edges the method must be modified in order to satisfy the Kutta condition. It is not clear whether the streamwise edge which will be considered in this section is actually the limit of a leading or a trailing edge. What is more, the character of the edge does not remain the same when it is subjected to an infinitesimal yawing velocity, so that it is not certain that a stability derivative, as such, even exists. Nevertheless, the solution obtained in chapter III will be applied to the tip of the rectangular wing.

When the pressure in the tip is finally obtained, it will be observed that there is a singularity along the streamwise tip. One might argue that for a trailing edge all that is necessary to permit the Kutta to be satisfied is to put this singular term equal to zero. In fact, this is so in the case of simple lifting wings. But this is an invalid argument for the wing undergoing a rate of yaw, because, although it is true that the Kutta condition implies that the pressure vanishes along the trailing edge, this does not imply that the partial derivative of the pressure with respect to $\dot{\beta}$ for small $\dot{\beta}$ also vanishes. In fact, the additional linearization with respect to β also gives rise to a singularity along the edge, and it is not clear, *per se*, which of the singular terms are singular because the pressure itself is singular and which are singular because of the linearization with respect to $\dot{\beta}$. In fact, the solution is found to be singular along the Mach line that passes through the juncture of leading and side edges, and this singularity is due, solely, to the linearization with respect to $\dot{\beta}$. Clearly, the pressure is in grave error in these neighborhoods; but, nevertheless, the integrated rolling moment may be expected to be in reasonable agreement with experiment.

The rectangular wing is depicted in Fig. 12 where the pertinent lines have been labeled in both Mach coordinates and Cartesian coordinates. Applying Eq. (53) to this configuration there is obtained

$$\begin{aligned} \phi = \frac{w\dot{\beta}}{\pi B}\left(t - \frac{Mx}{B^2a}\right)\Bigg\{ & y\cos^{-1}\left[1 - \frac{2(l - y)}{x/B}\right] - \\ & 2\sqrt{l - y}\,\sqrt{x/B - l + y}\Bigg\} - \\ & \frac{2w\dot{\beta}B}{\pi}\left[t - \frac{M(l - y)}{Ba}\right]\frac{(x/B + y - l)^{3/2}}{\sqrt{l - y}} \end{aligned} \quad (54)$$

The pressure is obtained from Eq. (13). If the term proportional to t is ignored, it is found that

$$\begin{aligned} p = \frac{\rho w\dot{\beta}}{\pi B^3}\Bigg\{ & -y\cos^{-1}\left[1 - \frac{2(l - y)}{x/B}\right] + \\ & M^2(y + x/B)\sqrt{\frac{l - y}{x/B - l + y}} + (2 + M^2B^2)\times \\ & \sqrt{(l - y)(x/B + y - l)} - \\ & 2B^4(x/B + y - l)^{3/2}/\sqrt{l - y}\Bigg\} \end{aligned} \quad (55)$$

The rolling moment is given by Eq. (38). Eq. (55) is to be used in the tip region, whereas Eq. (36) is proper in the "two-dimensional" region. The integrations in the tip region are easily performed if the integration variables x and y are changed to x' and θ, where $x = x'$; $y = l - x'(1 - \cos\theta)/2B$. The final result for the rolling moment coefficient is

$$C_{lr} + C_{l\dot{\beta}'} = \frac{4\alpha}{3B^3}\left[1 - \frac{3(M^2+1)}{2\,AR'} - \frac{(-7+7M^2-3M^4)}{2\,AR'^2} - \frac{(5-6M^2-3M^4)}{8\,AR'^3}\right] \quad (56)$$

where $AR'(= B.R)$ is the reduced aspect ratio. It is worth noting that the effect of aspect ratio can be such as to change the sign of the rolling moment coefficient from the two-dimensional value and thereby change the stability characteristics of the wing.

Part III—Rate of Change of Sideslip and Yaw—a Comparison

It is interesting to compare the results of previous investigators with those obtained herein. Harmon[2] by a heuristic approach has solved for C_{lr} for a two-dimensional wing, and when his result is expressed in terms of stability (wind) axes it concurs with the present one. Westley[3] has also computed C_{lr} for a two-dimensional wing by a more rigorous procedure. His result, which is computed directly in wind axes, agrees with Harmon's, although he seems unaware that the reason they seem to differ is because they are expressed in a different set of axes.

Lomax, Heaslet, and Fuller[4] have computed C_{lr} for the two-dimensional wing in body axes, and their result concurs with the other investigators.

Consider the following self-explanatory table which has been made for the two-dimensional wing.

	Body axes	Wind axes
$C_{l_{r\alpha}}$	$-2/3B^3$	$-2(2-M^2)/3B^3$
$C_{l_{r\alpha}} + C_{l_{\dot{\beta}\alpha}}$	$-2/3B^3$	$-2(2-M^2)/3B^3$

It is to be noted that C_{lr} and $C_{lr} + C_{l\dot{\beta}}$ are equal when computed in the same set of axes. Hence, if the two coefficients are subtracted, it is found that in any set of axes $C_{l\dot{\beta}} = 0$. Hence, rate of sideslip does not affect the rolling moment to the first order. It may be inferred from this that all strip theories for three-dimensional wings based on two-dimensional sectional results will always be devoid of the effect of rate of sideslip. A subtler three-dimensional approach, such as that given herein, is necessary in order to obtain distinct numerical values for the two different coefficients.

References

[1] Webster, A. G., *Partial Differential Equations of Mathematical Physics*, Chapter VI; G. E. Steckert & Co., New York, 1933.

[2] Harmon, Sidney M., *Stability Derivatives at Supersonic Speeds of Rectangular Wings with Diagonals Ahead of the Tip Mach Lines*, NACA Report 925, 1949.

[3] Westley, R., *The Potential due to a Source Moving Through a Compressible Fluid, and Applications to Some Rotary Derivatives of an Aerofoil*, The College of Aeronautics, Cranfield Report No. 54, 1952.

[4] Lomax, H., Heaslet M., and Fuller, F., *Three-Dimensional Unsteady Lift Problems in High Speed Flight-Basic Concepts*, NACA TN 2256, 1950.

[5] Ribner, Herbert S., *The Stability Derivatives of Low-Aspect Ratio Triangular Wings at Subsonic and Supersonic Speeds*, NACA TN 1423, 1947.

[6] Gardner, Clifford S., *Time-Dependent Linearized Supersonic Flow Past Planar Wings*, Com. Pure & Appl. Math., Vol. III, No. 1, 1950.

[7] Hadamard, Jacques, *Lectures on Cauchy's Problem*, Dover, 1952.

[8] Evvard, J. C., *Use of Source Distributions for Evaluating Theoretical Aerodynamics of Thin Finite Wings at Supersonic Speeds*, NACA Report 951, 1950.

[9] Martin, John C., and Gerber, Nathan, *On the Effect of Thickness on the Damping in Roll of Airfoils at Supersonic Speeds*, Journal of the Aeronautical Sciences, Vol. 20, No. 10, pp. 699–704, October, 1953.

[10] Martin, John C., and Gerber, Nathan, *The Effect of Thickness on Pitching Airfoils at Supersonic Speeds*, Jour. Math. & Physics, Vol. 33, pp. 46–56, April, 1954.

Discussion of the Lecture (*Continued from page 329*)

are to be flown at appreciable supersonic speeds. Evidently this problem is much more critical for the supersonic fighter than it has been for subsonic airplanes of this type. As is well known, appreciable dynamic load increments due to gusts have been observed at subsonic speeds on some of the larger airplanes now in use, and it seems evident that very thorough dynamic loads studies will be required for any large airplane which may be designed for operation at supersonic speeds. The major difference, as in the flutter case, between the large airplane and the fighter is largely a matter of increased complexity due to the greater number of vibration modes that must be considered.

Figs. 1–4 illustrate, on an exaggerated scale, the nature of the dynamic response of a large airplane during penetration of a discrete gust of 1-cosine type. Fig. 1 shows the relative proportions of the gust in relation to airplane size. Fig. 2 shows the wing deflection immediately before the gust encounter and at an early stage of penetration. Fig. 3 is an exaggerated view of the structural distortions of the wing when the airplane is approximately midway through the gust. It is quite evident here that there is a substantial torsional deflection of the wing in addition to the bending component. Finally, Fig. 4 shows the distortions existing as the airplane is leaving the gust area. The presence of bending components of higher than first order is evident here.

In conclusion I should like to say that it has not been my intention to indicate or imply any disagreement with the content of Professor Bisplinghoff's lecture. In presenting the Nineteenth Wright Brothers Lecture, he has performed an extremely valuable service by outlining the trends to be expected in a rapidly developing and vital technical field. I am sure that his comments will serve as a very useful guide for design analysis, indicating a number of possible pitfalls which we must guard against in designing aircraft for higher speeds.

The Flow Over a Body in a Choked Wind Tunnel and in a Sonic Free Jet*

BERNARD W. MARSCHNER†
California Institute of Technology

SUMMARY

The pressure distribution over a double wedge airfoil under free flight conditions with Mach Number 1 is compared with the pressure distribution over the same airfoil in a choked closed wind tunnel and in a sonic free jet.

The computation is carried out as a development with respect to a parameter which indicates the deviation from free flight conditions at Mach Number 1.

The results are of interest in considering the question of wind-tunnel corrections. The deviations from the free flight pressure distribution are of about the same magnitude for the choked flow in a closed tunnel as for a free jet of the same width—the sign of the deviations is different.

For the specific example of a wedge whose length is 13 per cent of the tunnel height and with a thickness ratio of 10 per cent, the deviations of the pressure distribution barely exceed the usual experimental scatter.

The results are quite encouraging for the application of closed throat wind tunnels in transonic testing, although the axial symmetric case may not show entirely the same behavior.

(1) INTRODUCTION

TEST RESULTS obtained in a closed wind tunnel under conditions at and close to choking are generally considered somewhat unreliable. It is believed that the data obtained are greatly distorted once the local supersonic region at the body grows to the wind-tunnel walls. In a recent theoretical investigation,[1] Guderley has shown that in the vicinity of the model a flow under choking conditions will have a close resemblance to a flow with a free-stream Mach Number 1 if the ratio between tunnel width and model thickness is sufficiently large. The important question is the order of magnitude of the deviation. If for a reasonable ratio of wind tunnel to model size the deviations are within limits which are acceptable from a technical point of view, then it would be possible to use the present closed test sections in an extended Mach Number range. For this reason the present paper determines numerical data for the example of a double wedge airfoil in a choked closed wind tunnel and in a sonic free jet of finite width. The results are compared with the pressure distribution over the body in a free stream of Mach Number 1, which are available in reference 2.

Received February 11, 1955.

* This paper is a condensed version of a Ph.D. thesis accepted at the California Institute of Technology.

† Formerly, Graduate Student, C.I.T. Now, Lt. Col., Arnold Engineering Development Center, USAF.

(2) FORMULATION OF THE BOUNDARY VALUE PROBLEM

Fig. 1 shows a double wedge airfoil in a closed wind tunnel under choking conditions. Similar flow patterns have been described previously,[1, 2] therefore we mention only some salient features. The sonic line CO extends with a downstream slope from the model to the wall. From the shoulder of the wedge a fan of rarefaction waves propagates out into the flow. Some of these waves will end at the sonic line, while those further downstream terminate at the wind-tunnel wall. The Mach wave DO, which is the last one to reach the sonic line—i.e., whose point of intersection with the sonic line lies at the wall—will be referred to as the limiting characteristic; it limits the part of the supersonic region which can influence the subsonic region.

The hodograph representation of this flow pattern is shown in Fig. 2. Corresponding points in the physical plane (Fig. 1) and in the hodograph plane (Fig. 2) have the same notation. The zero streamline starts at infinity point A with the choking Mach Number and goes to the stagnation point at the nose of the wedge, then it follows the side of the wedge to the shoulder. At the shoulder it undergoes a Prandtl-Meyer expansion represented by the line CD, which will be referred to as the shoulder characteristic. The wall streamline starts in the hodograph with the choking Mach Number and increases to sonic speed; since its slope is zero, it maps into a portion of the horizontal axis of the hodograph plane.

The wedge in a sonic free jet is shown in Fig. 3. All streamlines begin with the sonic velocity and at the entire boundary streamline sonic speed prevails. The zero streamline has qualitatively the same behavior as in a closed tunnel. The corresponding hodograph representation in Fig. 4 requires no further explanation.

As usual the hodograph equation will be reduced by the transonic approximation to the so-called Tricomi equation. The above boundary value problems are then of the type investigated by Tricomi,[3] thus the questions of existence and uniqueness of the solutions are settled. Regarding the manner in which the solutions will be constructed the following point of view is important. In transonic wind-tunnel testing the model is small in comparison to the wind-tunnel width, thus the choking Mach Number will be close to 1. Hence a development of the solution with respect to the deviation of the choking Mach Number from 1 (or with respect to a similar parameter in the case of the

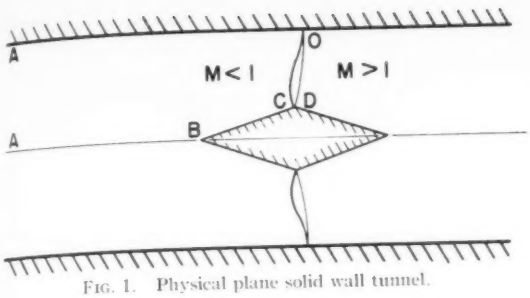

FIG. 1. Physical plane solid wall tunnel.

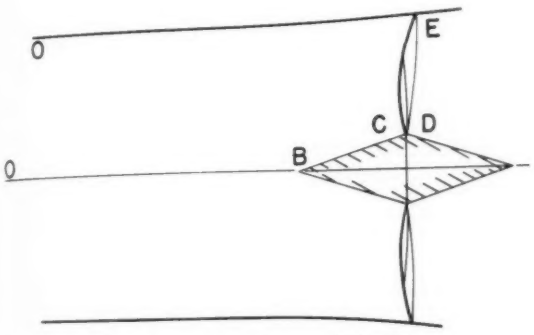

FIG. 3. Physical plane sonic free jet.

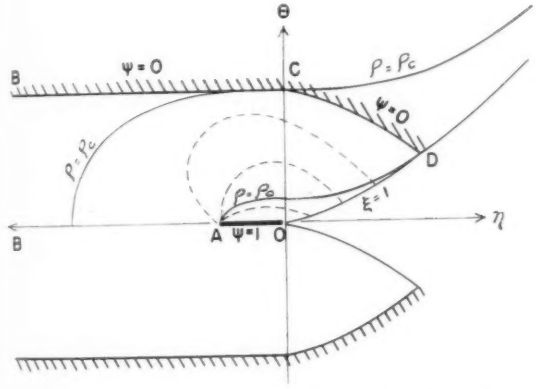

FIG. 5. Transonic hodograph plane solid wall tunnel.

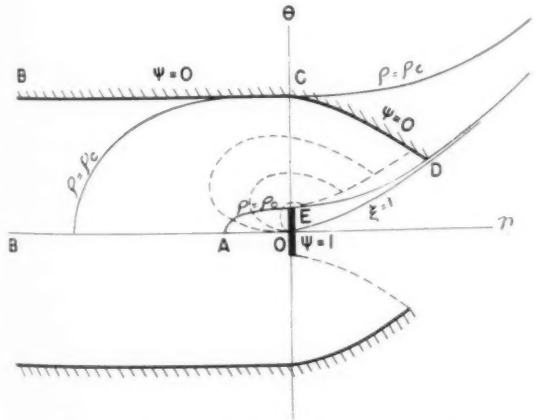

FIG. 6. Transonic hodograph plane sonic free jet.

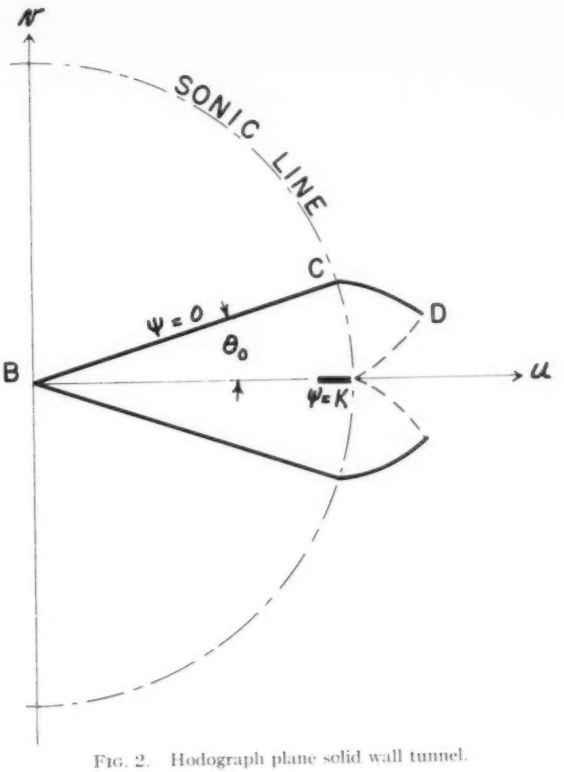

FIG. 2. Hodograph plane solid wall tunnel.

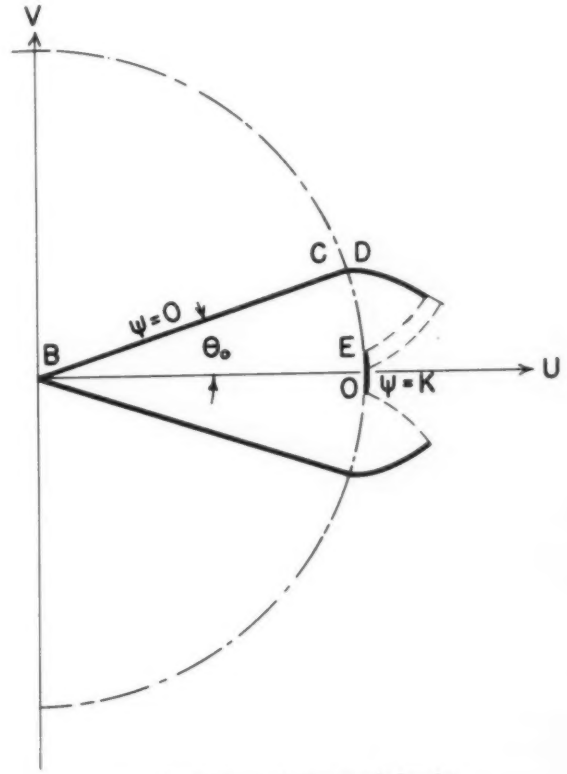

FIG. 4. Hodograph plane sonic free jet.

sonic free jet) can be expected to be advantageous. Such an approach has been proposed in reference 1. Details will be presented after a suitable system of particular solutions has been introduced.

(3) Symbols and Basic Equations

x, y = Cartesian coordinates in the physical plane
u, v = velocity components in the x, y directions
w = absolute magnitude of velocity vector
θ = angle of velocity vector with x-axis
w^* = sonic speed
$\bar{\rho}$ = density
ρ^* = density at sonic speed
p = pressure
γ = ratio of specific heats
Φ = velocity potential
ϕ = Legendre's transformed velocity potential
ψ = stream function
L = length of double wedge airfoil
H = width of tunnel
θ_0 = wedge half angle

In the actual computations the density will occur only of the value at sonic speed, and it can be placed equal to unity without loss of generality.

The differential equation for the potential in two-dimensional isentropic compressible flow is given by

$$[1 - (u^2/a^2)]\Phi_{xx} - 2(uv/a^2)\Phi_{xy} + [1 - (v^2/a^2)]\Phi_{yy} = 0 \quad (3.1)$$

Applying Legendre's transformation and introducing polar coordinates w, θ, and a new variable η by

$$w = w^*[1 + (\gamma + 1)^{-(1/3)}\eta] \quad (3.2)$$

and introducing simplifications known from the derivation of the transonic similarity law, one obtains from Eq. (3.1)

$$\phi_{\eta\eta} - \eta\phi_{\theta\theta} = 0 \quad (3.3)$$

In a similar fashion the equation for the stream function in the hodograph yields

$$\psi_{\eta\eta} - \eta\psi_{\theta\theta} = 0 \quad (3.4)$$

Eqs. (3.3) and (3.4) are of the form discussed by Tricomi.[3]

Between the stream function and the transformed potential there exist relations [see reference 4, Eqs. (4.6)] which in the present approximations reduce with $\rho^* = 1$ to

$$\psi = \phi_\theta \quad (3.5)$$

The coordinates in the physical plane are given in reference 4, Eq. (4.3); within the present approximations they are

$$x = [(\gamma + 1)^{1/3}/w^*]\phi_\eta \quad (3.6)$$

$$y = (1/w^*)\phi_\theta \quad (3.7)$$

The boundary value problems for the closed tunnel and the sonic free jet in the η, θ-plane are presented in Figs. 5 and 6, respectively. The notation of the corresponding points is the same as in the previous figures.

(4) A System of Particular Solutions

Let us introduce a new set of independent variables

$$\xi = \eta/[(3/2)\theta]^{2/3} \quad (4.1)$$

$$\rho = -\eta^3 + [(3/2)\theta]^2 \quad (4.2)$$

Fig. 7 shows lines of constant ρ and ξ in the η, θ-plane. With these independent variables Tricomi's equation for the stream function [Eq. (3.4)] becomes

$$\frac{(1 - \xi^3)^2}{\xi}\psi_{\xi\xi} - \frac{5}{2}\xi(1 - \xi^3)\psi_\xi + \frac{\psi}{16} = 9\rho^2\psi_{\rho\rho} + \frac{21}{2}\rho\psi_\rho + \frac{1}{16}\psi \quad (4.3)$$

By the product hypothesis

$$\psi = \rho^{-\frac{1}{12} \pm \frac{\lambda}{3}} G[\xi] \quad (4.4)$$

in which λ is an arbitrary constant, the following differential equation for G (written in its self-adjoint form) is obtained:

$$\frac{d}{d\xi}\left[(1 - \xi^3)^{5/6}\frac{dG}{d\xi}\right] + \left(-\lambda + \frac{1}{16}\right)\frac{\xi}{(1 - \xi^3)^{7/6}}G = 0 \quad (4.5)$$

This differential equation is closely related to the hypergeometric equation.[1]

For a given value of λ there exist two linearly independent solutions for $G(\xi)$. One can choose them such that the arising functions ψ are symmetric or antisymmetric with respect to the line $\xi = -\infty$. They may then be distinguished by a superscript (s) or (a) respectively. As the functions $G^{(a)}$ and $G^{(s)}$ depend upon ξ and λ, they will be written as $G^{(a)}(\xi, \lambda)$ and $G^{(s)}(\xi, \lambda)$.

Formulas for the functions $G^{(a)}(\xi, \lambda)$ and $G^{(s)}(\xi, \lambda)$ are given in Eqs. (18) and (19) of reference 1. Some functions G are tabulated in reference 5. The following table compares the notations used in reference 5 and in the present paper.

Reference 5	Present Paper
x	ξ
y	$\begin{cases} G^{(s)}\left[\xi, \left(\frac{3}{4} + 3K\right)^2\right] & \text{for even } K \\ G^{(a)}\left\{\xi, \left[\frac{9}{4} + \frac{3}{2}(K+1)^2\right]\right\} & \text{for odd } K \end{cases}$
y'	$dG/d\xi$ with the same coordination
w	$(-\xi)^{-(3/2)}$ with respect to K as above

(5) Choice of the Parameter λ

In the original hypothesis [Eq. (4.4)] the parameter λ can assume any value. For the present applications two families of particular solutions, defined by suitable boundary conditions, will be used. The boundary conditions are $\psi = 0$ along $\xi = \infty$ and along $\xi = \text{const.} = b$. The value of b will be specified later. With these boundary conditions the functions G and the values of λ are determined by an eigen value prob-

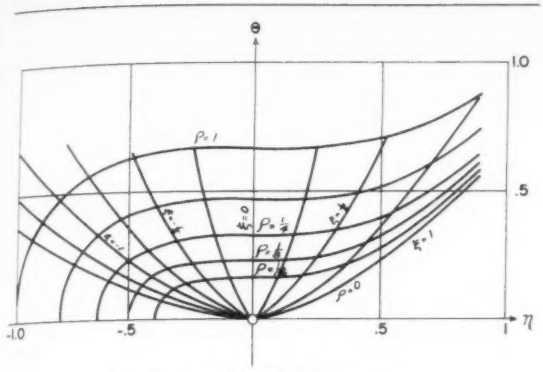

FIG. 7. ρ and ξ coordinate system.

lem which is of the classical type except for the fact that the coefficient of G in Eq. (4.5) changes its sign as ξ passes through zero—i.e., at the sonic line. The eigen function G has the following properties:

(a) They are orthogonal.

(b) The eigen values are positive or negative real numbers.

(c) The system of eigen functions is complete.

The eigen values will be arranged according to their magnitude and denoted by

$$\ldots \lambda_{-h} \ldots\ldots \lambda_{-2}, \lambda_{-1}, \lambda_1, \lambda_2, \ldots\ldots \lambda_h \ldots$$

where the negative and positive subscripts refer to negative and positive eigen values, respectively. The eigen functions are the function $G^{(a)}$ with the proper value of λ_h. The relations of orthogonality, derived in a standard method, are

$$\int_{-\infty}^{b} \frac{\xi}{(1-\xi^3)^{7/6}} G(\xi, \lambda_h)\, G(\xi, \lambda_k)\, d\xi = 0 \qquad h \neq k \tag{5.1}$$

$$\int_{-\infty}^{b} (1-\xi^3)^{5/6} \frac{dG(\xi, \lambda_h)}{d\xi} \frac{dG(\xi, \lambda_k)}{d\xi}\, d\xi = 0 \qquad h \neq k \tag{5.2}$$

The following notations for the particular solutions ψ formed with the eigen functions G may be introduced.

$$\psi_{\mathrm{I}_h} = G^{(a)}[\xi, \lambda_h]\, \rho^{-1/12+1/3\sqrt{\lambda_h}} \tag{5.3a}$$

$$\psi_{\mathrm{II}_h} = G^{(a)}[\xi, \lambda_h]\, \rho^{-1/12-1/3\sqrt{\lambda_h}} \tag{5.3b}$$

$$\psi_{\mathrm{III}_h} = G^{(a)}[\xi, \lambda_{-h}]\, \rho^{-1/12} \cos [(\sqrt{-\lambda_{-h}}/3) \log (\rho/\rho_0)] \tag{5.3c}$$

$$\psi_{\mathrm{IV}_h} = G^{(a)}[\xi, \lambda_{-h}]\, \rho^{-1/12} \sin [(\sqrt{-\lambda_{-h}}/3) \log (\rho/\rho_0)] \tag{5.3d}$$

where h is a positive integral number, ρ_0 is an arbitrary constant, and the sign of the roots is always positive.

One of the families of particular solutions used in the following arises if $b = 0$—i.e., if $\psi = 0$ along the sonic line. Incidentally, this family of particular solutions is the one used in Tricomi's memoir.[3] From the formulas for G in reference 1 one finds

$$\lambda_h = [-(1/4) + 3h]^2 \qquad h = 1, 2, 3, \ldots \tag{5.4}$$

The second family of particular solutions of Eq. (4.3) arises if one tries to represent certain solutions of Tricomi's equation in the region OB′CD of Fig. 8. This region is bounded by $\xi = -\infty$, $\rho = \rho_c$, the characteristic CD, and the characteristic OD. Along $\xi = -\infty$ the boundary condition $\psi = 0$ is prescribed. Along the boundary CD we have also $\psi = 0$, but along CD ξ is a function of ρ, so this condition is different from the one used in the formulation of the eigen value problem. This situation can be remedied by including into the region considered the area bounded by the characteristic CD, the characteristic DG, and the line $\rho = \rho_c$—this is the shaded area in Fig. 8. In this region we set $\psi = 0$. Since the boundary condition $\psi = 0$ is prescribed along the characteristic CD, the differential equation will then be satisfied everywhere in the region GDOB′CF. It is true that the first derivative of ψ will jump along CD, however this is not in contradiction with the fulfillment of the differential equation since CD is a characteristic. Now we draw a line $\xi = \text{const.} = b$ in Fig. 8 (line OD′D″) and the line $\rho = \rho_{D'}$ through point D'. Then in the region AB′CFD″-D′E the upper limit of ξ is b and along it the boundary condition $\psi = 0$ is fulfilled. This establishes an eigen value problem and a system of eigen functions which depend naturally upon the choice of b. This choice was arbitrary and the value of $\rho_{D'}$ becomes smaller when b approaches 1. Thus, the system of eigen functions obtained by prescribing $\psi = 0$ along $\xi = b$ and a subsequent limiting process that $b \to 1$, can be used to represent a solution with the boundary values $\psi = 0$ along OB and CD. The positive eigen values are obtained from Eq. (18) of reference 1 and are

$$\lambda_h = [-(3/4) + 3h]^2 \qquad h = 1, 2, 3, \ldots \tag{5.5}$$

The negative eigen values form a continuous spectrum.

For the eigen values just obtained the particular solutions defined in Eq. (5.3) may be denoted in the following manner:

$$\Psi_{\mathrm{I}_h} = \psi_{\mathrm{I}_h} \tag{5.6a}$$

$$\Psi_{\mathrm{II}_h} = \psi_{\mathrm{II}_h} \tag{5.6b}$$

$$\Psi_{\mathrm{III}_h} = \psi_{\mathrm{III}_h} \tag{5.6c}$$

$$\Psi_{\mathrm{IV}_h} = \psi_{\mathrm{IV}_h} \tag{5.6d}$$

with λ_h given by Eq. (5.5).

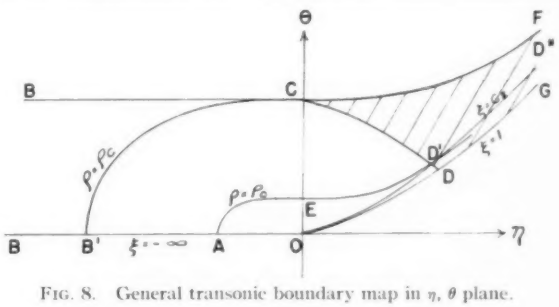

FIG. 8. General transonic boundary map in η, θ plane.

(6) Some Remarks about the Limiting Process that b Tends to 1

The determination of the negative eigen values in the limiting case that b tends to 1 is shown in reference 1. The process that $b \to 1$ is similar to that in which the upper limit of the interval in which a Fourier series is defined, tends to infinity such that a Fourier integral arises. Details are found carried out in reference 6. One might be tempted to replace the boundary condition

$$\lim_{b \to 1} \psi(\rho, b) = 0$$

by

$$\psi(\rho, 1) = 0$$

But then one would lose the particular solutions ψ_{III_h} and ψ_{IV_h}. Such a condition would also contradict Tricomi's formulation of a mixed boundary value problem.[3] According to these investigations no boundary condition can be prescribed along $\xi = 1$. For this reason the idea of a limiting process must be retained in the formulation of the eigen value problem. The investigations in references 1 and 6 show that, with the retention of the limiting process, no contradiction to Tricomi's formulation of the boundary value problem will be encountered. It must be admitted that the introduction of a limiting process at this point is unsatisfactory from a mathematical point of view, however, to the author's knowledge, no better approach has been given so far.

(7) Procedure for the Solution of the Boundary Value Problem

The two examples described above can be treated to a large extent in the same manner. The line $\rho = \rho_0$ through point A in Fig. 5 and point E in Fig. 6 divides the domain into two regions, the inner region ($\rho < \rho_0$) and the outer region ($\rho > \rho_0$).

Now we introduce a system of solutions $\bar{\psi}_h$ which consists of a singular portion given by one of the functions Ψ_{II_h} and of another portion $\tilde{\psi}_h$ which fulfills the conditions of Tricomi's uniqueness and existence proof[3]

$$\bar{\psi}_h = \Psi_{\mathrm{II}_h} + \tilde{\psi}_h \tag{7.1}$$

and is determined in such a manner that the functions $\bar{\psi}_h$ fulfill the boundary condition $\bar{\psi}_h = 0$ along the map of the body surface ABCD (see Fig. 8). Then any solution which fulfills for $\rho > \rho_0$ the boundary condition $\psi = 0$ along ABCD can be expressed by superposition of the functions $\bar{\psi}_h$. So, it is possible to express in Fig. 5, as well as in Fig. 6, the solution for the outer region ($\rho > \rho_0$) by a series with coefficients, undetermined so far, of the form

$$\psi = \sum_{h=1}^{\infty} C_h \bar{\psi}_h \tag{7.2}$$

The first term ($h = 1$) represents the flow over the body with a free-stream Mach Number 1. The other terms give the influence of the boundary conditions in the inner regions (see Figs. 5 and 6).

A slight modification is still necessary. A superposition of the above particular solutions will, in general, change the length of the side of the wedge. To be more specific: If one superimposes to each other certain expressions ψ in the hodograph plane, then in the physical plane the coordinates which belong in the different particular solutions—to the same velocity vector—are added. The particular solutions $\bar{\psi}_h$ will be constructed so that the nose of the wedge lies at the origin of the x,y-system. For the shoulder of the wedge the expressions $\bar{\psi}_h$ will, in general, give values of x different from zero. We form a linear combination of the $\bar{\psi}_h$ ($h = 2, 3 \ldots$) with ψ_1 such that the value of x for the combination at the shoulder is zero. This is always possible since for $\bar{\psi}_1$—i.e., in the flow with a free-stream Mach Number 1—the length of the wedge is different from zero. Thus, particular solutions

$$\bar{\bar{\psi}}_h = \bar{\psi}_h + b_h \bar{\psi}_1 \qquad h = 2, 3, 4 \ldots \tag{7.3}$$

will be used where b_h are constants chosen such that for $\bar{\bar{\psi}}_h$ one has $x = 0$ at the shoulder of the wedge. Then the outer solution is written as

$$\psi = c_1 \bar{\psi}_1 + \sum_{h=2}^{\infty} c_h \bar{\bar{\psi}}_h \tag{7.4a}$$

or

$$\psi = c_1(\Psi_{\mathrm{II}_1} + \tilde{\psi}_1) + \sum_{h=2} c_h[\Psi_{\mathrm{II}_h} + \tilde{\psi}_h + b_h(\Psi_{\mathrm{II}_1} + \tilde{\psi}_1)] \tag{7.4b}$$

The treatment of the inner region depends upon the boundary conditions prescribed. The boundary conditions are nonhomogeneous with ψ assuming a constant value at the boundary of the jet—i.e., along AO in Fig. 5 and along EO in Fig. 6. The inner solution will be split into a portion which fulfills the nonhomogeneous boundary condition just mentioned and a portion which has $\psi = 0$ along the boundary of the inner region. Since the lines EO and AO are lines of constant ξ, the nonhomogeneous portion will be found from Eq. (4.4) with $\sqrt{\lambda} = +\frac{1}{4}$. These solutions will be denoted by $H(\xi)$ [the functions $H(\xi)$ are not the same for the sonic jet and the closed tunnel]. The homogeneous portions originate from the eigen value problems discussed above; for the free jet $b = 0$ and for the closed tunnel we must carry out the limiting process $b \to 1$.

Thus, the inner solution for the closed tunnel is represented by the nonhomogeneous expression and a superposition of the expression

$$\psi = H(\xi) + \sum_{h=1}^{\infty} c_{\mathrm{I}_h} \Psi_{\mathrm{I}_h} + \sum_{h=1}^{\infty} c_{\mathrm{III}_h} \Psi_{\mathrm{III}_h} + \sum_{h=1}^{\infty} c_{\mathrm{IV}_h} \Psi_{\mathrm{IV}_h} \tag{7.5}$$

where c_{I_h}, c_{III_h}, and c_{IV_h} are suitable constants. Obviously terms Ψ_{II_h} will not occur in the inner representation since they would introduce a singularity at the origin. It is true also that the expressions Ψ_{III_h} and Ψ_{IV_h} are singular at point O, but in the limit $b \to 1$ the

singularities cancel out by the superposition. (Details are shown in references 1 and 6.)

Point O in Fig. 6 represents the free jet at some distance upstream of the model, therefore ψ at point O varies only between zero and some finite value which corresponds to the surface of the jet. If any singularity Ψ_{II_h} would be included in the inner solution, ψ would tend to infinity at point O, therefore, such functions cannot be admitted and the inner solutions will contain $H(\xi)$ and Ψ_{I_h}. Particular solutions Ψ_{III_h} and Ψ_{IV_h} do not exist in this case since the inner region is entirely subsonic. Thus

$$\psi = H(\xi) + \sum c_{I_h}\Psi_{I_h} \qquad \rho < \rho_0 \tag{7.6}$$

for the sonic free jet.

The unknown coefficients occurring in the inner and outer representation for ψ will be found by matching the representations along the line $\rho = \rho_0$.

A simplification arises if the investigation is limited to cases where ρ_0 is small—i.e., cases where the tunnel height is large relative to the dimensions of the model. Then in the outer solutions the terms Ψ_{II_h} in Eq. (7.1) will predominate along $\rho = \rho_0$, and for matching process only the expression

$$\psi = \sum c_h\Psi_{II_h} \tag{7.7}$$

need be considered.

Thus we have the following program for the computation:

(a) Determination of the expression $\bar{\psi}_h$. We shall see that the predominant correction for small values of ρ_0 is given by $\bar{\psi}_2$.

(b) Matching of the inner and outer representations.

(c) Determination of the quantities which are of physical interest in the solutions.

The determination of the expressions $\bar{\psi}_h$ is in principle the same as the determination of a flow at a free-stream Mach Number 1; the only difference lies in the fact that now a different singularity—i.e., Ψ_{II_2}—will prevail at point O. Thus the procedure of reference 2 is applicable.

(8) Matching of the Inner and Outer Solutions

Along the line $\rho = \rho_0$ one has the condition that the inner and outer solutions have the same values of the function and the normal derivative. From this condition it is rather easy to develop a numerical procedure for determining the unknown coefficients.

As an illustration the treatment of the closed wind-tunnel case will be shown.

Here the functions $H(\xi)$ mentioned above are defined by the differential Eq. (4.5) with $\sqrt{\lambda} = (1/4)$ and the boundary condition $H = 1$ at $\xi = -\infty$ and $H = 0$ at $\xi = 1$. The solution Eq. (7.5) in the inner region may be written as

$$\psi = H(\xi) + \sum_{h=1}^{\infty} c_{I_h}\rho^{-(1/3+h)}\, G\left[\xi, \left(-\frac{3}{4} + 3h\right)^2\right] + \sum_{1}^{\infty} c_{III_h}\,\rho^{-(1/12)} \cos\left[\frac{\lambda_{-h}}{3}\log\frac{\rho}{\rho_0}\right] G\,(\xi, \lambda_{-h}) + \sum_{1}^{\infty} c_{IV_h}\,\rho^{-(1/12)} \sin\left[\frac{\lambda_{-h}}{3}\log\frac{\rho}{\rho_0}\right] G(\xi, \lambda_{-h}) \tag{8.1}$$

In the last expression the limiting process $b \to 1$ has been carried out in the first sum only. The other sums are unimportant for the change of the pressure distribution over the body.

For the matching process, the outer solution in the form of Eq. (7.7) will be written as

$$\psi = \sum_{h=1}^{\infty} c_h\rho^{-(1/6)-h}\, G\left[\xi, \left(-\frac{3}{4} + 3h\right)^2\right] \tag{8.2}$$

Matching the values of the function along $\rho = \rho_0$ one obtains

$$H(\xi) + \sum_{h=1}^{\infty} c_{I_h}\,\rho_0^{-(1/3)+h}\, G\left[\xi, \left(-\frac{3}{4} + 3h\right)^2\right] + \sum_{1}^{\infty} c_{III_h}\rho_0^{-(1/12)}\, G[\xi, \lambda_{-h}] = \sum_{h=1}^{\infty} c_h\,\rho_0^{-(1/6)-h}\, G\left[\xi, \left(-\frac{3}{4} + 3h\right)^2\right]$$

Similarly for the derivative

$$\sum_{h=1}^{\infty}\left(\frac{1}{3} + h\right) c_{I_h}\,\rho_0^{(4/3)+h}\, G\left[\xi, \left(-\frac{3}{4} + 3h\right)^2\right] + \sum_{h=1}^{\infty} c_{III_h}\left(-\frac{1}{12}\right)\rho_0^{-(11/12)}\, G(\xi, \lambda_{-h}) + \sum_{1}^{\infty} c_{IV_h}\,\rho_0^{-(13/12)}\, G(\xi, \lambda_{-h}) = \Sigma\left(\frac{1}{6} - h\right) c_h\rho_0^{-(5/6)-h}\, G\left[\xi, \left(-\frac{3}{4} + 3h\right)^2\right]$$

The unknown coefficients can be readily found since for the functions G occurring the conditions of orthogonality Eq. (5.1) apply. Multiplying the last equation by

$$\frac{\xi}{(1-\xi^3)^{7/6}}\, G_k\left[\xi, \left(-\frac{3}{4} + 3h\right)^2\right]$$

integrating from $\xi = -\infty$ to $\xi = 1$ and introducing simultaneously

$$D_k = \int_{-\infty}^{1} \frac{\xi H(\xi)}{(1-\xi^3)^{7/6}}\, G_k\left[\xi, \left(-\frac{3}{4} + 3k\right)^2\right] d_\xi \tag{8.3}$$

$$C_k = \int_{-\infty}^{1} \frac{\xi}{(1-\xi^3)^{7/6}}\, G_k\left[\xi, \left(-\frac{3}{4} + 3k\right)^2\right] d\xi \tag{8.4}$$

one obtains

$$D_h + c_{I_h}\,\rho_0^{-(1/3)+h}\, c_h = c_h\,\rho_0^{(1/6)-h}\, c_h$$

$$[-(1/3) + h]\, c_{I_h}\,\rho_0^{-(4/3)+h}\, c_h = [(1/6) - h]\, c_h\rho_0^{-(5/6)-h}\, c_h$$

For the pressure distribution over the body only the terms of the outer solution are of importance. One finds

$$c_h = (D_h/C_h)\{[h-(1/3)]/[2h-(1/2)]\}\rho_0^{(1/6)+h} \tag{8.5}$$

The integral D_h can be evaluated by integrations by parts using the differential equation Eq. (4.5) and the properties of the functions G and H at the end points of the interval. One finds

$$D_h = \frac{-(3/2)}{[-(3/4)+3h]^2-(1/16)} \tag{8.6}$$

The evaluation of the C_h can be carried out according to (Appendix IV of reference 1):

$$C_h = \frac{\pi 3}{\left(2h-\frac{1}{2}\right)^2}\cdot\frac{-\frac{1}{6}\cdot\frac{5}{6}\cdots\left(-\frac{1}{6}+h-1\right)}{\frac{2}{3}\cdot\frac{5}{3}\cdots\left(\frac{2}{3}+h-1\right)}\times\frac{\frac{1}{6}\cdot\frac{7}{6}\cdots\left(\frac{1}{6}+h-1\right)}{\frac{1}{3}\cdot\frac{4}{3}\cdots\left(\frac{1}{3}+h-1\right)} \tag{8.7}$$

Thus, for the closed tunnel

$$c_1 = \gamma_1\rho_0^{5/6} \qquad \text{where } \gamma_1 = 0.586 \tag{8.8a}$$

$$c_2 = \gamma_2\rho_0^{11/6} \qquad \text{where } \gamma_2 = 0.611 \tag{8.8b}$$

for the sonic free jet

$$c_1 = \gamma_1\rho_0^{5/6} \qquad \text{where } \gamma_1 = 0.403 \tag{8.9a}$$

$$c_2 = \gamma_2\rho_0^{11/6} \qquad \text{where } \gamma_2 = -0.306 \tag{8.9b}$$

(9) The Pressure Distribution over the Body

The coefficient c_h depends on ρ_0, [Eq. (8.5)] in such a manner that in Eq. (7.4a) only the first terms are of importance if ρ_0 is sufficiently small and if considering a fixed point of the η,θ-plane. The first term in Eq. (7.4a) represents the flow with a free-stream Mach Number of 1; the second term is the lowest order correction due to the wall influence. Only these two terms will be considered in the following.

Eq. (7.4a) has been obtained with the boundary condition $\psi = 1$ along the wind-tunnel wall with the sonic density equal to unity. This corresponds to a wind tunnel of height $(2/w^*)$. Thus the solution for a wind tunnel of height H is given by

$$\psi = (Hw^*/2)\,(c_1\bar{\psi}_1 + c_2\bar{\psi}_2) \tag{9.1}$$

Next it is necessary to determine the x coordinate along the wedge as a function of η. Following the procedure of reference 2 we transfer from ψ to ϕ by Eq. (3.5), then apply Eq. (3.6). Denoting the expressions ϕ in the same manner used in ψ, one finds

$$x = (H/2)\,(c_1\bar{\phi}_{1\eta} + c_2\bar{\phi}_{2\eta}) \tag{9.2}$$

The expression $\bar{\phi}_{1\eta}$ has been found in reference 2—the expression $\bar{\phi}_{2\eta}$ is determined in an analogous manner. Up to the present the computations were concerned with the front part of the wedge only, the rear part of the wedge can be treated by the method of characteristics. Fig. 9 shows the results for a diamond profile.

As indicated, the quantities ϕ_η will contain certain powers of the wedge angle θ_0 as factors which arise in the course of the computations.

The length of the profile is obtained from Fig. 9 as the difference in the x coordinates of the leading and trailing edges. For this purpose, only $\bar{\phi}_{1\eta}$ need be considered because the function $\phi_{2\eta}$ is constructed in such a manner as to leave the dimensions of the profile unaffected. One finds for the length of the profile

$$L/H = 1.235\,c_1[(3/2)\theta_0]^{-(4/3)}\,(\gamma+1)^{1/3} \tag{9.3}$$

and by combining with Eq. (8.8a) we have

$$\rho_0 = \left(\frac{3}{2}\theta_0\right)^{8/5}\left[\frac{L}{H}\frac{(\gamma+1)^{-(1/3)}}{1.235\gamma_1}\right]^{6/5} \tag{9.4}$$

In determining the wall effect on the pressure distribution on the wedge surface, it is necessary to find the change of η at a fixed value of x. The expression $\bar{\psi}_{2\eta}$ indicates the wall influence on the x coordinate for a given value of η. In the flow with a free-stream Mach Number of 1,

$$x = (H/2)c_1\bar{\phi}_{1\eta}(\eta) \tag{9.5}$$

Then, if the value of η is changed by $\Delta\eta$ at a given point x, we have

$$x = (H/2)\,c_1\bar{\phi}_{1\eta}(\eta+\Delta\eta) + c_2\bar{\phi}_{2\eta}(\eta+\Delta\eta) \tag{9.6}$$

Considering $\phi_{2\eta}$ and $\Delta\eta$ as small so that higher order terms may be neglected and using Eqs. (9.5), (8.8), and (8.9) we have

$$\Delta\eta = -(\gamma_2/\gamma_1)\rho_0(\bar{\phi}_{2\eta}/\bar{\phi}_{1\eta\eta}) \tag{9.7}$$

The term $\bar{\phi}_{1\eta\eta}$ was calculated from the solution of the basic flow and is presented in Fig. 9. By Eq. (9.5) a change of independent variables from η to x can be accomplished, and the results written

$$\Delta\eta = -(\gamma_2/\gamma_1)\rho_0[(3/2)\theta_0]^{-(4/3)}F(x/L) \tag{9.8}$$

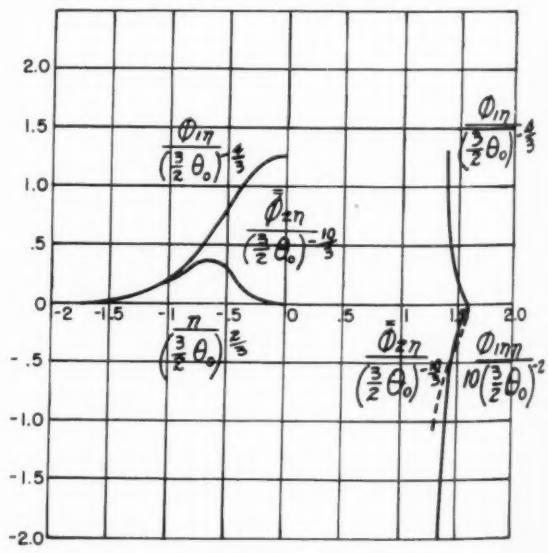

Fig. 9. Functions of ϕ_η along the wedge.

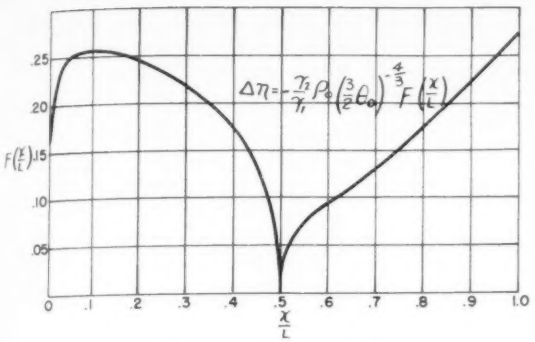

FIG. 10. Δ_η along the wedge.

The function $F(x/L)$ is shown in Fig. 10.

In the present approximation the pressure coefficient is given by

$$C_p = (P - P^*)/q^* = -2(\gamma + 1)^{-(1/3)}\,\eta \qquad (9.9)$$

Thus, the change of the pressure coefficient due to the wall influence can be obtained from combining Eqs. (9.4), (9.8), and (9.9).

$$\Delta C_p = 2(\gamma + 1)^{-(11/15)}\left(\frac{L}{1.235\gamma_1 H}\right)^{6/5} \times \left(\frac{3}{2}\theta_0\right)^{4/15}\frac{\gamma_2}{\gamma_1}F\left(\frac{x}{L}\right) \qquad (9.10)$$

Inserting the numerical values into the above equation we have

for the closed tunnel

$$\Delta C_p = 1.802\,\theta_0^{4/15}\,(L/H)^{6/5}\,F(x/L) \qquad (9.11)$$

for the sonic free jet

$$\Delta C_p = -2.037\,\theta_0^{4/15}\,(L/H)^{6/5}\,F(x/L) \qquad (9.12)$$

The pressure coefficient for the double wedge airfoil in a free flow of Mach Number 1 has been determined in reference 2 as

$$C_p = \theta_0^{2/3}\,g\,(x/L) \qquad (9.13)$$

The function $g(x/L)$ is shown by the solid line in Fig. 11. Then the pressure coefficient for the two cases under consideration may be written as

for the closed tunnel

$$C_p = \theta_0^{2/3}\,[g(x/L) + 1.802\,\theta_0^{-(2/5)}\,(L/H)\,F(x/L)]^{6/5} \qquad (9.14a)$$

for the sonic free jet

$$C_p = \theta_0^{2/3}\,[g(x/L) - 2.037\,\theta_0^{-2/5}\,(L/H)^{6/5}\,F(x/L)] \qquad (9.14b)$$

The pressure distribution on the surface of a double wedge air-foil of $\theta_0 = 0.1$ is presented in Fig. 11. The solid line indicates flow over a wedge with Mach Number 1, and the dashed line the wedge in a closed wind tunnel with $L/H = 0.13$. The sonic free jet would lie on the other side of the solid line with about the same displacement.

Determining the choking Mach Number for the solid tunnel, an inspection of Fig. 5 indicates that ρ_0 is closely connected to the tunnel dimension and the choking Mach Number. For the condition of $\theta_0 = 0$ at infinity and combining the definitions of η [Eq. (3.2)] and ρ [Eq. (4.2)] with Bernoulli's equation, we find

$$1 - M_{\text{choking}} = \frac{(\gamma + 1)^{3/15}}{2}\left(\frac{L}{1.235\ \gamma_1 H}\right)^{2/5}\left(\frac{3}{2}\theta_0\right)^{8/15} \qquad (9.15a)$$

and inserting the numerical values

$$1 - M_{\text{choking}} = 1.127(L/H)^{2/5}\,\theta_0^{8/15} \qquad (9.15b)$$

(10) Limitations of the Analysis

Besides the transonic simplifications which required that the Mach Number in the flow does not deviate too much from 1, the assumption has been made that the value of ρ_0 is small in comparison to the value of ρ which occurs along the contour. The smallest value of ρ which occurs along the subsonic part of the contour is found at point C in Figs. 5 and 6 and may be denoted by ρ_c, where $\rho_c = (9/4)\theta_0^2$. With Eq. (9.4) we thus find that for the closed tunnel

$$\rho_0/\rho_c = 1.01(L/H)^{6/5}\,\theta_0^{-2/5} \qquad (10.1)$$

must be small in comparison to 1. For the relatively extreme example of an airfoil of a length of 13 per cent of the tunnel height and a thickness ratio of 10 per cent, this ratio is found to be 0.219. Results obtained under these conditions can be considered as fairly reliable.

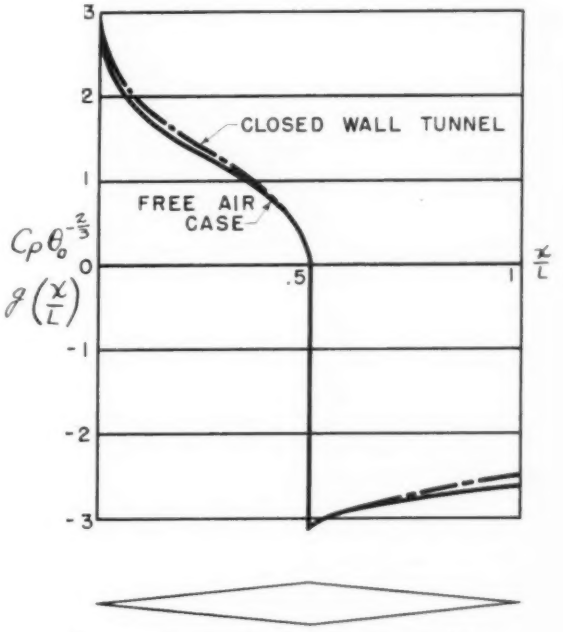

FIG. 11. Pressure distribution over the wedge.

(11) Discussion of the Results

The purpose of the present investigation is to illustrate in a quantitative manner the wall influences in the transonic region. A wedge of 10 per cent thickness ratio and a length of 13 per cent of the closed tunnel height has been considered and the results of Eq. (9.14a) are presented in Fig. 11. The solid line gives the pressure distribution over the wedge in free air with a Mach Number of 1, while the dashed line gives the distribution in the closed tunnel. It is to be observed that the wall influence is relatively small and this indicates that measurements of this type in a closed choked wind tunnel give a surprisingly good approximation of free flight data at Mach 1.

A comparison of the results of a similar computation for a sonic free jet of the same height would show that the deviations from free flight conditions would be about the same magnitude but of opposite sign. One would obtain a line slightly underneath the solid line in Fig. 11. Examining the coefficients of the superimposed solution in Eq. (9.14a) and Eq. (9.14b), one notes that the deviations of the pressure distribution are greater in the sonic free jet than in the choked closed wind tunnel. This indicates that a free jet tunnel cannot be considered as preferable solely on the basis that the desired free-stream Mach Number actually occurs at some distance of the model. The closed wind tunnel will never attain the free-stream Mach number 1, but the results obtained are even somewhat better than those obtained in a sonic free jet. Eqs. (9.11) and (9.12) show the influence of the model dimensions. Naturally, the deviation of the pressure distribution will become smaller if the model is smaller in comparison to the tunnel height. The deviation from free air results is proportional to $(L/H)^{6/5}$. In comparison with the deviation of the choking Mach Number from 1 [Eq. (9.15b)] which is proportional to $(L/H)^{2/5}$, the deviation of the pressure distribution decreases much faster with decreasing (L/H) than the deviation of the choking Mach Number from 1. Thus, considerations on the accuracy of measurements based solely on the choking Mach Number obtainable in a wind tunnel are not realistic.

The dependence of the wall influence on the thickness ratio of the model (in this case on θ_0) is given in Eq. (9.11) by the term $\theta_0^{4/15}$. The absolute deviation of C_p is reduced if θ_0 is decreased, but, as Eq. (9.14a) shows, the relative accuracy of the measurements becomes smaller. This behavior is understandable from consideration of transonic similarity. According to the transonic similarity law, a flow over a thin body in a wide tunnel will correspond to flow over a thicker body in a narrower tunnel if the lengthwise coordinate is kept the same. These considerations show that the measurement of very slender bodies in the transonic speed range offers certain difficulties, but from a structural point of view extremely thin bodies are of little interest for practical application.

Eq. (9.15b) gives the choking Mach Number in terms of the model dimension. Naturally, the validity of this formula is subject to the restriction that the ratio of (ρ_0/ρ_c) is small [Eq. (10.1)]. It shows that the choking Mach Number is not directly determined by the area available at the narrowest cross section, otherwise the powers of θ_0 and L/H would be 1/2.

Although the present results indicate that measurements in a closed wind tunnel may be quite valuable in the transonic region, one should be careful not to generalize this result too quickly. The result has been found for two-dimensional flow, and, while investigations of axial symmetric transonic flow show that the behavior is similar to planar flows, there are also marked differences.[8]

References

[1] Guderley, Gottfried, *Two Dimensional Flow Patterns with a Free Stream Mach Number Close to One*, Wright Field Report No. 6343, May 1951.

[2] Guderley, Gottfried, and Yoshikara, Hideo, *The Flow Over a Wedge Profile at Mach Number One*, Wright Field Report No. 5783, July, 1949.

[3] Tricomi, F., *On Linear Partial Differential Equations of the Second Order of Mixed Type*, Brown University Translation A9-T-26.

[4] Guderley, Gottfried, *Singularities at the Sonic Velocity*, Wright Field Report F-TR-1171-ND, June, 1948.

[5] The Computation Laboratory, Harvard University, Cambridge, Massachusetts: *Flow Patterns with a Free Stream Mach Number Close to One*, Report No. 16.

[6] Guderley, Gottfried, *The Wall Pressure Distribution in a Choked Tunnel*, WADC Technical Report 53-509.

[7] Guderley, Gottfried, *The Flow over a Flat Plate with an Angle of Attack*, WADC Technical Report 53-404.

[8] Guderley, Gottfried, *Axial-Symmetric Flow Patterns at a Free Stream Mach Number Close to One*, Wright Field Report No. 6285, October, 1950.

A Method for Predicting Lift Effectiveness . . . (*Continued from page 334*)

also to step spoilers of 0.10 semispan or less having their mid-spans distributed along a constant per cent chord line. The lift effectiveness of other types of spoilers such as slot-lip ailerons, flap-type spoilers, etc., could possibly be predicted by modifications to the results presented. For instance, a simple ratio of their section lift effectiveness to the plain-spoiler section lift effectiveness might be adequate. It is possible, however, that a better means of modification could be developed by further investigation of the overall differences between the characteristics of plain and other types of spoilers.

For spoiler alignments that are not along a constant per cent chord line these results do not apply and cannot, at present, be transformed to apply. It should be emphasized, however, that the approach used in developing this method has inherently, sufficient flexibility to permit the inclusion of the effects of additional factors such as more geometric parameters, other types of spoilers, and other spoiler alignments once sufficient data on the effects of these factors are available.

Readers' Forum

BRIEF REPORTS of investigations in the aeronautical sciences and discussions of papers published in the JOURNAL are presented in this special department. Entries must be restricted to a maximum of 1,300 words or the equivalent of one JOURNAL page including formulas and illustrations. Publication is completed as soon as possible after receipt of the material. The Editorial Committee does not hold itself responsible for the opinions expressed by the correspondents.

Contents

Negative Magnus Force ..... E. KRAHN 377

On the Method of Averaging Stagnation Pressures ..... RAYMOND L. CHUAN 378

The Skewness Factor According to Obukhoff's Transfer Theory ..... W. H. REID 379

Iteration in Semidefinite Eigenvalue Problems ..... SAMUEL PINES 380

The Laminar Free-Convective Heat Transfer from the Surfaces of a Vertical Circular Cylinder ..... KNOX MILLSAPS AND KARL POHLHAUSEN 381

Propulsive Ducts at the Tips of Rotor Blades ..... J. V. FOA, A. GAIL, AND T. R. GOODMAN 381

The Downstream Effect of a Thickening of the Laminar Boundary Layer ..... D. G. HURLEY 383

Effect of Diffusion in an Isothermal Boundary Layer ..... E. R. G. ECKERT AND P. J. SCHNEIDER 384

Bending Moments in an Initially Bent, Spring Restrained Column ..... M. J. FORRAY AND S. R. BODNER 387

Similar Solutions in Compressible Laminar Free Mixing Problems ..... LUIGI G. NAPOLITANO 389

Comments on Supersonic Diffuser Instability ..... W. C. RANDELS 390

Deflection of Inelastic Columns ..... DOV HAZONY (HASANOVITSH) 390

On the Convergence of an Iterative Procedure in Solving Dynamic Response Problems ..... HUA LIN 391

Torsional Vibration of Rotating Twisted Bars ..... J. L. BOGDANOFF AND J. T. HORNER 393

On Viscous Heating ..... H. M. DEGROFF 395

A Device for Vortex-Core Measurements ..... EDWARD J. HOPKINS AND NORMAN E. SORENSEN 396

Interpolation Formulas for Supersonic-Hypersonic Airfoils ..... RICHARD D. LINNELL AND JERRY Z. BAILEY 398

Linearized Theory of Water Drop Impingement ..... THEODORE R. GOODMAN 399

Negative Magnus Force

E. Krahn

U.S. Naval Ordnance Laboratory, White Oak, Silver Spring, Md.

October 27, 1955

AT CERTAIN LOW ROTATIONAL speeds spheres and cylinders in cross-flow exhibit Magnus forces which have directions opposite to those at high speeds. The effect will be explained here for the rotating cylinder as a transition effect of the boundary layer from laminar to turbulent flow.* The critical Reynolds Number of the transition depends on many parameters—e.g., turbulence of the air, surface roughness, etc.—but has a definite value for a given experimental setup. It varies between 10^5 and 10^6 for the nonrotating cylinder in incompressible flow. In this investigation it is arbitrarily assumed to be 1.4×10^5 in accord with measurements of Fage and Falkner (reference 1, p. 422). The Reynolds Number is formed with the velocity of the undisturbed stream and the diameter of the cylinder.

If the cylinder does not rotate then the laminar boundary layer separates from the surface of the cylinder at 82° from the forward stagnation point (reference 1, p. 152), whereas if the boundary layer is turbulent it separates at about 130° (reference 1, p. 438). The transition to turbulence occurs on both sides of the cylinder if Re exceeds 1.4×10^5.

If the cylinder rotates then there is no longer symmetry in the flow and turbulence will appear on the two sides at different velocities of the undisturbed stream—i.e., at different Reynolds Numbers. The transition will depend on the speed of the flow relative to the wall.

On the side where the wall moves in the direction of the flow, the relative speed of the flow with respect to the wall is smaller than the speed relative to a stationary wall, and at the Reynolds Number 1.4×10^5 no transition to turbulence will occur. Con-

* This method of approach was suggested by Dr. H. H. Kurzweg.

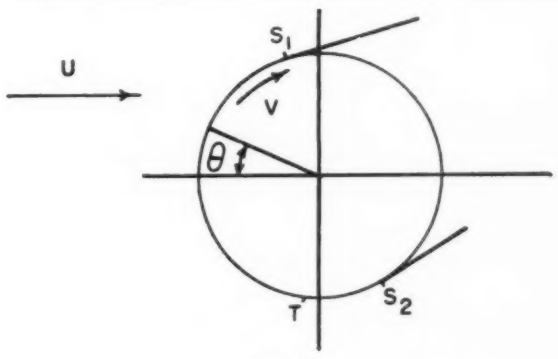

FIG. 1.

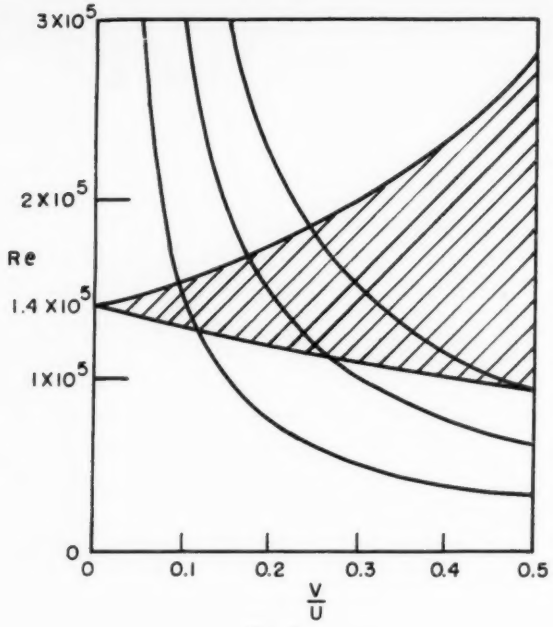

FIG. 2.

sequently the critical Reynolds Number for this side of the cylinder is higher than 1.4×10^5 and increases with (V/U), where V is the velocity of the wall and U is the velocity of the undisturbed stream.

On the other side of the cylinder, where the flow has the opposite direction to the motion of the wall, a flow at a smaller Reynolds Number than 1.4×10^5 will cause transition.

Thus for $Re = (Ud/\nu)$ close to 1.4×10^5 the boundary layer on one side of the rotating cylinder is laminar and on the other side turbulent. In Fig. 1 the separation point of the laminar boundary layer is at S_1, the separation point of the turbulent boundary layer is at S_2, and T is the point of transition.

With increasing (V/U) the point S_1 will move farther away from the forward stagnation point and S_2 will come nearer to the forward stagnation point. From known pictures of flow one can estimate that for $(V/U) = 1$ the laminar flow is attached beyond 130° and the turbulent one on the other side of the cylinder has receded to a smaller angle than 130°. For some value $(V/U) = K$ between 0 and 1 the points of separation on the laminar side and on the turbulent side will be at equal distances from the forward stagnation point. We will assume here $K = 0.5$ which seems to be in agreement with experiments (reference 1, p. 546).

For $0 < (V/U) < K$ and a Reynolds Number sufficiently near to 1.4×10^5 to leave laminar flow on one side of the cylinder and cause turbulent boundary layer on the other side, the turbulent flow is attached over a larger portion of the cylinder than the laminar flow. This causes a smaller pressure over most of the turbulent side and a negative Magnus force results.

To get the order of magnitude of the negative Magnus force we use pressure distributions given in reference 1, p. 422 for $Re = 1.06 \times 10^5$ and 1.66×10^5, the first corresponding to a laminar flow, the second to a turbulent one. Regarding them as flows on two sides of the same cylinder we can assume that the cylinder is rotating with a speed ratio (V/U) equal roughly to 0.2 and will further assume that the pressure in the wake varies linearly between the two points of separation—i.e., from -1.25 at 90° to -1.05 at 240°. Multiplying the given pressures by $\sin\theta$ and integrating around the cylinder we find that the Magnus force coefficient is equal to -0.15. This is of the right order of magnitude.

In Fig. 2 the region of the negative Magnus force is indicated in the (V/U), Re-plane by the shaded area. Assuming that the critical Reynolds Number does not depend on the absolute velocity of the stream but on the velocity relative to the wall one gets $Re_{crit.} = (1.4 \times 10^5)/[1 \pm (V/U)]$. These two curves border the shaded area. Between the (V/U)-axis and the lower curve is the area representing laminar flow on both sides of the cylinder, and above the shaded area is the region in which the flow is turbulent on both sides of the cylinder. In Fig. 2 the condition of constant U and variable V can be represented by a straight line parallel to the (V/U)-axis. Each hyperbola corresponds to a constant V and variable U.

We get the following picture for the change of the Magnus force coefficient K_F with the rate of rotation at a constant Reynolds Number in the range $1 \times 10^5 < Re < 2.8 \times 10^5$.

For small rotational speeds and Re not equal to 1.4×10^4 the flow is either laminar or turbulent on both sides of the cylinder and the Magnus force small but positive. With increasing (V/U) a stage will be reached when the boundary layer is laminar on one side and turbulent on the other side of the cylinder. Then there will be an abrupt change of the Magnus force which becomes negative (AB in Fig. 3). A further increase of (V/U) decreases the amount of the negative Magnus force, which becomes zero at about $(V/U) = 0.5$. The more Re differs from its critical value the larger the value of (V/U) for which the jump AB will occur.

Due to the uncertainty of the critical Reynolds Number and the position of the point of separation on a moving surface, the numerical data in this paper can give only the order of magnitude.

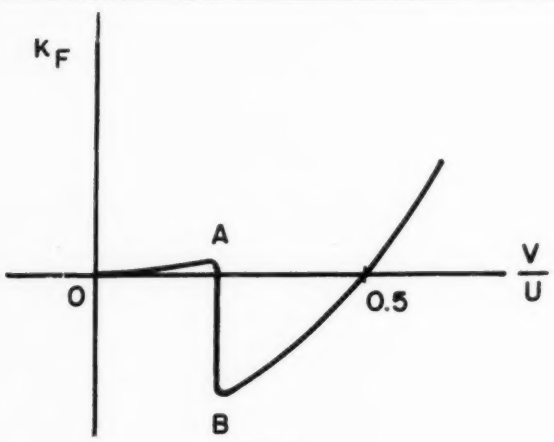

FIG. 3.

REFERENCE

[1] Goldstein, S., (Ed.), *Modern Developments in Fluid Dynamics*, 2 Vols., The Clarendon Press, Oxford, 1938.

On the Method of Averaging Stagnation Pressures

Raymond L. Chuan
Research Associate, Engineering Center, University of Southern California, Los Angeles, Calif.
October 31, 1955

IN INVESTIGATION dealing with dissipative flows—such as flows in ducts, diffusers, drag of bodies by wake measurements, etc.—the question of how properly to arrive at an average stagnation pressure from a measured distribution of stagnation pressure has often arisen. Some investigators place a number of pitot tubes, spaced equally, in the flow, read the tubes indi-

vidually, and compute an arithmetic mean. Others manifold all the pitot tubes together to yield one reading of stagnation pressure. Still others prefer to find a mass-flow weighted average. This note will attempt to show, by resorting to simple considerations of thermodynamics, that all three methods fail to give the correct average, and that, by these same considerations, a meaningful upper limit on the correct average stagnation pressure can be established.

It should be recognized at the outset that in dissipative flows the quantity which measures the dissipativeness is the entropy of the system at the point of interest and that the stagnation pressure is only one of the readily measurable manifestations of the state of the entropy of the system. Therefore, in defining an average stagnation pressure, one should really deal with the entropy first and proceed then to the stagnation pressure, thereby avoiding confusion and erroneous conclusions.

Consider the adiabatic flow of a gas with Prandtl Number 1.0, starting from rest in a uniform state, p_1, T_1, s_1 and passing through certain dissipative processes so that it arrives at the point of observation in a nonuniform state, say, for simplicity, $p_2(y)$, $T_2(y)$, $s_2(y)$. Fig. 1 shows schematically the history of one stream tube. The entire flow is made up of many such stream tubes, each at a different state at 2. The stagnation pressure $p_3(y)$ is the pressure any stream tube will assume when brought isentropically to the fictitious stagnation chamber 3 from 2. Then, $s_3(y) = s_2(y)$, and $s_3(y)$ is related to $p_3(y)$ and the initial state of the gas by the following

$$s_3(y) - s_1(y) = R \log [p_1/p_3(y)] \tag{1}$$

Now, $T_2(y)$ is not a constant; but, if all the stream tubes are brought to rest, remembering that the flow is adiabatic, $T_3(y)$ is a constant and is equal to T_1. Since all the stream tubes now in the fictitious stagnation chamber have the same temperature, their entropies can be added to yield the entropy for the whole flow by allowing them to attain reversibly a common uniform state. It is apparent that this total entropy must be the minimum, since, in bringing the stream tubes to rest and to equilibrium by processes other than isentropic, the resulting total entropy must be higher. It must be noted that we cannot sum the entropies $s_2(y)$ because the stream tubes at the observation point are not at the same temperature. Summing $s_3(y)$ we have

$$S_3 = \int s_3 dm_3$$

where dm_3 is the mass contained in a stream tube. By virtue of the manner in which we brought the stream tubes to rest

$$s_3 dm_3 = s_2 dm_2$$
$$dm_2 = \rho_2 u_2 \, dy$$

Therefore

$$S_3 = \int s_2 \rho_2 u_2 \, dy = \int s_3 \rho_2 u_2 \, dy$$

where the integration is performed over all the stream tubes, is the total entropy of the flow brought to rest isentropically from the point of observation. The average specific entropy is then

$$\bar{s}_3 \equiv \frac{S_3}{\int \rho_2 u_2 dy} = \frac{\int s_3 \rho_2 u_2 \, dy}{\int \rho_2 u_2 \, dy} \tag{2}$$

From this we can compute a mean stagnation pressure $\bar{p}_3$ by Eq. (1), realizing that, since $\bar{s}_3$ is the lowest possible entropy, $\bar{p}_3$ thus arrived at is the maximum possible.

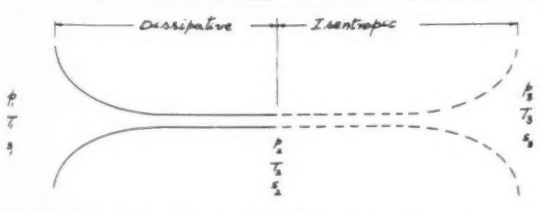

FIG. 1. Schematic representation of one stream tube.

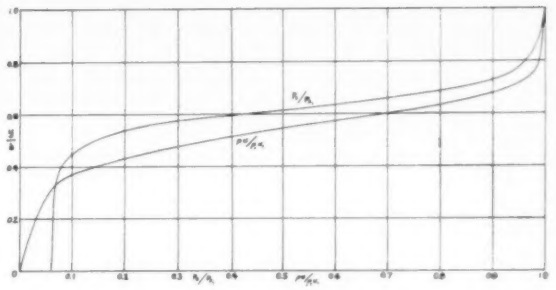

FIG. 2. Distribution of mass flow and stagnation pressure.

$$\bar{p}_3 = p_1 e^{-(\bar{s}_3 - s_1)/R} \tag{3}$$

From Eqs. (2) and (1)

$$\bar{s}_3 = (1/\int \rho_2 u_2 \, dy) \int (s_1 + R \log p_1/p_3) \, \rho_2 u_2 \, dy \tag{4}$$

Since p_1 is a constant, Eq. (4) becomes

$$\bar{s}_3 = (s_1 + R \log p_1) - (R/\int \rho_2 u_2 \, dy) \int \rho_2 u_2 \log p_3 \, dy \tag{5}$$

Eq. (3) then becomes

$$\bar{p}_3 = e^{\int \rho_2 u_2 \log p_3 \, dy / \int \rho_2 u_2 \, dy} \tag{6}$$

Dropping the subscripts and regarding p_3 as the locally measured isentropic stagnation pressure, p_s, in a nonuniform stream, we have, as an *upper limit* to the average stagnation pressure

$$\bar{p}_3 = e^{\int \rho u p_s \, dy / \int \rho u \, dy} \tag{7}$$

To show that appreciable discrepancies can arise by using incorrect averaging methods, an example is given below using actual measurements of a separated laminar boundary layer at a free-stream Mach Number of 2.4. The distributions of $\rho u/\rho_1 u_1$ and p_s/p_{s1} (where ρ_1, u_1, and p_{s1} are conditions outside the boundary layer) are presented in Fig. 2. Three averages are taken, the correct maximum as given by Eq. (7) and two others as follows:

$$\bar{p}_s = \int_0^\delta \rho u p_s \, dy \Big/ \int_0^\delta \rho u \, dy \tag{8}$$

$$\bar{p}_s = \frac{1}{\delta} \int_0^\delta p_3 \, dy \tag{9}$$

Eq. (7) yields $\bar{p}_s/p_{s1} = 0.641$, while Eqs. (8) and (9) give 0.756 and 0.432, respectively. Any average value higher than that given by Eq. (7) is a violation of the Second Law of Thermodynamics; while the validity of any average lower than that of Eq. (7) must be examined in the light of the method whereby it is obtained.

This note results from an investigation on boundary-layer flows sponsored by the Office of Scientific Research, USAF. The author wishes to acknowledge the discussions leading to this note with Mr. K. Krishnamurty.

The Skewness Factor According to Obukhoff's Transfer Theory

W. H. Reid
Exterior Ballistics Laboratory, Aberdeen Proving Ground, Md.
October 31, 1955

FOR SUFFICIENTLY LARGE Reynolds Numbers for which a universal equilibrium exists, Millsaps[1] has shown that Obukhoff's transfer theory leads to an equilibrium spectrum of the form

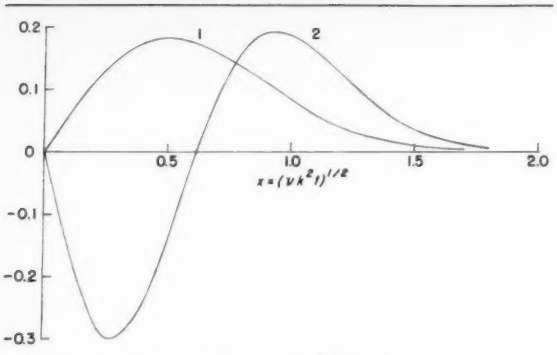

FIG. 1. Curve 1: The "zero Reynolds Number" energy spectrum, $F_2(x)$—independent of transfer theory. Curve 2: The first approximation to the transfer function, $10\ U_3(x)$—Obukhoff's transfer theory.

$$\left.\begin{aligned} E(k) &= \frac{1}{k^2}\frac{d}{dk}\left[(A+B)^{1/2}+(A-B)^{1/2}\right]+\frac{2\nu^2}{3\gamma^2}k \\ &\qquad\qquad \text{for } 0 \le k \le k_\eta \\ &= 0 \qquad\qquad \text{for } k_\eta < k < \infty \end{aligned}\right\} \tag{1}$$

where $k_\eta = (\epsilon\gamma^2/4\nu^3)^{1/4}$

$$A = \frac{k^4}{432\gamma^6}\left(27\epsilon^2\gamma^4+18\epsilon\gamma^2\nu^3k^4+2\nu^6k^8\right)$$

$$B = \frac{\epsilon k^4}{48\gamma^3}\left[(27\epsilon^2\gamma^2+4\epsilon\nu^3k^4)/3\right]^{1/2}$$

In these equations, γ is the arbitrary constant usually denoted by this symbol which occurs in Obukhoff's expression for the transfer function. From this solution it is possible to obtain the behavior of the ratio S/γ, where S is the skewness factor of $-\partial u_1/\partial x_1$, both for $\nu = 0$ and for $\nu \to 0$.

In the case $\nu = 0$ this is particularly simple; for, the solution (1) then reduces to

$$E(k) = (2/3)\,(\epsilon/\gamma)^{2/3}k^{-5/3} \qquad \text{for } 0 \le k < \infty, \tag{2}$$

and if this result is compared with the Kolmogoroff prediction[2]

$$E(k) = \frac{55}{81}\frac{1}{(1/3)!}\left(\frac{4\epsilon}{5S}\right)^{2/3}k^{-5/3} \tag{3}$$

one finds that

$$\frac{S}{\gamma} = \frac{4}{135}\left[\frac{55}{6\,(1/3)!}\right]^{3/2} = 0.9745 \tag{4}$$

On the other hand, this ratio can also be calculated from the relation

$$S = \frac{3}{7}(30)^{1/2}\,\nu\left\{\int_0^\infty k^4E(k)(k)dk\Big/\left[\int_0^\infty k^2E(k)dk\right]^{3/2}\right\} \tag{5}$$

which is asymptotically correct as $\nu \to 0$. Thus, by using the solution of (1), or the alternative form of it given by Goldstein,[3] one finds that

$$\frac{S}{\gamma} = \frac{12}{7}(15)^{1/2}\left(\frac{\pi}{4}-\frac{2}{3}\right) = 0.7883 \tag{6}$$

This "double limit" behavior is similar to the situation encountered in Heisenberg's transfer theory;[2] it is only the second value, of course, that is physically meaningful.

It is also possible to obtain very simply the value of S/γ for small values of the Reynolds Number (i.e., as $\nu \to \infty$). Thus, by assuming the usual type of initial period similarity for the energy spectrum and transfer functions

$$\left.\begin{aligned} E(k,t) &= \gamma^{-2}\nu^{5/2}t^{-1/2}F(x) \\ T(k,t) &= \gamma^{-2}\nu^{5/2}t^{-3/2}U(x) \end{aligned}\right\} \tag{7}$$

where $x = (\nu k^2 t)^{1/2}$, and by assuming a solution in the form of a power series in the Reynolds Number of the turbulence

$$\left.\begin{aligned} F(x) &= \sum_{n=2}^{\infty} F_n(x)\,(\gamma R_\lambda)^n \\ U(x) &= \sum_{n=3}^{\infty} U_n(x)\,(\gamma R_\lambda)^n \end{aligned}\right\} \tag{8}$$

one finds that, according to Obukhoff's transfer theory, the leading terms in these expressions are given by

$$\left.\begin{aligned} F_2(x) &= \frac{3}{5}xe^{-2x^2} \\ U_3(x) &= -\frac{3(15)^{1/2}}{200}\frac{d}{dx}e^{-2x^2}\left[1-(1+2x^2)e^{-2x^2}\right]^{1/2} \end{aligned}\right\} \tag{9}$$

which are shown graphically in Fig. 1. The ratio S/γ can now be calculated from this solution by using the relation

$$\frac{S}{\gamma} = \frac{400}{7}\int_0^\infty x^2U_3(x)dx + O(\gamma R_\lambda) \tag{10}$$

which follows directly from the definition of S; an approximate evaluation of this integral then gives

$$S/\gamma \to 0.75 \text{ as } R_\lambda \to 0 \tag{11}$$

which is remarkably close to the value 0.79, obtained for $R_\lambda \to \infty$.

Thus, the variation of the ratio S/γ with Reynolds Number is even less for Obukhoff's transfer theory than it is for Heisenberg's.[2] Although the physical transfer theories of this type no longer occupy the center of interest in research on isotropic turbulence, nevertheless, it is interesting to note how remarkably consistent they are.

REFERENCES

[1] Millsaps, K., *The Obukhoff Spectrum of Homogeneous Isotropic Turbulence*, Journal of the Aeronautical Sciences, Vol. 22, No. 7, p. 511, July, 1955.

[2] Reid, W. H., *Two Remarks on Heisenberg's Spectrum of Isotropic Turbulence*, Quart. Appl. Math. (to be published).

[3] Goldstein, S., *On the Law of Decay of Homogeneous Isotropic Turbulence and the Theories of the Equilibrium and Similarity Spectra*, Proc. Cambridge Phil. Soc., Vol. 47, Part 3, pp. 554–574, July, 1951.

Iteration in Semidefinite Eigenvalue Problems

Samuel Pines
Chief Dynamics Engineer, Republic Aviation Corporation, Farmingdale, N. Y.

November 1, 1955

THE PROBLEM OF obtaining the eigenvectors and characteristic frequencies of a system of equations involving both elastic and rigid-body modes is of sufficient interest to warrant the presentation of an additional method to the set already outlined in the reference paper.

We are given the matrix equation

$$(C - w^2M)x = 0 \tag{1}$$

where M is positive definite of order and rank n, and C is semidefinite of order n and rank $n - r$. If C were nonsingular, it could be inverted and Eq. (1) would read

$$[I(1/w^2) - C^{-1}M]x = 0 \tag{2}$$

and solution for the characteristic vector x could be obtained in a standard fashion. Since C is singular, an alternate procedure is presented which will retain the basic elastic properties and increase the rank of C to n.

The individual equations of the matrix Eq. (1) consists of r equations (not involving elastic terms) of the form

$$\sum_{j=1}^{n} m_{ij}x_j = 0 \qquad (i = 1, 2, \ldots r) \tag{3}$$

The coefficients m_{ij} come from the matrix M, and the corre-

sponding elements of the matrix C are all zero, since no elastic energy is involved. In addition, the matrix Eq. (1) consists of $n - r$ equations (involving elastic terms) of the form

$$\sum_{j=r+1}^{n} c_{ij}x_j - w^2 \sum_{j=1}^{n} m_{ij}x_j = 0 \qquad (i = r+1, \ldots n) \qquad (4)$$

The elements c_{ij} come from the C matrix. It is seen that the matrix M is complete while C contains an elastic nucleus in the lower corner bounded by r rows and r columns of zeros.

From Eq. (3), since a number equal to zero is equal to a constant times itself, it follows that we may replace the r equations of the form in Eq. (3) by their equivalent form

$$\sum_{j=1}^{n} m_{ij}x_j - w^2 \sum_{j=1}^{n} m_{ij}x_j = 0 \qquad (i = 1, 2 \ldots r) \qquad (5)$$

In this fashion the first r rows of the C matrix are altered from their original value of zero to

$$c_{ij} = m_{ij} \qquad (i = 1, 2 \ldots r) \qquad (6)$$

The matrix C may now be written

$$\left.\begin{aligned} C &= \begin{pmatrix} M_1 & \vdots & M_2 \\ 0 & \vdots & K \end{pmatrix} \\ C^{-1} &= \begin{pmatrix} M_1^{-1} - M_1^{-1}M_2K^{-1} \\ 0 \qquad\qquad K^{-1} \end{pmatrix} \end{aligned}\right\} \qquad (7)$$

It is plain that the matrix C can always be inverted as long as K^{-1} exists and M_1^{-1} exists. Since M_1 is a minor of the positive definite matrix M, its inverse exists. K^{-1} exists since the rank of C is $n - r$.

We may now write Eq. (1) in the form of Eq. (2) and solve for the vector x.

The same procedure may be adapted to the problem of building in the orthogonality conditions into the matrix.

Assume that the first vector has been determined and we seek a second. We have from Eq. (3)

$$\sum_{j=1}^{n} m_{ij}x_{j2} = 0 \qquad (i = 1, 2 \ldots r) \qquad (3)$$

From the orthogonality condition we have

$$x_2 M x_1 = 0 \qquad (8)$$

or

$$\sum_{i=1}^{n} d_i x_{i2} = 0 \qquad (8a)$$

where the elements d_i result from the product of the matrix M into the previously determined characteristic vector x_1. We may combine Eqs. (8) and (8a) into a single equation of the form

$$\sum_{j=1}^{n} (m_{ij} + d_j)x_{j2} - w^2 \sum_{j=1}^{n} (m_{ij} + d_j)x_{j1} = 0 \qquad (9)$$

In this case, the coefficients of the matrix C for the first r equations become

$$c_{ij} = m_{ij} + d_j \qquad (i = 1, 2 \ldots r) \qquad (10)$$

Whereas the coefficients for the first r equations in the matrix M become

$$m_{ij} \rightarrow m_{ij} + d_j \qquad (11)$$

The matrix C is now inverted as shown above and the process is continued.

The resulting solutions will contain all n components, including the so-called rigid body amplitudes and will automatically form an orthogonal set of vectors.

Bibliography

Fraeys de Veubeke, B. M., *Iteration in Semidefinite Eigenvalue Problems*, Journal of the Aeronautical Sciences, Vol. 22, No. 10, pp. 710–720, October, 1955.

The Laminar Free-Convective Heat Transfer from the Surfaces of a Vertical Circular Cylinder

Knox Millsaps and Karl Pohlhausen
Department of Mechanical Engineering, Massachusetts Institute of Technology, and Wright Air Development Center, United States Air Force, Respectively
November 7, 1955

THE PROBLEM OF determining the laminar free-convective heat transfer from the surfaces of a vertical circular cylinder is attracting some attention.[1] Consequently, it may be interesting to note that the case of the linear variation of surface temperature with height of the cylinder admits a similar boundary-layer solution that is roughly analogous to the case of the vertical plate with a constant surface temperature.

The partial differential equations describing the problem are

$$\frac{\partial(ru_r)}{\partial r} + \frac{\partial(ru_z)}{\partial z} = 0$$

$$u_z\frac{\partial u_z}{\partial z} + u_r\frac{\partial u_z}{\partial r} = \nu\left(\frac{\partial^2 u_z}{\partial r^2} + \frac{1}{r}\frac{\partial u_z}{\partial r}\right) + \beta\vartheta$$

$$u_z\frac{\partial \vartheta}{\partial z} + u_r\frac{\partial \vartheta}{\partial r} = \alpha\left(\frac{\partial^2 \vartheta}{\partial r^2} + \frac{1}{r}\frac{\partial \vartheta}{\partial r}\right)$$

It is easily shown that the differential system has a similar solution when one lets

$$\begin{aligned} \partial\psi/\partial r &= ru_z \\ \partial\psi/\partial z &= -ru_r \\ \psi(r, z) &= zf(r) \\ \vartheta(r, z) &= zr^{-4}g(r) \end{aligned}$$

The resulting two ordinary differential equations for $f(r)$ and $g(r)$ are Eulerian equations that may be advantageously transformed by putting $t = \ln r$. The final equations for $f(t)$ and $g(t)$ are

$$\nu f''' + ff'' - \nu f'' - (f')^2 - ff' + \nu f' + \beta g = 0$$

$$\alpha g'' + (f - 7\alpha)g' + (16\alpha - 4f - f')g = 0$$

where primes denote differentiation with respect to t. The boundary conditions are

$$f(\ln a) = f'(\ln a) = f'(\infty) = g(\infty) = 0$$

$$g(\ln a) = \text{const.}$$

where a is the radius of the cylinder.

The complete details with numerical results for various surface temperatures slopes and Prandtl Numbers may be presented in a later paper.

References

[1] Sparrow, E. M., and Gregg, J. L., *Laminar Free-Convective Heat Transfer from the Outer Surface of a Vertical Circular Cylinder*, Paper No. 55-A-25, November Meeting, ASME.

Propulsive Ducts at the Tips of Rotor Blades

J. V. Foa,* A. Gail,† and T. R. Goodman‡
November 17, 1955

THE COMBUSTION CHAMBERS of ram-jets or ram rockets at the tips of rotor blades are subject to fairly high temperatures, internal overpressure, and high centripetal accelerations. The

* Rensselaer Polytechnic Institute.
† Cornell Aeronautical Laboratory, Inc.
‡ Formerly, at Cornell Aeronautical Laboratory, Inc. Now, at Allied Research Associates, Inc.

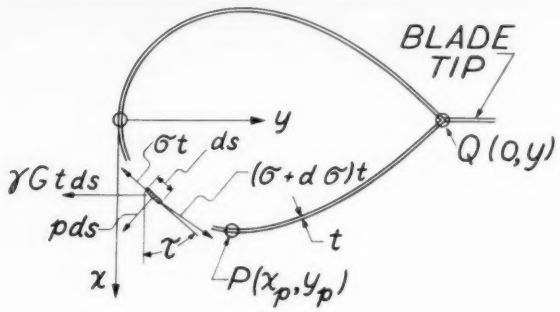

FIG. 1.

weight of the combustion chamber is a major part of the weight of the jet engine and exerts, in turn, a critical influence upon the weight and/or stress level of the whole rotor. The cross-sectional area, A, included within the combustion chamber contour determines the jet thrust or power at any given condition of operation. The problem of optimum combustion chamber design involves the selection of a cross-sectional contour of minimum periphery, $2S_Q$, minimum wall thickness, t, compatible with the allowable stress, and maximum cross-sectional area, A. This problem is treated briefly in the present note.

Consider an infinitely flexible combustion chamber in equilibrium between the internal overpressure, p, and the inertia forces of its wall. A combustion chamber with this equilibrium contour would be subject to tensile stresses only and would be lighter than any differently shaped chamber having the same strength, chordwise length, and contour periphery, $2S_Q$. There is no danger of collapse of such a chamber since the internal overpressure, p, (approximately the diffuser recovery pressure) will not vanish unless the rotor rotation, and with it the inertia forces, vanish also.

Consider the case of a wall of constant thickness, t. Moreover, let the centripetal acceleration be constant throughout the chamber wall which is a good approximation in view of smallness of the combustion chamber dimensions compared to the blade radius, R.

In Fig. 1, the notation and coordinate system are shown.

The equilibrium for any element of chamber wall of unit chordwise length requires

$$\left.\begin{aligned} -(d/ds)(\sigma\cos\tau) &= (p/t)\sin\tau \\ (d/ds)(\sigma\sin\tau) &= (p/t)\cos\tau + \gamma G \end{aligned}\right\} \tag{1}$$

where

σ = tensile stress
γ = specific weight of combustion chamber wall material
$G = \omega^2 R/g$ = centripetal acceleration in units of g
ω = angular velocity of rotor

Multiply the first of Eq. (1) by cos τ, the second by sin τ, and subtract. The resulting equation can be integrated to give

$$\sigma = \sigma_0 + \gamma G y \tag{2}$$

where σ_0 is a constant. Multiply the first of Eq. (1) by sin τ, the second by cos τ, and add. There is then obtained

$$\left.\begin{aligned} \sigma\frac{d\tau}{ds} &= \frac{p}{t} + \gamma G\cos\tau \\ \text{or}\qquad \sigma\frac{d\tau}{d\sigma}\frac{d\sigma}{dy}\frac{dy}{ds} &= \frac{p}{t} + \gamma G\cos\tau \end{aligned}\right\} \tag{3}$$

Using Eq. (2) and the identity $(dy/ds) = \sin\tau$, this may be be integrated to yield

$$\sigma = [\sigma_0(1+\beta)]/(1+\beta\cos\tau) \tag{4}$$

where $\beta = \gamma Gt/p$, the ratio of inertia forces to pressure forces and the condition $y = 0$, $\tau = 0$, $\sigma = \sigma_0$ has been applied. Combining Eq. (4) with Eq. (2) there is obtained

$$\eta = y/y_P = (1-\cos\tau)/(1+\beta\cos\tau) \tag{5}$$

where $y_P = \sigma_0 t/p$ is the value of y for which x is maximum or $\tau = 90°$ [see Fig. (1)]. The length of arc is

$$\left.\begin{aligned} \Sigma = \frac{s}{y_P} &= (1+\beta)\int_0^\tau \frac{d\tau}{(1+\beta\cos\tau)} \\ &= \frac{1}{1-\beta}\left[\frac{-\beta\sin\tau}{1+\beta\cos\tau} + \frac{1}{\sqrt{1-\beta^2}}\cos^{-1}\left(\frac{\beta+\cos\tau}{1+\beta\cos\tau}\right)\right];\ \beta<1 \\ &= 2\sin\tau\frac{(2+\cos\tau)}{3(1+\cos\tau)^2};\ \beta = 1 \\ &= \frac{1}{\beta-1}\left[\frac{\beta\sin\tau}{1+\beta\cos\tau} - \frac{1}{\sqrt{\beta^2-1}}\times\cosh^{-1}\left(\frac{\beta+\cos\tau}{1+\beta\cos\tau}\right)\right];\ \beta>1 \end{aligned}\right\} \tag{6}$$

the x coordinate is

$$\left.\begin{aligned} \xi = \frac{x}{y_P} &= (1+\beta)\int_0^\tau \frac{\cos\tau\, d\tau}{(1+\beta\cos\tau)^2} \\ &= \frac{1}{1-\beta}\left[\frac{\sin\tau}{1+\beta\cos\tau} - \frac{\beta}{\sqrt{1-\beta^2}}\times\cos^{-1}\left(\frac{\beta+\cos\tau}{1+\beta\cos\tau}\right)\right];\ \beta<1 \\ \sin\tau &= \frac{(1+2\cos\tau)}{3(1+\cos\tau)^2};\ \beta = 1 \\ &= \frac{1}{\beta-1}\left[\frac{-\sin\tau}{1+\beta\cos\tau} + \frac{\beta}{\sqrt{\beta^2-1}}\times\cosh^{-1}\left(\frac{\beta+\cos\tau}{1+\beta\cos\tau}\right)\right];\ \beta>1 \end{aligned}\right\} \tag{7}$$

Eqs. (5) and (7) together constitute the parametric equations of the equilibrium contour. It is of interest to know the value of τ at the point Q (see Fig. 1), viz., τ_Q. This is obtained by setting $\xi = 0$. The variation of τ_Q with β is shown in the chart for $0 < \beta < 2$. The radial dimension η_Q, as well as the width ξ_P, is given in the chart. The total perimeter, $2\Sigma_Q$, which is a measure of the weight of the chamber, is given also. The area enclosed by the contour, which is a measure of the thrust, is given by

$$\left.\begin{aligned} \alpha = \frac{A}{y_P^2} &= \frac{2}{y_P^2}\int_0^{\tau_Q} x\frac{dy}{d\tau}d\tau \\ &= \frac{(1+\beta)\sin\tau_Q(1+2\beta\cos\tau_Q)}{\beta(1-\beta)(1+\beta\cos\tau_Q)^2};\ \beta\le 1 \\ &= (8/5)\sqrt{3};\ \beta = 1 \end{aligned}\right\} \tag{8}$$

Numerical values of α are shown in the accompanying table.

The combustion chamber design requires advantageous choices of β and y_P. The shape of the chamber contour is determined by β, its size by y_P. The quantity β should be as small as possible in order to obtain a maximum of combustion chamber cross section (and hence thrust) for a given chamber periphery (chamber weight). At $\beta = 2$ the contour has a shape resembling a 30-per cent-thick symmetrical airfoil. If β cannot be kept below 2, one may well prefer an elongated chamber of rectangular shape adapted to the blade design. If $\beta \le 1$ can be attained, the equilibrium contours will be sufficiently bulging as to leave no doubt about the desirability of this design.

If ωR is subsonic, $p \approx (\rho/2)(\omega R)^2$ and $\beta \approx (2\gamma t/\rho g R)$, or for steel chambers near sea level $\beta \approx 12{,}767\,(t/R)$.

In the supersonic case, ωR is likely to be near 2,000 ft./sec. and $p = 52$ lb./in.^{2} (near sea level and assuming a diffuser recovery factor of 0.8). Thence, for the steel chamber of a supersonic ram-jet rotor at low altitude, $\beta = 8112\,(t/R)$. Assuming that $t = 0.02$ in. $= 0.00166$ ft. is a practical minimum thickness of the chamber wall, the blade radius would have to be $R > 21$ ft.

TABLE 1

β	τ_Q	η_Q	$2\Sigma_Q$	α	ξ_P	$\frac{2\Sigma_Q}{1+\beta\eta_Q}$	$\frac{\alpha}{(1+\beta\eta_Q)^2}$
0	180.00°	2.000	6.283	3.142	1.0000	6.283	3.142
0.2	154.25°	2.318	6.359	3.101	0.9006	4.345	1.448
0.4	139.94°	2.544	6.492	3.023	0.8235	3.218	0.7426
0.6	130.86°	2.723	6.640	2.937	0.7614	2.521	0.4234
0.8	124.59°	2.872	6.784	2.850	0.7100	2.057	0.2621
1.0	120.00°	3.000	6.928	2.771	0.6670	1.732	0.1732
1.2	116.50°	3.113	7.062	2.695	0.6295	1.491	0.1202
1.4	113.74°	3.214	7.192	2.623	0.5973	1.308	0.08672
1.6	111.50°	3.304	7.310	2.545	0.5687	1.163	0.06440
1.8	109.65°	3.386	7.420	2.475	0.5424	1.046	0.04917
2.0	108.10°	3.462	7.530	2.414	0.5211	0.9503	0.03845

for subsonic rotors and $R > 13.5$ ft. for supersonic rotors in order to obtain $\beta < 1.0$.

Supersonic rotors are likely to be larger for other reasons. Subsonic rotors of small helicopters are apt to be smaller—i.e., require $\beta > 1$ and make the application of this chamber design marginally advantageous.

The size of the chamber is limited by the maximum allowable stress, σ_c, of the combustion chamber—i.e., its value at point Q. It follows from Eq. (2) that $y_{P_{max.}} = \sigma_c t/p(1 + \beta\eta_Q)$, and consequently the maximum cross-sectional area at a given β and maximum stress is

$$A_{max.} = \left(\frac{\sigma_c t}{p}\right)^2 \frac{\alpha}{(1+\beta\eta_Q)^2} \text{ (see Table 1)} \tag{9}$$

and the maximum arc length is

$$2S_{Q_{max.}} = \frac{\sigma_c t}{p} \frac{2\Sigma_Q}{1+\beta\eta_Q} \text{ (see Table 1)} \tag{10}$$

If the desired minimum chamber wall thickness (say $t = 0.02$ in.) leads to an insufficiently large combustion chamber cross section and consequently an insufficient jet thrust, a larger t will always yield a larger $A_{max.}$ in the domain of β considered here.

The cylindrical combustion chambers of supersonic jet engines will deform in operation since p and consequently β will change with altitude.

For a given combustion chamber, the arc or periphery $2S_Q = 2y_P\Sigma_Q = \text{const.}$ For two states of operation characterized by β_0 and β_1

$$\frac{A_1}{A_0} = \left(\frac{2\Sigma_{Q0}}{2\Sigma_{Q1}}\right)^2 \frac{\alpha_1}{\alpha_0}$$

The approximate relation $\Delta A/A = -0.3\Delta\beta$ may serve as a quick estimate.

An example may illustrate the order of magnitude of the significant deformations: In an ascent from sea level to approximately 30,000 ft., altitude β is approximately doubled, the combustion chamber area decreased by between 6 to 18 per cent ($0.2 < \beta < 0.6$), and the angular deformation of the chamber at the attachment point Q is approximately 15°.

The Downstream Effect of a Thickening of the Laminar Boundary Layer

D. G. Hurley
Senior Scientific Officer, Department of Supply, Australia
November 7, 1955

SUMMARY

A simple approximate method of calculating the downstream effect of a thickening of the laminar boundary layer is given. It is shown that the thickening dies away very rapidly in a favorable pressure gradient but is magnified by an adverse pressure gradient. This confirms a conclusion that was drawn from experiments on the effects of surface roughness on the stalling characteristics of a thin airfoil.

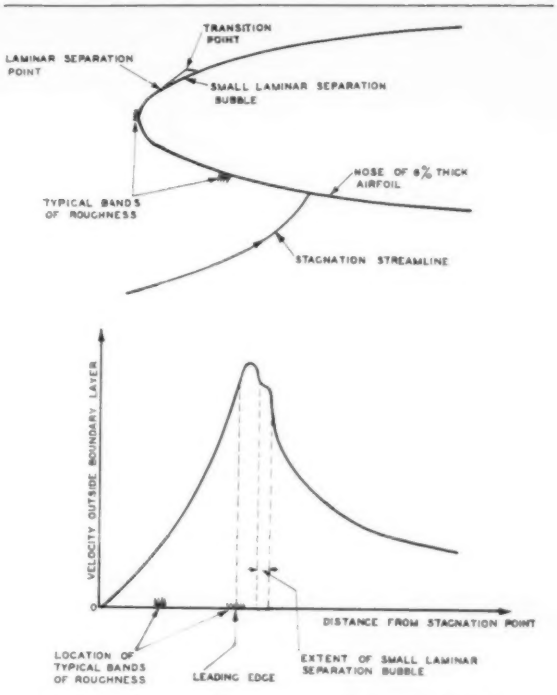

FIG. 1. Diagrams illustrating roughness experiments.

INTRODUCTION

THE PRESENT WORK was prompted by the results of an experimental investigation[1] of the effects of a narrow spanwise strip of surface roughness on the stalling characteristics of a 6 per cent thick airfoil. In these experiments strips of different sized roughness elements were in turn located on the lower surface of the airfoil at various positions close to the leading edge. When the airfoil was at a small incidence, the stagnation point was behind the strip of roughness which was then located in a very thin and hence stable laminar boundary layer. (See Fig. 1.) It was found that the roughness could be considered as having the following two effects on the flow:

(1) The roughness thickened the laminar boundary layer downstream of it.

(2) The roughness introduced disturbances into the flow which were carried downstream to the small laminar separation bubble where they provoked earlier transition in the separated boundary layer thereby reducing the size of the bubble.

Under certain conditions the nose stalling incidence* was increased by the roughness, and it was found that the increase could be correlated with the thickening of the boundary layer at the laminar separation point produced by the roughness. When this thickening was negligible, the increase in the stalling incidence was greatest provided the roughness introduced disturbances sufficient to cause transition almost immediately downstream of the laminar separation point. In this case the stall was due to the turbulent boundary layer separating a short distance downstream of the then very small separation bubble. These effects were produced by a narrow strip (0.0010 chord†) of relatively large roughness (0.030-in.) at a point on the lower surface where the velocity outside the boundary layer was low. Much smaller roughness (0.005-in.) located at the leading edge where the velocity was higher produced a greater thickening

* As the incidence is increased a critical value is reached when the small laminar separation bubble changes abruptly into a large bubble extending downstream from the leading edge; this critical value is called the nose stalling incidence.

† The chord was 10 ft. and the chord Reynolds Number 3.85×10^6.

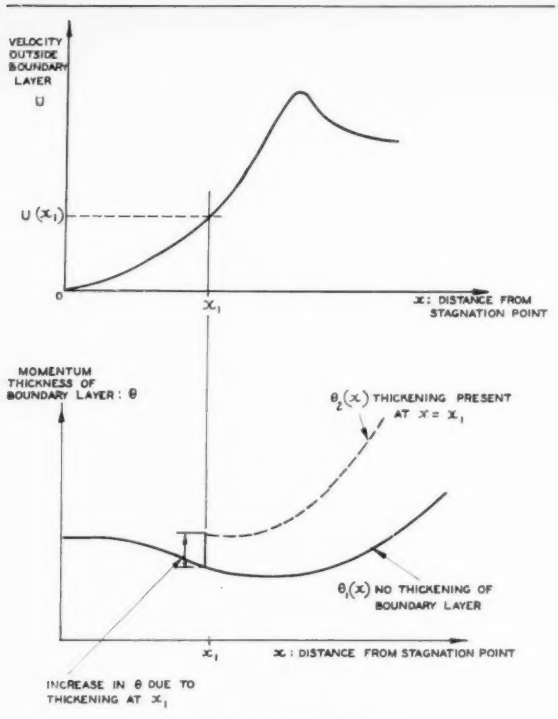
VELOCITY OUTSIDE BOUNDARY LAYER
U
U (x1)
0
x1
x: DISTANCE FROM STAGNATION POINT
MOMENTUM THICKNESS OF BOUNDARY LAYER: θ
θ2(x) THICKENING PRESENT AT x = x1
θ1(x) NO THICKENING OF BOUNDARY LAYER
x1
x : DISTANCE FROM STAGNATION POINT
INCREASE IN θ DUE TO THICKENING AT x1

FIG. 2. Definitions of symbols.

of the boundary layer at the separation point and a smaller increase in the nose stalling incidence.

These findings prompted the investigation of the downstream effect of a thickening of the laminar boundary layer which is described below.

THEORY

It will be assumed that the thickening effect of a narrow band of roughness can be represented by a discontinuous change in the boundary-layer parameters (momentum thickness, displacement thickness, etc.) and that after the thickening, the boundary layer rapidly adjusts itself to the new value of its shape parameter* so that its subsequent development can be calculated approximately in the usual way. Let $\theta_1(x)$ be the momentum thickness of the boundary layer when there is no thickening and $\theta_2(x)$ the momentum thickness when thickening occurs at $x = x_1$ (see Fig. 2).

According to the method of reference 2, the boundary-layer momentum equation may be approximated by

$$U(x)\frac{d\theta^2(x)}{dx} = 0.45\,\nu - 6\,\frac{dU(x)}{dx}\,\theta^2(x) \qquad (1)$$

where ν is the kinematic viscosity and the other symbols are defined in Fig. 2. This can be integrated to give

$$\theta^2(x) = \frac{0.45\nu}{U^6(x)}\int_0^x U^5(x)\,dx + \frac{C}{U^6(x)} \qquad (2)$$

Now at the stagnation point, $x = 0$, $U(x)$ is zero, and $\theta(x)$ finite so that $C = 0$. Thus, for the case of no thickening at $x = x_1$,

$$\theta_1^2(x) = \frac{0.45\,\nu}{U^6(x)}\int_0^x U^5(x)\,dx \qquad \text{for all } x > 0 \qquad (3)$$

When thickening occurs at $x = x_1$, Eq. (2) will still hold for $x > x_1$ but the value of the constant C will be changed. Its value is determined by the condition that at $x = x_1$, $\theta(x)$ should equal some prescribed value $\theta_2(x_1)$.

Thus from Eqs. (2) and (3)

$$\theta_2^2(x_1) = \frac{0.45\nu}{U^6(x_1)}\int_0^{x_1} U^5(x)\,dx + \frac{C}{U^6(x_1)}$$

$$= \theta_1^2(x_1) + \frac{C}{U^6(x_1)} \qquad \text{respectively}$$

so that $C = U^6(x_1)\,[\theta_2^2(x_1) - \theta_1^2(x_1)]$

Substituting into Eq. (2) gives for the case of thickening

$$\theta_2^2(x) = \frac{0.45\nu}{U^6(x)}\int_0^x U^5(x)\,dx + \frac{U^6(x_1)}{U^6(x)}\,[\theta_2^2(x_1) - \theta_1^2(x_1)]$$

Substituting for the first term of the R.H.S. from Eq. (3) gives

$$\theta_2^2(x) - \theta_1^2(x) = \frac{U^6(x_1)}{U^6(x)}\,[\theta_2^2(x_1) - \theta_1^2(x_1)] \qquad \text{for all } x > x_1 \quad (4)$$

This is the required result.

DISCUSSION

Eq. (4) shows that the increase, $\theta_2^2(x) - \theta_1^2(x)$, in θ^2 at a point where the velocity outside the boundary layer is $U(x)$, that arises from an increase, $\theta_2^2(x_1) - \theta_1^2(x_1)$, in θ^2 at some upstream point where the velocity is $U(x_1)$ is simply

$$\frac{U^6(x_1)}{U^6(x)}\,[\theta_2^2(x_1) - \theta_1^2(x_1)]$$

i.e., it is directly proportional to the velocity ratio at the two points raised to the sixth power and is independent of the manner in which the velocity change is effected.

In a favorable velocity gradient $U(x) > U(x_1)$ so that any thickening will die out very quickly. In an adverse velocity gradient $U(x) < U(x_1)$ so that the thickening will increase rapidly.

It is seen that Eq. (4) provides a qualitative explanation of the thickening effects of roughness referred to in the Introduction.

REFERENCES

[1] Hurley, D. G., and Ward, G. F., *Experiments on the Effects of Air Jets and Surface Roughness on the Boundary Layer Near the Nose of an NACA 64A006 Aerofoil*, A.R.L. Aero Note 128, September, 1953.

[2] Thwaites, B., *Approximate Calculation of the Laminar Boundary Layer*, Aero. Quart., Vol. 1, Part III, p. 245, November, 1949.

* Some justification for this assumption was obtained from the measured boundary-layer profiles, which at a short distance downstream of the roughness showed no unusual features.

Effect of Diffusion in an Isothermal Boundary Layer*

E. R. G. Eckert and P. J. Schneider

Professor of Mechanical Engineering and Research Associate in Mechanical Engineering, Respectively, Heat Transfer Laboratory, University of Minnesota

August 16, 1955

SYMBOLS

C_i	=	integration constants
c_f	=	dimensionless local skin-friction coefficient
D_{12}	=	coefficient of ordinary diffusion
f	=	dimensionless stream function ($df/d\eta = 2\,\varphi_\rho\,u/u_\infty$)
J_i	=	diffusion currents
M	=	molecular weight
Sc	=	Schmidt Number $= \nu_\infty/D_{12}$
u,v	=	velocity components in x and y directions
W	=	mass fraction of diffusing component in binary mixture

* These investigations are part of a larger program of theoretical and experimental studies of mass-transfer cooling being carried out by the Heat Transfer Laboratory at the University of Minnesota under the auspices of the Air Research and Development Command, Air Force Contract No. AF-18(600)-1226. The authors also acknowledge their debt to Wayne R. Lundberg, currently with Pratt and Whitney Aircraft at Hartford, Conn., for assistance in the numerical calculations.

X = mole fraction of diffusing component in binary mixture
x,y = coordinates parallel and perpendicular to plate surface
η = independent similarity coordinate = $(1/2)y\sqrt{u_\infty/\nu_\infty x}$
μ = viscosity of mixture
ν_∞ = kinematic viscosity of free-stream fluid
ρ = density of mixture
φ_μ = viscosity ratio = μ/μ_∞
φ_ρ = density ratio = ρ/ρ_∞

Subscripts

1 = diffusing gas
2 = free-stream gas
w = surface
∞ = free stream

Introduction

Recent studies have suggested that the method of mass-transfer cooling can offer an effective means of protecting the surfaces of high-speed vehicles against the influence of viscous dissipation. By this method, a coolant is forced through the porous surfaces of the vehicle. The coolant may be a gas, or it may be a liquid that covers the porous surface as a film and evaporates into the boundary layer. An alternate technique is represented by sublimation cooling in which the walls of the vehicle are constructed of a solid material whose surface continuously evaporates into the high-temperature boundary-layer air. In all such processes the heat and momentum transport are accompanied by a simultaneous diffusion of the injected or generated gas away from the surface. This diffusion process has a marked effect on the boundary-layer development, particularly when the properties of the diffusing foreign gas are widely different from the properties of the free stream.

A relatively recent paper in the Journal by Smith[1] has considered the effects of molecular diffusion in a laminar boundary layer for cases of zero and finite heat transfer to porous flat plates. In both cases a diffusion phenomenon is present if the physical and thermal properties of the fluid injected into the boundary layer are different from those of the main boundary-layer fluid. In the isothermal case the diffusion is principally caused by nonuniformity of composition in the binary fluid mixture, while in the nonisothermal case both composition and thermal diffusion are present.

The purpose of this note is to indicate a number of improvements in Smith's solutions. While only results for the isothermal case will be presented here, the improvements are applicable to the heat-transfer case as well.

Analysis

The boundary-layer equations of continuity, momentum, and diffusion for steady, laminar, two-dimensional, isothermal flow over a flat plate of a fluid with variable properties μ and ρ and under the condition of fluid injection from the surface are

$$(\partial/\partial x)(\rho u) + (\partial/\partial y)(\rho v) = 0 \tag{1}$$

$$\rho u(\partial u/\partial x) + \rho v(\partial u/\partial y) = (\partial/\partial y)[\mu(\partial u/\partial y)] \tag{2}$$

$$\rho u(\partial W/\partial x) + \rho v(\partial W/\partial y) = (\partial/\partial y)[\rho D_{12}(\partial W/\partial y)] \tag{3}$$

The standard transformation in terms of a dimensionless stream function f and a dimensionless similarity coordinate η automatically satisfies Eq. (1), and reduces the partial-differential Eqs. (2) and (3) to the set of total differential equations for momentum and diffusion*

$$f\frac{d}{d\eta}\left(\varphi_\rho{}^{-1}\frac{df}{d\eta}\right) + \frac{d}{d\eta}\left[\varphi_\mu\frac{d}{d\eta}\left(\varphi_\rho{}^{-1}\frac{df}{d\eta}\right)\right] = 0 \tag{4}$$

$$(d/d\eta)[Sc^{-1}\varphi_\rho(dW/d\eta)] + f(dW/d\eta) = 0 \tag{5}$$

Although these variables effect a transformation to total differential equations, they impose the condition that the normal velocity at the surface must vary inversely with the square root of x.

* As communicated in a later note[2] by Smith, the diffusion equation used in reference 1 was in error.

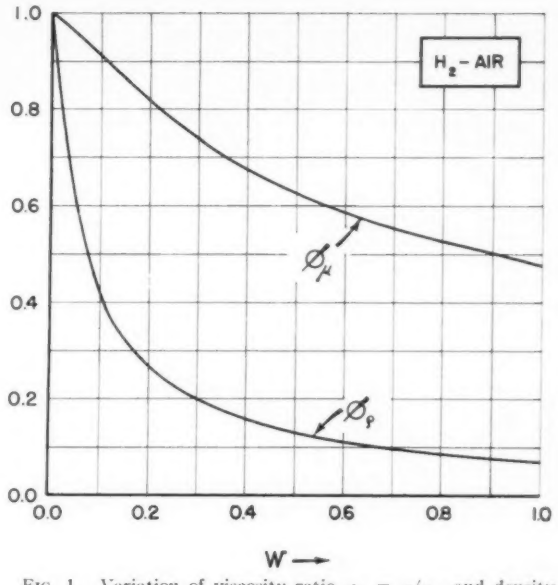

Fig. 1. Variation of viscosity ratio $\varphi_\mu = \mu/\mu_\infty$ and density ratio $\varphi_\rho = \rho/\rho_\infty$ with mass concentration W for an isothermal hydrogen-air mixture.

One of the principal differences between the present solution of the isothermal case and that obtained by Smith[1] is the selection of boundary conditions for the momentum equation. Smith assumed that the normal convective velocity at the plate surface is zero. However, a diffusive velocity of the gas ejected from the surface is always present due to the concentration gradient through the boundary layer. In order to make the convective velocity zero, this diffusive velocity would have to be compensated by a diffusive velocity of the air into the plate. Since this does not occur in practical applications of interest, a nonvanishing normal convective velocity at the surface is allowed in the present study. There is a connection between this convective velocity and the mass fraction of diffusing gas at the surface which can be expressed as follows:

The diffusion current for the air is given by

$$J_2 = (1 - W)\rho(v_2 - v)$$

and in a finite mixture this must be equal to the diffusion current of the injected foreign gas. At the plate surface the diffusive velocity of the air is assumed to be zero,

$$v_2 = 0 \text{ at } y = 0$$

According to this the surface diffusion current for the foreign gas becomes

$$J_{1_w} = -J_{2_w} = (1 - W_w)\rho_w v_w = -\rho_w D_{12}(\partial W/\partial y)_w$$

By transforming this to f and η, we have

$$f_w = \{\varphi_{\rho_w}/[Sc(1 - W_w)]\}(dW/d\eta)_w \tag{6}$$

instead of $f_w = 0$ as assumed by Smith. The value of f_w thus depends on the selection of a mass fraction at the surface; either f_w or W_w can be chosen independently and the other calculated by Eq. (6) and the concentration gradient $(dW/d\eta)_w$.

The set of five boundary conditions which must be satisfied by the third-order momentum and second-order diffusion equations is therefore

$$\left.\begin{aligned} f' &= 0\ (u = 0) \\ f &= \{\varphi_{\rho_w}/[Sc(1 - W_w)]\}(dW/d\eta)_w \\ W &= W_w \end{aligned}\right\} \text{ at } \eta = 0$$

$$\left.\begin{aligned} f' &= 2\ (u = u_\infty) \\ W &= 0 \end{aligned}\right\} \text{ at } \eta = \infty$$

Solutions of the differential Eqs. (4) and (5) are obtained by the method of successive approximations, for which these equa-

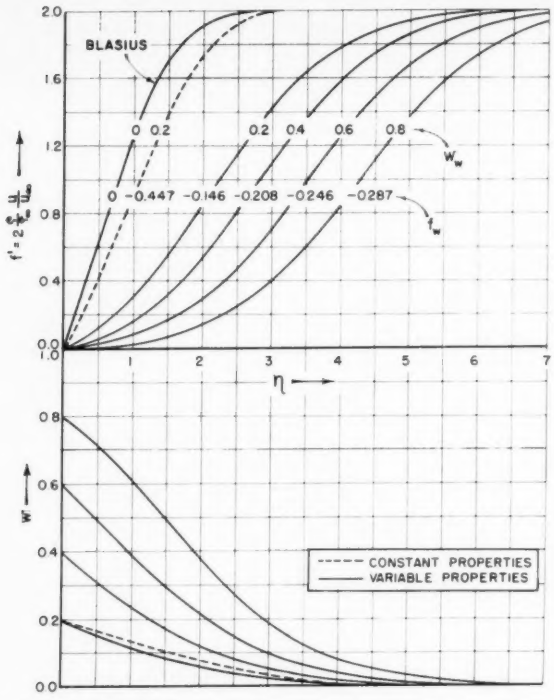

FIG. 2. Mass-velocity and concentration profiles in an isothermal hydrogen-air boundary layer as a function of the dimensionless distance from the plate surface $\eta = (1/2)y\sqrt{u_\infty/\nu_\infty x}$, surface concentration W_w, and corresponding dimensionless blowing parameter $f_w = -2(\zeta_w/\zeta_\infty)v_w\sqrt{x/\nu_\infty u_\infty}$.

tions are reduced to the required integral forms

$$f = f_w + C_1\int_0^\eta \varphi_\rho \int_0^\eta \varphi_\mu^{-1} \exp\left(-\int_0^\eta \varphi_\mu^{-1} f d\eta\right) d\eta d\eta \quad (7)$$

$$W = W_w + C_2\int_0^\eta \varphi_\rho^{-1} \exp\left(-Sc\int_0^\eta \varphi_\rho^{-1} f d\eta\right) d\eta \quad (8)$$

in which $f_w = C_2/Sc(1 - W_w)$. The Schmidt Number is assumed to be constant, since in the first approximation the coefficient of ordinary diffusion D_{12} is a function of temperature alone (see reference 3, page 539).

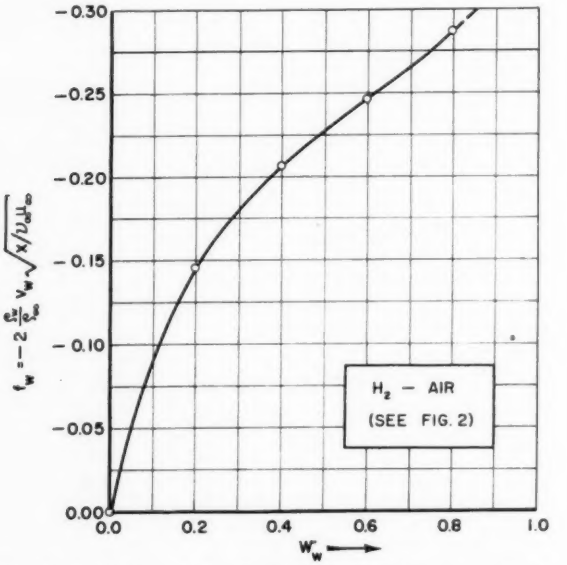

FIG. 3. Variation of the dimensionless blowing parameter f_w with mass concentration at the surface W_w.

TABLE 1
Viscosity Ratio for an H_2-O_2 Mixture

X_1	μ/μ_2 Calculated	μ/μ_2 Experimental	Per Cent Error
0.0	1.0	1.0	...
0.1835	0.968	0.978	−1.02
0.3945	0.918	0.925	−0.76
0.6030	0.838	0.846	−0.95
0.7808	0.720	0.715	+0.70
1.0	0.424	0.424	...

In the new set of calculations, the viscosity of an isothermal binary mixture is not assumed to vary linearly with composition. Based on kinetic theory, Wilke[4] developed the following approximate expression for this concentration dependence:

$$\mu = \frac{\mu_1}{1 + \zeta_{12}(X_2/X_1)} + \frac{\mu_2}{1 + \zeta_{21}(X_1/X_2)} \quad (9)$$

where $$\zeta_{ij} = \frac{[1 + (M_j/M_i)^{1/4}\sqrt{\mu_i/\mu_j}]^2}{(4/\sqrt{2})\sqrt{1 + (M_i/M_j)}}$$

and in which the X_i, M_i, and μ_i represent the mole fraction, molecular weight, and viscosity of the pure component i. The accuracy of this relation can be tested with reference to a hydrogen-oxygen mixture for which experimental data are available. In the temperature range 300–1,000°K. the ratio of viscosities for the pure components is $\mu_1/\mu_2 = 0.4240$, so that

$$\frac{\mu}{\mu_2} = \frac{0.4240}{1 + 1.2600(X_2/X_1)} + \frac{1}{1 + 0.2675(X_1/X_2)}$$

A comparison of calculated and experimental values is shown in Table 1 to be within approximately 1 per cent. For a hydrogen-air mixture with $\mu_1/\mu_2 = 0.4790$, Eq. (9) reduces to

$$\varphi_\mu = \frac{0.4790}{1 + 0.1299[(1 - W)/W]} + \frac{1}{1 + 3.9512\,[W/(1 - W)]} \quad (10)$$

where W is the mass fraction of diffusing hydrogen.

In terms of W, the density of an isothermal binary mixture of perfect gases is given by

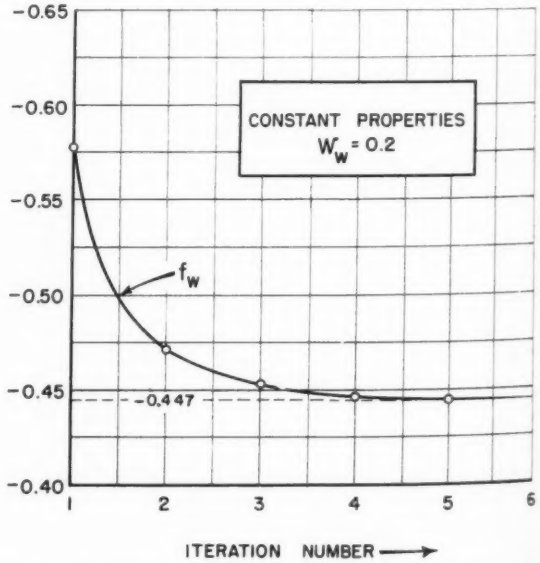

FIG. 4. Convergence of the blowing parameter f_w with successive iterations.

$$\varphi_\rho = \frac{1}{1 + [(M_2/M_1) - 1]W} = \frac{1}{1 + 13.5\,W} \qquad (11)$$

The viscosity and density ratios for an H_2-Air mixture are plotted according to Eqs. (10) and (11) in Fig. 1.

Results

Calculated results based on the new set of equations, boundary conditions, and property variations are shown in Fig. 2 for surface concentrations $W_w = 0.2, 0.4, 0.6$, and 0.8. A solution for the case of constant properties (based on air, $\varphi_\mu = 1 = \varphi_\rho$) is also shown in Fig. 2 for $W_w = 0.2$. It is evident that even at this low concentration the constant-property solution does not represent a good approximation to the actual case, particularly with regard to the mass-velocity profile f'. It is also seen that for the constant-property case a much higher blowing velocity ($f_w \sim v_w$) is required to reach a given surface concentration.

Values of f_w corresponding to the surface concentrations in Fig. 2 are plotted in Fig. 3. The point of inflection in this curve occurs in the same range of W_w for which the concentration profiles of Fig. 2 change from concave to inflected curves.

In the actual calculations based on selecting a W_w, the calculated value of f_w changes with each iteration in accordance with the changing concentration gradient $(dW/d\eta)_w = C_2/\varphi_{\rho w}$ at the surface. If one begins the first iteration with the Blasius profile and a zero concentration profile, then for successive iterations f_w converges from one side as illustrated in the typical convergence curve of Fig. 4. In general, the number of iterations required for convergence of f_w to three significant figures is approximately five, although this increases slightly as $W_w \to 1$.

The binary boundary-layer velocity profiles are given in Fig. 5. These curves indicate that the effect of injection and diffusion is to decrease the velocity gradients through the boundary layer, the effect becoming more pronounced as the injection and surface concentration increases. For a given surface concentration, the velocity at any point is overestimated by the constant-property solution.

Dimensionless local skin-friction coefficients computed as

$$c_{f_\infty} = \frac{\varphi_{\mu_w}}{\sqrt{Re_{x_\infty}}}\left[\frac{d}{d\eta}\left(\frac{u}{u_\infty}\right)\right]_w$$

are shown in Fig. 6 as a function of the wall injection parameter f_w. With increasing injection the drag coefficient decreases from the Blasius solid-plate value of $0.664/\sqrt{Re_x}$. Corresponding friction coefficients for the constant-property isothermal case are shown for comparison in Fig. 6. The Reynolds Number for both curves is based on a free-stream kinematic viscosity ν_∞, and on this basis the constant-property solution greatly overestimates the drag. If, on the other hand, one computes the

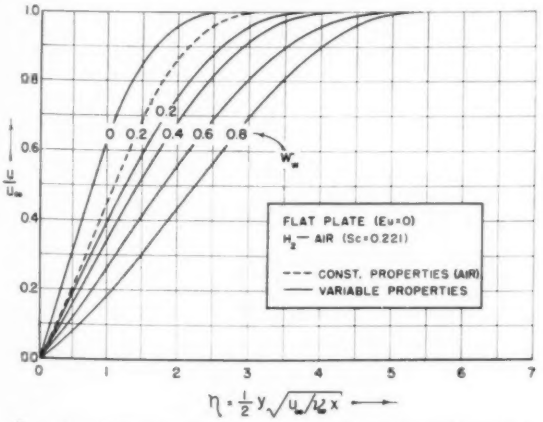

Fig. 5. Velocity profiles in an isothermal hydrogen-air boundary layer as a function of the dimensionless distance from the plate surface and surface concentrations W_w.

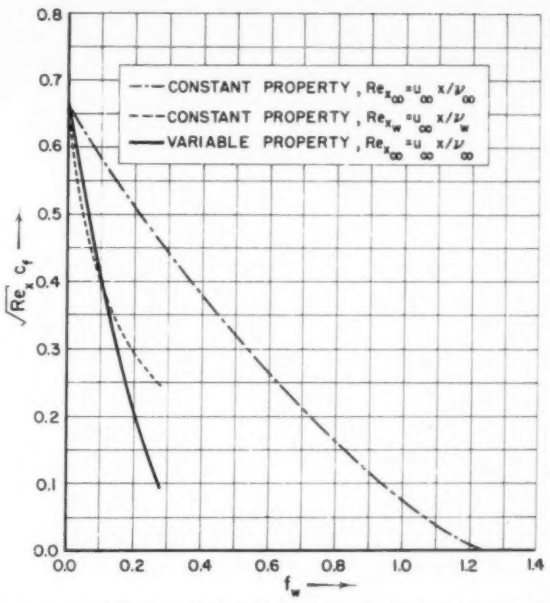
CONSTANT PROPERTY, $Re_{x_\infty} = u_\infty x/\nu_\infty$
CONSTANT PROPERTY, $Re_{x_w} = u_\infty x/\nu_w$
VARIABLE PROPERTY, $Re_{x_\infty} = u_\infty x/\nu_\infty$
$\sqrt{Re_x}\, c_f$
f_w

Fig. 6. Variation of local skin-friction coefficient with wall injection parameter.

Reynolds Number of the constant-property case with a wall kinematic viscosity ν_w, then the constant-property drag $\left[\sqrt{Re_{x_w}} \times c_{f_w} = (\nu_\infty/\nu_w)^{1/2}\sqrt{Re_{x_\infty}}\, c_{f_\infty}\right]$ more closely approximates the variable-property drag based on the free-stream kinematic viscosity. This approximation is shown in Fig. 6.

Results for the heat-transfer case will be available at a later date. In view of the excessive computational effort by hand calculations, the problem is being programmed for solution on a digital computer.

References

[1] Smith, J. W., *Effect of Diffusion Fields on the Laminar Boundary Layer*, Journal of the Aeronautical Sciences, Vol. 21, No. 3, pp. 154–162, March, 1954.

[2] Smith, J. W., *Addendum—Effect of Diffusion Fields on the Laminar Boundary Layer*, Journal of the Aeronautical Sciences, Reader's Forum, Vol. 21, No. 9, pp. 640–641, September, 1954.

[3] Hirschfelder, J. O., Curtis, C. T., and Bird, R. B., *Molecular Theory of Gases and Liquids*; John Wiley & Sons, New York, 1954.

[4] Wilke, C. R., *A Viscosity Equation for Gas Mixtures*, J. of Chem. Phys., Vol. 18, No. 4, pp. 517–519, April, 1950.

Bending Moments in an Initially Bent, Spring Restrained Column

M. J. Forray† and S. R. Bodner‡
Republic Aviation Corporation, Farmingdale, N. Y.
November 28, 1955

The deflection and bending moment of a simply supported spring restrained column of length L and flexural rigidity EI (Fig. 1) are determined in this note. The shape of the column when unloaded is assumed to be given by

$$y_0 = 4\Delta[(x/L) - (x/L)^2] \qquad (1)$$

This initial deflection reaches its maximum value, Δ, at the column midpoint $x = L/2$. The column is restrained at the point $x = a$ by a linear spring of spring constant K.

† Senior Stress Analyst.
‡ Senior Mathematician.

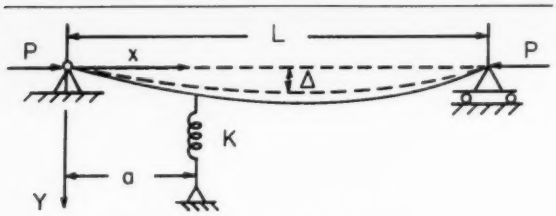

FIG. 1. Elastically restrained beam-column.

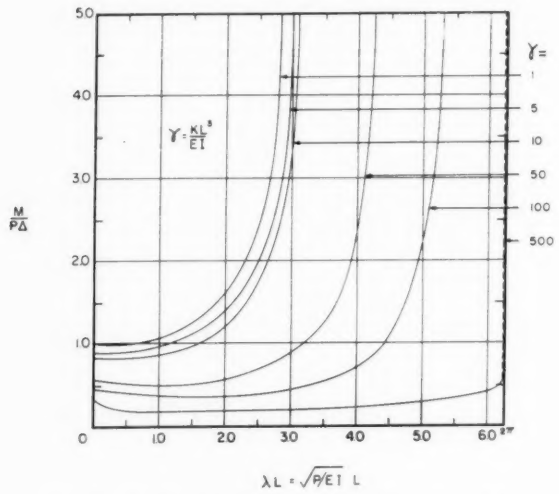

FIG. 2. Bending moment, load curves for $a/L = 0.5$.

The classical beam equation is solved to give the following expression for the elastic deflection y

$$y = A \cos(\lambda x) + B \sin(\lambda x) + Hx^2 + Jx + M \qquad 0 \le x \le a \quad (2)$$

where

$$A = 8\Delta/(\lambda L)^2$$

$$B = A \tan(\lambda L/2) + [\gamma/(\lambda L)^3]y^* [\sin(\lambda a) \cot((\lambda L) - \cos(\lambda a)]$$

$$\gamma = KL^3/EI$$

$$\lambda L = \sqrt{P/EI}\, L$$

$$y^* = \frac{A[\cos(\lambda a) + \sin(\lambda a)\tan(\lambda L/2)] + 4\Delta\{(a/L)^2 - (a/L) - [2/(\lambda L)^2]\}}{1 - \{\gamma a[1 - (a/L)]/L(\lambda L)^2\} - \{\gamma \sin \lambda a[\sin(\lambda a)\cot(\lambda L) - \cos(\lambda a)]/(\lambda L)^3\}}$$

$$H = 4\Delta/L^2$$

$$J = -4\Delta/L + \gamma y^*[1 - (a/L)]/L(\lambda L)^2$$

$$M = -8\Delta/(\lambda L)^2$$

and

$$y = C \cos(\lambda x) + D \sin(\lambda x) + H^* x^2 + J^* x + M^* \qquad a \le x \le L \quad (3)$$

where

$$C = A - \gamma y^* \sin(\lambda a)/(\lambda L)^3$$

$$D = \{[8\Delta \csc(\lambda L)]/(\lambda L)^2\} - C \cot(\lambda L)$$

$$H^* = 4\Delta/L^2$$

$$J^* = -4\Delta/L - [\gamma a y^*/L^2(\lambda L)^2]$$

$$M^* = -A + \gamma a y^*/L(\lambda L)^2$$

y^* = the elastic deflection at the spring (defined above)

The values of the relative maximum bending moments in the regions $0 \le x \le a$ and $a \le x \le L$ are

$$(M_1/P\Delta) = (1/\Delta)(-A + \sqrt{A^2 + B^2}) \qquad 0 \le x \le a \quad (4)$$

$$(M_2/P\Delta) = (1/\Delta)(-A + \sqrt{C^2 + D^2}) \qquad a \le x \le L \quad (5)$$

where the quantities A, B, C, D are defined above. If a relative maximum value does not exist in an interval, then the maximum bending moment for that region is the value at the spring location $x = a$. This quantity, M_a, is given by

$$(M_a/P\Delta) = (A/\Delta)(\cos \lambda a - 1) + B \sin(\lambda a)/\Delta \quad (6)$$

The maximum bending moment for the column is the maximum of the absolute values of M_1, M_2, and M_a.

The variation of the maximum value of the bending moment parameter $(M/P\Delta)$ with λL for various spring stiffnesses (KL^3/EI) and positions (a/L) is shown in Figs. 2, 3, 4, and 5. The maximum stress in the column can be calculated from the formula

$$\sigma = (P/A) + (Mc/I) \quad (7)$$

In the small deflection theory used here, buckling is indicated by the column deflection becoming infinitely large. The vertical asymptotes of the bending moment curves in the charts are, therefore, the buckling loads of the columns. The irregular behavior of the curves corresponding to the higher spring stiffnesses is due to the change in the deflection shape as the buckling load is approached. For columns restrained by relatively stiff

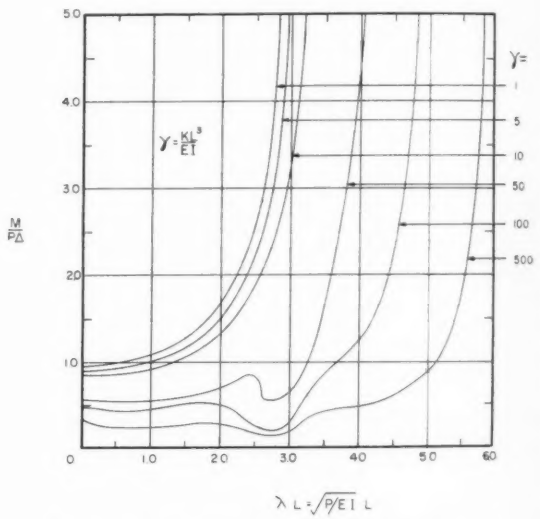

FIG. 3. Bending moment, load curves for $a/L = 0.4$.

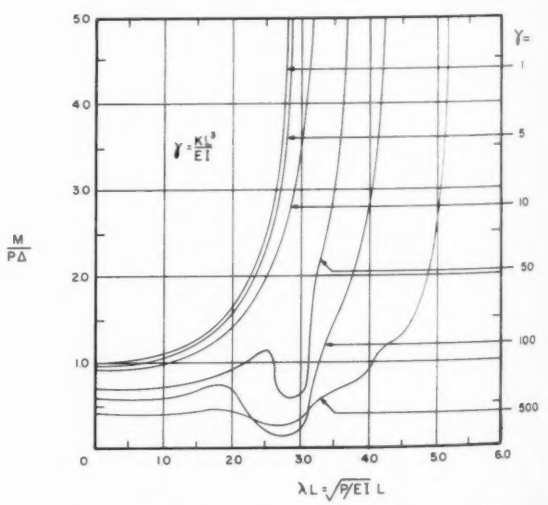

FIG. 4. Bending moment, load curves for $a/L = 0.3$.

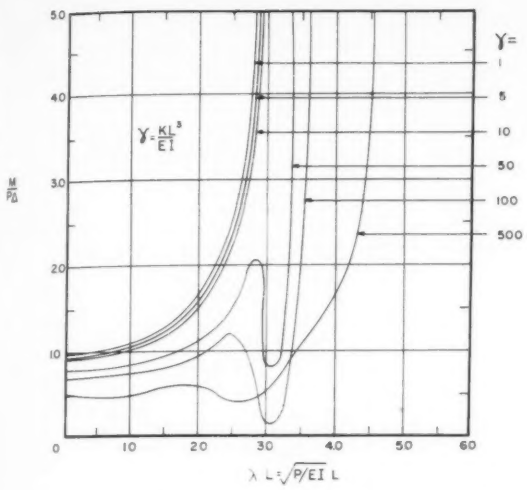

FIG. 5. Bending moment, load curves for $a/L = 0.2$.

springs, the buckling mode consists of two half waves. In these cases the column departs from the single half wave shape of the initial configuration at high loads.

Similar Solutions in Compressible Laminar Free Mixing Problems

Luigi G. Napolitano
Research Group Leader, Polytechnic Institute of Brooklyn, Brooklyn, N.Y.

November 17, 1955

THERE ARE IN supersonic aerodynamics many situations of practical interest wherein streams of different velocities and, in general, different stagnation pressures mix with one another. In the majority of these problems the interaction between the two streams takes place in the presence of an axial pressure gradient. Its effect on the characteristics of the mixing may influence significantly the performances of the devices wherein the phenomena cited above occur. A theoretical and experimental program of research to study mixing in the presence of axial pressure gradients is being carried on at the Polytechnic Institute of Brooklyn under the direction of Professor Antonio Ferri and has resulted in several preliminary publications.[1, 2] The work is sponsored by and conducted with the financial assistance of the National Advisory Committee for Aeronautics.

In the present note the possibility of obtaining similar solutions for the laminar mixing of two infinite streams with a common axial pressure gradient is discussed. Further details and developments of the analysis and experimental results are to be found in forthcoming reports. In reference 3 it was shown that for c_p = constant, $Pr = 1$, and $(\rho\mu)_y = 0$, the basic compressible boundary-layer equations, through the definition of the new dependent and independent variables

$$\left.\begin{aligned} \psi &= \xi^c U_1^d f(\zeta) \\ \eta &= \xi^b U_1^q \zeta \\ S &= S(\zeta) \end{aligned}\right\} \tag{1}$$

can be reduced to

$$\left.\begin{aligned} f''' - k_1(f')^2 + k_2 f f'' &= -k_3(1+S) \\ S'' + k_2 f S' &= 0 \\ k_i &= \text{constants} \end{aligned}\right\} \tag{2}$$

provided that the velocity distributions $U_1(\xi)$ in the Stewartson plane satisfy three simultaneous differential equations. As was subsequently pointed out[4] this requirement leads to only two distinct velocity distributions defined by appropriate values of the constant b, c, d, q. (Symbols are essentially the ones used in reference 3 or have otherwise an evident meaning.)

Since the present case differs from the boundary-layer problems only in the boundary conditions which read

$$\left.\begin{aligned} \zeta = +\infty \quad & f' = 1 && S = 0 \\ \zeta = -\infty \quad & f' = U_2/U_1 = k_{10} && S = S_2 = (H_2/H_1 - 1) \\ & f(0) = 0 \end{aligned}\right\} \tag{3}$$

the velocity distributions leading to similar solutions will be the same as the ones found in reference 3 if the additional condition

$$U_2/U_1 = k_{10} = \text{const.} \tag{4}$$

is satisfied.

Thus with the accepted hypothesis of zero normal pressure gradient, the final requirement to be fulfilled for similar solutions to be possible is expressed by

$$(\rho_{1s}/\rho_{2s})^{(\gamma-1)}\,[1 + (\gamma-1)\,M_2^2/2] \div [1 + (\gamma-1)\,M_1^2/2] = k_{10}^{2(\gamma-1)} \tag{5}$$

where the subscript s indicates stagnation values. The general solution of this equation is

$$M_2^2 = 2(m-1)/(\gamma-1) + mM_1^2 \tag{6}$$

where

$$m = (k_{10}^2\,\rho_{2s}/\rho_{1s})^{\gamma-1} \tag{7}$$

Moreover, the stagnation quantities will be related through the equations

$$p_{2s}/p_{1s} = m^{\gamma/(\gamma-1)} \qquad T_{2s}/T_{1s} = (k_{10})^2 m^{-1}$$

Interesting particular cases of Eq. (6) are:

(a) The simple case M_1 = const. and M_2 = const. $\neq M_1$ corresponding to two uniform streams already solved by Pai.[5] It is however of interest to point out that the solution of the Blasius equation, to which the present case reduces, depends only on k_{10}, while the energy equation, naturally, is identically satisfied by

$$S = S_2(f' - 1)/(k_{10} - 1)$$

For a given value of k_{10} the ratios u/u_1 and $(H - H_1)/(H_2 - H_1)$ are only functions of the similarity parameter $\zeta = \eta(a_{1s}/a_1)^{1/2} \times u_1^{1/2}\,\xi^{-1/2}$. The effects of the temperatures of the streams on the mixing characteristics are already embodied in ζ and will become apparent when velocity and temperature profiles are transformed back into the physical plane. With this method, for given values of u_1 and u_2, only one solution of the equation is necessary to investigate all the range of temperatures in which one may be interested. Compressibility effects are simply contained in the stretching of coordinates as exemplified by Eqs. (1) since the same function $u/u_1 = g(\eta a_{1s}^{1/2}\,a_1^{-1/2}\,u_1^{1/2}\,\xi^{-1/2}$ describes the incompressible velocity profile $U/U_1 = g(\eta U_1^{1/2} \times \xi^{-1/2})$ for two incompressible streams whose velocities are in the ratio (a_{1s}/a_1) to those of the corresponding compressible streams.

(b) $M_2(x) = M_1(x)$. This corresponds to $m = 1$ in Eq. (6). The constant k_{10} is determined from the stagnation quantities according to

$$\rho_{1s}/\rho_{2s} = T_{2s}/T_{1s} = (k_{10})^2$$

and the stagnation pressures of the two streams are equal.

(c) The determined solutions can be applied for any Mach Number distribution in the two main streams provided small perturbations in $(M_2 - M_1)$ are considered.

If the incompressible case is considered it becomes readily apparent that the similarity in the boundary condition and the requirement of equal axial pressure gradient cannot be both satisfied unless the streams are uniform.

It is therefore concluded that:

(a) In a compressible fluid similar solutions are possible when the velocity in the Stewartson plane is given as either a power or an exponential function of the coordinate ξ. The Mach Number distribution must satisfy, in either case, the relation given by

(6). The equations to which the problem is reduced are identical with the ones given in reference 3. The energy equation must not be considered when the two compressible streams have the same stagnation enthalpy for the equality in stagnation enthalpy is a necessary and sufficient condition for the validity of the Busemann energy integral. The solution is in any case independent of the Mach Number distributions in the two outer streams. The free laminar mixing of two infinite streams is only a particular case and is governed by the Blasius equation.

(b) In an incompressible fluid the additional similarity condition imposed at the second boundary reduces the possible cases to the elementary one of mixing of two infinite uniform streams. The phenomenon is again described by the Blasius equation.

(c) Apparently, no correlation is possible between compressible and incompressible flow in mixing problems except for the simple case of uniform streams.

References

[1] Napolitano, L. G., and Ferri, A., *Preliminary Results from the Mixing Tunnel of the Polytechnic Institute of Brooklyn Aerodynamics Laboratory*, PIBAL Report No. 267, November, 1954.

[2] Napolitano, L. G. *Theoretical and Experimental Investigations in the Mixing of Two Homogeneous Streams*, Ph.D. Thesis, Polytechnic Institute of Brooklyn, June, 1955.

[3] Li, T. Y., and Nagamatsu, H. T., *Similar Solutions of Compressible Boundary-Layer Equations*, Readers' Forum, Journal of the Aeronautical Sciences, Vol. 20, No. 9, p. 653, September, 1953.

[4] Cohen, C. B., *Similar Solutions of Compressible Laminar Boundary-Layer Equations*, Reader's Forum, Journal of the Aeronautical Sciences, Vol. 21, No. 4, p. 281, April, 1954.

[5] Pai, S. I., *Two-Dimensional Jet Mixing of a Compressible Fluid*, Journal of the Aeronautical Sciences, Vol. 16, No. 8, p. 463, August, 1949.

Comments on Supersonic Diffuser Instability

W. C. Randels

Research and Development Department, Crown Cork and Seal Company, Inc., Baltimore 3, Md.

November 30, 1955

THE AUTHOR of reference 1 makes the statement " . . . it would not be expected that the well-known phenomena of compressor surge and alternate stalling and unstalling of parallel ducts filling the same plenum chamber could be explained by the same mechanism." It should then be of general interest that the theory of Senger, reference 2, does exactly this.

By simple physical reasoning, Senger established the theorem that (to the extent of a first-order analysis) compressor flow will be unstable if the pressure-volume flow characteristic has a positive slope, giving a physical explanation for a fact which had often been noticed empirically. Supersonic diffuser buzz also occurs under the same conditions for the same reason. The data of Fig. 4a, reference 1, do not contradict this, since the one-dimensional analysis of Senger cannot be expected to apply to the eccentric configuration reported on there.

Other dissimilar phenomena which can be explained by this type of reasoning include some forms of combustion instability, the Hartman noise generator, and, in the electrical field, the neon tube oscillator.

Reference 2 may be difficult to procure but the reasoning is given in reference 3 and also in some standard gas turbine textbooks, notably one by Vincent and one by Adams.

References

[1] Daily, Charles Lee, *Supersonic Diffuser Instability*, Journal of the Aeronautical Sciences, Vol. 22, pp. 733–749, November, 1955.

[2] Senger, *The Operating Characteristics of Multistage Compressors*, VDI Lecture, 1940, BUSHIPS(338), May, 1946.

[3] Pearce, R. B., *Causes and Control of Power Plant Surge*, Aviation Week, January 16, 1950.

Deflection of Inelastic Columns

Dov Hazony (Hasanovitsh)

Junior Research Engineer, Department of Engineering, University of California at Los Angeles

November 22, 1955

Summary

A differential equation describing the deflection of inelastic columns is formulated. A specific case is considered in which the material deforms linearly up to a specified value of stress beyond which it exhibits a parabolic stress-strain relationship. Further, fibers which undergo unloading behave linearly.

Symbols

A = cross-sectional area
a = maximum initial deflection
$\gamma = \frac{3Ga\pi^2}{16l^2} \times \frac{E_0 + E_1}{E_0 E_1} \times \frac{E_1 - 3E_0}{(\sqrt{E_0} + \sqrt{E_1})^2}$
E_0 = modulus of elasticity
E_1 = initial slope of the parabola (see Fig. 2)
E_c = tangent modulus at the centroidal axis
E_r = von Kármán's reduced tangent modulus = $[4E_0E_1/(\sqrt{E_0} + \sqrt{E_1})^2]$
ϵ = strain of an arbitrary fiber
ϵ_1 = strain at the position of the inelastic boundary
ϵ_c = strain at the centroidal axis
G = modulus of curvature
h = width of the cross section
η = deflection of the beam, $\eta' = d\eta/dz$, $\eta'' = d^2\eta/dz^2$
I = moment of inertia of the cross section
l = column length
μ = initial deflection assumed equal $a \cos (\pi/l)z$
P = load
σ = stress in an arbitrary fiber
σ_c = stress at the centroidal axis
y, z = coordinate system (see Fig. 1)
$z' = \pi z/l$ = normalized coordinate
y' = position of the inelastic boundary on the cross section
$\psi = \eta/a$ = normalized deflection
$\omega^2 = P/(\pi/l)^2 E_r I$

Discussion

LET THE CROSS SECTION of the column (see Fig. 1) be a rectangle in which h is the width along the y axis (see Symbols) and the breadth is unity.

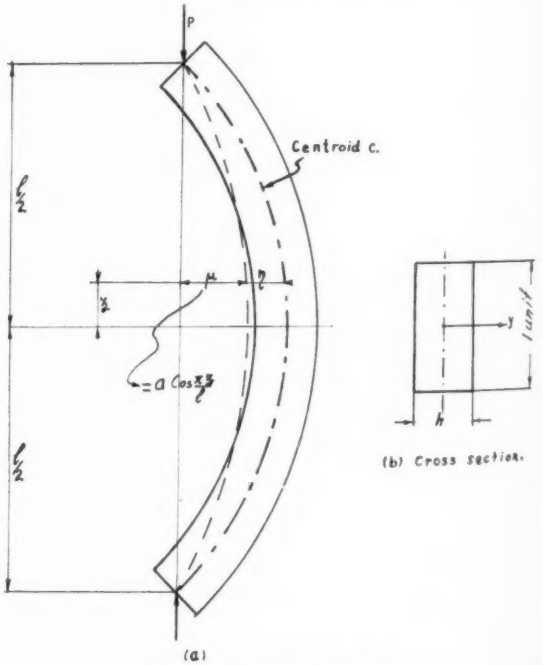

FIG. 1. A deflected column.

Let Hooke's Law be obeyed by all fibers for which the stress is less than $\sigma = \sigma_1 = \rho/h$ (see Fig. 2). The rest of the fibers are assumed to obey a parabolic stress-strain relationship. These assumptions may be summarized by the following equations:

$$\sigma - \sigma_c = E_c(\epsilon - \epsilon_c) + G(\epsilon - \epsilon_c)^2 \qquad -h/2 < y < y' \qquad (1)$$

$$= E_0(\epsilon - \epsilon_c) - (E_0 - E_c)(\epsilon_1 - \epsilon_c) + G(\epsilon_1 - \epsilon_c) \qquad y' < y < h/2 \qquad (2)$$

By assuming that plane sections remain plane and that η', the derivative of the deflection in respect to the coordinate z, is much smaller than unity; we can write for the fiber strain[1]

$$\epsilon - \epsilon_c = \eta'' y \qquad \text{and} \qquad \epsilon_1 - \epsilon_c = \eta'' y' \qquad (3)$$

Eliminating $\epsilon - \epsilon_c$ and $\epsilon_1 - \epsilon_c$ from Eqs. (1), (2), and (3) gives

$$\sigma - \sigma_c = (E_1 - 2G\eta'' y')\eta'' y + G(\eta'' y)^2 \qquad -h/2 < y < y' \qquad (4)$$

$$= E_0\eta'' y - (E_0 - E_1)\eta'' y' - G(\eta'' y')^2 \qquad y' < y < h/2 \qquad (5)$$

Now apply the conditions of equilibrium of forces and moments[2, 3]

$$\rho = \int \sigma \, dA \qquad (6)$$

$$\rho(\eta + \mu) = \int \sigma y \, dA \qquad (7)$$

to Eqs. (4) and (5) and perform the integration. It follows that

$$\frac{(E_0 - E_1)h^2}{4} + \frac{G\eta'' h^3}{12} - \left[(E_0 + E_1)h - \frac{G\eta'' h^2}{2}\right] y' + (E_0 - E_1 + G\eta'' h)y'^2 + \frac{2G\eta'' y'^3}{3} = 0 \qquad (8)$$

$$\frac{E_0 + E_1}{24}\eta'' h^3 - \frac{G\eta''^2 h^2}{64} - \left[(E_0 - E_1)\frac{\eta'' h^2}{8} + \frac{G\eta''^2 h^3}{12}\right] y' + \frac{G\eta''^2 h^2}{8} y'^2 + \frac{(E_0 - E_1)}{6}\eta'' y'^3 + \frac{G\eta''^2 y'^4}{12} + \rho(\eta + \mu) = 0 \qquad (9)$$

An exact differential equation for the deflection of the column can be obtained by eliminating y' from Eqs. (8) and (9). For most applications, it is sufficient to approximate the resulting differential equation. This can be accomplished by first expanding y' in a power series of $(G\eta''/E_r)$ which satisfies Eq. (8). The value of y' so obtained is substituted in Eq. (9).

Ignoring terms in $(G\eta''/E_r)^n$ for n larger than unity in the resulting expression, we find

$$(1 + \gamma\psi'')\psi'' + \omega^2(\psi + \cos z') = 0 \qquad (10)$$

For a pin-ended column, a solution of Eq. (10) is required which satisfies the homogeneous boundary conditions $\psi_{\pi/2} = \psi_{-\pi/2} = 0$. The solution of Eq. (10) subject to these conditions is presented in reference 3. The results are shown in Fig. 3.

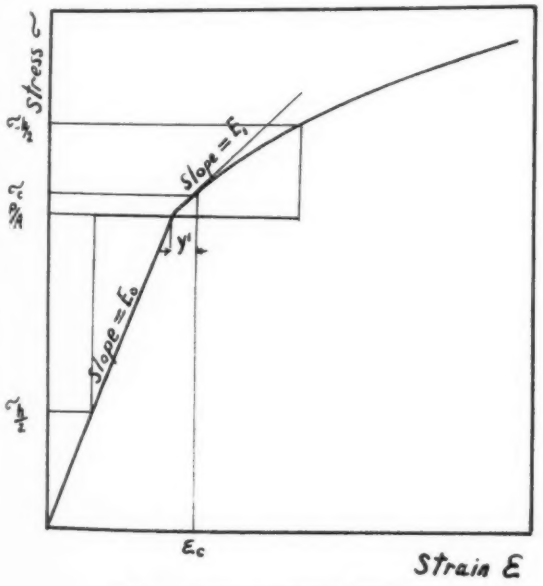

FIG. 2. Stress vs. strain diagram.

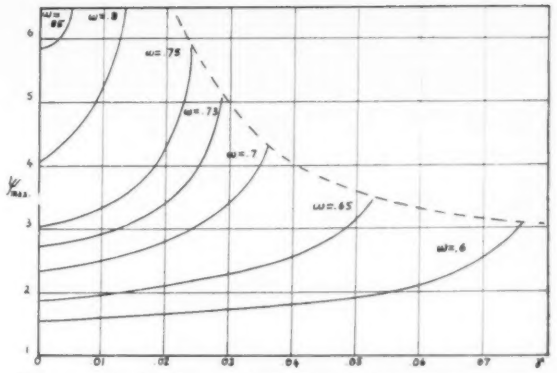

FIG. 3. Solution for ψ_{max} (satisfying the homogeneous boundary conditions $\psi \pm \pi/2 = 0$) of the equation $(1 + \gamma\psi'')\psi'' + \omega^2(\psi + \cos z') = 0$.

The region to the right of the broken line in Fig. 3 arises because of the fact that the parabola approximating the stress-strain diagram of the material has a maximum. Beyond this maximum, the material has a negative tangent modulus. Whether such a material is physically realizable or not is beyond the scope of this note. If such a material exists, fibers with a negative tangent modulus will have negative elastic energies. The region to the right of the broken line in Fig. 3 represents the fact that the sum total of all the energy of the fibers is negative. At this stage the column will continue to deform even if the load is removed. Thus the above region represents the region of instability.

REFERENCES

[1] von Kármán, Th., *Untersuchungen über Knickfestigkeit*, Mitteilungen über Forschungsarbeiten auf dem Gebiete des Ingenieurwesens, No. 81, p. 12, 1910.

[2] Timoshenko, S., *Theory of Elastic Stability*, pp. 158–161; McGraw-Hill Book Company, Inc., New York, 1936.

[3] Rosenthal, D., and Hasanovitsh, D., *Creep Buckling*, Final Report prepared under AF contract No. AF 33(616)-379, WADC, 1954.

On the Convergence of an Iterative Procedure in Solving Dynamic Response Problems

Hua Lin
Research Aeronautical Engineer, Aeroelastic and Structures Laboratory, Massachusetts Institute of Technology, Cambridge, Mass.

December 23, 1955

IN DETERMINING THE dynamic response of an airplane structure to time-dependent forces, it has been proposed in the literature, for example reference 1, that an iterative procedure may be used to account for aerodynamic damping. The first approximation is obtained by calculating a damping force corresponding to the undamped velocity response and by treating the damping force so obtained as an additional term in the external input. Successive iterations can be made by recalculating the damping force according to the velocity response of the preceding cycle.

It is interesting to examine the rate of convergence of such an iterative procedure. For clarity, let us consider a simple spring-mass-pot system—sketched in Fig. 1—acting by a step force, F, at time, $t = 0$. The governing equation of motion and the initial conditions are, respectively,

$$\left.\begin{aligned} m\ddot{x} + c\dot{x} + kx &= F \\ x(0) = \dot{x}(0) &= 0 \end{aligned}\right\} \qquad (1)$$

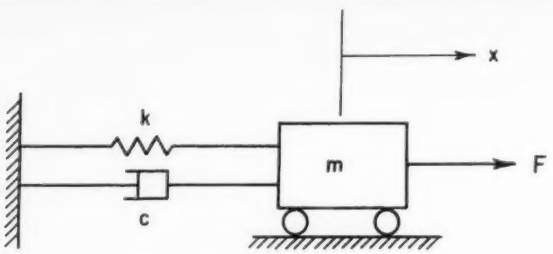

FIG. 1. A spring-mass-pot system.

where

x = displacement of the mass from its initial position at rest
m = mass
c = velocity-damping coefficient
k = linear spring constant
$(')$, $('')$ = first and second time derivatives, respectively

Eq. (1) can be rewritten into the nondimensional form

$$\left.\begin{aligned} \xi'' + 2\zeta\xi' + \xi &= 1 \\ \xi(0) = \xi'(0) &= 0 \end{aligned}\right\} \tag{2}$$

by defining

ξ = $m\omega_n^2 x/F$ = nondimensional displacement
ω_n = $\sqrt{k/m}$ = undamped natural frequency
ζ = $c/2m\omega_n$ = damping ratio
τ = $\omega_n t$ = nondimensional time
$( )', ( )''$ = first and second derivatives with respect to τ

The exact solution of Eq. (2) is

$$\xi = 1 - e^{-\zeta\tau}\left[\cos\sqrt{1-\zeta^2}\,\tau + (\zeta/\sqrt{1-\zeta^2}) \times \sin\sqrt{1-\zeta^2}\,\tau\right] \tag{3}$$

If the damping term in Eq. (2) is discarded, we have

$$\left.\begin{aligned} \xi_0'' + \xi_0 &= 1 \\ \xi_0(0) = \xi_0'(0) &= 0 \end{aligned}\right\} \tag{4}$$

The subscript, 0, indicates the zero order of approximation, namely the solution of the undamped system.

The solution of Eq. (4) is simply

$$\xi_0 = (1 - \cos\tau) \tag{5}$$

$$\xi_0' = \sin\tau \tag{6}$$

According to the iterative procedure described previously, the governing equation for the first approximation of the damped system becomes

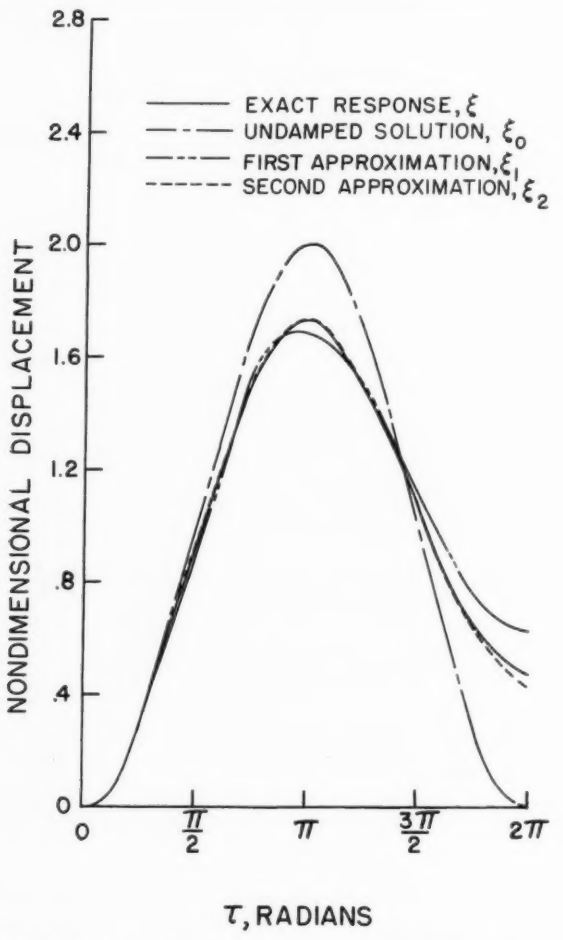

FIG. 2. Exact and approximate responses of a damped system, $\zeta = 0.1$.

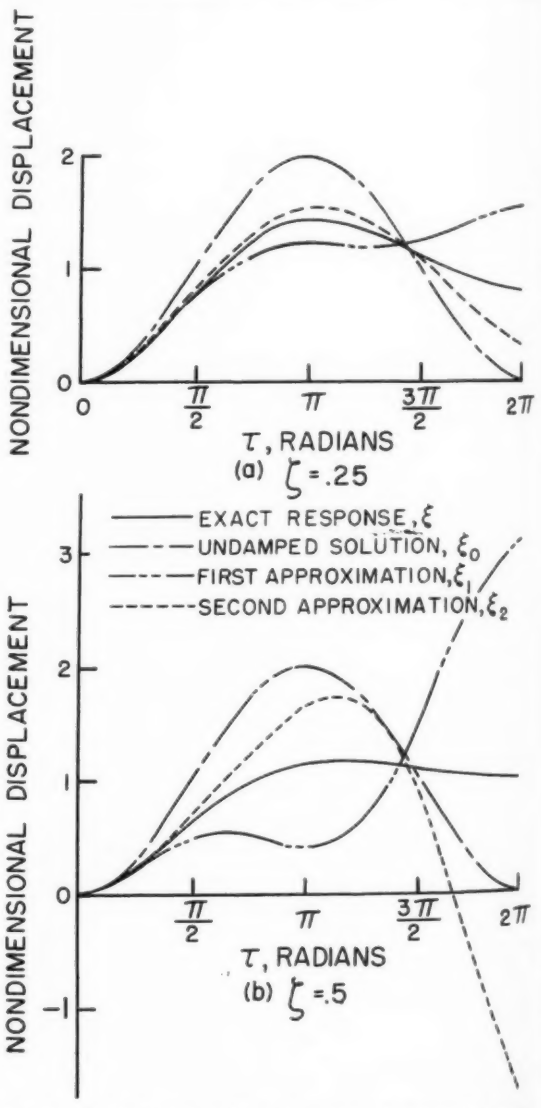

FIG. 3. Exact and approximate responses of a damped system, $\zeta = 0.25$ and $\zeta = 0.5$.

$$\xi_1'' + 2\zeta\xi_0' + \xi_1 = 1$$

or

$$\left.\begin{aligned} \xi_1'' + \xi_1 &= 1 - 2\zeta\xi_0' \\ \xi_1(0) &= \xi_1'(0) = 0 \end{aligned}\right\} \quad (7)$$

Substituting Eq. (6) into Eq. (7), we find the solution

$$\left.\begin{aligned} \xi_1 &= (1 - \cos\tau) + \zeta(\tau\cos\tau - \sin\tau) \\ &= \xi_0 + \zeta(\tau\cos\tau - \sin\tau) \end{aligned}\right\} \quad (8)$$

$$\xi_1' = \sin\tau - \zeta\tau\sin\tau \quad (9)$$

In a similar manner, the second approximation of the damped system leads to the equation

$$\left.\begin{aligned} \xi_2'' + \xi_2 &= 1 - 2\zeta(\sin\tau - \zeta\tau\sin\tau) \\ \xi_2(0) &= \xi_2'(0) = 0 \end{aligned}\right\} \quad (10)$$

which yields the solution

$$\begin{aligned} \xi_2 &= (1 - \cos\tau) + \zeta(\tau\cos\tau - \sin\tau) - \\ &\qquad (\tau/2)\zeta^2(\tau\cos\tau - \sin\tau) \\ &= \xi_1 - (\tau/2)\zeta^2(\tau\cos\tau - \sin\tau) \end{aligned} \quad (11)$$

The exact solution, ξ, and the three approximations, ξ_0, ξ_1, and ξ_2 are plotted in Figs. 2 and 3 versus nondimensional time, τ, for three values of damping ratio, ζ.

It can be observed that the successive approximate results tend to overcorrect themselves by each additional iterative step. For small damping ratios, the overcorrection is small and the iterated results converge rapidly. However, the convergence rate deteriorates rapidly with higher damping ratio and particularly at large values of time, τ.

Reference

[1] Williams, D., and Jones, R. P. N., *Dynamic Loads in Aeroplanes Under Given Impulsive Loads with Particular Reference to Landing and Gust Loads on a Large Flying Boat*, British R. & M. No. 2221, September, 1945.

Torsional Vibration of Rotating Twisted Bars

J. L. Bogdanoff and J. T. Horner
Professor of Engineering Science, Purdue University, Lafayette, Ind., and Supervisor, Engineering Calculations, Allison Division of General Motors Corporation, Indianapolis, Ind., Respectively

December 23, 1955

(I) Introduction

It has been noted by previous investigators[1, 2, 3] that the torsional natural frequencies of rotating bars are influenced by the angular velocity—the amount of this influence being dependent upon the base setting angle, the radius of the base, and the pretwist. Some approximate numerical results on the fundamental frequencies of a uniform fixed free bar without pretwist have been given.[3]

In this brief note, we present numerical results on the influence of rotation on the first three natural frequencies of a uniform fixed free bar having different base setting angles and constant pretwist rates. We also give an approximate formula for the fundamental frequency of such bars, and the total pretwist does not exceed 45°.

(II) Basic Equations

Referring to Fig. 1, the mass axis of the bar is assumed to coincide with a radial line which lies in the central plane of a disc rotating at a constant angular velocity Ω. The orthogonal axes A_0x_{10} and A_0x_{20} are along the principal axes of the base cross section and are perpendicular to the mass axes. At a typical cross section, at a distance x_3 from the base plane, the principal axes in the undeformed configuration are Ax_1 and Ax_2. Let $\mathbf{i}_1$ and $\mathbf{i}_2$ denote unit vectors along Ax_1 and Ax_2, respectively;

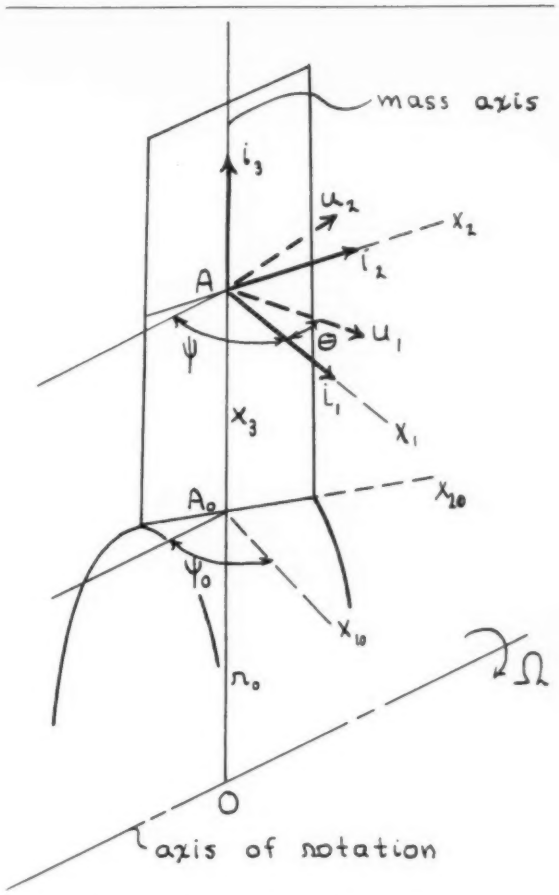

FIG. 1. Schematic diagram of twisted bar.

and let $\mathbf{i}_3$ denote a unit vector along the mass axis. The pretwist is specified by the angle, $\Psi(x_3)$, between $\mathbf{i}_1$ and a line through A parallel to the axis of rotation, as shown.

The torsional displacement of the cross section at A about $\mathbf{i}_3$ is denoted by $\theta(x_3, t)$, which is assumed to be small. Let the displaced positions of $\mathbf{i}_1$ and $\mathbf{i}_2$ be $\mathbf{u}_1$ and $\mathbf{u}_2$, respectively. It follows from kinematical considerations that the angular velocity, $\mathbf{w}$, of the unit orthogonal triad $\mathbf{u}_1$, $\mathbf{u}_2$, $\mathbf{i}_3$ is

$$\mathbf{w} = (\Omega_1 - \theta\Omega_2)\mathbf{u}_1 + (\Omega_2 + \theta\Omega_1)\mathbf{u}_2 + (\partial\theta/\partial t)\mathbf{i}_3 \quad (1)$$

where $\Omega_1 = -\Omega\cos\Psi$, $\Omega_2 = \Omega\sin\Psi$. Hence, the angular momentum per unit length of the bar, with respect to A, is given by the expression

$$\mathbf{h} = I_1(\Omega_1 - \theta\Omega_2)\mathbf{u}_1 + I_2(\Omega_2 + \theta\Omega_1)\mathbf{u}_2 + I_3(\partial\theta/\partial t)\mathbf{i}_3 \quad (2)$$

if $I_1(x_3)$, $I_2(x_3)$, $I_3(x_3)$ denote the principal moments of inertia per unit length.

The components about $\mathbf{i}_3$ of the couple due to the traction on the cross section is taken to be given by the formula

$$G_3 = C\frac{\partial\theta}{\partial x_3} + \left[\frac{J\Omega^2}{A}\int_{x_3}^{l}(R_0 + \xi)m\,d\xi\right]\left(\frac{\partial\theta}{\partial x_3} + \frac{\partial\Psi}{\partial x_3}\right)^* \quad (3)$$

where $C(x_1)$ is the usual torsional stiffness, $A(x_3)$ and $J(x_3)$ the area and second moment of area about $\mathbf{i}_3$, respectively, of the cross section, $m(x_3)$ is the mass per unit length, and $\partial\Psi/\partial x_3$ is assumed small.[4, 5]

The equation of torsional *motion* can now be obtained from the principle of angular momentum, on making use of Eqs. (2), (3), and the definitions of Ω_1 and Ω_2.

* For a more involved expression see reference 2.

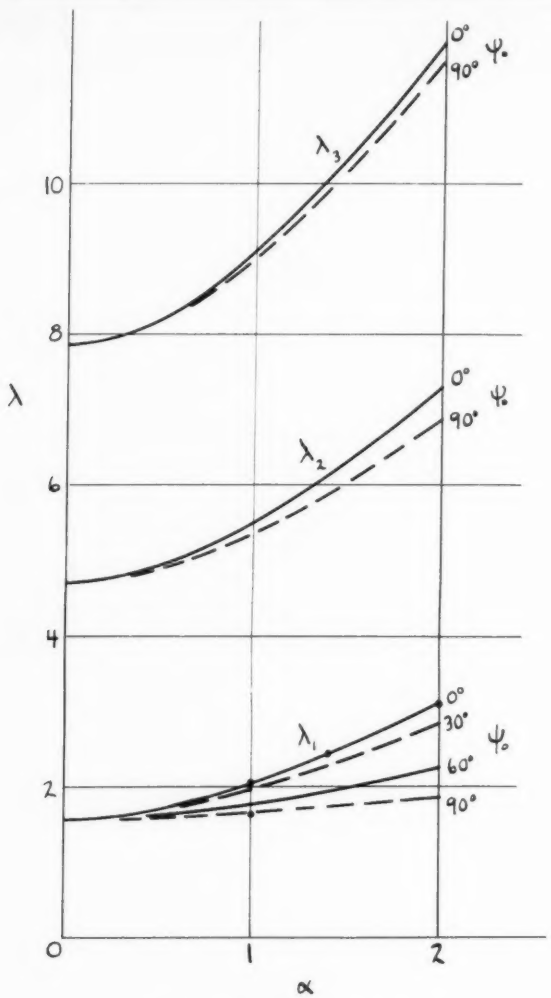

FIG. 2. Influence of ψ_0, $\nu = 0$.

$$\frac{\partial}{\partial x_3}\left\{C\frac{\partial\theta}{\partial x_3} + \left[\frac{J\Omega^2}{A}\int_{x_3}^{l}(R_0+\xi)\,m\,d\xi\right]\frac{\partial\theta}{\partial x_3}\right\} = I_3\frac{\partial^2\theta}{\partial t^2} - (I_2 - I_1)\,\Omega^2\theta\cos 2\Psi \quad (4)$$

where only linear terms in θ have been retained, and where the nonhomogeneous terms which are functions of x_3 and Ω^2 and represent distributed couples due to rotation have been dropped. The boundary conditions are

$$\left.\begin{aligned}\theta(0,\,t) &= 0\\ (\partial\theta/\partial x_3)_{x_3\,=\,l} &= 0\end{aligned}\right\} \quad (5)$$

To determine the natural frequencies and principal modes of torsional vibration, let

$$\theta(x_3,\,t) = \varphi(x_3)e^{i\omega t} \quad (6)$$

Then, Eqs. (4) and (5) become

$$\frac{d}{dx_3}\left\{\left[C + \frac{J\Omega^2}{A}\int_{x_3}^{l}(R_0+\xi)m\,d\,\xi\right]\frac{d\varphi}{dx_3}\right\} = -\left\{I_3\omega^2 + (I_2 - I_1)\Omega^2\cos 2\Psi\right\}\varphi \quad (7a)$$

$$\left.\begin{aligned}\varphi(0) &= 0\\ (d\varphi/dx_3)_{x_3\,=\,l} &= 0\end{aligned}\right\} \quad (7b)$$

respectively. These equations, or their dimensionless forms

$$(d/d\zeta)\left\{\left[c(\zeta) + \alpha^2 a(\zeta)\int_{\zeta}^{1}(r_0+\eta)\,b(\eta)\,d\eta\right](d\varphi/d\zeta)\right\} = -[\lambda^2\,d(\zeta) + \alpha^2\beta\,f(\zeta)\cos 2\Psi]\,\varphi \quad (8a)$$

$$\varphi(0) = 0 \qquad (d\varphi/d\zeta)_{\zeta\,=\,1} = 0 \quad (8b)$$

where $\zeta = x_3/l$, $r_0 = R_0/l$, $A(0) = A_0$

$C(0) = C_0$, $J(0) = J_0$, $I_3(0) = I_{30}$

$$\left.\begin{aligned} m(0) &= m_0\\ a(\zeta) &= J(\zeta)\,A_0/J_0A(\zeta), \quad b(\zeta) = m(\zeta)/m_0\\ c(\zeta) &= C(\zeta)/C_0, \quad d(\zeta) = I_3(\zeta)/I_{30}\\ f(\zeta) &= [I_2(\zeta) - I_1(\zeta)]/I_{30}\\ \alpha^2 &= m_0J_0l^2\Omega^2/A_0C_0, \quad \beta = I_{30}A_0/m_0J_0\\ \lambda^2 &= I_{30}\,l^2\omega^2/C_0\\ \Psi &= \nu\zeta + \Psi_0, \qquad \nu = \text{const.}\end{aligned}\right\} \quad (8c)$$

determine the natural frequencies and principal modes.

(III) Numerical Solution

To obtain a numerical solution, Eq. (8a) may be written as

$$\left.\begin{aligned} d\varphi/d\zeta &= T/[c(\zeta) + \alpha^2 a(\zeta)\,g(\zeta)]\\ dT/d\zeta &= -[\lambda^2 d(\zeta) + \alpha^2\beta\,f(\zeta)\cos 2\Psi]\,\varphi\end{aligned}\right\} \quad (9a)$$

$$\varphi(0) = 0, \quad T(\zeta = 1) = 0 \quad (9b)$$

where $g(\zeta) = \int_{\zeta}^{1}(r_0+\eta)\,b\,(\eta)\,d\eta$

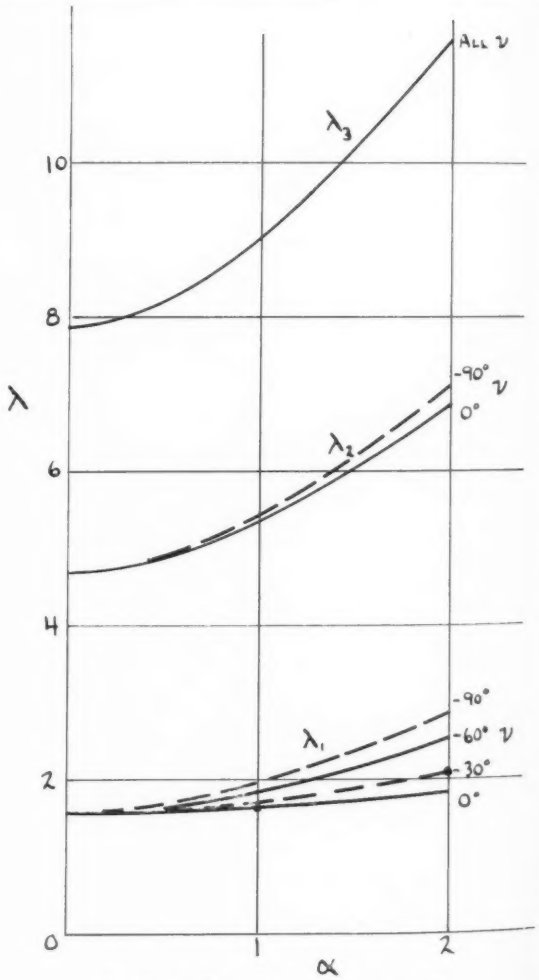

FIG. 3. Influence of pretwist, $\psi_0 = 90°$.

TABLE 1

α^2	ψ_0	ν	λ_1	λ_2	λ_3
0			1.511	4.714	7.874
1.0	0	0	2.063	5.520	9.109
1.0	30	0	1.981	5.479	9.086
1.0	30	-30	2.067	5.504	9.101
1.0	60	0	1.768	5.406	9.042
1.0	60	-30	1.911	5.430	9.071
1.0	60	-60	2.032	5.477	9.084
1.0	90	0	1.651	5.368	9.020
1.0	90	-30	1.718	5.383	9.028
1.0	90	-60	1.862	5.416	9.048
1.0	90	-90	1.968	5.446	9.066
2.0	0	0	2.457	6.176	10.14
2.0	30	0	2.316	6.122	10.10
2.0	30	-30	2.46	6.168	10.13
2.0	60	0	1.940	5.990	10.03
2.0	60	-30	2.203	6.064	10.07
2.0	60	-60	2.404	6.121	10.10
2.0	90	0	1.722	5.923	9.986
2.0	90	-30	1.850	5.950	10.00
2.0	90	-60	2.113	6.012	10.04
2.0	90	-90	2.324	6.068	10.07
4.0	0	0	3.134	7.312	11.68
4.0	30	0	2.867	7.202	11.82
4.0	30	-30	3.102	7.282	11.86
4.0	60	0	2.241	6.976	11.68
4.0	60	-30	2.710	7.106	11.76
4.0	60	-60	3.013	7.205	11.81
4.0	90	0	1.849	6.861	11.61
4.0	90	-30	2.065	6.910	11.64
4.0	90	-60	2.541	7.021	11.70
4.0	90	-90	2.886	7.119	11.76

Now let

$$\varphi = \rho(\zeta)\,\varphi(1)$$
$$T = \sigma(\zeta)\,\varphi(1)$$

Substituting into Eq. (9), we obtain

$$\left.\begin{aligned} d\rho/d\zeta &= \sigma/[c(\zeta) + \alpha^2 a(\zeta)\, g(\zeta)] \\ d\sigma/d\zeta &= -[\lambda^2 d(\zeta) + \alpha^2\beta f(\zeta)\cos 2\Psi]\,\rho \end{aligned}\right\} \quad (10a)$$

$$\left.\begin{aligned} \rho(1) &= 1, \quad \sigma(1) = 0 \\ \rho(0) &= 0 \end{aligned}\right\} \quad (10b)$$

For any particular bar, the functions $a(\zeta)$, $b(\zeta)$, $c(\zeta)$, $d(\zeta)$, $f(\zeta)$, $g(\zeta)$, and $\cos 2\Psi(\zeta)$ may be tabulated, and α^2 may be calculated. Next values for ω^2 or λ^2 may be assumed, and a numerical integration of Eqs. (10a) carried out using, for example, the Runge-Kutta or the Milne method. When the final condition, $\rho(0) = 0$, is satisfied, a natural frequency has been obtained. The values of ρ for this ω^2 give the normalized mode shape.

For a uniform bar with $R_0 = 0$ and a uniform rate of twist, Eq. (10a) becomes

$$\left.\begin{aligned} d\rho/d\zeta &= \sigma/[1 + (\alpha^2/2)(1 - \zeta^2)] \\ d\sigma/d\zeta &= -[\lambda^2 + \alpha^2\beta f_0 \cos 2(\nu\zeta + \Psi_0)]\,\rho \end{aligned}\right\} \quad (11a)$$

Fig. 2 shows the influence of the setting angle on first three natural frequencies of bars having no pretwist for which $f_0\,\beta = -0.80$. The effect of pretwist for a setting angle of 90° is shown in Fig. 3. Table 1 gives the complete numerical results. The computations were carried out on the IBM 701 computer.

(IV) Approximate Formula for λ_1 when the Bar Is Uniform and σ Small

An approximate formula for λ_1, when the bar is uniform and $\nu < \pi/8$, may be obtained from Eqs. (8) by means of the first approximation in an iterative method due to Schwarz, Stodola, Temple, etc.[3, 4] This formula is

$$\lambda_1 = 1.58/\{1 - n^2[(1 + 25\,r_0/16)/\beta - (p_2 - p_1)(1 - 8\sigma^2/7) \times \cos 2\,\Psi_0 + \sigma(p_2 - p_1)(3\sigma/24 - 5\sigma^2/8)\sin 2\,\Psi_0]\}^{1/2} \quad (12)$$

where $\Omega = n\,\omega, \quad p_1 = I_{10}/I_{20}, \quad p_2 = I_{20}/I_{30}$

Hence

$$\omega_1 = (C_0/I_{30}l^2)^{1/2}\,\lambda_1$$

The points in the Figures indicated by "dots" were calculated from Eq. (12).

References

[1] Turner, M. J., and Duke, James B., *Propeller Flutter*, Journal of the Aeronautical Sciences, Vol. 16, No. 6, pp. 323–336, June, 1949.

[2] Houbolt, John C., *Coupled Bending and Torsional Deformations of Twisted Rotating Blades under Arbitrary Loading*, presented at the 23rd Annual Meeting of the IAS, January 24–27, 1955.

[3] Bogdanoff, J. L., *Influence of Secondary Inertia Terms on Natural Frequencies of Rotating Beams*, J. Appl. Mechanics (to be published).

[4] Goodier, J. N., *Elastic Torsion in the Presence of Initial Axial Stress*, J. Appl. Mech., Vol. 17, No. 4, p. 383.

[5] Chu, Chen, *The Effect of Initial Twist on the Torsional Rigidity of Thin Prismatical Bars and Tubular Members*, Proc. First U.S. Nat. Congress on Applied Mech., p. 265.

[6] Morse, P. M., and Feshbach, H., *Methods of Theoretical Physics*, Chapt. 9, McGraw-Hill, New York, 1953.

On Viscous Heating

H. M. DeGroff

Head, School of Aeronautical Engineering, Purdue University, Lafayette, Ind.

December 22, 1955

Viscous heating in incompressible gas flow has received considerable attention in the literature. Specifically, Schlichting[1] has stated the familiar result that the temperature profile arising from viscous heating in Couette and Poiseuille flow is parabolic. He assumed constant fluid properties.

Illingworth[2] and Tarapov[3] generalized the Couette flow analysis of Schlichting to the extent that the viscosity coefficient, μ, and the thermal conductivity coefficient, k, were assumed temperature-dependent. These analyses are essentially correct but no specific conclusions are drawn by either author.

In a recent report,[4] the writer of this note has presented a more direct analysis of this problem and has pointed out the principal conclusions. A brief summary of reference 4 is the objective of this note.

Consider Couette flow of an incompressible, viscous, heating conducting gas between parallel plates in which the lower plate ($\eta = 0$) is fixed, and the upper plate ($\eta = 1$) moves with unit velocity. Further, assume that the plates are maintained at unit temperature. (Other temperature boundary conditions can be employed, but the isothermal condition is sufficient to demonstrate the important results.)

The velocity, u, and temperature, T, distributions within the fluid are then determined by the following forms of the equations of conservation of momentum and energy

$$(d/d\eta)\,[\mu(du/d\eta)] = 0 \quad (1)$$

$$(d/d\eta)\,[k(dT/d\eta)] + 2\sigma^2\mu(du/d\eta)^2 = 0 \quad (2)$$

where

$$2\sigma^2 = P_r(\gamma - 1)M_0$$
$$P_r \equiv \text{Prandtl Number} = \mu c_p/k$$
$$M_0 \equiv \text{Mach Number} = 1/\sqrt{\gamma RT}$$

and where these parameters are based upon the temperature boundary conditions. (γ = ratio of specific heats, c_p = specific heat at constant pressure, R = gas constant.)

In the case where all fluid properties are assumed constant, the above mathematical problem yields the well-known solution

$$\left.\begin{aligned} u &= \eta \\ T &= 1 + \sigma^2\eta(1 - \eta) \end{aligned}\right\} \quad (3)$$

But suppose, following the example of references 2 and 3, it is assumed that $\mu = T$, P_r = constant, and c_p = constant. This then also requires that $k = T$, and Eqs. (1) and (2) become

$$(d/d\eta)\,[T(du/d\eta)] = 0 \quad (4)$$

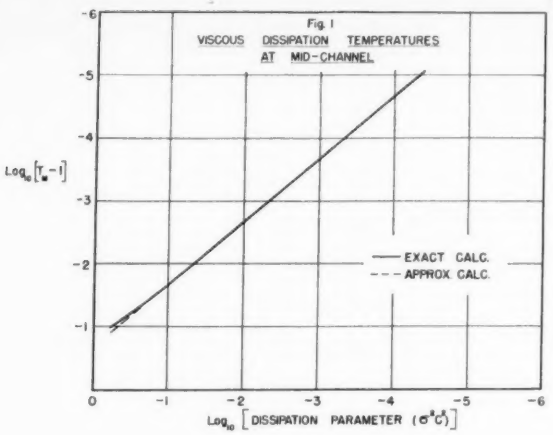

$$(d/d\eta)\,[T\,(dT/d\eta)] + 2\sigma^2 T\,(du/d\eta)^2 = 0 \qquad (5)$$

This mathematical problem can be solved as follows. The first integral of Eq. (4) is a constant, C, which can be identified as the slope of the velocity profile at either plate. If this is substituted into Eq. (5), the following differential equation for the temperature is obtained

$$[d^2(T)^2/d\eta^2] + 4\sigma^2 C^2 T = 0 \qquad (6)$$

This can be integrated by conventional techniques and, after applying the boundary conditions, one obtains

$$\left[1 - \frac{T-1}{T_m - 1}\right]^{1/2}\left[1 + \frac{(1/3)\,(T-1)}{1 + (2/3)\,(T_m - 1)}\right] = 1 - 2\eta \qquad (7)$$

where T_m is the temperature at mid-channel and is obtainable from

$$(T_m - 1)^{3/2} + (3/2)\,(T_m - 1)^{1/2} - (3\sigma C/4) = 0 \qquad (8)$$

Eqs. (7) and (8) serve to define the temperature distribution exactly. The velocity then can be determined as a function of the known temperature distribution. If the second integral of Eq. (4) is obtained and the boundary conditions applied, the result is

$$u = \int_0^\eta \frac{d\eta}{T} \Big/ \int_0^1 \frac{d\eta}{T} \qquad (9)$$

Hence, Eqs. (7) and (9) serve to define the velocity profile.

Two aspects of the above result complicate its reduction to numerical form. One is the rather involved expression for the temperature and the other is the presence of the constant, C, which depends upon the temperature. However, numerical results can be obtained by the following steps:

(1) Assume typical values of σC. (C is known to be of order unity as a consequence of the analysis based upon constant fluid properties.)

(2) Calculate corresponding values of $(T_m - 1)$ from Eq. (8).

(3) Substitute the values of $(T_m - 1)$ as obtained from Step (2) into Eq. (7), and integrate the expressions in Eq. (9) either numerically or graphically.

(4) Since

$$\frac{1}{C} = \int_0^1 \frac{d\eta}{T}$$

the constant, C, is determined in Step (3) and the corresponding value of σ can then be obtained from the assumed values of σC employed in Step (1).

Before indicating the results of this "exact" analysis, it should be added that the quantity $(T_m - 1)$ can be expected to be quite small for many gas flows. If such a restriction is introduced into Eqs. (7) and (8), it can be shown that they reduce to

$$T_m - 1 = \sigma^2 C^2/4 \qquad (10)$$

$$T = 1 + \sigma^2 C^2 \eta(1 - \eta) \qquad (11)$$

Further, Eq. (9) can be integrated in closed form and one obtains

$$u = \frac{\log\left[\left|\frac{p}{q}\right|^{\left|\frac{\eta - q}{\eta - p}\right|}\right]}{\log\left[\left|\frac{p}{q}\right|^{\left|\frac{1 - q}{1 - p}\right|}\right]} \qquad (12)$$

where $$p, q = (1/2)\,[1 \pm \sqrt{1 + (4/\sigma^2 C^2)}] \qquad (13)$$

On the basis of the above results, the effect of temperature dependent viscosity and heat conductivity coefficients on viscous heating can be indicated very clearly.

In Fig. 1, the amount of viscous heating as evaluated at mid-channel is plotted as a function of the parameter $\sigma^2 C^2$. The exact calculation heading refers to Eq. (8) and the approximate calculation heading to Eq. (10). Note that the approximation is excellent for values of the parameter as high as $\sigma^2 C^2 = 0.5 \times 10^{-1}$. If the fluid is assumed to be air, this value of the parameter corresponds to a plate "Mach Number" equal to 0.573. The constant, C, has the value 1.0083. If, on the other hand, $\sigma^2 C^2 = 0.5$, then the air "Mach Number" is 1.691 and the corresponding value of C is 1.0797.

Now since $C = 1$ in the case of constant viscosity and conductivity, this means that consideration of fluid property variations with temperature increases the viscous heating and the slope of the velocity profile. In other words, both the skin friction and the heat transfer are increased by variable viscosity and heat conductivity in a gas. However, in the case of skin friction this increase is proportional to C and in the case of heat transfer it is proportional to C^2. Therefore, the skin friction is increased to a lesser extent than the heat transfer. This means that heat-transfer coefficients based on skin-friction analysis will underestimate the heat transfer to a degree that depends upon the magnitude of the parameter σ unless an appropriate correction is applied.

One final comment regarding the velocity profile is in order. An inspection of Eq. (12) will show that an inflection point in the velocity curve exists at mid-channel. Dr. Sydney Goldstein has pointed out that this makes this an extremely interesting example for use in instability analysis.

References

[1] Schlichting, von H., *Einige Exakte Losungen fur die Temperaturverteilung in Einer Laminaren Stromung*, F. Angew, Zeitschrift fur Angewandte Mathematik und Mechanik, Vol. 31, No. 3, pp. 78–83, 1951.

[2] Illingworth, C. R., *Some Solutions of the Equations of Flow of a Viscous, Compressible Fluid*, Cambridge Phil. Soc. Proc., Vol. 46, pp. 469, 1950.

[3] Tarapov, I. E., *Solutions of the Problem of Viscous Gas Flow Between Two Moving Parallel Plates with Heat Transfer*, Prikladnaya Matematika I Mekhanicka, Vol. 19, No. 3, March, 1955.

[4] DeGroff, H. M., *Viscous Heating in Couette Flow*, Purdue School of Aero. Engrg. Report No. A-55-2, (Army Ordnance Research Contract No. DA-33-008-ord-888), September, 1955.

A Device for Vortex-Core Measurements

Edward J. Hopkins and Norman E. Sorensen
Aeronautical Research Scientists, NACA, Ames Aeronautical Laboratory, Moffett Field, Calif.

December 22, 1955

CERTAIN VISUAL-FLOW TECHNIQUES, such as the tuft grid described in reference 1 and the vapor screen described in reference 2, have been used in the past to indicate the approximate locations of vortex cores. To establish accurately both the positions of vortex cores in a transverse plane and their paths in the stream direction, a new technique was investigated. The technique employed a device which consisted of a small circular cylinder, free to rotate about an axis perpendicular to the axis of the cylinder, placed in the flow field with its axis of rotation

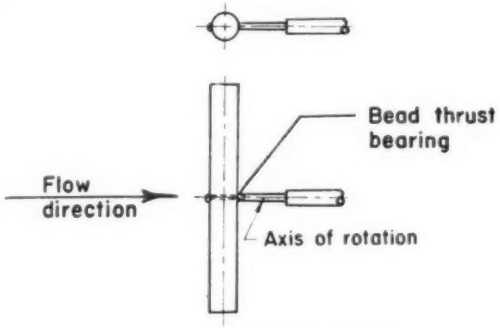

Fig. 1. A typical vortometer.

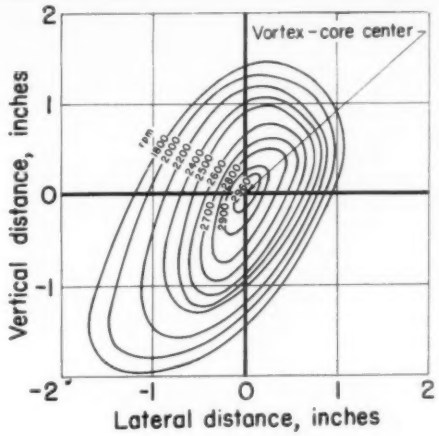

Fig. 2. Contour lines of constant rotational speeds of the 1-inch vortometer as seen looking downstream from the left wing panel.

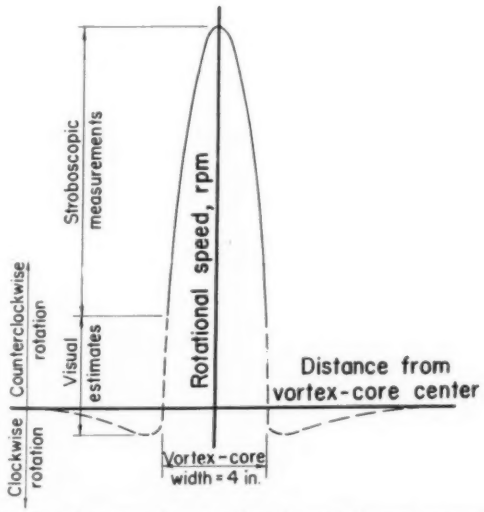

Fig. 3. Observed variation in rotational speed of the 1-inch vortometer as it was moved through the vortex core.

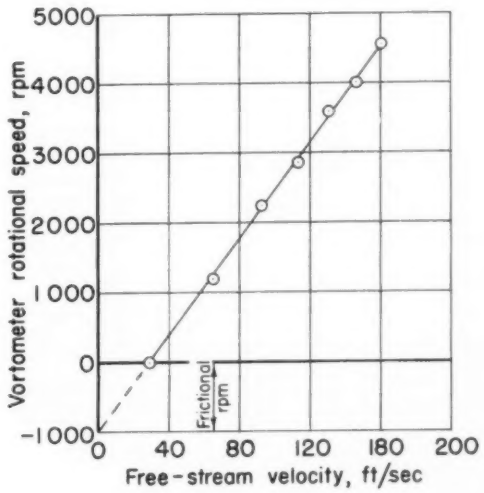

Fig. 4. Variation in rpm at the vortex-core center.

aligned in the free-stream direction. It was reasoned that the rotational speed of this device would change as it was moved across a vortex core because of the large flow-angle gradients near the core. The device, hereinafter called a "vortometer," is shown in Fig. 1.

A limited survey was made to determine the variation in the rotational speed of a 1-in.-long vortometer as it was moved across the vortex core formed by a triangular wing having a span of 42 in. and an aspect ratio 2.0 at an angle of attack of 14°. The measurements were made in a transverse plane 11.2 in. behind the wing trailing edge. The rotational speeds of the vortometer at various positions within the vortex core were measured with a stroboscope. These results are plotted in the form of contour lines of constant rotational speed in Fig. 2. At the center of the vortex core, the rotational speed is maximum. As the vortometer was moved away from the center of the vortex core, it was found that its rotational speed decreased to zero, reversed direction, and attained a relatively small maximum negative value, and then it decreased again to zero. It was not possible to establish these lower rotational speeds by means of the stroboscope because the minimum frequency of the light source was about 500 cycles per min. It was observed visually, however, that the rotational speeds of the vortometer varied in a manner similar to that shown in Fig. 3. It is believed that the size of the vortex core, indicated as the vortex-core width in Fig. 3, can be defined accurately provided the vortometer is small relative to the core and the low rotational speed can be measured. It was also found possible to establish the paths and origins of vortices by surveying with the vortometer in a number of transverse planes.

Measurements of the variation of the rotational speed of the vortometer with free-stream velocity made at the center of the vortex core are presented in Fig. 4. It is evident that the rotational speed was a linear function of free-stream velocity. An extrapolation of the curve to zero velocity gives an indication of the reduction in the rotational speed due to shaft friction. The vortometer in its present form does not appear suitable for use at transonic or supersonic speeds because of the very high rotational speeds that would be encountered as indicated by Fig. 4. An alternate device has been considered consisting of a small sweptback flat vane which is restrained from rotating by a torque-measuring instrument. The torque measured on such a device would vary in a manner similar to the r.p.m. shown in Fig. 3.

The main advantage of the vortometer technique over other techniques is its greatly imporved accuracy in determining the center and size of vortex cores. It should be possible to effect considerable refinement in the vortometer design and in the method of measuring its rotational speed, thereby improving the usefulness of a vortometer as a research tool.

References

[1] Bird, John D., and Riley, Donald R., *Some Experiments on Visualization of Flow Fields Behind Low-Aspect-Ratio Wings by Means of a Tuft Grid*, NACA TN 2674, 1952.

[2] Allen, H. Julian, and Perkins, Edward W., *A Study of Effect of Viscosity on Flow Over Slender Inclined Bodies of Revolution*, NACA Rep. 1048, 1951.

Interpolation Formulas for Supersonic-Hypersonic Airfoils

Richard D. Linnell* and Jerry Z. Bailey†
Convair, A Division of General Dynamics Corporation, Fort Worth, Texas

December 14, 1955

Analytical interpolation formulas for the aerodynamic characteristics of airfoils in supersonic-hypersonic flow provide compact prediction methods with reasonable accuracy. The formulas are based on curve fitting numerical data obtained from linear theory, shock-expansion hypersonic theory, and the method of characteristics. The nature of the aerodynamic properties of airfoils in hypersonic flows is shown by the formulas.

The Flat Plate

Modified shock-expansion theory with $\beta = \sqrt{M^2 - 1}$ gives the upper and lower surface pressure coefficients for a flat plate at angle of attack, α, as

* Formerly, Project Aerodynamics Engineer. Now, Functional Engineer, General Electric Company, Schenectady, N.Y.
† Technical Analyst.

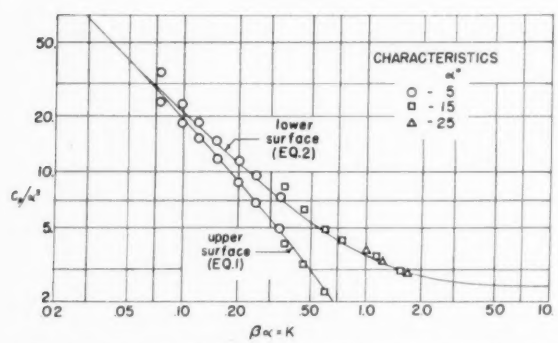

Fig. 1. Supersonic-hypersonic flat-plate pressure coefficients.

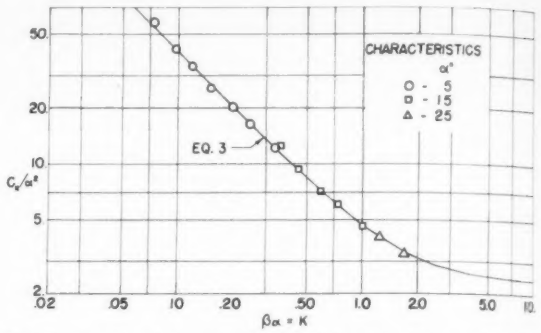

Fig. 2. Supersonic-hypersonic flat-plate normal force coefficient.

$$C_{pu}/\alpha^2 = (2/\gamma K^2)\left\{[1 - (1/2)(\gamma - 1)K]^{2\gamma/(\gamma-1)} - 1\right\} \quad (1)$$

$$C_{pl}/\alpha^2 = (1/2)(\gamma + 1) + 2\sqrt{1 + [(1/4)(\gamma + 1)K]^2}/K \quad (2)$$

where $K = \beta\alpha$ and the bracket $[1 - (1/2)(\gamma - 1)K]$ is taken to be zero when negative. Eqs. (1) and (2) give the correct forms for the linear-theory regime also. A comparison of these equations with the oblique-shock and Prandtl-Meyer exact inviscid theory values for $\gamma = 1.4$ is shown in Fig. 1. Except near shock detachment, the interpolation equations are accurate within ± 10 per cent.

An interpolation formula for flat-plate normal-force coefficient is

$$C_N/\alpha^2 = (4/K)\sqrt{1 + [(1/4)(\gamma + 1)K]^2} \quad (3)$$

which has been checked numerically only for $\gamma = 1.4$. This correlation is shown in Fig. 2. The accuracy is better than 10 per cent except near shock detachment. The factor $4/K$ is the linear-theory result. The square root term is a hypersonic correction factor.

The correction factor provides a simple method for estimating the importance of hypersonic effects. Thus when

$K = 0.1$, the correction is 0.2 per cent
0.5, the correction is 4.5 per cent
1.0, the correction is 17 per cent
2.0, the correction is 56 per cent

The correction factor also applies for the other flat plate coefficients which are $C_L = \cos\alpha C_N$, $C_{DL} = \sin\alpha C_N$, $C_{DW} = 0$, and $C_{M\frac{1}{4}} = 0$.

The Double-Wedge Airfoil

Numerical results for the double-wedge airfoil indicate that there are several differences between its properties in supersonic and hypersonic flow. In hypersonic flow:

(1) Lift coefficient increases more rapidly than the first power of angle of attack.

(2) Lift coefficient is affected by airfoil thickness.

(3) Zero lift pressure drag is greater than the supersonic value predicted by linear theory.

(4) Thickness wave drag (defined as pressure drag minus the streamwise component of normal force) is affected by angle of attack.

Evaluation of these effects is difficult when numerical data must be used. Interpolation formulas facilitate such study.

Curve fitting based on the flat-plate results gives similar formulas for the double-wedge airfoil with thickness ratio δ.

$$C_N/\alpha^2 = 4x\sqrt{1 + [(1/4)(\gamma + 1)/x]^2} \quad (4)$$

where

$$x = \sqrt{1 + [(1/2)(\gamma + 1)K_\delta]^2}/K_\alpha \quad (5)$$

Here K_δ is the thickness ratio similarity parameter, $\beta\delta$, and K_α is the angle of attack parameter. The form of Eq. (4) is identical to Eq. (3) with x replacing K. The parameter x includes the effect of thickness.

Eqs. (4) and (5) are based on a correlation for $\gamma = 1.4$ only. The correlation is shown in Fig. 3. The accuracy of the inter-

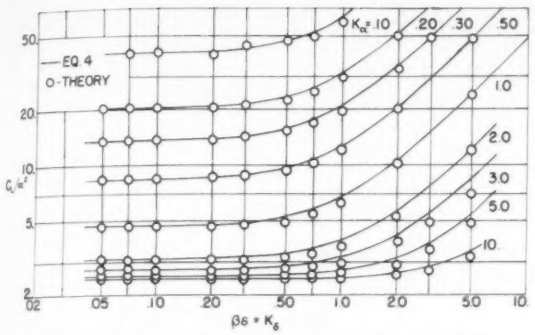

FIG. 3. Supersonic-hypersonic double-wedge airfoil lift coefficient.

polation formula is better than ±10 per cent in the region which was checked. The figure also shows how significant the effect of K_δ can be.

From Eq. (4), we find that in supersonic flow the thickness affects the lift coefficient only as an additive squared term. If K_δ and K_α are both large, the lift coefficient is not affected by thickness. But if K_α is less than 1 while K_δ is much greater than 1, thickness significantly affects the lift coefficient. In fact, under these conditions the lift coefficient is proportional to the thickness ratio, $C_L = 2(\gamma + 1)\delta\alpha$.

The interpolation formula for the zero lift pressure drag coefficient of the double-wedge airfoil is

$$C_{D0_p}/\delta^3 = (4/K_\delta)\sqrt{1 + [(1/4)(\gamma + 1)K_\delta]^2} \qquad (6)$$

which has the same form as Eq. (3). The square root is in effect a correction factor to the linear-supersonic theory value given by the first term.

For convenience define the drag due to lift coefficient by

$$C_{DL} = C_N \sin\alpha \qquad (7)$$

and define the thickness wave-drag coefficient as in linear supersonic theory by

$$C_{DW} = C_D - C_{DL} \qquad (8)$$

for inviscid flow. Numerical results show that C_{DW} is not independent of angle of attack in hypersonic flow. The interpolation formula for C_{DW} is similar to Eq. (4) with the roles of K_α and K_δ reversed.

$$C_{DW}/\delta^3 = 4y\sqrt{1 + [(1/4)(\gamma + 1)/y]^2} \qquad (9)$$

where

$$y = \sqrt{1 + [(1/2)(\gamma + 1)K_\alpha]^2}/K_\delta \qquad (10)$$

Eq. (9) has been checked only for $\gamma = 1.4$. The correlation with the numerical results is so similar to the comparison shown in Fig. 3 that it is not presented. The strongest effect of angle of attack on wave drag occurs when K_α is large and K_δ small. In this case the wave-drag coefficient becomes proportional to angle of attack, $C_{DW} = 2(\gamma + 1)\alpha\delta^2$.

The interpolation formula for the pitching-moment coefficient about the mid-chord of the double-wedge airfoil is

$$C_{M\frac{1}{2}} = (1/2)(\gamma + 1)\alpha\delta \qquad (11)$$

This expression correlates with the numerical data for $\gamma = 1.4$ with essentially no error until α/δ increases above 3.0. At α/δ of 10 the error is −10 per cent.

Linearized Theory of Water Drop Impingement*

Theodore R. Goodman†
Cornell Aeronautical Laboratory, Inc., Buffalo, N.Y.
December 22, 1955

INTRODUCTION

THE PROBLEM OF computing the trajectories of particles in the presence of a body when both particles and body are immersed in air has been studied by a number of authors. To name but a few: M. Glauert[1] computed them using Stokes' law of resistence. Langmuir and Blodgett[2] improved the calculations using an experimentally determined resistance law. Guibert, Janssen, and Robbins[3] performed a large number of numerical integrations on the differential analyzer which were formulated into empirical laws by Bergrun.[4]

The problem of calculating the aerodynamic performance of a thin airfoil is usually computed using linearized thin airfoil theory, and the velocity field about the airfoil is then known only to this order. It is consistent, therefore, to compute particle trajectories, which depend on the velocity field about a thin airfoil, to the same order as the velocity field itself.

The linearized equations of particle trajectories will be derived, and the results applied to determine the impingement efficiency of a flat plate at angle of attack.

INTEGRATION OF THE EQUATIONS OF MOTION

The equations of motion of a particle which moves in the x, y plane have been derived in reference 3. In dimensionless form they are

$$\left.\begin{aligned} du/d\tau &= \lambda(C_DR/24)\,[u_0(x, y) - u] \\ dv/d\tau &= \lambda(C_DR/24)\,[v_0(x, y) - v] \end{aligned}\right\} \qquad (1)$$

where u, v are the x and y components of velocity, τ is time, u_0, v_0 are the x and y components of the velocity field of the airfoil. According to reference 2, the quantity $(C_DR/24)$ is given empirically by

$$C_DR/24 = 1 + 0.197R^{0.63} + 2.6 \times 10^{-4}R^{1.38} \qquad (2)$$

where R is the local relative Reynolds Number

$$R = (2rU\rho_a/\mu)\sqrt{(u_0 - u)^2 + (v_0 - v)^2} \qquad (3)$$

where ρ_a is mass density of air. If the particles obeyed Stokes' resistance law, then $C_DR/24$ would be unity. $\lambda = (9/2)(C\mu \div r^2\rho_pU)$ where C is airfoil chord, μ is kinetic viscosity of air, r is particle radius, ρ_p is particle mass density, U is free-stream velocity. (λ is a measure of the particle size relative to the wing size.) The unit of velocity is U, the unit of length, C, and the unit of time, C/U. The trajectory obeys the initial conditions: at $\tau = -\infty$, $x = -\infty$, $y = \bar{y}$, $u = 1$, $v = 0$. Let ϵ be a dimensionless thickness parameter. The thin airfoil theory was derived by assuming $u_0 = 1 + \epsilon u_0'$, $v_0 = \epsilon v_0'$. Let $u = 1 + \epsilon u'$, $v = \epsilon v'$, $x = \tau + \epsilon x'$, $y = \epsilon y'$, $\bar{y} = 0(\epsilon)$. The last two assumptions mean that attention is confined to trajectories which are near the airfoil. It is clear from Eq. (3) that $R = 0(\epsilon)$. Hence, from Eq. (2) $C_DR/24 = 1 + 0(\epsilon^{0.63})$. Substituting into Eqs. (1) and linearizing with respect to ϵ, there is obtained

$$\left.\begin{aligned} du'/d\tau &= \lambda[u_0'(\tau, 0) - u'] \\ dv'/d\tau &= \lambda[v_0'(\tau, 0) - v'] \end{aligned}\right\} \qquad (4)$$

It is to be noted that, due to the linearization, the resistance law has reduced to Stokes. The general solutions are

$$\left.\begin{aligned} u' &= \lambda\exp(-\lambda\tau)\int_{-\infty}^{\tau}\exp(\lambda\tau_1)u_0'(\tau_1)d\tau_1 \\ v' &= \lambda\exp(-\lambda\tau)\int_{-\infty}^{\tau}\exp(\lambda\tau_1)\,v_0'(\tau_1)d\tau_1 \end{aligned}\right\} \qquad (5)$$

* The author would like to thank Prof. A. Robinson, whose lecture on this subject provided the impetus for the present investigation.

† Formerly, Principal Engineer, Aerodynamic Research Department. Now, Senior Engineer, Allied Research Associates, Inc., Boston, Mass.

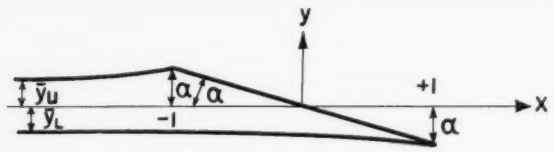

FIG. 1. Flat plate and limit trajectories (schematic).

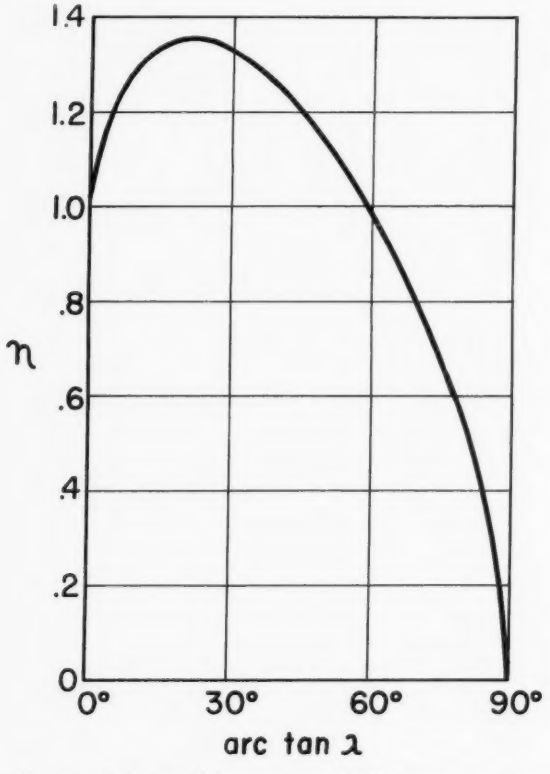

FIG. 2. Collector efficiency vs. particle size parameter, λ.

where the dependence of u_0' and v_0' on the second variable has been ignored. Since $u' = dx'/d\tau$, $v' = dy'/d\tau$, the equations may be integrated once more to yield

$$\left.\begin{aligned} x &= \tau + \int_{-\infty}^{\tau} u_0'(\tau_1)\{1 - \exp[-\lambda(\tau - \tau_1)]\}d\tau_1 \\ y &= \bar{y} + \int_{-\infty}^{\tau} v_0'(\tau_1)\{1 - \exp[-\lambda(\tau - \tau_1)]\}d\tau_1 \end{aligned}\right\} \quad (6)$$

Eqs. (6) constitute the parametric form of the trajectory.

Application to a Flat Plate at Angle of Attack

For a flat plate according to thin airfoil theory, $u_0'(\tau) = 0$ ahead of the plate, which means that the particle does not accelerate ahead of the plate. But it is the deflection of the particle which is of primary interest. In order to determine this, it is necessary to know $v_0'(\tau)$ ahead of the airfoil. On the under side of the airfoil, the kinematic boundary condition prescribes that $v_0'(\tau) = -\alpha$. Assume that the flat plate lies along the x axis from $x = -1$ to $x = +1$ so that the chord is 2. Furthermore, let ψ' be the perturbation stream potential, $v_0'(\tau) = -\partial\psi'/\partial\tau$. The second of Eq. (6) may then be written

$$y = \bar{y} - \psi'(\tau) + \psi'(-\infty) - e^{-\lambda\tau}\int_{-\infty}^{\tau} v_0'(\tau_1)\, e^{\lambda\tau_1} d\tau_1 \quad (7)$$

According to two-dimensional airfoil theory, $\psi'(-\infty)$ is logarithmically infinite. However, if a three-dimensional wing were considered then ψ' would vanish far upstream as the reciprocal of the distance. Hence, if two-dimensional theory is considered to be the limit of three-dimensional theory, $\psi'(-\infty)$ will vanish. Define the limit trajectory to be that trajectory which just touches the airfoil. There are obviously two such trajectories—an upper and a lower as shown in Fig. 1. Associated with each is a $\bar{y}$ designated by $\bar{y}_u$ and $\bar{y}_L$, respectively. The efficiency of the airfoil as a collector of particles is defined to be $(\bar{y}_u - \bar{y}_L)$ divided by the frontal area which for the present case is 2α. The velocity ahead of the flat plate according to thin airfoil theory is

$$\left.\begin{aligned} v_0(\tau) &= \alpha\left[\sqrt{\frac{(\tau-1)}{(\tau+1)}} - 1\right] \qquad \tau < -1 \\ &= -\alpha \qquad\qquad\qquad -1 < \tau < +1 \end{aligned}\right\} \quad (8)$$

Whence, setting $\tau = -1$ in Eq. (7), and $y = \alpha$, $\bar{y} = \bar{y}_u$, there is obtained

$$\bar{y}_u = \alpha - \frac{\alpha}{\lambda} + \psi'(-1) + \alpha e^{\lambda}\int_{-\infty}^{-1}\sqrt{\frac{\tau_1 - 1}{\tau_1 + 1}}\, l^{\lambda\tau_1} d\tau_1 \quad (9)$$

The last integral can be expressed in terms of modified Bessel functions[5] as follows:

$$\bar{y}_u = \alpha - (\alpha/\lambda) + \psi'(-1) + \alpha e^{\lambda}[K_0(\lambda) + K_1(\lambda)] \quad (10)$$

In a similar manner by setting $\tau = 1$

$$\bar{y}_L = -\alpha - (\alpha/\lambda) + \psi'(1) + \alpha e^{-\lambda}[K_0(\lambda) + K_1(\lambda)] \quad (11)$$

The difference $\bar{y}_u - \bar{y}_L$ is

$$\bar{y}_u - \bar{y}_L = 2\alpha + [\psi'(-1) - \psi'(1)] + 2\alpha \sinh\lambda[K_0(\lambda) + K_1(\lambda)] \quad (12)$$

But

$$\psi'(-1) - \psi'(1) = \int_{-1}^{+1} v_0'(\tau)d\tau = -2\alpha \quad (13)$$

Hence, the efficiency η, according to the definition is

$$\eta = \sinh\lambda\,[K_0(\lambda) + K_1(\lambda)] \quad (14)$$

This result has been plotted in Fig. 2 using the tables of Jahnke and Emde.[6] The fact that the efficiency is greater than one for some values of λ may at first be surprising, but if the chord were used as normalizer instead of the frontal area, this would not happen.

Conclusion

The linearized theory of impingement can be applied to airfoils with camber and thickness, as well as angle of attack. The results for these more general cases cannot be expressed in terms of tabulated functions, but, by the principle of superposition, the results are additive.

References

[1] Glauert, M., *A method of constructing the paths of raindrops of different diameters moving in the neighborhood of (1) a circular cylinder, (2) an aerofoil, placed in a uniform stream of air; and a determination of the rate of deposit of the drops on the surface and the percentage of drops caught.* R & M no. 2025, British A.R.C., 1940.

[2] Langmuir, I., and Blodgett, K., *A mathematical investigation of water droplet trajectories,* General Electric Company Report 1945 (Also published as A.A.F. Tech. Report 5418; also, Dept. of Commerce Pub. PB 27565.)

[3] Guibert, A. G., Janssen, E., and Robbins, W. M., *Determination of rate, area, and distribution of impingement of waterdrops on various airfoils from trajectories obtained on the differential analyzer,* NACA RM 9A05.

[4] Bergrun, R., *An empirical method permitting rapid determination of the area, rate, and distribution of waterdrop impingement on an airfoil of arbitrary section at subsonic speeds,* NACA TN 2476, September, 1951.

[5] Magnus, W., Oberhettinger, F., *Formulas and Theorems for Special Functions of Mathematical Physics,* Chelsea, 1949.

[6] Jahnke, E., and Emde, F., *Tables of functions with formulas and curves,* Fourth Ed., Dover, 1945.

∞) is loga-
l wing were
ne reciprocal
s considered
will vanish.
which just
ajectories—
d with each
ciency of the
$\bar{y}_L$) divided
The velocity
is

(8)

$= \bar{y}_u$, there

$\lambda\tau_1}\, d\tau_1$ (9)

ified Bessel

$_0(\lambda)]$ (10)

$_1(\lambda)]$ (11)

$_0(\lambda)]$ (12)

(13)

(14)

of Jahnke
an one for
chord were
would not

to airfoils
The re-
d in terms
erposition,

of different
an aerofoil,
of deposit of
M no. 2035,

on of water
o published
27565.)
tion of rate,
irfoils from
.
ation of the
of arbitrary

for Special

and curves,